

NASA TMX-67562

U.S. AIR FORCE -NATIONAL AERONAUTICS AND SPACE ADMINISTRATION

JOINT CONFERENCE ON LIFTING MANNED HYPERVELOCITY AND REENTRY VEHICLES

April 11 - 14, 1960

A COMPILATION OF THE PAPERS PRESENTED

PART II April 13-14, 1960

LANGLEY RESEARCH CENTER Langley Field, Virginia

CLASSIFIED DOCUMENT - TITLE UNCLASSIFIED

This material contains information affecting the National Defense of the United States within the meaning of the espionage laws, Title 18, U.S.C., Secs. 793 and 794, the transmission or revelation of which in any manner to an unauthorized person is prohibited by law.

CLASSIFICATION OHANGE

By authority of MASA MOMA C. Changed by M. Rucka. Date

S/ Py H- Maines

2.27



U.S. AIR FORCE -

NATIONAL AERONAUTICS AND SPACE ADMINISTRATION

JOINT CONFERENCE

on

LIFTING MANNED HYPERVELOCITY

AND REENTRY VEHICLES

April 11-14, 1960

A Compilation of the Papers Presented

Part II April 13-14, 1960

Langley Research Center Langley Field, Virginia





TABLE OF CONTENTS

			Page
INTRODUCTION	•	•	vii
LIST OF CONFEREES	•	•	ix
TECHNICAL PAPERS PRESENTED			
April 13, 1960			
1. Introduction by Brig. Gen. Homer A. Boushey, USAF	•	•	1
2. Dyna-Soar Program Status by Col. W. L. Moore, Jr., USAF	•	•	3
I. PHASE ALPHA AND CONFIGURATION EVOLUTION			
SESSION CHAIRMAN: John H. Goldie			
3. Introduction to Boeing Papers on Dyna-Soar Project by John H. Goldie		•	9
4. Review of Dyna-Soar Reentry-Vehicle-Configuration Studies by John F. Milton			15
5. Assessing Capability of Modified Titan ICBM Boosters for Dyna-Soar Type Vehicles by G. E. Ledbetter	•		47
6. Summary Comparison of Dyna-Soar Reentry Devices by Max T. Braun	•	•	61
7. Dyna-Soar Glider-Configuration Evolution by R. L. Rotelli	•	•	71
8. Dyna-Soar Aerodynamic Performance by James S. Lesko .	•	•	85
9. Stability Flight Control, and Energy Management of the Dyna-Soar Glider by A. H. Lee and L. J. Mason	•	•	101



SESSION CHAIRMAN: Calvin B. Hargis, Jr.

10.	Self-Adaptive Flight-Control Studies Applicable to Dyna-Soar by 1st Lt. Philip C. Gregory, USAF	119
	II. AERODYNAMIC HEATING, STRUCTURES, AND MATERIALS	
11.	Accuracy of Aerodynamic-Heating Prediction by A. L. Nagel and R. A. Hanks	133
12.	Dyna-Soar-Glider Flight-Envelope Structural Parameters by Edwin G. Czarnecki and Gordon N. Davison	147
13.	Development of Truss-Type Dyna-Soar Glider Structure by Andrew K. Hepler, Bruce E. Landry, and Melvin A. Nelson	161
14.	Dyna-Soar Skin Panel Development by Andrew K. Hepler, Walter E. Backus, and George B. Smith	179
15.	Current Status of Refractory Metals for Structural Applications by T. Sgt. Jesse C. Ingram, Jr., USAF	193
16.	Hot-Gas Tests for Dyna-Soar Structures and Materials Development by E. L. Kaminski and H. W. Klopfenstein	203
17.	Booster-Structure-Modification Studies for Winged Dyna-Soar Vehicles by R. M. Haynes, R. T. Boll, and M. T. Braun	215
	April 14	
	III. PILOT FUNCTIONS AND FLIGHT TESTING	
	SESSION CHAIRMAN: William E. Lamar	
18.	Design Considerations for the Transparent Vision Areas in Orbital Glide Vehicles by Kennerly H. Digges	233
19.	Dyna-Soar Pilot Functions, Utilization, Information, and Display by Harold E. Bamford, Jr	245
20.	Utilization of the Pilot During Boost Phase of the Step I Mission by Euclid C. Holleman	261





21.	Pilot Factors Influencing Dyna-Soar Glider Design by Robert L. Campbell and Herbert G. Shepler	273
22.	Secondary Power and Environmental Control for Dyna-Soar by Earl M. Donnen	285
23.	Contributions of Free-Flight Model Testing to the Development of Boost-Glide Vehicles by Tung-Sheng Liu	30 5
24.	Dyna-Soar Step I Flight Test Program by Lt. Col. Harold G. Russell, USAF, B. Lyle Schofield, and Thomas F. Baker	311
25.	Instrumentation and Communications Considerations for Dyna-Soar by Gerald M. Truszynski and Paul O. Lindfors	325
	April 11	
	(These two papers were presented under the "Aerodynamic and Heat Transfer" section on April 11 and are being included in this compilation because of their classification.)	
26.	The Effect of Real-Air Properties Upon Aerodynamic Forces, Moments, and Heat-Transfer Rates for Reentry Vehicle by Nathaniel B. Cohen, Ivan E. Beckwith, and Robert L. Trimpi	33 5
27.	Studies of Stability and Control of Winged Reentry Configurations by Robert W. Rainey and William H. Close	3 61



Page intentionally left blank



INTRODUCTION

This document is Part II of a compilation of papers presented at a USAF/NASA Conference on Lifting Manned Hypervelocity and Reentry Vehicles held at the Langley Research Center on April 11-14, 1960. This conference was held jointly by the U.S. Air Force and the National Aeronautics and Space Administration to provide industry and government agencies the most recent results of research and development activities relating to manned hypervelocity and reentry vehicles which have lifting capability and ability to maneuver in the atmosphere. The papers were presented by the Air Force, NASA, and the Dyna-Soar contractor, Boeing Airplane Company.

Page intentionally left blank



LIST OF CONFEREES

The following were registered at the Joint Conference on Lifting Manned Hypervelocity and Reentry Vehicles, Langley Field, Virginia, April 13-14, 1960.

ABBEY, Capt. George W. ABBOTT, Ira H. ABRAHAMS, Robert P. ALBERI, Americo ALDERSON, Ross C. ALEXANDER, Grover L. AMUNDSON, Maj. Floyd ANDERSON, Harvey L. ANDERSON, Melvin S. ANDERSON, Roger A. ARCIDIACONO, Thomas ARMSTRONG, William O.

BADERTSCHER, Robert F. BADGER, Frank S., Jr. BAILEY, Capt. Cecil BAILEY, Harry E. BAKER, Thomas F. BAKER, William W. BARR, Dr. Norman L. BARRON, Capt. Douglas R. BARTON, Maj. Marshall M. BATES, George BATTERSON, Sidney A. BEAVER, Wallace W. BECKER, John V. BECKMAN, Capt. Edward L. BECKWITH, Ivan E. BELL, Marion W. J. BEISLEY, Steven E. BERESFORD, Thomas E. BERLOT, Robert R. BERTRAM, Mitchel H. BIKLE, Paul F. BIRD, King D. BOBCO, Richard P. BOND, Aleck C. BOOTH, Lt. Col. Raymond W. W.

BOUSHEY, Brig. Gen. H. A.

Wright Air Development Div.

NASA - Headquarters

Kearfott Co., Inc.

Republic Aviation Corp.

Minneapolis-Honeywell Regulator Co.

Wright Air Development Div.

Air Force Missile Test Center

Wright Air Development Div.

NASA - Langley Research Center

NASA - Langley Research Center

Fairchild Engine and Airplane Corp.

NASA - Langley Research Center

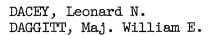
Battelle Memorial Institute Haynes Stellite Co. ARDC, Liaison Office, Langley Field NASA - Ames Research Center NASA - Flight Research Center Wright Air Development Div. Republic Aviation Corp. Wright Air Development Div. AF Warfare Systems School NASA - Headquarters NASA - Langley Research Center The Brush Beryllium Co. NASA - Langley Research Center Naval Air Development Center NASA - Langley Research Center North American Aviation, Inc. NASA - Ames Research Center Northrop Corp., Radioplane Div. G. M. Giannini and Co., Inc. NASA - Langley Research Center NASA - Flight Research Center Cornell Aeronautical Laboratory Northrop Corp., Nortronics Div. NASA - Space Task Group Office of the Director of Research & Development, DCS/Development Asst. for Advanced Technology, DCS/Development



BOYKIN, James A., Jr.
BRAUN, Gerhard W.
BRAUN, Max Thomas
BRAY, Richard S.
BREBNER, George G.
BREUHAUS, Waldemar O.
BRIDGE, Charles S.
BRODSKY, Robert F.
BROWN, Clinton E.
BUELL, Donald
BUNN, Lloyd T.
BURTON, George T., Jr.
BUSEMANN, Dr. Adolf

CAMPBELL, Robert Leon CAMPBELL, William F. CARNER, Harold A. CARR, Robert E. CARTER, Cecil V. CARTER, James W. CARTER, Roger D. CAUDLE, Capt. Ralph E. CHAMBERLIN, James A. CHAPIN, William T. CHAPLICK, Robert G. CHAPMAN, Philip W. CHARPENTIER, Allyn CHASE, Stanley R. CHILDERS, Milford G. CLARK, Charles C. CLARK, James W. CLARK, John R. CLOSE, Robert R. CLOSE, William H. COHEN, Nathaniel B. COMPTON, William A. CONCHA, Joseph I. CONLON, Emerson W. CONNOR, Harvey F., Jr. COOLEY, Dale E. CORNOG, Robert COUGHLIN, Kenneth J. CRAMER, Granville R. CREEL, R. L. CREER, Brent Y. CRONVICH, Lester L. CZARNECKI, Edwin Gregory Wright Air Development Div.
Air Force Missile Development Center
Boeing Airplane Co.
NASA - Ames Research Center
British Joint Services Mission
Cornell Aeronautical Laboratory
Litton Industries
Aerojet-General Corp.
NASA - Langley Research Center
NASA - Ames Research Center
E. I. du Pont de Nemours & Co., Inc.
Bendix Aviation Corp.
NASA - Langley Research Center

Boeing Airplane Co. Canadian Joint Staff Avco Manufacturing Corp. North American Aviation, Inc. Chance Vought Aircraft, Inc. Redstone Arsenal Analytic Services, Inc. Wright Air Development Div. NASA - Space Task Group General Electric Co. NASA - Goddard Space Flight Center American Bosch Arma Corp. American Machine and Foundry Co. Bendix Aviation Corp. Lockheed Aircraft Corp. International Nickel Co., Inc. United Aircraft Corp. Chance Vought Aircraft, Inc. Bendix Aviation Corp. NASA - Langley Research Center NASA - Langley Research Center Solar Aircraft Co. Air Technical Intelligence Center NASA - Headquarters Western Electric Co. Wright Air Development Div. Ramo-Wooldridge The Martin Co. Thickol Chemical Corp. Bureau of Naval Weapons NASA - Ames Research Center Applied Physics Laboratory - J. H. U. Boeing Airplane Co.



DAHM, Werner K. DAIGLE, Furnand F. DAVISON, Gordon N. DAWSON, John B. DEAN, J. W. DECREVAL, Roland DEGEN, Max DIGGES, Kennerley H. DISHER, John DOBRZANSKI, Janusz S. DOMIZI, Dario DONELY, Philip DONLAN, Charles J. DONNELL, William F. DONNEN, Earl Martin DOUGLASS, William M. DRAKE, Hubert M. DRALEY, Eugene C. DUKES, Wilfred DUNAVANT, James C. DUNCAN, Lt. Comdr. Robert C.

EAKINS, Lt. Col. William W. EDWARDS, George G. EDWARDS, Howard B. EDWARDS, Richard EGGLESTON, John M. ELLIS, Macon C. ERICKSON, Myles D. EULBERG, Alvin C. EVANS, A. J. EVANS, William L. EZRA, Arthur A. H.

FAGET, Maxime A.
FARNHAM, Leon
FEDZIUK, Henry A.
FEIGEN, Morris
FELLER, William V.
FELT, Morris E., Jr.
FERER, Lt. Col. Benjamin H.

FIKES, Joseph E. FLATZ, John S.

Operations Analysis Office (AFCOA) Director of Operational Requirements, DCS/Operations Redstone Arsenal Radio Corp. of America Boeing Airplane Co. Ampex Corp., Instrumentation Div. McDonnell Aircraft Corp. Bell Aircraft Corp. The Raytheon Co. Wright Air Development Div. NASA - Headquarters Hughes Aircraft Co. National Carbon Co. NASA - Langley Research Center NASA - Space Task Group Texas Instruments, Inc. Boeing Airplane Co. Douglas Aircraft Co., Inc. NASA - Flight Research Center NASA - Langley Research Center Bell Aircraft Corp. NASA - Langley Research Center

AF Cambridge Research Center
NASA - Ames Research Center
NASA - Langley Research Center
Grumman Aircraft Engineering Corp.
NASA - Langley Research Center
NASA - Langley Research Center
NASA - Ames Research Center
Convair
NASA - Headquarters
Convair
The Martin Co.

Office of Chief of Naval Operations

NASA - Space Task Group
General Electric Co.
NASA - Langley Research Center
Space Technology Laboratories, Inc.
NASA - Langley Research Center
The Martin Co.
Asst. for Advanced Technology,
DCS/Development
Army Ordnance Missile Command
Wright Air Development Div.



FLYNN, Warren A. FORREST, Clarence FOWLER, Robert M.

FOWLER, Roy G. FRANK, Robert G. FREEMAN, Robert R. FRIEND, Carl F. FULLING, Roger W.

GARRICK, I. E. GAY, Lt. Clarence C., Jr. GIESEMAN, Maj. Earl R., Jr.

GILDEA, David J. GILKEY, Kenneth J. GILMER, William N. GILRUTH, Robert R. GLODECK, Edward GLOVER, Col. Walter P. GOETT, Harry J. GOLDBAUM, George C. GOLDIE, John Harrison GOODWIN, Glen GORANSON, R. Fabian GOTTSCHALL, Richard C. GRANT, Frederick C. GREENE, Lawrence P. GREGORY, Lt. Phillip C. GRIMES, David L. GUY, Lawrence D. GUYTON, Robert D.

HABER, Bernard Dov HALE, Capt. Roy E. HALL, Edward N. HALL, R. W. HAMLIN, Benson HAMMOCK, David M. HANLEY, Gerald M. HARGIS, Calvin B. HARRIS, Ralph J. HARRIS, T. Aubrey HARTWIG, Frederic W. HAVEL, Charles J. HAYES, Lt. Thomas C. HAYNES, Robert Miller Temco Aircraft Corp. Bell Aircraft Corp. Metals Research Laboratory, Union Carbide Metals Co. Convair General Electric Co. Climax Molybdenum Co. of Michigan Ryan Aeronautical Co. E. I. du Pont de Nemours & Co., Inc.

NASA - Langley Research Center Wright Air Development Div. Office of the Director of Research & Development, DCS/Development North American Aviation, Inc. Wright Air Development Div. Experiment, Inc. NASA - Space Task Group Boeing Airplane Co. Wright Air Development Div. NASA - Goddard Space Flight Center Douglas Aircraft Co., Inc. Boeing Airplane Co. NASA - Ames Research Center NASA - Headquarters Bendix Aviation Corp. NASA - Langley Research Center North American Aviation, Inc. Wright Air Development Div. Narmco Industries, Inc. NASA - Langley Research Center Wright Air Development Div.

North American Aviation, Inc. ARDC, Andrews AFB United Aircraft Corp. NASA - Lewis Research Center Boeing Airplane Co. Redstone Arsenal Convair Wright Air Development Div. Naval Air Material Center NASA - Langley Research Center Space Technology Laboratories, Inc. Kelsey-Hayes Co. Wright Air Development Div. Boeing Airplane Co.



HEDGEPETH, John M. HELDENFELS, Richard R. HELMS, Bobbie F. HENDERSON, Arthur, Jr. HENSEL, Rudolph W. HEPLER, Andrew Karl HERTLER, Eugene G. HESS, George K., Jr. HEWES, Donald E. HIBBERT, Col. Richard B. HILDEBRAND, Robert B. HILTON, David A. HINZ, Hans HODGE, John M. HOLLEMAN, Euclid C. HOLZAPPLE, Brig. Gen. J. R. HOUBOLT, John C. HOUGHTON, Richard HUBBARD, Harvey H. HUBER, Paul W. HUFFINGTON, James E. HUNTINGTON, Robert C. HUNTIZICKER, John H. HURSH, John W. HURWICZ, Henryk

INGRAM, T. Sgt. Jesse C. ISENBERG, Dr. Joel S.

JESTER, Lt. Comdr. M.
JOHNS, Frank R.
JOHNSON, Caldwell C., Jr.
JOHNSON, James H.
JOHNSON, J. Malcolm
JOHNSON, Joseph L., Jr.
JONES, David J., Jr.
JONES, Dewey I.
JORDAN, Gareth H.
JUNTILLA, Harry W.

KAPLAN, Abner
KEARNEY, Lt. Comdr. Stuart D.
KEHLET, Alan B.
KIRK, Robert L.
KLEINHESSELINK, Glenn J.
KLEPINGER, Richard H.
KNAPP, Russell H.

NASA - Langley Research Center Arnold Engineering Development Center Boeing Airplane Co. Chrysler Corp. Bendix Aviation Corp. NASA - Langley Research Center Office of Asst. Chief of Staff, USAF Boeing Airplane Co. NASA - Langley Research Center Grumman Aircraft Engineering Corp. U. S. Steel Corp. NASA - Flight Research Center Dir. of Syst. Management, WADD NASA - Langley Research Center Grumman Aircraft Engineering Corp. NASA - Langley Research Center NASA - Langley Research Center Boeing Airplane Co. Motorola, Inc. The RAND Corp. Massachusetts Institute of Technology Avco Manufacturing Corp.

Wright Air Development Div. Flight Science Laboratory

Naval Air Development Center
Naval Air Development Center
NASA - Space Task Group
North American Aviation, Inc.
North American Aviation, Inc.
NASA - Langley Research Center
Convair
Wright Air Development Div.
NASA - Flight Research Center
Air Defense Command, Ent AFB

Space Technology Laboratories, Inc.
Office of Chief of Naval Research
NASA - Space Task Group
Litton Industries
General Motors Corp.
Wright Air Development Div.
Boeing Airplane Co.





KOCH, Charles J. KOHLHASE, Charles E., Jr. KORDES, Eldon E. KORYCINSKI, Peter F. KOSTOCH, Francis R. KRIEGER, Robert H.

LAMAR, William E. LAMPROS, Alexander F. LANGE, Roy H. LARRABEE, Prof. E. E. LASSEN, Herbert A. LAWLER, Edward D. LEDBETTER, Girvis Erwin LEE, Alan Hilman LEFLER, Emery D. LEONARD, Robert W. LESKO, James Stephen LEVIN, Ellis LEVIN, Kenneth LINDLEY, Charles A. LITTELL, Robert E. LIU, Dr. Tung-Sheng LOFTIN, Laurence K., Jr. LOFTUS, Lt. Joseph P. LOHSE, Edward LONG, Joseph E. LOVE, Eugene S. LOVELL, P. M. LOW, George M. LOWELL, Herman H. LU, Hoshen R. LUIDENS, R. W. LUKESH, John S.

MAC MORRIS, David MADDEN, Robert T. MADSEN, Alfred P. MAGGIN, Bernard MAGRANE, Capt. Joseph H. MARSHALL, Edmund V. MARTIN, Richard E. MARTZ, Ronald B. MASON, Dr. John L.

MASON, Leroy John MATHAUSER, Eldon E.

The Martin Co. NASA - Jet Propulsion Laboratory NASA - Langley Research Center

NASA - Langley Research Center

North American Aviation, Inc. Ballistic Research Laboratories

Wright Air Development Div.

Pacific Missile Range

Lockheed Aircraft Corp.

Massachusetts Institute of Technology

Space Technology Laboratories, Inc.

Naval Air Development Center

Boeing Airplane Co.

Boeing Airplane Co.

Wright Air Development Div.

NASA - Langley Research Center

Boeing Airplane Co.

Boeing Airplane Co.

Bell Aircraft Corp.

Marquardt Aircraft Co.

NASA - Headquarters

Wright Air Development Div.

NASA - Langley Research Center

Wright Air Development Div.

Burroughs Corp.

Office of Scientific Research, ARDC

NASA - Langley Research Center

NASA - Headquarters

NASA - Headquarters

NASA - Goddard Space Flight Center

Republic Aviation Corp.

NASA - Lewis Research Center

Northrop Corp., Nortronics Div.

Sundstrand Aviation Goodyear Aircraft Corp. Convair

NASA - Headquarters

Air Proving Ground Center

Chance Vought Aircraft, Inc.

Convair

Wright Air Development Div.

The Garrett Corp., AiResearch Mfg.

Boeing Airplane Co.

NASA - Langley Research Center



MAY, Ralph W. MAYES, William H. McCOMB, Harvey G., Jr. McKENZIE, Lt. Col. M. A. McLAUGHLIN, John R. McLELLAN, Charles H. McMAHON, Howard H. MEAD, Merrill H. MELLEN, David L. MERCER, Jack R. MIGOTSKY, Eugene MILLER, Bernard P. MILTON, John F. MOORE, Col. Walter L. MORAN, William R. MORGAN, Homer G. MOSSMAN, Emmet A. MULTHOPP, Hans MUNTER, Paul L. MUSE, Thomas C.

MUZZEY, Benjamin C.

NAGEL, Adelbert Leslie
NAY, Harvey O.
NEISON, Melvin A.
NEISON, R. L.
NESTINGEN, Irvin M.
NEVINS, James L.
NICHOLS, Mark R.
NIELSEN, Jack N.
NING, Ted C.
NORTH, Warren J.

ORSINI, Antonio OVERALL, John W.

PAGLIANETE, Francis J.
PASCHALL, Lt. Col. Benjamin F.
PAUL, Robert H.
PAULSON, John W.
PEARSON, E. O.
PECK, Robert F.
PELLINI, William S.
PENN, Col. William W.
PENTECOST, Joseph L.
PEPPING, Raymond A.

NASA - Headquarters NASA - Langley Research Center NASA - Langley Research Center Wright Air Development Div. The Raytheon Co. NASA - Langley Research Center Canadian Joint Staff NASA - Ames Research Center Minneapolis-Honeywell Regulator Co. United Aircraft Corp. Avco Manufacturing Corp. Radio Corp. of America Boeing Airplane Co. Wright Air Development Div. NASA - Langley Research Center The Martin Co. The Martin Co. Republic Aviation Corp. Office of the Director of Defense, Research & Engineering Boeing Airplane Co.

Boeing Airplane Co.
Hughes Tool Co.
Boeing Airplane Co.
Lockheed Aircraft Corp.
Convair
Massachusetts Institute of Technology
NASA - Langley Research Center
VIDYA, Inc.
Wright Air Development Div.
NASA - Headquarters

Walter Kidde & Co., Inc. Lockheed Aircraft Corp.

Bureau of Naval Weapons
Wright Air Development Div.
North American Aviation, Inc.
NASA - Langley Research Center
NASA - Headquarters
General Electric Co.
Naval Research Laboratory
ARDC, Andrews AFB
Aeronca Manufacturing Corp.
McDonnell Aircraft Corp.



PERKINS, Courtland D.

PERRINE, Calvin H., Jr. PETERSON, Homer C. PHILLIPS, Warren L. PHILLIPS, William H. PIERCE, Roger J. PITTMAN, W. D. PLASCOTT, Roland H. POSTLE, Robert POWELL, James L., Jr. PRATT, George L. PRIDE, Richard A. PURSER, Paul E. PUTNAM, Dale W.

RABER, Christopher L. RAINEY, A. Gerald RAINEY, Robert W. RARING, Richard REESE, Bruce A. REESE, David E., Jr. REGER, Joseph E. REID, Dr. H. J. E. RELLER, John O., Jr. RHODE, R. V. RICHARDSON, Francis H. RICLES, Robert RIEDINGER, Louis A. RITCHEY, Wallace M., Jr. ROBERTS, Leonard ROBINSON, Russell G. ROBINSON, Theodore ROCHEN, Herb RODRIGUEZ, Edward ROETHE, Floyd A. ROSCHE, M. G. ROSE, Peter H. ROSS, Dr. Franklin

ROSS, Robert S. ROTELLI, R. L. ROYSTER, Dick M. RUNYAN, Harry L. RUSSELL, Lt. Col. Harold G. RUTKOWSKI, Joseph RYKEN, John

Asst. Secretary of the Air Force, R&D The Martin Co. M.I.T. Lincoln Laboratories Hughes Aircraft Co. NASA - Langley Research Center Collins Radio Co. McDonnell Aircraft Corp. British Joint Services Mission Bell Aircraft Corp. The Martin Co. Arnold Engineering Development Center NASA - Langley Research Center NASA - Space Task Group Boeing Airplane Co.

General Electric Co. NASA - Langley Research Center NASA - Langley Research Center NASA - Headquarters Purdue Research Foundation NASA - Ames Research Center General Electric Co. NASA - Langley Research Center NASA - Ames Research Center NASA - Headquarters Air Force Flight Test Center Republic Aviation Corp. Lockheed Aircraft Corp. Wright Air Development Div. NASA - Langley Research Center NASA - Ames Research Center Wright Air Development Div. NASA - Headquarters Litton Industries Librascope, Inc. NASA - Headquarters Avco Manufacturing Corp. Office of the Asst. Secretary of the Air Force Goodyear Aircraft Corp. Boeing Airplane Co. NASA - Langley Research Center NASA - Langley Research Center Air Force Flight Test Center Bendix Aviation Corp. Bell Aircraft Corp.



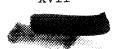
SAILOR, J. Douglas
SANDO, Robert M.
SANDORF, Prof. Paul E.
SANIAL, Thomas
SAUER, John G.
SAVIN, Raymond C.
SCHMITT, Thomas J.
SCHNEIDER, William C.
SCHUBERTH, Edward R.
SCHWICHTENBERG, Dr. A. H.

SCOVILLE, Maj. Curtis L. SEAGER, Donald B. SEATON, Charles H. SEIFF, Alvin SHANKS, Robert E. SHORTAL, Joseph A. SHOWS, J. C. SIVELLS, James C. SMITH, Charles G. SMITH, G. Allan SMITH, James C., Jr. SNODGRESS, Richard B. SODERBERG, Laurence R. SOEHNGEN, Erich E. SOLLENBERGER, Comdr. Robert L. SOMSON, Alfred S. SOULE, Hartley A. SPURR, Harold G. STAINBACK, P. Calvin STALK, Maj. George STALZER, Lt. Charles E. STATUM, Maj. Cyril M.

STAUBACH, Richard L.

STEINMETZ, H. F.
STEVENS, John E.
STEVENS, Victor I., Jr.
STEWART, John D.
STITT, L. E.
STOECKER, Lawrence R.
STREETT, Capt. James K.
STROUD, C. W.
SUMMER, A. J.
SVIMONOFF, Maj. Constantence
SWOFFORD, Maj. Gen. R. P., Jr.

Lockheed Aircraft Corp. Westinghouse Electric Corp. Massachusetts Institute of Technology Grumman Aircraft Engineering Corp. Universal-Cyclops Steel Corp. NASA - Ames Research Center Bureau of Naval Weapons Chief of Bureau of Naval Weapons Lockheed Aircraft Corp. Lovelace Foundation for Medical Education and Research ARDC, Andrews AFB Lockheed Aircraft Corp. Aeronutronic Systems, Inc. NASA - Ames Research Center NASA - Langley Research Center NASA - Langley Research Center McDonnell Aircraft Corp. Arnold Engineering Development Center Boeing Airplane Co. NASA - Ames Research Center Chrysler Corp. NASA - Headquarters The Martin Co. Wright Air Development Div. U.S. Naval Air Test Center Sperry Gyroscope Co. NASA - Langley Research Center British Joint Services Mission NASA - Langley Research Center Chief of Defense Atomic Support Agency Pacific Missile Range Office of Director of Personnel Procurement & Training Pratt & Whitney Aircraft Div., United Aircraft Corp. McDonnell Aircraft Corp. Chance Vought Aircraft, Inc. NASA - Ames Research Center General Electric Co. NASA - Lewis Research Center Beech Aircraft Corp. Wright Air Development Div. NASA - Langley Research Center McDonnell Aircraft Corp. Wright Air Development Div. Air University





SYVERTSON, C. A.

TAYLOR, Robert T.
TEMPLE, Jack L.
TEPLITZ, Jerome
THOMAS, Richard E.
THOMPSON, Floyd L.
THOMPSON, Jim Rogers
THOMPSON, Kenneth O.
THRALL, Edward W., Jr.
TOLEFSON, Harold B.
TOUMANOFF, George I.
TRIBBET, Louis W.

TRIMPI, Robert L.
TRUEBLOOD, Joseph R.
TRUSSELL, Donald H.
TRUSZYNSKI, Gerald M.
TUOVILA, Weimar J.
TURETZKY, Arthur A.
TUSCH, Carl W.

UIMANN, Edward

VALE, Robert E. VAN BUITEN, Robert D. VAN GOSSICK, Col. Lee

VELTON, Edward Jon

WAKEFORD, Ronald C. WALDRON, Howard F. WALKER, Harold J. WARREN, Walter WEBER, Charles M., Jr. WEIL, Nicholas A. WENTSCH, Robert E. WESESKY, John L. WHITE, John S. WHITE, Richard P., Jr. WICK, Bradford H. WILBUR, Stafford W. WILLIAMS, Harry E. WILLIAMS, Walter C. WILLIAMS, Maj. Wayland W. WILSON, Herbert A., Jr. WISEMAN, Homer E. WOLKO, Howard S. WOOD, Clotaire

NASA - Ames Research Center

NASA - Langley Research Center Boeing Airplane Co. Bureau of Naval Weapons Ohio State Univ. NASA - Langley Research Center Lockheed Aircraft Corp. Univ. of Minnesota Douglas Aircraft Co. NASA - Langley Research Center Airborne Instruments Laboratory Director of Development Planning, DCS/Development NASA - Langley Research Center ARDC, Andrews AFB NASA - Langley Research Center NASA - Flight Research Center NASA - Langley Research Center American Machine & Foundry Co. ARDC, Liaison Office, Moffett Field

General Electric Co.

NASA - Space Task Group National Academy of Sciences Office of the Asst. Secretary of the Air Force, R & D Convair

Melpar, Inc. Canadian Joint Staff NASA - Flight Research Center General Electric Co. The RAND Corp. Armour Research Foundation Ramo-Woolridge Air Force Flight Test Center NASA - Ames Research Center Cornell Aeronautical Laboratory NASA - Ames Research Center NASA - Headquarters NASA - Jet Propulsion Laboratory NASA - Space Task Group Strategic Air Command, Offutt AFB NASA - Langley Research Center Strategic Air Command, Offutt AFB Office of Scientific Research, ARDC NASA - Headquarters





INTRODUCTION

By Brig. Gen. Homer A. Boushey
Asst. for Advanced Technology, Deputy Chief of Staff,
Development Headquarters, U.S. Air Force

The NASA papers that have been heard during the past 2 days illustrate the tremendous contribution of time and the irreplacable scientific talent that NASA has made to the Dyna-Soar project. Not all of them apply directly to the U.S. Air Force development; for instance, it is not intended that the Air Force Dyna-Soar vehicle operate at speeds higher than orbital speed. The NASA work, however, along with the more specific work of Air Force contractors, form the theoretical and technical basis for our future development.

L

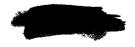
1

0

5

It should be remembered that the NASA and the U.S. Air Force will continue to pursue the Dyna-Soar development on a cooperative basis. A joint memorandum of understanding signed in November of 1958 by Dr. T. Keith Glennan for NASA and by General Thomas D. White for the Air Force says that the Air Force will fund and manage the Dyna-Soar development but with the advice and consultation of NASA. It is the intention of the Air Force to insure full and authoritative NASA participation. The memorandum of understanding states that the two partners will jointly participate in the technical development to maximize the vehicle capabilities from both the military-system development and aeronautical-research viewpoints. NASA has been represented in the Dyna-Soar Project Office, and it is hoped that as active development begins, this representation will be increased.

The Dyna-Soar project represents true pioneering into a new and extremely promising field of flight. The Air Force is convinced that many of its future systems will have to operate in space and furthermore that these systems must and inevitably will include man. An essential ingredient of these systems will be some device that can return man from orbital flight in a routine, nonadventurous manner that can be supported operationally. The pilot of the return vehicle must be able to control his return to earth. He must have some freedom in choosing the time when he will initiate reentry and he must have control of the point at which he will land. Also, his landing should be made without damage. It is this essential capability that is sought in Dyna-Soar. In achieving this goal, Dyna-Soar I must first demonstrate satisfactory solutions to many design problems and must validate design assumptions in areas such as aerodynamic heating and radiation cooling. Dyna-Soar I will do this by researching the flight corridor.





The Dyna-Soar project is also a pioneer in the management area. It is the Air Force intention to participate in much greater detail in the management of this project than has been the practice in the recent past. A project management, engineering, and contracting team is being created for this purpose.

There has been some controversy as to the value of man in space. There are many tasks in which it can be imagined that man's unique flexibility and judgment might be applied. Proponents of the unmanned systems will quickly point out the weight advantage that they offer. It is inconceivable, however, that our future in space will always be entrusted to machines.

Just as the Wright Brothers in their time could not imagine airplanes like the B-70 or modern jet transports, so it seems that man today cannot imagine the extent to which space flight will be used. The things that can be done now are rigidly restricted by the thrust and the large cost of the boosters that are available. As the proficiency and knowledge in space grow, we will want to do more and more.

Dyna-Soar is one of the steps toward that future. The Air Force believes that the Dyna-Soar development can now be begun with ample confidence. It is our intention to design, build, and fly a full-scale test system as quickly as the detailed problems can be solved.





DYNA-SOAR PROGRAM STATUS

By Col. W. L. Moore, USAF Wright Air Development Division

This conference has thus far been devoted to the presentation of results of generalized research in a broad field of lifting, manned, hypervelocity, and reentry vehicles. For the rest of the conference, discussions will be focused on Dyna-Soar. This joint U. S. Air Force-NASA program is the embodiment of the general scientific knowledge available to date in terms of a specific system development effort. In order to set the stage for the ensuing presentation of the engineering foundation derived from the Dyna-Soar program, a brief review will be given of the overall program objectives, the Dyna-Soar system requirements, and the program status. As is well known, considerable scientific thinking and interest were generated in boost glide and lifting reentry by such projects as ROBO, BRASSBELL, BOMI, and HYWARDS. Many of the ideas and objectives of these programs were incorporated in the Dyna-Soar program, and in January 1958, a large section of industry was involved in preliminary proposals for doing the job. In July 1958, the competitive field was narrowed to two companies - Martin and Boeing. This phase I competition continued through an Air Force-NASA sourceselection evaluation which was completed in June 1959. For several reasons, the results of the source-selection activity were not made known until November 1959. Now, at this point the project itself will be discussed and subsequently further remarks as to its status will be made.

The fundamental objective of the Dyna-Soar program is to establish a technological basis for the development of future military weapon systems. The particular nature of these future systems is not presently fully known. Considerable research effort has already gone into the problem of space military application and will continue throughout the program. Dyna-Soar, as a military test system, will help crystallize the mission characteristics of these future weapon systems. These future systems operating in the hypersonic and orbital regimes should exploit the inherent potential of the atmosphere and the intrinsic capability of man used in an active role in the judgment and command loops. The desired technological basis, which is needed as a springboard to achieve future military capabilities, has placed certain specific requirements on the nature of the Dyna-Soar system, as follows:



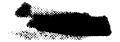
- (1) It must be piloted. The term "piloted" is used in opposition to "manned" to denote the active role that the operator would play in the operation of the system.
- (2) Dyna-Soar must be capable of a controlled landing. This requirement stems from operational considerations the necessity to return from orbit to touchdown on a routine basis.
- (3) The system must be capable of exploring a sufficiently large spectrum of hypersonic regimes in order to provide data which can be extrapolated for the design of future systems.
- (4) Dyna-Soar must be maneuverable not only for providing flexibility of operation but also as a corollary to its data acquisition capability.
- (5) Dyna-Soar must be able to test military equipment and the manmachine relationship.
 - (6) Dyna-Soar must achieve orbital capability.

The last-mentioned item is underlined to separate the requirements listed in items 1 to 5, which are illustrative of what can be done now in terms of available booster capability, from that of item 6, which will be done in the future when larger boosters become available.

The overall Dyna-Soar program can be viewed as consisting of three major steps:

- (1) Step I is the development and test of the glider in conjunction with a modified Titan ICBM. The test program in Step I would consist of, first, air drops at Edwards Air Force Base, then ground launches on the Atlantic Missile Range, unmanned initially, then manned.
- (2) During Step II, the same glider boosted by a larger booster would achieve global and orbital flight. At the end of Step II, an interim operational capability could be realized through the use of available equipment.
- (3) Step III is the development of a fully operational weapon system based on the technology derived from the Dyna-Soar program in view of existing military requirements.

As of November 1959, the configuration shown as figure 1 is the one planned for use in Dyna-Soar Step I. Shown is the Boeing glider with a lift-drag ratio L/D of about 2 mounted on the modified version of the SM-68 Titan booster. The modifications consisted primarily of the fins for stability and increased wall thickness to withstand increased bending moments caused by the glider.



The status of Dyna-Soar since November is shown in the following table:

PROGRAM STATUS

Program approved, November 1959

Contractors selected, November 1959 Boeing Martin

Further study directed by USAF Phase Alpha

Aero-Space vehicle panel briefed, December 2, 1959 Dyna-Soar program Proposed Phase Alpha study

Phase Alpha started, December 11, 1959

Aero-Space vehicle panel briefed, March 28, 1960

Report study results to ASAF, April 8, 1960

After the three-step program was approved by Headquarters, U. S. Air Force, source-selection results were announced. Based on the preliminary design competition between two teams of contractors, the Boeing Airplane Company was selected in November 1959 as the major contractor responsible for the glider and The Martin Company as the associate booster contractor. Then, in consonance with direction from Headquarters, USAF, a preliminary study phase, Phase Alpha of Step I, was initiated on December 11, 1959, and was completed on March 11, 1960. Note that the Aerospace Vehicle Panel of the Scientific Advisory Board was briefed concerning the Phase Alpha study before it began and then again at the end of March on the study results. The results of the study and a recommended program plan were presented to the Assistant Secretary for Research and Development April 8, 1960. The objectives of Phase Alpha are as follows:

- (1) To identify the technical problem areas associated with the development of Dyna-Soar.
- (2) To formulate a systematic plan of attack to cope with these problem areas.



(3) To define the developmental test program which would be required. Particular emphasis was placed on the areas of aerodynamics, structures, and materials.

In order to analyze these general problems in terms of required specifics, various system designs were studied with an assessment for each of the degree of technical risk involved, the nature of the developmental tests which would be required, the value of that design with respect to the program objectives, and the time and cost of such programs. On the basis of these various system design studies, the best system approach could then be selected in terms of a general configuration and an associated program plan. The scope of the effort comprising Phase Alpha is illustrated in the following list of the organizations that were involved:

1

Configuration studies by:				
Co	Air Force			
AVCO . Bell Boeing	Chance Vought Lockheed McDonnell	WADD/ASC		

Technical assistance from:
NASA General Electric
Goodyear

Booster	application	studies	by:
	Boeing BMD/STL Martin Aerojet		

Specific system design studies were completed by the contractors named in the first block, as well as by the Air Force. Technical assistance was provided by NASA in all of these endeavors and in certain specific areas by the two contractors named. Under the direction of the Air Force Ballistic Missile Division and Space Technology Laboratories, Boeing, Martin, and Aerojet have completed booster application studies.



7



Phase Alpha has resulted in the selection of a general configuration and the establishment of a preliminary program plan. The Air Force has selected a configuration having a medium L/D - that is, an L/D of 1.5 to 2.5 - and a wing loading of less than 30 pounds per square foot. The program plan as of this date is up for approval in the Pentagon.

The plan for the remainder of the Dyna-Soar presentation at this conference is as follows: Phase Alpha results will be presented by Boeing personnel, then Boeing, Air Force, and NASA personnel will discuss pertinent information on the Phase I design evolution. After this there will be an Air Force summation of the selected approach for Dyna-Soar and the program plan.

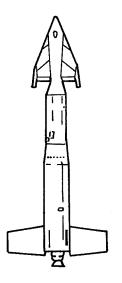
Before these discussions are begun, two points should be made clear:

- (1) The Dyna-Soar program is not intended to advance the state of the art in boosters; so most of the discussions will concern the glider.
- (2) Even though major contributions to Dyna-Soar have been made by others in industry Chance Vought, Martin, Bell, for example presentation sources have been restricted to the Air Force, NASA, and Boeing in deference to subcontractor competitions yet to come.





DYNA SOAR STEP I



WEIGHT 236,500 LBS

THRUST 300,000 LBS

Figure 1



INTRODUCTION TO BOEING PAPERS ON DYNA-SOAR PROJECT

By John H. Goldie Boeing Airplane Company

The preceding papers of this conference have been largely descriptions of research activities and results. The papers following the present paper will present discussions of the engineering applications of these data to specific problems of the Dyna-Soar. For example, the mission planned for Dyna-Soar is limited to earth-orbital flight or less. Therefore, data and trends presented in the paper by Thomas J. Wong, Glen Goodwin, and Robert Sly and in the paper by Frederick C. Grant do not apply directly to Dyna-Soar.

L

1

1

0

7

Papers by John F. Milton, G. E. Ledbetter, and Max T. Braun, which follow the present paper, will describe the results of Phase Alpha. One general question frequently asked about Phase Alpha is, "Why, of all possible reentry bodies, were only nine specific shapes chosen for detailed study?" Many additional concepts were examined at least briefly. It was believed vital that at least one configuration be examined in each of the four following prominent classes of reentry devices: modified ballistic, lifting bodies, winged bodies, and variablegeometry shapes. Within each of these classes, several shapes were considered to determine whether the results were common to all designs within that class. If so, the choice was rapidly narrowed. For example, two modified ballistic shapes were analyzed for several weeks to discover whether adding a variable-angle skirt or movable fins to a simple shape would provide better $(L/D)_{MAX}$ and lower weight than other ideas. When these shapes did not prove to be better, they were abandoned. lifting-body class, a shape similar to the Ames M-2a was examined and discarded for stability reasons. Two different structural concepts for the Ames M-2b were considered; one proved to be somewhat inferior and was dropped.

It was believed very desirable to have data on a spectrum of glider configurations having values of $(L/D)_{MAX}$ from 1 to 3 in order to determine the trends of weight and performance. Four different designs with low $(L/D)_{MAX}$ were investigated and the choice was narrowed to one. For variable-geometry configurations, a number of suggestions were eliminated with essentially no formal design work; an autogiro was one of these.



It would have been very desirable to carry all these configurations through complete design and evaluation rather than narrowing from 21 configurations to 9 as was actually done. The effective design period of Phase Alpha was only eight weeks and the funds were limited. Attempting even as many as nine preliminary design studies in parallel was considered risky, but all of these were carried to conclusion. The final design of each is believed to be feasible although varying amounts of development time and risks are required.

Completion of even limited preliminary designs of this many bodies needed a great deal of help from other highly competent industrial organizations. In some cases, the idea for the reentry device originated with one of these companies and all the subsequent design was done by them. In other cases, the company provided necessary technical data and consultation. In every instance, Boeing Airplane Company supervised the work and must accept full responsibility for the final designs to be submitted at this conference.

Ι

In order to enable rational comparisons between such different reentry techniques, a common set of ground rules, requirements, and objectives for Phase Alpha only was established. The significant requirements are shown in table I.

Piloted means the maximum use of the man to reduce subsystem complexity. A single crew member is used to reduce weight and cost. One thousand pounds of research-equipment payload does not include weight of structure, auxiliary power, and cooling to support the 1,000 pounds of payload. If those were included, the total would exceed 2,000 pounds. The 75-cubic-foot volume, combined with the large payload weight, allows flight tests of almost any military or scientific subsystem desired. "Once-around" operating capability means that the design shall be capable of Step IIA orbital operation although Step I reaches only about 19,000 ft/sec.

"Safe" boost means the boost trajectory shall not penetrate the recovery ceiling. The recovery ceiling is that altitude-velocity condition at $\gamma=0$, from which the unpowered vehicle can just pull back into equilibrium glide without exceeding its temperature or load limits.

The requirement for landing within 10 square miles was established to avoid continued expensive marine recovery operations. This area was chosen to permit the use of military airports; thus trees and hills would not interfere with parachute landings. Consistent subsystems (and also consistent ground-support equipment) were used where logical to prevent differences in vehicle weight resulting only from different levels of refinement in subsystem design. Reusability for four flights (with refurbishment) was a contractual requirement.



The requirement for at least neutral static stability during first-stage boost and reentry was established to provide better safety. During second-stage boost, the divergence rate is low enough to allow reasonable escape. Escape provisions were not required, but a requirement for safety approaching 100 percent led the designers to use escape systems. Ballistic reentry devices generally needed escape only during first-stage boost. The 6,000-foot margin above the critical heating limit requires that the vehicle not approach its structural limit too closely. This statement is only applicable for gliders; a similar rule was used for ballistic shapes.

Certain other ground rules have been used both prior to and during Phase Alpha. These include structural factors of 1.4 on booster tanks and 1.5 on the remaining structure and a conservative heating assumption which requires the structure to withstand heating rates for either laminar, turbulent, or transition flow, whichever is worst.

None of the preceding ground rules are considered firm for the remainder of the Dyna-Soar program. Certain of these are being reevaluated now; the requirement for neutral static stability throughout the entire first-stage boost may be changed to require stability only at first-stage burnout. This will permit a coast period between stages one and two.

Certain items which were used as ground rules during earlier design efforts were abandoned as ground rules during Phase Alpha but were maintained as dependent variables, and the designs were compared with respect to these variables. Examples of these include the amount of lateral maneuverability, ability to land conventionally, ability to gather research data, and potential for eventual military use.

Certain terms have been used in this paper which need additional clarification. Figure 1 shows a typical variation of altitude h with velocity v for a glider. This plot can be used to define some of the less familiar terms of this paper and of subsequent papers.

The equilibrium glide lines for $C_{L,MAX}$ and $(L/D)_{MAX}$ are shown in figure 1. These lines bound the normal flight regime. Flight at a C_L less than that for $(L/D)_{MAX}$ is possible but not desirable. When the glider is banked to approximately 45° and flown at the C_L for $(L/D)_{MAX}$, the largest lateral range is attained. The glider seeks an equilibrium line at a somewhat lower altitude due to the bank angle.

The temperature limit line shown in the figure is actually a composite limit for either the nose, leading edge, or bottom surface



depending upon the angle of attack. The q limit represents a dynamic pressure of 500 lb/sq ft during reentry. At this pressure the elevon surface actuator is load-limited. Under certain flight conditions, a load factor of 7.33 is limiting instead.

The distance shown as the flight corridor is a measure of the research ability of the glider. The 6,000-foot margin has been previously mentioned and is graphically described on the figure. The recovery ceiling is shown only in its approximate location. A glider inserted without power at that ceiling has insufficient velocity to maintain equilibrium flight at that altitude and hence falls. By pulling maximum lift, the aircraft can just barely arrest the fall before encountering the temperature or structural limit.

L

1

In conclusion, the technical effort during and prior to Phase Alpha has formed a solid foundation for the remainder of the Dyna-Soar program.



TABLE I GROUND RULES

- PILOTED (ONE CREWMAN)
- LOOO-POUNDS RESEARCH EQUIPMENT
- 75 CUBIC FEET VOLUME FOR EQUIPMENT
- ONCE-AROUND OPERATING CAPABILITY
- "SAFE" BOOST
- LAND WITHIN 10 SQUARE MILES
- CONSISTENT SUBSYSTEMS
- REUSABLE FOR FOUR FLIGHTS
- AT LEAST NEUTRAL STABILITY
- ESCAPE PROVISIONS
- 6,000-FOOT MARGIN WITH CRITICAL HEATING



h

TYPICAL REENTRY CORRIDOR

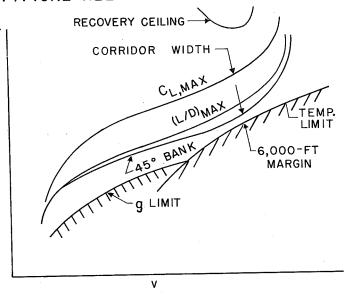


Figure 1

L 1

1

0

8

REVIEW OF DYNA-SOAR REENTRY-VEHICLE-CONFIGURATION STUDIES

By John F. Milton Boeing Airplane Company

SUMMARY

All known types of reentry vehicles were investigated to determine the structural and aerodynamic characteristics of each when designed to conform to standardized design criteria and ground rules. Preliminary analyses were performed on twenty-one shapes which were subsequently reduced to nine configurations for a more definitive evaluation. From this number a single reentry system was selected as meeting the objectives of the Dyna-Soar military test system.

INTRODUCTION

The reentry vehicles studied during the Phase Alpha program are divided into four categories. These are as follows:

- (1) The modified ballistic shapes which are characterized by $\mbox{L/D}$ values below 0.5.
- (2) The lifting-body shapes which are characterized by L/D values from 0.5 to 1.5 and wing loadings from 40 to 120 lb/sq ft.
- (3) The winged gliders which are characterized by L/D values from 1.5 to 3.0 and wing loadings between 20 and 30 lb/sq ft.
- (4) Variable-geometry gliders which are characterized by intermediate L/D values and wing loadings below 15 lb/sq ft. These devices change their external configuration between boost and reentry to take advantage of low planform area during boost to reduce the booster stability and structural penalties, and high wing areas during reentry are utilized to reduce the wing loading and temperatures.

The booster-reentry vehicle Step I performance and the growth capabilities during Step IIA are presented. Reentry trajectories are discussed with potential altitude-velocity exploration corridors available





for each vehicle. The maneuver capability available during reentry, the structural concepts utilized, and summary weight statements are presented for each of the configurations.

The configurations studied with some of their pertinent characteristics are presented in table I. In this table, the companies contributing technical assistance are indicated in parentheses after each configuration. The wing loading of each of these vehicles as a function of L/D is shown in figure 1.

Low L/D vehicles utilize the entire vehicle for escape and rely on large rockets for "off the pad" emergencies. The variable-geometry and glider vehicles utilize the forward portion of the body as a separate escape capsule. The modified ballistic vehicles and the M-l lifting body rely on parachute recovery due to the low subsonic L/D characteristics. The other configurations have suitable tangential landing capabilities.

 \mathbf{L}

1

1

0

Because the temperatures on the vehicle vary in severity due to differences in reentry trajectories and wing loading, the heat protection systems discussed include both ablation and reradiating systems. The M-2b lifting body, the gliders, and the variable-geometry vehicles rely primarily on radiation and passive water cooling. The high L/D glider utilizes active water cooling on the nose cap and a water-glycol system (on the pressurized compartments). The M-1 lifting body utilizes an ablation system over an aluminum load-bearing shell. The drag brake has an ablation shield at the stagnation point but relies on radiation on the extended umbrella-like structure. Weight statements are provided for each configuration.

BALLISTIC REENTRY DEVICES

Modulated Drag Brake

The modulated-drag-brake reentry device shown in figure 2 achieves variable drag by means of a foldable umbrella-like structure surrounding a payload capsule. This reentry-device configuration was developed by the Everett Division of AVCO. This configuration was not developed to meet the ground rules established in the Phase Alpha study, but rather the available designs and data were adapted to satisfy the payload and manning design criteria. This configuration enjoys advantages in weight and simplicity; however, if the design were modified to meet all the Phase Alpha criteria, these advantages would be decreased.



TABLE I SUMMARY OF REENTRY VEHICLE CHARACTERISTICS

Caudi munti on	(L/D) _{HYPERSONIC}	(L/D) _{SUBSONIC}	Maneuve	r capability ^a	Altitude corridor,	Boost weight,	Step I,f
Configuration	HYPERSONIC	(2/3/SUBSONIC	Lateral (b)	Longitudinal (c)	ft (d)	lb (e)	V _{BO} , fps
Drag-brake device (AVCO)	0	0	. 0	0	0	5,260	22,350
Modified Mercury (McDonnell)	-	Not presented					
M-1 lifting body (Boeing)	•5	.8	±140	1,000	60,000	7,275	21,600
M-2b lifting body (Boeing - General Electric)	1.3	3.5	±895	1,980	22,000	9,391	19,700
Lów L/D glider (Chance Vought)	1.5	4.2	±1,180	3,150	51,000	8,590	19,200
Intermediate L/D glider (Boeing)	2.2	4.5	±2,150	4,500	51,000	9,719	^g 19,638
High L/D glider (Bell Aircraft)	3.0	4.0	±3,500	6,900	67,000	11,291	17,050
Inflatable-wing glider (Boeing - Goodyear)	1.7	4.5	±1,400	2,950	37,000	11,069	19,150
Folding-wing glider (Lockheed)	2.0	4.4	±1,700	8,300	27,000	8,298	19,300

All maneuvers are initiated at a relative velocity of 23,000 fps.

bLateral maneuver is in nautical miles from the orbital path.

 $^{^{\}mathrm{c}}$ Longitudinal maneuver is difference in nautical miles between maximum and minimum range.

 $d_{Minimum}$ altitude corridor between $C_{L,max}$ and structural limit except for drag-brake device and M-1 lifting body (see text). e^{-1} Weight at second-stage jettison (Step IIA, one-orbit mission).

fModified Titan booster.

gSecond-iteration data.

During boost the drag brake is folded around the pilot and equipment compartment. The upper section of the vehicle consists of abort rockets and fairings. After a successful first-stage boost, these items are jettisoned. During orbit the drag brake remains closed and vehicle attitude is controlled by reaction jets.

The drag brake is modulated to achieve reentry at a preselected altitude, position, and velocity. At the reentry point, defined by the magnitude of the deceleration, the drag brake is locked in the fully opened position. Modulation to a deceleration of 0.1g results in a longitudinal dispersion of ±150 miles and a lateral dispersion of ±18 miles from the preselected landing point. Modulation to a deceleration of 1.5g will reduce the longitudinal dispersion distances to ±18 miles. Lateral-range control is not possible during reentry.

The open drag brake serves in lieu of a parachute for landing. An alighting gear in the form of 24 metal bellows is inflated to limit ground impact decelerations. Impact occurs at a velocity of 55 fps.

Escape from the booster is accomplished by firing the escape rockets mounted on the nose fairing assembly. When a safe altitude is reached, the fairing and rockets are jettisoned and the drag brake is opened for descent to the ground. Escape from orbit is accomplished by fully opening the drag brake.

The drag-brake device is currently designed for one reentry trajectory. Although some altitude variation could be achieved by varying drag, the current device is designed for complete deployment of the brake during reentry.

The booster considered for the Step I nonorbital program (fig. 3) is a modified version of the standard Titan booster. The modifications required are a 13-percent increase in tank wall stiffening and the addition of 238 square feet of stabilizing fin area. This combination of reentry device and booster results in a burnout velocity of 22,350 fps and a range of 1,775 nautical miles. The Step IIA orbital booster can orbit this vehicle with a potential growth in weight of 111 percent.

The maximum design temperatures are 1,710° F on the stagnation plate and 1,425° F on the side of the brake. The drag brake is a foldable umbrella-like structure. The outside skin of the drag brake is composed of a flexible woven mesh of 0.0015-inch-diameter René 41 wire, 200 to the inch. A coating of glass frits, held in a silicone rubber base, is applied to the skin in order to achieve nonporosity. Twenty-four ribs, spaced at 15° intervals, support the wire-mesh skin. These ribs consist of two side-by-side trusses which are joined at the top by common chord members and separated at the bottom to form an included angle of approximately 29°. Crossmembers between the bottom chords





complete the truss assembly. The truss members are tubular and fabricated from Udimet 500 alloy. The actuator struts react the major portion of the rib loading and are essentially compression members. They also serve to position the ribs during drag modulation through their attachment to the actuator mechanism. These struts are circular in cross section with essentially a frame-stringer type of construction. The material used is Udimet 500.

The pressurized body structure contains a 75-cubic-foot pilot's compartment pressurized to 10 lb/sq in. and a 100-cubic-foot equipment section pressurized to 6 lb/sq in. These two compartments are integrally attached by seam welding to a main structural cone. This structural cone carries the compartment inertial loads and the reaction loads of the drag brake, the actuator, and the booster transition section. A 103-inch-diameter stagnation plate, covered with Teflon, forms the bottom of the body structure. The entire body is covered with a 2-inch layer of Thermoflex insulation. Entrance to the pilot's compartment is provided by a 20-inch-diameter hatch located on the compartment side wall. Access to the equipment compartment is provided by a 4-foot-diameter hatch located in the center of the compartment floor.

A summary weight statement for the drag-brake device is as follows for a one-orbit mission:

	Weigl	ht, lb
Reentry vehicle (boost) at launch		5,260
Reentry vehicle at second-stage jettison		4,140
Airframe	•	1,789
Landing gear		200
Secondary power	•	208
Flight controls		88
Electronics		298
Environmental control		208
Crew operations		349
Payload		1,000
Tay Load 1 1 1 1 1 1 1 1 1 1 1 1 1 1 1 1 1 1 1		,
Reentry vehicle (reentry)	•	4,123
Reentry vehicle (landing)		4,084



Modified Mercury

A modified ballistic reentry vehicle similar to the Project Mercury capsule was also considered. For proprietary reasons, it will not be presented herein.

LIFTING-BODY CONFIGURATIONS

M-l Lifting Body

L

l

0

The M-l lifting-body reentry device, shown in figure 4, is a blunted cone shape that is 8 feet long with a 12-foot base diameter and a 30° half-apex angle. This vehicle enjoys weight and cost advantages, a capability for growth to superorbital missions with minimum modifications, and a wide range of reentry trajectories. The upper surface is flattened to obtain a hypersonic lift-drag ratio of 0.5. Control is provided by reaction control jets and four low-aspect-ratio electrically actuated control flaps hinged near the cone base perimeter. Rear vision is provided the pilot through the use of a single mirror system. The conditioned equipment and payload compartment extends from the pilot's compartment to the interior structural shell. The 75-cubic-foot payload bay is located to the right of the pilot's compartment.

The M-l configuration includes a parachute recovery system since the subsonic L/D of approximately 0.8 is too low for a conventional landing. Drogue parachutes are deployed at an altitude of 80,000 feet and the main parachutes, at 14,000 feet. In order to insure landing within the required 10-square-mile area, terminal guidance is required during approach to the landing site to correct for wind conditions prior to deploying the drogue parachute. Both radio and inertial guidance systems are used for terminal guidance during reentry and landing to provide continuous, accurate terminal guidance. Vehicle control during reentry and approach to the landing site may be either automatic or manual.

Maneuver capability of the M-l device during reentry can provide a lateral-range deviation from the orbital path of 140 nautical miles when maneuver is initiated at 23,000 fps.

The normal reentry exploration corridor for the M-l configuration is considered to lie within the trajectory for $C_{L,max}$, $\emptyset = 0^{\circ}$, and a ballistic trajectory ($C_{L} = 0$) which imposes limiting decelerations on the pilot (reentry angle of -2.5°). The corridor is approximately 60,000 feet in the hypersonic region and 30,000 feet in the lower supersonic region.

Weight 1h



The booster for the Step I suborbital program is a standard Titan booster (fig. 5) modified to provide stability and to carry the loads imposed by the presence of the reentry device. An 18-percent increase in tank wall stiffening and an additional 12^{14} square feet of fin area increase the booster weight by 1,111 pounds. This modified Titan booster is capable of attaining a burnout velocity of 21,600 fps with the M-l reentry vehicle. A 400,000-pound-thrust Titan-Centaur booster can provide orbital velocity with a potential growth in allowable weight of 52 percent.

The basic structural concept for the M-l vehicle utilizes a cool, semimonocoque aluminum pressurized structure which is protected from high external flight temperatures by a polyethylene ablation cover. The ablation-cooled structural approach is used because it is more efficient for the short reentry times and high heating rates which are typical of a low L/D reentry trajectory. The ablation material is polyethylene which ablates at 375° F and has good insulation properties. The ablation thickness is based on a structural skin design temperature of 120° F.

The M-l structure consists of a pressurized load-carrying aluminum external shell which is reinforced with frames, bulkheads, and longerons. The frames are spaced at 8 inches and are used with the skin to withstand internal pressure loads. In addition, they provide longeron column stabilization and serve as panel shear stiffeners to the skin. Bulkheads are used to separate the various pressurized compartments. Four longerons resist fuselage bending loads and distribute booster, parachute, escape rocket, and landing loads to the external shell. The pilot's environmental compartment is an aluminum-frame structure, attached to the four longerons. Access to the pilot's compartment is provided by an inward opening hatch. Access to the equipment and payload compartments is provided by panels in the vehicle's top surface and in the aft bulkhead.

The weights of the M-l device for a one-orbit mission are summarized as follows:

																						W	<u>- 18</u>	كلت وكلتك
Reentry vehicle at	ЪС	os	t	bı	ırı	101	ıt	•																7,275
Airframe	•	•	•	•		•	•	•	•	•	•	•	•	•	•		•	•	•	•	•	•	•	2,720
Landing gear																								
Propulsion																								
Secondary power																								
Flight controls																								
Electronics																								
Environmental co	ntr	ol		•	•	•	٠	•	•	•	•	•	•	•	•	•	•	•	•	•	•	•	•	527





· · · · · · · · · · · · · · · · · · ·	weign	C, LD
Crew operations		
Reentry vehicle (reentry)	. 6	5,509
Reentry vehicle (landing)	. 5	5, 453

M-2b Lifting Body

The M-2b lifting-body configuration shown in figure 6 is a blunted conical lifting-body shape consisting of a 13° half-apex cone angle and a flat upper surface. This configuration has conventional landing capabilities, a low weight relative to the glider systems, and requires less booster modification than the systems with a large planform. The afterbody surfaces are boattailed to minimize the base drag for subsonic flight and to achieve trim with a noseup angle of attack. The vehicle is sized to keep the weight as low as possible and retain the center of gravity in an appropriate location. Technical assistance in the development of this vehicle was received from the Missiles and Space Vehicle Division of the General Electric Company. Ames wind-tunnel data shows a hypersonic L/D of 1.3 and a subsonic L/D of 3.5 for the M-2b configuration. This high subsonic L/D allows the M-2b lifting body to make a conventional landing with a minimum touchdown speed of 187 knots.

Normal landing is accomplished by touchdown on aft skids using a mechanical energy-absorbing system. The forward gear consists of an air-charged oleo and dual wheels which are stored in a pressurized and cooled compartment during flight. Direct pilot vision is provided as an aid in landing and for observation during the other phases of flight. The forebody section separates for pilot escape during the various phases of the flight. The escape capsule is recovered by parachute and utilizes crushable structure on the bottom of the capsule for energy absorption. The payload compartment is located in the pressurized aft section of the vehicle. Expendables are located in the extreme rear in individual pressurized containers. This arrangement allows the pilot to separate himself from the payload, auxiliary power unit (APU), expendables, and control surfaces in the event of an emergency condition.

Maneuver capability of the M-2b device during reentry can provide a lateral-range variation of 895 nautical miles from the orbital path and a longitudinal-range variation of 1,980 nautical miles, when maneuver is initiated at 23,000 fps.





The normal reentry exploration corridor for the M-2b configuration lies between the trajectories for $C_{L,max}$, $\phi = 0^{\circ}$ and $(L/D)_{max}$, $\phi = 45^{\circ}$. The corridor is approximately 22,000 feet in the hypersonic region and 60,000 feet in the lower subsonic region.

The standard Titan booster for the Step I suborbital program (fig. 7) is modified to increase tank stiffening and add 253 square feet of fin area, with a total weight change of 2,103 pounds. This booster can attain a burnout velocity of 19,700 fps and a range of 2,440 nautical miles. A 400,000-pound-thrust Titan-Centaur booster provides orbital velocity with a potential growth in allowable weight of 14 percent.

Various structural concepts were investigated for the M-2b vehicle. A reradiation heat-protection system was considered most suitable because of the high heating rates which are experienced for long periods of time. Nose equilibrium temperatures are 3,900° F. The bottom surface varies from 2,700° F immediately aft of the nose cone to 2,000° F on the lower surface behind the escape capsule. The leading edges of the fins and control surfaces reach temperatures above 2,280° F.

A concept was investigated in which the reradiative heat-protection shield also carried the primary air loads. Coated niobium alloy was proposed as the primary structural material, because of the low oxidation rate of niobium as compared with coated molybdenum alloys. This hot load-carrying structural concept provides a lighter weight vehicle. However, the materials, processes, and fabrication techniques involved with refractory alloys will require considerable development before sufficient confidence could be established to permit its use on a manned vehicle.

The insulated and cooled structural concept which has been chosen for the M-2b vehicle consists of a hot, nonstructural outer shell, made of refractory materials, insulation, and passive water walls, which protects the inner aluminum load-carrying structure. Greater confidence exists in the structural integrity of this concept since aluminum is used for primary load-carrying structure.

A Chance Vought developed "Zirod" design is used to withstand the 3,900° F temperature experienced on the nose of the vehicle. In the areas on the vehicle where the temperature is between 2,000° F and 3,400° F, combinations of zirconium oxide foam, molybdenum, fibrous alumina insulation, and a water wall are used. For areas with temperatures below 2,000° F, René 41 sheet is used for the external surface, backed up by a René 41 corrugated sheet, MIN-E-2000 insulation, and a water wall. The thickness of the structure is sized for a maximum temperature limit of 120° F on the internal aluminum structure.



The internal load-carrying structure consists of an aluminum shell, supported by conventional aluminum frames, bulkheads, longerons, and shear beams. Pressurized compartments, formed by the load-carrying skin, bulkheads, and shear beams, are used for the pilot and the equipment. Access to these areas is provided by access doors or panels. Structural continuity for body axial and bending loads is provided by the four longerons which also distribute the boost loads. Explosive attachments are provided for separation of the escape capsule from the vehicle. Shear continuity between the escape capsule and the vehicle is provided at the separation bulkhead by the use of fore-and-aft shear pins.

Aluminum frames, attached to the load-carrying structural shell, distribute the shear loads throughout the vehicle. These frames are also designed to minimize structural deformation under the outer insulation shell.

L 1

1

O

A M-2b summary weight statement for a one-orbit mission is as follows:

																				We	eig	ht, lb
Reentry vehicle at																						
Airframe		•	•	•	•	•	•	•	•	•	•	•	٠.		•	•	•	•	•	•		3,440
Landing gear																						270
Propulsion				•	•	•	٠	•	•	•	•	•	•	•		•	•	٠		•		
Secondary power		•	•		•	•		•	•	•		•	•	•	•	•	•	•	•	•	•	1,049
Flight controls		•	•	•		•	•		•		•	•	•	•	•	•		٠	•		•	230
Electronics .																						786
Environmental co																						1,661
Crew operations			•	•		٠		•	•	•	•	•	•	•	•	•	•	•	•	•	•	610
Payload		•	•	•	•	•	•	•		•	٠	•	•	•	•	•	•	•		•		1,000
Reentry vehicle (reentry	•)	•	•	٠	•	٠	•	•	•	•	•	٠	٠	•		•	9	9	٠.	•	9,196
Reentry vehicle (Landing	:)	•	•	•	9	•			•		9				•	•		9	•		8,169

GLIDER CONFIGURATIONS

Low L/D Glider

The low L/D glider model is shown in figure 8. The purpose of this design was to explore the relatively more compact arrangement obtainable with lower L/D shapes. This glider has an $(L/D)_{max}$ of 1.5 at Mach 20, and an $(L/D)_{max}$ of 4.25 at landing which provides





conventional landing capability and good research-data-gathering ability. This configuration was developed by Chance Vought Aircraft, Inc., Astronautics Division. The glider has a wing loading of 29.1 lb/sq ft at a weight of 8,590 pounds.

The complete glider consists of two major sections. The forward section is the escape capsule, which may be separated at any point in the flight path and return to earth as a stable unit. The capsule contains the pilot, his controls, environmental protection, and necessary survival equipment. Forward and side vision are provided the pilot to assist in observation and landing. The forward window is shielded during reentry and exposed when required for landing. The cockpit is protected from aerodynamic heating effects by a cooled and insulated structure. The capsule is aerodynamically similar to the glider and provides escape from all portions of the flight regime. The maximum temperatures during escape are no more severe than during normal reentry. A separation rocket is provided for ground-level escape from the booster. The aft portion of the glider body is a pressurized and conditioned compartment containing all glider equipment, except that which functionally must be forward or that which the pilot needs during escape.

The equipment compartment has usable volume of 490 cubic feet. This large volume provides for the 75 cubic feet of payload, the necessary subsystems, and space for a crawl-way. The equipment is arranged with the basic electronics, guidance, pressurization, and cooling equipment on the left side of the compartment and the payload, secondary-power equipment, and fuel on the right side.

Conventional unpowered landing approach capability is considered to be good because of the high subsonic L/D and low wing loading which reduce equilibrium sink rates and approach speeds.

Maneuver capability during reentry when initiated at 23,000 fps allows a lateral-range variation of 1,180 nautical miles from the orbital path and a longitudinal-range variation of 3,150 nautical miles.

The minimum normal exploration corridor between the trajectories for $C_{L,max}$ and the lower flight limit is 51,000 feet at 21,000 fps. This lower limit, determined by structural temperature limits, is 6,000 feet below the trajectory for $(L/D)_{max}$ with $\emptyset = 45^{\circ}$.

The Titan booster (fig. 9), modified to include 1,700 pounds for tank stiffening and 2,520 pounds for stabilizing fins, will provide the reentry device with a burnout velocity of 19,200 fps and a range of 2,500 nautical miles during the suborbital program. Orbital velocity can be obtained with a 400,000-pound-thrust Titan-Centaur booster. The potential growth capability with this booster is 8 percent of glider launch weight.



Structurally, the glider has a pressurized body with a water-cooled basic structure, and radiation-cooled wing, wing leading edge, and nose cap. The basic body is an ellipsoidal-shaped semimonocoque structure of 15-7 stainless-steel alloy. Open-faced honeycomb forms a retainer for the water-wick heat sink. An 0.008-gage, 15-7 stainless-steel vapor barrier separates the water wall and insulation.

Fiberfrax insulation is used for all applications up to 2,000° F and fibrous alumina, where temperatures exceed 2,000° F. An exterior shield is attached to the pressure wall by segmented channel frames. This shield is a 0.012-gage, 0.5-percent titanium-molybdenum in areas where the temperature exceeds 2,000° F and a 0.012-gage, René 41 nickelbase alloy in all other areas.

The nose cap is made up of zirconium oxide rods retained by a siliconized graphite spherical shell. This cap is attached to a 0.5-percent titanium-molybdenum skirt. Siliconized graphite tiles are applied to the exterior surfaces where the temperature exceeds 2,700° F.

The wing structure consists of a radiation-cooled truss structure with a covering of light-gage skin. Upper skins are 0.012-gage, René 41 with channel stiffeners spotwelded to the skin. The lower skins are built up of a 0.012-gage, 0.5-percent titanium-molybdenum outer shield with Fiberfrax or fibrous alumina insulation and René 41 corrugations.

Wing leading edges are 0.05-gage, 0.5-percent titanium-molybdenum alloy with fusion-welded ribs. The leading edges are segmented and supported from a René 41 beam. Fibrous alumina insulation protects the beam from the hot leading-edge surface.

A summary weight statement for the low L/D glider for a one-orbit mission is as follows:

																			We	eig	ht, lb
Reentry vehicle at boost	; bı	ırı	101	ıt	•	9	•	•	9			9	•	•					•	٠	8,590
Airframe	٠	•	•	۰	•			•	•			•		۰	•	•		۰	9	٠	3 , 255
Landing gear				•	•	•	•		9	•	•	•	•		•	9.		•	•		270
Propulsion			•	•		٠				•			•	•		•	•	•		•	230
Secondary power				۰		٠		•		•	•		•	•	•		•			•	1,062
Flight controls				•					٠	•		•	•	٠		•	9	•	a		332
Electronics			•	•	۰		•	•			•		•	•	•	۰	•	•	•	•	786
Environmental control	•	•		•	•	•		•	•	•			•	•	•	•		•		•	1,125
Crew operations				•	٠	9	٠	•		9	•			٠	•			•	•	•	530
Payload	•	٠	•	•	•	•	•	•	•	•	•	•	۰	•	•	•		•	۰	•	1,000
Reentry vehicle (reentry	7)	9	•	•		•				٠		•	•		•	9	0	9	٠	0	8,346
Reentry vehicle (landing	g)		٠		•	•						•		•	•	•	•		•	•	8,023



Intermediate L/D Glider

The intermediate L/D glider is shown in figure 10. This glider has been configurated with the objective of developing a design with a hypersonic L/D around 2 and a wing loading commensurate with reentry temperature limits. The configuration shown has a hypersonic L/D of 2.2 and a subsonic L/D of 4.5 with a wing loading of 28.7 lb/sq ft. This reentry device offers the advantages of moderate design temperatures and booster modifications, conventional landing capability, and a very good research potential.

The complete glider consists of two major sections. The forward section, which serves as the escape capsule, includes the pilot's compartment and all his emergency equipment. This section may be separated from the aft portion of the glider at any point in the flight path and returned to earth as a stable unit. The aft section of the glider contains all equipment except that required in the forward portion (escape capsule) for functional or emergency reasons.

The lateral-range control of the intermediate L/D glider, starting from a relative velocity of 23,000 fps, is 2,150 nautical miles. From the orbital flight path the minimum longitudinal range occurs at $C_{L,max}$ and is 3,100 nautical miles. The maximum longitudinal range at $(L/D)_{max}$ is 7,600 nautical miles.

Due to slightly lower landing approach speed and a higher L/D during landing approach the intermediate glider should be superior to the X-15 research airplane in landing capability. Landing runout distances are acceptable since the nominal touchdown speed is 150 knots.

The flight envelope for the intermediate L/D glider is limited by structural capabilities which are established by the temperature capability of the structure. The normal exploration corridor between $C_{L,max}$ and the minimum flight limit has a minimum value of 51,000 feet at a velocity of 21,500 fps.

The Titan booster for the suborbital program (fig. 11) will require modification to accommodate the intermediate glider. This modification includes the addition of 613 square feet of stabilizing fins and stiffening of the tank structure with a total added weight of 4,469 pounds. This modified booster will provide the intermediate glider with a relative burnout velocity of 19,638 fps and a longitudinal range of 4,500 nautical miles. Preliminary studies of the Titan-Centaur booster for the orbital program indicated the need for an 8-percent weight reduction on the glider; however, improvements in transition weights and the



use of storable propellants in the Titan stage will allow the attainment of orbital velocities with a potential growth in glider weight of 5 percent.

The glider structure utilizes Rene 41 radiation-cooled determinate trusswork with a covering of thin-gage corrugation-stiffened skins.

Controlled-environment compartments are provided for the pilot, glider equipment, and payload. These compartments are supported from the basic trusswork in a manner designed to minimize thermally induced stresses.

L

1

0

8

Weight, lb

The pilot's compartment is constructed of 15-7 stainless-steel alloy, brazed honeycomb with a water-wall passive heat sink. This compartment is fusion-welded at all joints except the entry hatch and windows.

The equipment and payload container is a large cylindrical "can" supported between the two main fore-and-aft trusses. It is constructed of 2014 aluminum and insulated with Refrasil or comparable silica fiber insulation. A thin-foil Hastelloy "X" cover is added on the exterior of the insulation for containment and radiation shielding.

The nose cap is a Chance Vought developed "Zirod" design using zirconium oxide rods retained in a graphite spherical shell. This cap is attached to an insulated René 41 truss structure. Skins on the lower surface and sides just aft of the cap are insulated panels of 0.5-percent titanium-molybdenum shield and René 41 or HS-25 corrugations.

The leading edge is constructed of 0.5-percent titanium-molybdenum segments supported from a René 41 corrugated web support beam. This beam attaches to the wing spar trusses and is discontinuous at the joints to prevent interaction due to differential thermal expansion.

The skin panels on the lower surface are subjected to temperatures in excess of 2,000° F. These panels are constructed of an outer shield of 0.5-percent titanium-molybdenum, fibrous alumina insulation, a Hastelloy "X" screen retainer, and René 41 load-carrying corrugations.

A summary weight statement for the intermediate L/D glider for a one-orbit mission is as follows:

•																			· · · / -
Reentry vehicle at	boost	burnout	•	•	•			•					•				•	•	9,719
Airframe					•		٠	•			•	•		•					4,321
Landing gear			•			•	•	•	•	•	•		٠	•	٠			•	270
Propulsion					•	•	•	•		•	•	•	•	•	•	•		•	230





Weight, 1b . . . 1,104

Secondary power		1,104
Flight controls		293
Electronics		786
Environmental control	•	1,185
Crew operations	٠.	530
Payload	•	1,000
Reentry vehicle (reentry)	•	9,455
Reentry vehicle (landing)	•	9,063

High L/D Glider

The basic design objective for the glider shown in figure 12 was to provide a high hypersonic L/D design with a wing loading sufficiently low to maintain acceptable reentry temperatures. The $(L/D)_{max}$ is 3.0 at Mach 20 and is 4.0 at landing speed. The glider has a wing loading of 26.1 lb/sq ft at a reentry weight of 10,570 pounds. This configuration was developed by the Bell Aircraft Corporation. This configuration has the advantages of relatively lower temperature, excellent lateral-maneuver capability, and excellent potential for gathering research data.

The complete glider consists of two major sections. The forward section is the escape capsule, which may be separated at any point in the flight path and can be returned to earth as a stable unit. The entire basic structure is cooled to a maximum temperature of 250° F by a system that circulates a solution of water and glycol.

The capsule contains the pilot, his controls and environmental protection, and necessary survival equipment. Side vision is provided during the entire flight. A forward window is protected by a fairing until after reentry when it is necessary for landing. It is aerodynamically similar to the glider and provides escape from all portions of the flight regime. The maximum temperatures during escape are no more severe than during normal reentry. A separation rocket is provided for ground level escape from a burning or exploding booster. The aft portion of the glider body is a pressurized and conditioned compartment containing all glider equipment except that which functionally must be forward or that which the pilot needs during escape.

Due to the high subsonic L/D and low wing loading, this reentry vehicle has very good landing characteristics with a lower sink rate and approach speed than the X-15 research airplane. This reentry vehicle



has excellent lateral maneuver capability and range control since these characteristics are primarily affected by the hypersonic L/D. This vehicle has a lateral capability of 3,500 nautical miles from the orbital path and longitudinal-range control from a minimum of 4,500 nautical miles to 11,400 nautical miles when maneuver is initiated at a relative velocity of 23,000 fps.

The normal exploration corridor for this vehicle, between the ${\rm C_{L,max}}$ trajectory and the lower flight limit, which is determined by dynamic pressure and temperature limitation, has a minimum of 67,000 feet at 21,000 fps.

The standard Titan (fig. 13) for the Step I suborbital program will provide a burnout velocity of 17,050 fps and a 3,780-nautical-mile range. The modifications required include 2,120 pounds of tank stiffening and 5,090 pounds of fin (889 square feet). The 400,000-pound-thrust Titan-Centaur booster was considered for the once-around orbital mission; however, the vehicle weight would have to be decreased by 34 percent to achieve this capability with this booster.

Structurally, the glider embodies the concept of a pressurized body with the basic structure cooled by a circulated water-glycol system. The wing leading edges are radiation cooled. The glider primary load-carrying structure is conventional, semimonocoque aluminum insulated from the aerodynamic heat. The insulation is contained by outer shell panels of refractory or super alloys. These outer panels are small with gaps between panels for accommodation of differential thermal expansion. Where temperatures exceed 2,000° F, a corrugation-stiffened 0.012-gage, 0.5-percent titanium-molybdenum outer panel is used. Where temperatures are 2,000° F or less, the panel is made of brazed HS-25 honeycomb with 0.0035-gage face skins and 0.002-gage core. Between the outer shell and the aluminum primary structure is a layer of alumina powder insulation contained in foil wrappers. This foil is Inconel 702 where the outer panel is HS-25 and platinum where the outer panel is molybdenum.

The nose cone utilizes a water-spray cooling system to maintain the HS-25 machined nose cap at temperatures below 1,600° F. Steam generated as the water cools the nose cap is bled overboard at the edge of the cap. The HS-25 trusses with a covering of 0.012-gage, 0.5-percent molybdenum skin are used to attach the nose cap to the cooled aluminum fuselage.

The leading edges are heat-sustaining siliconized graphite segments supported by molybdenum channels to the cooled aluminum wing structure. A small panel of corrugation-stiffened 0.040 molybdenum is used on the lower surface just aft of the graphite segments.



The control surfaces are radiation-cooled, semimonocoque structures using Inconel corrugated skin panels and spanwise beams. The lower surface is protected by a 0.012-gage corrugation-stiffened 0.5-percent titanium-molybdenum outer skin with alumina powder insulation.

A summary weight statement for the high L/D glider for a one-orbit mission is as follows:

	Weight, 1b
Reentry vehicle at boost burnout	
Airframe	. 5,318
Landing gear	. 338
Propulsion	. 508
Secondary power	
Flight controls	. 494
Electronics	. 751
Environmental control	. 1,332
Crew operations	. 569
Payload	. 1,000
Reentry vehicle (reentry)	. 10,570
Reentry vehicle (landing)	. 10,153

VARIABLE-GEOMETRY CONFIGURATIONS

Inflatable Reentry Device

The inflatable vehicle is a manned, variable-geometry device with orbital flight capabilities. In the launch configuration, it is a pointed, cylindrical body with a deflated planform area of less than 300 square feet; prior to reentry it is inflated and assumes a delta planform of 1,800 square feet as shown in figure 14. The relatively small size during boost permits use of an ICBM booster with very little modifications. The large inflated wing area makes possible reentry at high altitudes where vehicle surface temperatures and heating rates are minimized.

The basic arrangement of the inflatable vehicle reentry configuration consists of a rigid metal crew compartment/escape capsule at the forward end, a rigid payload and equipment pod housed within the wing as far aft as possible, and an inflatable fabric structure developed by the Goodyear Aircraft Company connecting these extremities. The crew compartment/escape capsule contains only equipment required during



escape, and displays and equipment which are necessary during normal flight. Forward vision is provided during the landing phase by jettisoning the upper half of the nose cap, exposing a window. The escape capsule is of the ballistic type, employing a separation rocket, flaps, and parachutes during the escape sequence.

Contents of the aft pod include secondary power, most of the vehicle electronics, payload, compartment environmental control system, and a liquid-helium inflation system for the fabric structure. Only wire bundles (no fluids, gases, or wave guides) are led through the inflatable structure between the crew compartment and aft pod. A short, rigid section just aft of the crew compartment houses the vehicle's dual reaction control systems, normal O_2 - N_2 supply, certain electronics, and other items which are located in the forward section during normal flight but are left behind in event of escape. Surface-mounted hydraulic actuators are provided for rudders and elevons. Rigid-metal fairings protect these actuators.

The 5-lb/sq ft inflatable vehicle has good tangential landing capabilities. The performance is superior to the X-15 research airplane due to lower wing loading and a higher L/D on approach. Touchdown speed is 73 knots which allows a very short runout distance.

The maximum and minimum longitudinal ranges for the inflatable vehicle (wing loading of 5 lb/sq ft) are 5,850 and 2,900 nautical miles, respectively, and the lateral-range variation from the orbital flight path is 1,400 nautical miles when the maneuver is initiated at 23,000 fps.

The normal altitude exploration corridor between the $\rm C_{L,max}$ equilibrium trajectory and the lower flight limit for this vehicle is 37,000 feet at a relative velocity of 19,000 fps.

The Step I, suborbital Titan booster (fig. 15) modifications include 535 pounds of tank stiffening and 956 pounds of fins (242 square feet). This booster will provide the reentry device with a burnout velocity of 19,150 fps and a range of 2,830 nautical miles. A 400,000-pound-thrust Titan-Centaur booster will provide orbital velocity to this vehicle with a potential growth in weight of 120 pounds.

The aft pod is cantilevered off the booster upper stage, with the deflated fabric structure folded around and forward of it. A structural fairing surrounds the fabric, protecting it and providing the necessary structural connection between the glider nose section and the booster. The fairing is jettisoned just prior to the inflation sequence, which must be performed under low q conditions.





The crew compartment/escape capsule portion of the inflatable vehicle consists of an aluminum-honeycomb inner shell isolated from a high-temperature René 41 outer shell by Fiberfrax insulation. Thingage frames of appropriate materials stiffen these shells, and steel longerons support the aluminum structure. The outer shell is coated with a nickelous oxide ablation material of sufficient thickness to insure that the René skin never exceeds 2,000° F. The design surface temperature is below that required for ablation at all times during normal flight. The short, rigid section between the crew compartment and forward fabric area is nonpressurized and consists of René skin over a frame-type structure. Thin-skin water-wall construction with a 0.25-inch layer of Min-K insulation is used for the aft pod. Tracks are provided to facilitate pod installation and removal in the surrounding fabric structure. The fairings which house the control surface servoactuators are formed René 41 sheets.

The fabric used for inflatable portions of the vehicle is woven of René 41 wire. This material is coated with a silicone elastomer for pressure retention. Maximum allowable temperature is 1,600° F. However, a higher temperature capability is indicated for fabric structures with an inner coating of René 41 foil. The elastomeric coating hardens after exposure to temperatures above 1,000° F and may not be folded again to the small radii required for the launch configuration.

The fabric wing, fins, and control surfaces are constrained to their noncircular cross sections by "drop threads" which are closely spaced René wires which connect the upper and lower surfaces of the section. Neither tubular "backbone" nor the semicircular leading and trailing edges require drop threads.

The inflatable structure is pressurized so that a net compression load cannot exist at any point in the fabric. Shear load provisions include vertical "shear mats" within the wing and two high-pressure tubes located between the fabric backbone and wing upper surface. Gas flow must be modulated to maintain the correct pressure under the constantly varying ambient conditions encountered in flight.

The weights for the inflatable-wing glider for a one-orbit mission are summarized as follows:

				Weight, Ib
Reentry vehicle at	boost	burnout	 	 11,069
Airframe			 	 4 , 945
Landing gear			 	 210
Propulsion				
Secondary power			 	 1,284



														We	eie	ht, lb
Flight controls																
Electronics Environmental control .	:		•		•	•	:	:	:	•	:	:				1,189
Crew operations Inflation system																530
Payload																
Reentry vehicle (reentry)		•		•									•			9,860
Reentry vehicle (landing)	•	•	•	•					•				•			8,727

Folding-Wing Reentry Device

The folding-wing reentry device (fig. 16) is a low-wing-loading (13.4 lb/sq ft) glider capable of reentering the atmosphere from orbit. This configuration was developed by the Lockheed Aircraft Corporation. The low wing loading permits deceleration at high altitudes resulting in relatively low surface heating rates and temperatures. Low temperatures permit the use of presently known and available metals for practically the entire structure. The folding wings reduce the planform area of the vehicle on the booster to that of the intermediate L/D vehicle (330 square feet), yet provide 959 square feet of wing area when extended. The pilot flies the folding-wing glider from a ballistic crew compartment/escape capsule which makes escape possible throughout the flight.

Dual hydrazine APU's generate electrical, hydraulic, and compartment blower power. Dual hydrazine reaction control systems maintain reentry-device attitude during orbit. A separate hydrazine-fueled reaction control system controls the attitude of the escape capsule during emergency reentry. After second-stage burnout, a rocket is used to separate the vehicle from the interstate structure.

The folding wing is a thick slab approximately 4 feet thick. Nose and wing leading-edge radii are 18 inches. The wings fold forward over the top for boost. A ballistic crew compartment/escape capsule is nested in a recess near the nose of the vehicle. Fairings are added ahead of and behind the capsule.

The folding-wing vehicle has good tangential landing capability. At $(L/D)_{max} = 4.4$, the start flare speed is 145 knots and the sink rate is 53 fps.

When maneuver is started at 23,000 fps, this vehicle provides a lateral-range variation of 1,700 nautical miles from the orbital flight path and a potential longitudinal-range variation of 8,300 nautical miles. The normal exploration corridor lies between $C_{\rm L,max}$ and the lower structural limit. The minimum corridor of 27,000 feet occurs at a 20,000-fps velocity.

Modifications on the standard Titan (fig. 17) include the addition of 1,737 pounds of tank stiffening and 3,275 pounds of fins (627 square feet). The burnout velocity achieved with the Step I suborbital booster is 19,300 fps, with a range of 3,485 nautical miles.

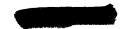
The Titan-Centaur booster can provide orbital velocities with a potential growth capability of 8 percent of the gross weight.

The basic material for vehicle skin and structure is René 41 sheet. Spot and seam welding are the principal fastening methods. The body is built around four fore-and-aft trusses consisting of U-shaped caps and box section verticals and diagonals. Gussets are used at the joints. Across the longitudinal trusses run main frames and subframes. The main frames are trusses built in the same manner as the longitudinal frames. The subframes are U-shaped members next to the skin. The material from which these members are fabricated is 0.006 to 0.040 gage. Lower-surface skin panels consist of a smooth 0.004-gage outer sheet with 0.003-gage corrugations. Corrugations without an outer skin are exposed on the upper surfaces.

A heat shield is provided which covers the vehicle nose and forward 16 feet of the undersurface. The shield consists of 0.012 molybdenum separated from the René 41 skin by a thin layer of Fiberfrax insulation. The maximum surface temperature in the protected region is 2,700° F. The maximum temperature of the aft areas, where René 41 is used, is $2,000^{\circ}$ F.

The crew compartment/escape capsule structure consists of inner and outer shells separated by insulation. Four stainless-steel longerons plus aluminum Z-frames and skin form the inner pressure shell.

A combination of pin and floating connections at the ends of the longerons supports the inner shell in the high-temperature outer structure. The outer shell is a René 41 skin on Z-frames. Refrasil and Fiberglas insulation reduce heat flow into the capsule. The nose section includes a crushable honeycomb structure to absorb landing impact. A single-point capsule release system is used for maximum reliability.



A weight summary for the folding-wing glider for a one-orbit mission is as follows:

															We	eig	ht, lb
Reentry vehicle at boost burn																	
Airframe																	2,973 340
Landing gear Propulsion																	200
Secondary power																	
Flight controls																	424
Electronics																	786
Environmental control																	985
Crew operations																	530
Payload		•	•	•	•	• •	•	٠	•	•	•	•	•	٠	•	•	1,000
Reentry vehicle (reentry) .	• .•	•	•	•	•		•	•	•	•	•	•	•	•	•	•	7,952
Reentry vehicle (landing) .				•	•												7,715

Ι

CONCLUSION

It is concluded that all the vehicles studied are feasible and capable of achieving reentry from orbital flight. Some of the vehicles represent longer development time and others do not accomplish the Dyna-Soar test mission. The evaluations of the vehicles are presented in a subsequent paper by Max T. Braun entitled "Summary Comparison of Dyna-Soar Reentry Devices."

REENTRY DEVICE CONFIGURATION SPECTRUM

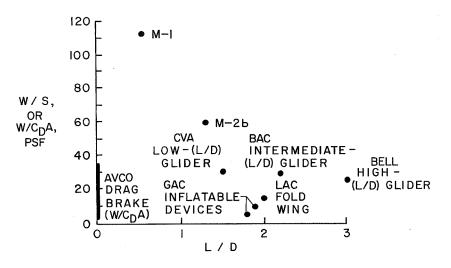


Figure 1

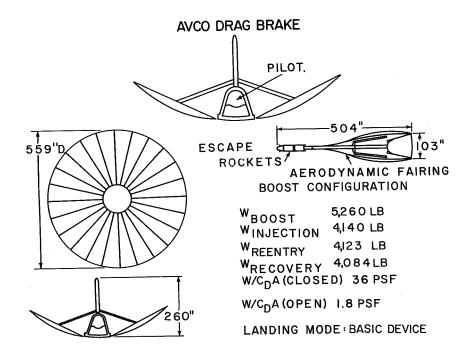


Figure 2





VEHICLE ARRANGEMENT

AVCO DRAG-BRAKE

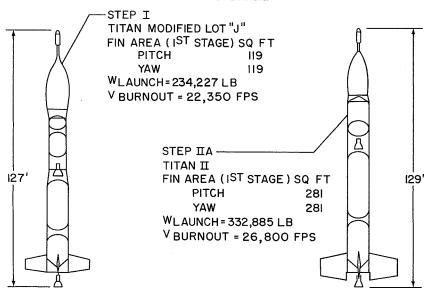


Figure 3

LIFTING BODY, M-I

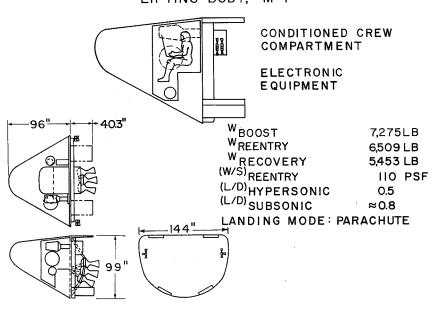


Figure 4





VEHICLE ARRANGEMENT M-I LIFTING BODY

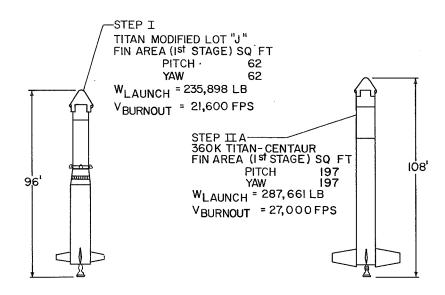


Figure 5

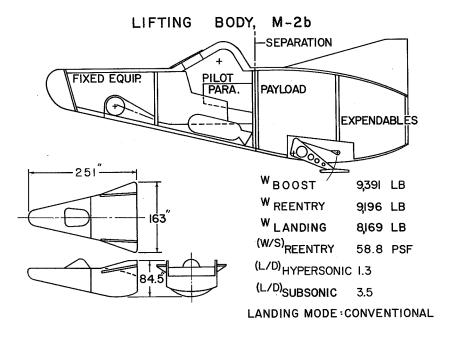


Figure 6





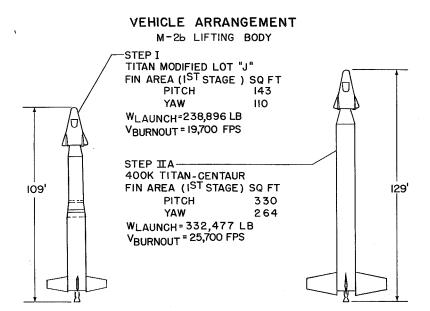


Figure 7

CVA GLIDER, LOW L/D

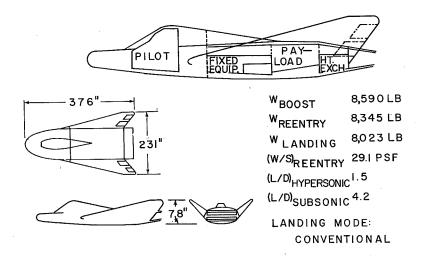


Figure 8





VEHICLE ARRANGEMENT

CVA GLIDER, LOW L/D

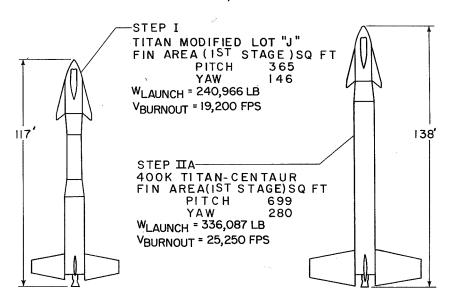


Figure 9

BAC GLIDER, INTERMEDIATE L/D

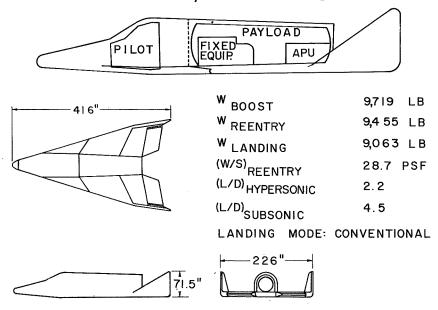


Figure 10





VEHICLE ARRANGEMENT BAC GLIDER, INTERMEDIATE L/D

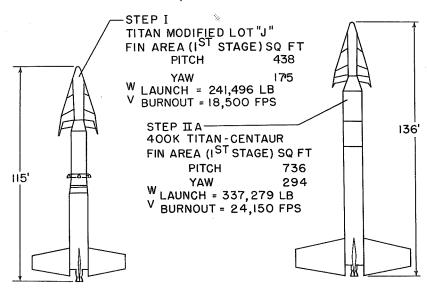


Figure 11

BELL GLIDER, HIGH L/D

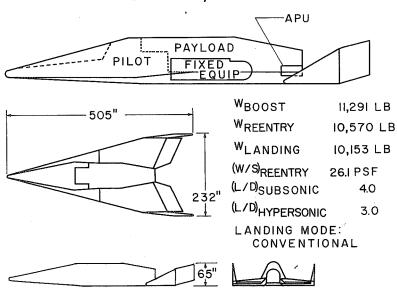


Figure 12





VEHICLE ARRANGEMENT BELL GLIDER, HIGH L/D

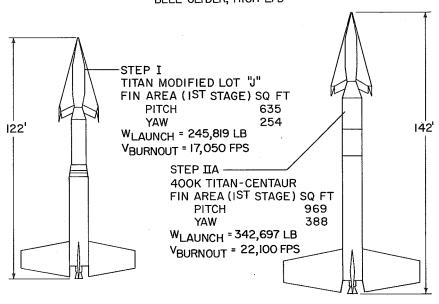


Figure 13

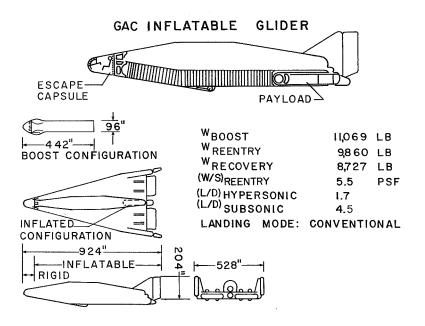


Figure 14





VEHICLE ARRANGEMENT GAC INFLATABLE

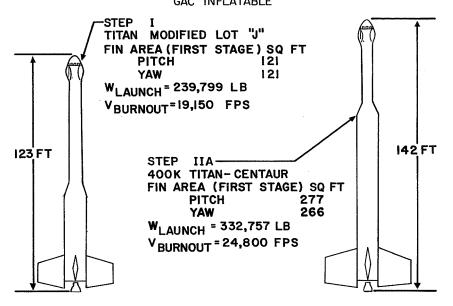


Figure 15

LAC FOLD-WING GLIDER ESCAPE CAPSULE ELEVON PAYLOAD COMPARTMENT W_{BOOST} 8298 LB WREENTRY 7,952 LB WLANDING **BOOST CONFIGURATION** 7,715 LB (W/S)REENTRY 13.4 PSF (L/D)_{HYPERSONIC} 2.0 (L/D) SUBSONIC 336" LANDING MODE: CONVENTIONAL 600" 96"

Figure 16





VEHICLE ARRANGEMENT LAC FOLD WING

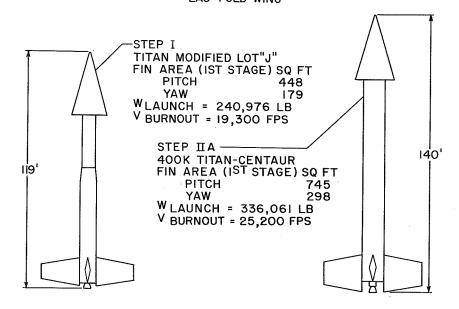


Figure 17

Page intentionally left blank

5



ASSESSING CAPABILITY OF MODIFIED TITAN ICBM BOOSTERS

FOR DYNA-SOAR TYPE VEHICLES

By G. E. Ledbetter Boeing Airplane Company

SUMMARY

This Dyna-Soar Phase Alpha booster study has shown that the Titan ICBM, when modified to the Dyna-Soar booster mission ground rules, can be used for a Step I booster for any of the reentry devices examined. It cannot place any of these devices in orbit for Step I. The changes required to the ICBM for Dyna-Soar Step I are approximately the same regardless of the reentry device selected; for example, fins are required for all devices, as are structural modifications. The differences involved are not basic but are only differences in degree to which the given change must be made.

For Step IIA, this study has also indicated that the Titan II is not useful except for very small or lightweight reentry devices. For larger devices a "maximum growth" version of the Titan-Centaur will probably be required.

TNTRODUCTTON

Phase Alpha of Dyna-Soar Step I was a systematic evaluation of a wide variety of reentry devices for selection of the best configurational approach to the Dyna-Soar program. Extensive studies were made of the Titan and Atlas boosters to determine the effects of reentry device and mission requirements on booster modifications and performance. Since the Titan has been selected to be the Dyna-Soar Step I booster, this paper contains results of studies of the Titan, Titan II, and Titan-Centaur boosters.

REENTRY DEVICES TO BE BOOSTED

The Dyna-Soar reentry devices studied during Phase Alpha are shown in figure 1. The variety in shape of the boosted configurations is





apparent. During boost the reentry device is mounted on a conical transition section atop the booster. The lifting characteristics of the device are the predominant factor in determining booster modifications. "Wing area" varies from 58.5 square feet for the M-l lifting body to 405 square feet for the glider with a lift-drag ratio L/D of 3.0, as shown in table 1. Boosted weight, including the weight of the transition cone of the device, ranges from 5,380 pounds for the drag brake to 12,250 pounds for the L/D = 3.0 glider.

TABLE 1.- REENTRY-DEVICE WING AREA AND BOOSTED WEIGHT

Device	Wing area ^a ,	Boosted	weight, 1b
Device	sq ft	Step I	Step IIA
Drag brake M-1 lifting body M-2b lifting body L/D = 1.5 glider L/D = 2.2 glider L/D = 3.0 glider Folding wing Inflatable	219 58.5 155 284 330 405 330 298	b5,380 7,410 9,700 9,370 9,960 11,230 8,590 10,930	b5,550 7,820 10,000 9,590 10,440 12,250 9,000 11,360

^aWing area of the device is the plan area of the view shown in figure 1. The drag brake, M-l lifting body, and inflatable devices are nearly symmetrical. All other devices have side areas which are substantially different from plan areas.

Each of these devices jettisons approximately 1,100 pounds at booster first-stage burnout.

BOOSTER STUDIES

Several of the Dyna-Soar booster mission requirements are substantially different from those applied in the Titan ICBM design.

Step I of the Dyna-Soar program requires the use of a modified standard Titan ICBM booster to place a minimum-size manned reentry device in or near its equilibrium glide corridor for subsequent exploration of as large a portion of the hypersonic reentry regime as practicable. Burnout altitude for insertion of the reentry device into its equilibrium glide corridor varies, as a function of boost burnout velocity and lifting characteristics of the device, between 220,000 feet and 300,000 feet for most of the shapes. A zero (or horizontal) flight-path angle is required at burnout.



Step IIA will use a larger booster to place the manned reentry device into orbital flight. A once-around orbit is a minimum requirement. The orbital mission for a lifting device starts at an altitude of approximately 300,000 feet with a zero flight-path angle at a burnout velocity (relative for eastward launch) in excess of 24,500 feet per second.

Several additional rules were established to improve safety during boost:

1. Fins are required on all boosters studied to make the booster and reentry-device assembly have at least neutral aerodynamic stability during the first-stage boost.

L

1

1

0 9

- 2. The booster flight control system is designed to accept pilot control inputs both directly and superimposed on automatic commands. The pilot will also have a manual means of thrust termination.
- 3. The minimum factor of safety on limit loads for the booster basic structure for manned flight will be 1.40. The flight factor may be reduced to 1.25 for unmanned flights to allow more severe environmental tests.
- 4. The reentry device shall never be boosted to any condition from which it cannot safely recover. The boost trajectory must not pass through the reentry-device recovery ceiling either in normal operation or as the result of premature thrust termination.

The Phase Alpha booster studies were for the most part conducted concurrently with the design studies of the various reentry devices shown in figure 1. As a result of this study procedure it was necessary to conduct the booster studies on a parametric basis which involved making numerous assumptions regarding the reentry-device characteristics and total vehicle configurations. First, a nine-point matrix of reentrydevice weights (6,000, 9,000, and 12,000 pounds) and wing areas (40, 250, and 500 square feet) were established. The smaller wing-area devices were assumed to be ballistic shapes, whereas the larger wing-area devices were assigned lift and drag characteristics as a function of wing loading. It was then necessary to assume typical center-ofpressure and center-of-gravity locations and to assume a configuration and weight for the transition section between the reentry device and the booster. A standard lift-curve slope of 0.03 per degree was used for all reentry devices throughout the parametric study. A limit angle of attack of 50 was used at maximum dynamic pressure for structural sizing of the boosters.

For performance calculations, appropriate drag characteristics were assumed for each reentry device. The vehicle was launched from



Cape Canaveral at an azimuth angle of 110°. The thrust-weight ratio at launch was generally maintained above 1.25 to avoid drift problems.

Typical boosters studied for Phase Alpha are shown in figure 2. The Titan ICBM is shown only for comparison, with the Lot J type having been used as a technical reference point. The modified Titan for Step I and the three larger Step IIA Titan boosters are shown for the midpoint of the parametric weight-area study matrix.

Characteristics of these typical boosters are shown in table 2. The Step I modified Titan represents the minimum changes required to the ICBM for performance of the Dyna-Soar Step I mission.

L

1

0

9

For Step IIA orbital capability, the Titan II and two different versions of the Titan-Centaur were studied. Primary interest for Step IIA was centered around the 400,000-pound-thrust Titan-Centaur. The Titan first stage used for this combination was increased in size to allow the addition of 105,000 pounds of IO2/RP-1 propellant, and the two ICBM engines are uprated to 200,000 pounds of thrust. The second stage CENTAUR B uses optimum propellant loading for the combination and has two 20,000-pound-thrust (Pratt and Whitney) RL10B-2 IO2/hydrogen engines. Since the growth of the first stage of the larger Titan in terms of both size and engine thrust, was considered to be near the growth limits of the 10-foot-diameter Titan, a smaller version was also investigated for orbital capability. This 360,000-pound-thrust Titan first stage had 66,000 pounds of propellant added to the ICBM first-stage capacity and used engines uprated to 180,000 pounds of thrust.

Fin sizes required to provide static stability during first-stage boost are shown in figure 3. Note that fins are required even for the smallest size reentry device, since all the boosters are inherently unstable without fins. These fin sizes are determined by assuming a normal-force-curve slope of 0.03 per degree for the reentry device and 0.06 per degree for the fins. Body lift and aeroelastic effects were included. The curves of figure 3 show only pitch-fin area required. In addition, yaw fins were required, which were the same size as the pitch fins for symmetrical ballistic reentry devices. The various glider reentry devices required yaw fins whose area was only 40 percent of the pitch-fin area. The fins used in all cases had a taper ratio of 2 with an unswept 50-percent-chord line.

Booster-structural-weight increases were computed for a given reentry device by using a limit angle of attack of 5° at maximum dynamic pressure to establish body bending loads. The weights required for such structural modifications were combined with the fin and fin-attachment weights to produce the total structural-weight increase for the Titan



and Titan-Centaur as shown in figure 4. The reference weights shown are basic dry-structure weights of each booster before modification. Note that for the Titan a boosted 9,000-pound device with a wing area of 400 square feet requires doubling the basic structural weight. The Titan-Centaur curve is for the 400,000-pound-thrust Titan first stage previously described. Nonlinearity of these curves is due primarily to the predominance of axial loads for small reentry-device wing areas, whereas bending loads predominate for the larger lifting shapes.

A typical Step I boost trajectory is shown in figure 5. The recovery ceiling, dynamic-pressure q limit, and temperature limit are indicated for an intermediate L/D glider reentry device. The initial phase of the trajectory is a vertical boost to 200 feet per second followed by a gravity turn through first-stage burnout. After first-stage separation, a gravity turn is continued to a relative velocity of approximately 14,000 feet per second at an altitude of 260,000 feet, at which time a constant angle-of-attack pitch program of 12° is initiated and maintained until just prior to second-stage burnout. This pitch program, with the angle of attack held constant for approximately 40 seconds, is required to produce a zero burnout angle in the proper glide corridor.

L

1

1

9

The staging operation for separation of the first stage from the second-stage—reentry-device combination was varied somewhat, depending on the booster. Initial staging concepts for the Titan booster included a 20-second coast period between the first-stage burnout and separation. Such a Step I coast was used throughout the parametric studies. However, results of feasibility studies of the "fire-in-the-hole" technique indicated that the second-stage engines could be ignited and brought up to a 70-percent nominal thrust prior to separation. This technique then allowed staging at considerably higher dynamic pressures than were originally considered feasible, so that Step I staging could be accomplished without coast following first-stage burnout. The Step I performance trade shown in figure 6 indicates a burnout velocity $\rm V_{B.O.}$ increase of approximately 150 feet per second if no staging coast is required.

A staging refinement study was not conducted for the Titan-Centaur. All Step IIA data include a 10-second coast between first-stage burnout and Centaur separation. For Step IIA this coast occurred at a higher altitude than for Step I, and the dynamic pressure at Centaur separation was in all cases less than 10 pounds per square foot.





BOOSTER PERFORMANCE SUMMARY

The booster parametric-performance summary for Step I is shown in figure 7. Step I boosted weights and equivalent wing areas for each of the eight reentry devices considered are also shown. These reentry-device points have been corrected in terms of equivalent wing area to account for actual physical characteristics of the reentry device in such a fashion that the burnout velocities read from figure 7 for each device are truly comparative. The Step I burnout-velocity—weight trades are as follows:

$$\frac{\Delta V_{\text{B.O.}}}{\Delta W_1} = -0.10$$

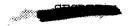
$$\frac{\Delta V_{B.O.}}{\Delta W_{2}} = -0.59$$

where V_{B.O.} is the burnout velocity and W₁ and W₂ are the weights of stages 1 and 2, respectively. Although figure 7 represents comparative Step I performance data from the parametric booster study, it does not necessarily represent the ultimate Step I performance achievable for any specific booster—reentry-device combination. For example, a design refinement conducted for the intermediate L/D glider—Titan-booster combination indicated that a burnout-velocity improvement of approximately 1,000 feet per second over the parametric-data value might be achieved through improved transition and fin design and with careful trajectory optimization for such a specific vehicle combination.

Step IIA orbital capability of the various Titan boosters is shown in approximate form in figure 8. It was assumed for this comparison that a relative burnout velocity of 24,600 feet per second would be required at an altitude of 300,000 feet to produce a once-around orbital mission. These data indicate that the Titan II will be adequate for Dyna-Soar Step IIA only for very light, small reentry devices. The 400,000-pound-thrust Titan-Centaur, on the other hand, will be adequate for a large number of the reentry devices studied.

The Step IIA booster-performance trades are as follows:

$$\frac{\Delta V_{\text{B.O.}}}{\Delta W_{1}} = -0.15$$





$$\frac{\Delta V_{B.O.}}{\Delta W_2} = -0.82$$

Again, it should be noted that these parametric data are somewhat conservative in terms of orbital capabilities shown herein. A design refinement which results in an increase in thrown weight on the order of 1,000 pounds would make the Titan-Centaur adequate for Step IIA for all the reentry devices except the high L/D glider. Such a capability increase can probably be achieved through (a) use of a Titan II storable first stage with increased propellant loading, (b) optimization of fins, structure, and transition section, and (c) reduction of the fin requirements.

During the final portion of the Phase Alpha studies, primary interest in the reentry devices centered about several intermediate L/D glider configurations. A study refinement was conducted for one such device on a Titan(storable 400,000-pound thrust)-Centaur booster as shown in figure 9. Fins were reduced in area below that required for stability throughout the first-stage boost, but they were maintained large enough to provide a 5° angle-of-attack control authority within the first-stage engine gimbal limits $\left(4\frac{1}{2}\right)$ and to provide static stability at first-stage burnout. Burnout velocity, with the glider shown, was increased to 24,800 feet per second (relative). Further growth capability may be achieved through additional uprating of the first-stage engine thrust.





TABLE 2.- TYPICAL BOOSTER CHARACTERISTICS

Booster	Launch weight, kilopounds	Propellant	Usable propellant, lb	Thrust, kilopounds	I _{sp} ,
Titan Lot J ICBM Stage 1 (sea level)		10 ₂ /RP-1	164,240	300	249
Stage 2 (vacuum)	227.3	LO ₂ /RP-1	41,250	80	307
Titan modified, Step I Stage 1 (sea level)	270.0	lo ₂ /rp-1	164,240	300	249
Stage 2 (vacuum)	239.2	LO ₂ /RP-l	47,270	80	307
Titan II, Step IIA Stage 1 (sea level)	335. ⁴	N ₂ O ₄ /50% UDMH - N ₂ H ₄	244,810	400	253
Stage 2 (vacuum)	777.4	N ₂ O ₄ /50% UDMH - N ₂ H ₄	61,030	80	310
Titan-Centaur, Step IIA 360K stage 1 (sea level)		lo ₂ /rp-1	230,000	360	253
Stage 2 (vacuum)	290.1	LO ₂ /LH ₂	31,250	40	418
Titan-Centaur, Step IIA 400K Stage 1 (sea level)		lo ₂ /rp-l	269,170	400	254
Stage 2 (vacuum)	331.9	го ⁵ /гн ⁵	31,250	40	418

Ó

44



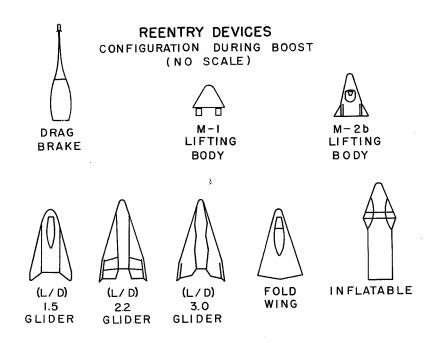
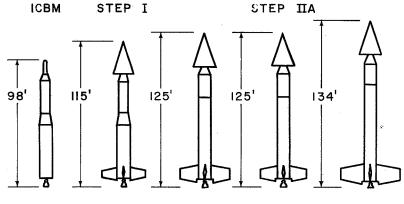


Figure 1

TYPICAL BOOSTERS STUDIED

REENTRY-DEVICE WING AREA = 250 SQ FT REENTRY-DEVICE WEIGHT = 9,000 LB



360K 400 K 227,300 LB 239,200 LB 335,400 LB 290,100 LB 331,900 LB TITAN LOT"J" TITAN MOD. TITAN II TITAN-CENTAUR

Figure 2





FIN SIZE REQUIRED 9,000-LB REENTRY DEVICE

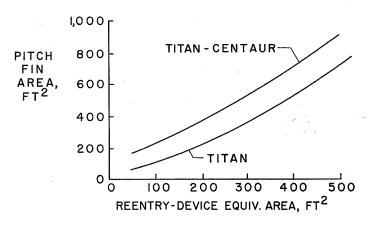


Figure 3

STRUCTURAL-WEIGHT ADDITIONS 9,000-LB REENTRY DEVICE

STRUCTURAL-WEIGHT INCREASE INCLUDING FINS, LB

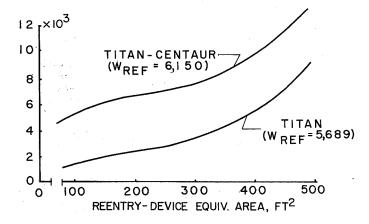


Figure 4





TYPICAL STEP I BOOST TRAJECTORY

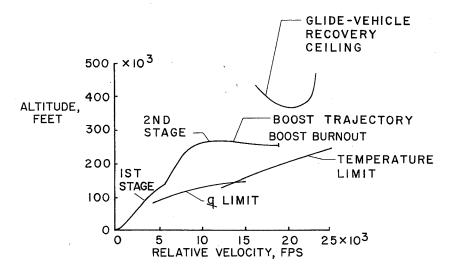


Figure 5

STAGING DURING BOOST

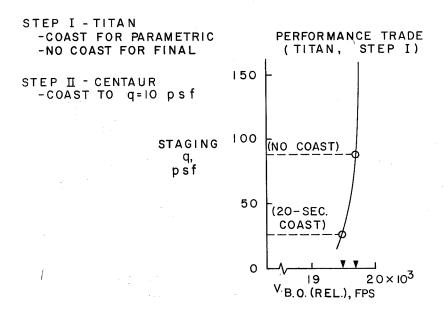


Figure 6





STEP I PERFORMANCE SUMMARY TITAN LOT "J" MOD.

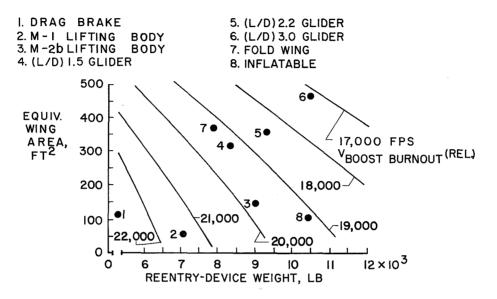


Figure 7

STEP IIA PERFORMANCE SUMMARY

ORBITAL CAPABILITY COMPARISON (VBOOST BURNOUT = 24,600 FPS RELATIVE AT 300,000 FT ALTITUDE)

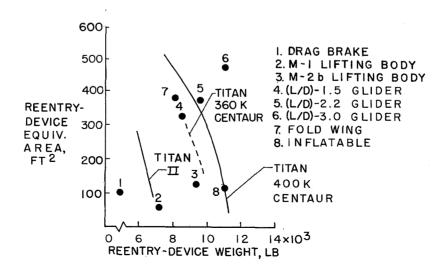


Figure 8





STEP IIA BOOSTER REFINEMENT TITAN (400 K-STORABLE) CENTAUR

INTERMEDIATE L/D GLIDER REENTRY DEVICE

VBOOST BURNOUT (REL.) = 24,800 FPS

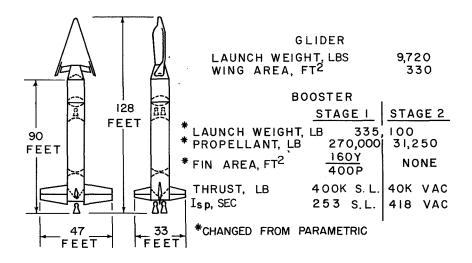


Figure 9

Page intentionally left blank

SUMMARY COMPARISON OF DYNA-SOAR REENTRY DEVICES

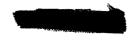
By Max T. Braun Boeing Airplane Company

A significant part of Dyna-Soar Phase Alpha studies was the preliminary design, to consistent ground rules, of broadly selected configurations on which research on the problem of controlled, manned
reentry could be conducted. After the preliminary investigation of
21 configurations, 9 devices, shown in figure 1 along with the name
of the principal contributor, were selected for detailed investigation. Technical details of these devices are presented in other
papers at this conference. It is significant that these devices, with
the exception of the drag brake, were designed for a common set of ground
rules shown in table I. Hence, for the first time, these devices can be
compared directly. The scope of the nine devices covers the broad range
of parameters shown in table II. The wing-loading range from approximately 5 to 110 lb/sq ft and a range of hypersonic lift-drag ratios
from 0 to 3.0 were studied. For proprietary reasons, the parameters
and technical data for the Modified Mercury will not be presented.

One of the first areas of comparison is the weights of these devices. This comparison is shown in table III. Since a variety of structural concepts and heat-protection systems are used on the devices, it is appropriate to compare the sum of the structure and environmental-control weights rather than just the structure weight.

Arriving at the optimum system to accomplish a specific mission or objective is an evaluation process with emphasis on cost. When evaluation of the merits of the nine devices for the Dyna-Soar mission was formulated, it became apparent that there are four separate elements involved in the evaluation of these systems. These parts are not addable or combinable by any method other than considered judgment. The four parts are: technical confidence, value of technical results, development phasing, and costs.

The following portions of the paper include Boeing Airplane Company ratings in technical evaluation of the devices. Table IV presents the rank of the devices in technical confidence in aerodynamic technology required to accomplish successfully the program objectives. These ratings reflect predesign development-program timing to bring the devices to similar confidence levels. The aerodynamic rating is based on flight control, performance, and heating.



First in aerodynamic confidence rating is the drag brake. The flight-control problems are not severe because of its pure ballistic shape. The heating technology for this blunt shape is well known, and the ability to predict the performance is very high. It has a possible problem because the cloth which covers the umbrella-like drag device sags. The only heating problem is the sagging and heating of the partially open device.

Next in aerodynamic confidence are the M-1, 2.2 $\frac{L}{D}$ glider, and $3.0\frac{L}{D}$ glider. The M-1 has possible flight-control problems from its blunt, close-coupled shape which changes by ablation during the reentry process and possible center-of-gravity problems. The heating confidence is very high except around the control surfaces where stagnation areas occur. The performance-predicting ability is only slightly less than that for pure ballistic devices. The 2.2 $\frac{L}{D}$ glider has had extensive windtunnel testing up to the present time. There are some problems in the flight-control area, but these are not serious. The heating of this device is fairly well understood, except in certain detail areas. The ability to predict performance is not rated as high as that of the pure ballistic devices or as high as that of the M-1, but it is still relatively high. The 3.0^{L}_{n} glider has also had extensive development time and is rated the same as the 2.2 $\frac{L}{\overline{D}}$ glider. The 1.5 $\frac{L}{\overline{D}}$ glider ranks next. It has had some subsonic testing; however, there are some possible hypersonic problems because the shape of this device has not been tested as yet. Very little is known about this glider in the flight-control area.

L

1

1

1

0

The fold-wing device ranks next. There are unknown flight-control answers of this device, particularly in the subsonic directional-stability and subsonic pitchup problems. Heating confidence for this glider is relatively high, ranking only slightly less than that for the $2.2\frac{L}{D}$ and $3.0\frac{L}{D}$ gliders. Performance-prediction ability is the same as for the other glider devices.

Next in rank is the M-2b. The flight-control problems would be better than those of the M-1 except that this device has a landing problem as well. It has the least confidence of any of the systems in heating, particularly around the tip controls. The performance-predicting confidence is the same as that for any glider.

Last in ranking is the inflatable device. The problems of the flexible system and reaction control problems are reflected in low flight-control-system confidence. Also, new systems are required to make the flight-control system work. The heating problem is not very





different from that of the $2.2\frac{L}{D}$ glider except for possible sagging problems. The ability to predict the performance of this device ranks the same as any glider.

The structures confidence of these devices ranks the M-l structure as having the highest confidence. Possible problems are the hot control areas and long time ablators.

The gliders all rank approximately the same. They all employ refractory metals in one form or another, just to different degrees. The order of ranking is close with the $2.2\frac{L}{D}$ glider, $1.5\frac{L}{D}$ glider, fold wing, M-2b, and $3.0\frac{L}{D}$ glider in that order. There is a drop in confidence in the fold wing, however, due to the fact that its weights are considered optimistic. The fold-wing device employs extremely thin gages of nickel-base alloys, and more work would have to be done to ensure that this is a reliable structure. The basis for this ranking is the structural test programs, both successful and unsuccessful, which have been conducted to date during the Dyna-Soar study. The $3.0\frac{L}{D}$ glider employs a cooled nose cap which has not been tested to date. This is the main reason for its ranking lower in this rating.

The hot-fabric-covered devices are lowest on the scale, but the drag brake does not require air tightness to the same degree as the air inflatable device and, therefore, has higher confidence. Development of the wiremesh fabrics which are covered by a silicon compound with glass frits in it is not complete at this time. The confidence in the weight of the drag device is low, however, mainly because it does not satisfy the ground rules in the areas of landing sites and reusability. If this device is rated on its performance in other areas based on this weight, the confidence must be lowered.

Table V shows the rank of these devices in value of technical results for Dyna-Soar objectives. Many facets of comparison were examined to arrive at this rating. They are listed without detail. The devices were examined for ability to make lateral aerodynamic maneuvers, for ability to grow to superorbital reentry capability, for ability to make a conventional landing, rather than merely impacting intact, for ability to explore various corridors during reentry, for ability to obtain a wide variety of research data applicable to future military reentry systems, for ability to obtain research data not available from the extension of existing programs, for the ability of the pilot to make orbit corrections, for the ability of the pilot to assist in landing-site selections, for the ability of the pilot to assist in landing-site selections, for the ability of the pilot to aid in the emergency modes, for the ability of the devices to sustain orbit, for the ability of the devices to research military subsystems, for the ability of the devices

for potential military payloads, for the ability of the devices to incorporate military equipment, and for the growth capability of the devices.

When all of these facets of value of technical results were taken into account, the following ranking results. First in value is the 3.0 $\frac{L}{D}$ glider. Second in value is the 2.2 $\frac{L}{D}$ glider closely followed by the fold wing and the 1.5 $\frac{L}{D}$ glider, in that order. Next comes the inflatable-wing device closely followed by the M-2b. The M-1 is followed by the drag brake which is last in the rating.

Next some of the technical aspects of the study will be examined. Figure 2 shows the efficiency ratio, which is the ratio of weight of payload plus pilot to the boost weight of the reentry device, as a function of L/D. As might be expected, low values of L/D result in higher efficiency.

L

1

1

0

Figure 3 shows the efficiency ratio in terms of the boost weight of the reentry device as a function of lateral maneuverability. Here, the basic reentry device has been provided with a maneuver rocket (with a specific impulse of 410 and a propellant-loading fraction of approximately 0.88), which is fired a quarter of the earth's circumference before landing. This rocket is considered as part of the boost weight of the reentry device. The plot shows that for different lateral maneuverabilities the relative ranking of these devices changes completely. The solid portions of the curves are those devices which can be boosted with a modified Titan-Centaur booster; the dashed portions of the curves are those devices which cannot be pushed into orbit by that booster.

Table VI presents the comparison of the aerodynamic maneuverability of these devices and a comparison of their landing characteristics with those of the X-15 device. This comparison has been made with the method of reference 1. It is interesting to note that providing for a conventional landing capability insures a hypersonic L/D of 1.5 or greater.

In closing it is appropriate to remark upon the evaluation process used. Shown in figure 4 is a 3-axis system, schematically representing the evaluation process used. Each device has an appropriate value as a research system, a cost of the research program, and time to accomplish the program objective. Technical confidence comes into this evaluation process in that time and money have been provided to the best of present ability to bring the technical confidences to a similar level. However, lack of technical confidence at this time must also be considered as possible perturbations in time, money, and value. Selection of the optimum device to accomplish the objectives of the Dyna-Soar program will then depend upon considered judgment as to combination of these factors of technical confidence, value, time, and cost. The rankings





contained herein reflect an evaluation made by Boeing Airplane Company and do not reflect or imply results of evaluations made by any other group that had access to the Phase Alpha design studies.

REFERENCE

1. Matranga, Gene J., and Armstrong, Neil A.: Approach and Landing Investigation at Lift-Drag Ratios of 2 to 4 Utilizing a Straight-Wing Fighter Airplane. NASA TM X-31, 1959.

. L

1

1

1





TABLE I GROUND RULES

- PILOTED (ONE CREWMAN)
- 1,000-POUNDS RESEARCH EQUIPMENT
- 75 CUBIC FEET VOLUME FOR EQUIPMENT
- ONCE-AROUND OPERATING CAPABILITY
- "SAFE" BOOST
- LAND WITHIN IO SQUARE MILES
- CONSISTENT SUBSYSTEMS
- REUSABLE FOR FOUR FLIGHTS
- AT LEAST NEUTRAL STABILITY
- ESCAPE PROVISIONS
- 6,000-FOOT MARGIN WITH CRITICAL HEATING

TABLE II

PARAMETER COMPARISON

STEPHA (ONCE - AROUND)

DEVICE	W _{BOOST} , LB	W _{REENTRY} , LB	(W/S) REENTRY, LB/SQ FT	^(L/D) M = 20
DRAG BRAKE	z 5,260	4,1 23	W/CDA=1.8/36	o
M-I LIFT BODY	7,275	6,509	LB/SQ FT	.5
M-2bLIFT BODY	9,391	9,196	59.1	1.3
1.5 (L/D) GLIDER	8,590	8,346	29.4	1.5
2.2(L/D) GLIDER	9,719	9,455	28.7	2.2
3.0 (L/D) GLIDER	11,291	10,570	26.1	3.0
INFLAT. WING	11,069	9,860	5.5	1.7
FOLD WING	8,298	7,952	13.4	2.0

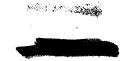




TABLE III

SUMMARY WEIGHT COMPARISON

STEP II A (ONCE-AROUND)

DEVICE	W _{INJECT} , LB	WSTRUCT. ENVIRON. CONTROL (INJECT.), LB	WOTHER SUBSYSTEM (INJECT.), LB	W _{PILOT} AND PAYLOAD, LB
DRAG BRAKE	4,140	2,197	743	1,200
M-I LIFTING	6,657	3,617	1,840	1,200
M-2 bLIFTING BODY	9,391	5,371	2,820	ι,200
1.5 (L/D) GLIDER	8,590	4,650	2,740	1,200
2.2(L/D) GLIDER	9,719	5,776	2,743	1,200
3.0 (L/D) GLIDER	11,291	6,988	3,103	1,200
INFLAT. WING	1,1069	6,334	3,5 25	1,200
FOLD WING	8298	4,298	2,800	1,200

TABLE IV

RELATIVE TECHNICAL CONFIDENCE

RANK IN AERODYNAMICS	RANK IN STRUCTURES AND MATERIALS
DRAG BRAKE	M-I
M-1	2.2 L/D GLIDER
2.2 L/D GLIDER	1.5 L/D GLIDER
3.0 L/D GLIDER	M-2b
1.5 L/D GLIDER	3.0 L/D GLIDER
FOLD WING	FOLD WING
M-2b	DRAG BRAKE
INFLATABLE WING	INFLATABLE WING
	·





TABLE V

VALUE OF TECHNICAL RESULTS RANK IN VALUE FOR DYNA-SOAR OBJECTIVES

3.0 L/D GLIDER
2.2 L/D GLIDER
FOLD WING
1.5 L/D GLIDER
INFLATABLE WING
M-2b
M-I
DRAG BRAKE

TABLE VI.

MANEUVER AND LANDING COMPARISON

LATERAL MANEUVER FROM 23,000 FPS	LANDING METHOD AND COMPARISON TO X-15
0	BASIC DEVICE (55 FPS)
150	PARACHUTE (30 FPS)
800	CONVENTIONAL - EQUAL
1,100	CONVENTIONAL - BETTER
2,150	CONVENTIONAL - BETTER
3,500	CONVENTIONAL - BETTER
1,400	CONVENTIONAL — BETTER
1,700	CONVENTIONAL BETTER
	FROM 23,000 FPS 0 150 800 1,100 2,150 3,500 1,400





REENTRY DEVICES EVALUATED

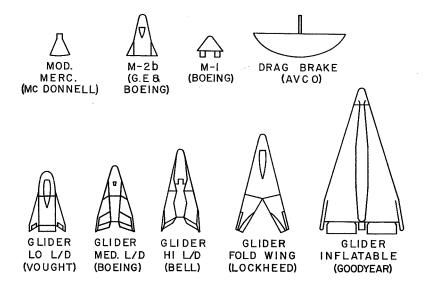


Figure 1

Ь

VARIATION OF EFFICIENCY RATIO WITH L/D REENTRY-DEVICE BOOST WEIGHT BASIS

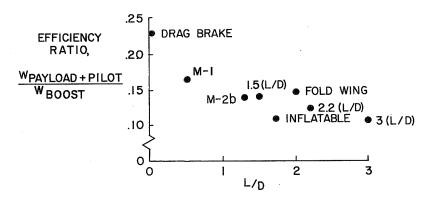


Figure 2





LATERAL MANEUVER CAPABILITY

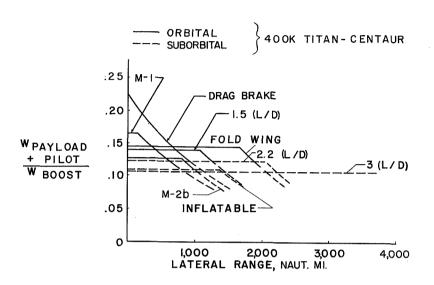


Figure 3

EVALUATION PROCESS (SCHEMATIC)

- DEGREE OF TECHNICAL CONFIDENCE ALREADY ACCOUNTED FOR IN TIME AND COST
- DEGREE OF TECHNICAL CONFIDENCE ALSO CONSIDERED AS POSSIBLE PERTURBATIONS ON VALUE, TIME, AND COST
- CONSIDERED JUDGEMENT TO ARRIVE AT DECISION

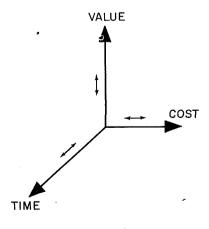


Figure 4



DYNA-SOAR GLIDER-CONFIGURATION EVOLUTION

By R. L. Rotelli Boeing Airplane Company

INTRODUCTION

The major effort of the Boeing Airplane Company on Dyna-Soar reentry devices has been in the development of a winged glider. The purpose of this paper is to show the external configuration evolution of the glider from the time of the initial proposal in March 1958 to the current status. Time does not permit a review of all of the configuration steps taken during this two-year period, nor is a comprehensive review of any one configuration possible. Four configuration steps with brief explanations of significant reasons for each transition will be presented.

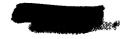
The first configuration was developed by an Industry team headed by Boeing to meet the requirements of the U.S. Air Force request for a proposal. All subsequent configurations have been influenced by Air Force-NASA critiques, Air Force, NASA, and Boeing analytical and test programs, industrial companies collaborating with Boeing as team members, scientific consultants throughout the nation, and any other source from which data were obtainable.

There have been a total of 51 configuration steps, of which 9 were sufficiently significant to warrant construction of models and 4 are worthy of further discussion here. As shown in figure 1, these models include (1) the initial configuration proposed in March 1958, (2) the Phase I model of December 1958, (3) the Phase I model of April 1959, and (4) the Phase Alpha model of March 1960.

INITIAL CONFIGURATION OF MARCH 1958

At the time of the initial Dyna-Soar competition the design objectives were as noted in figure 2. Throughout the 2-year development period these objectives have not changed and remain the same today.

The design approach used in meeting these objectives was as noted in figure 3. The small size is necessary to keep booster costs and



development time to a minimum by modification of existing ICBM boosters. The use of existing hardware is to minimize the development costs and time not essential to Dyna-Soar research. The versatile test stores bay is to provide research flexibility. The simple passive structure is to get maximum reliability with structure that is dependent upon itself for survival rather than upon an active subsystem. Maneuverability provides large course corrections so that a maximum of research flight envelope and a maximum means for the pilot to get the machine back safely are available. The growth to military use is to avoid "dead-end" testing by planning a logical transition to an operation system. The "once-around" range is to demonstrate an orbital capability.

Based on this design approach the configuration is as shown in figure 4. The weight at launch is 8,260 pounds, wing area is approximately 250 square feet, the test payload is 510 pounds, and the landing speed is 150 knots. The configuration has a leading-edge sweep of 75°, and the lower-surface dihedral is a constant 20°. There is one dorsal fin and two ventral fins. A single-pilot canopy is located forward for landing vision. Pilot escape is by a stable capsule which occupies the forward third of the glider.

The initial work of the Phase I effort started with this configuration, and some major problems soon evolved. These were

- (1) The large base area produced high subsonic drag with a corresponding low lift-drag ratio L/D of 3.25
 - (2) The hypersonic L/D of 1.85 gave insufficient lateral range
- (3) The 20° dihedral together with the interaction effects of two upper and two lower control surfaces produced large roll-yaw cross-coupling effects
- (4) At hypersonic high angles of attack the beam line (intersection of the lower dihedral surfaces) and the leading edges of the ventral fins were experiencing temperatures in excess of known passive materials capability
- (5) Because of the wedge shape the location of equipment caused the center of gravity to be too far aft so that stability characteristics were very poor and trim could not be obtained with surfaces of reasonable size
- (6) The impingement of the ventral-fin shock wave on the lower surface produced temperatures in excess of passive material capability.





PHASE I CONFIGURATION OF DECEMBER 1958

The solutions to these problems and the creation of new ones is shown in the configuration identified as Phase I model of December 1958. The design objectives at that time were the same as in March 1958. The design approach differences from those used in the March configuration are shown in figure 5.

Landing without thrust power is necessary to avoid the massive costs to produce and to use a booster capable of putting a glider sized and weighted to carry such an engine installation into orbit, particularly if the engine has no other purpose than to assist the pilot in landing. Escape throughout the flight profile was considered a good idea for any manned system if it could be done within acceptable cost penalties. Full time stability augmentation was found to be necessary for good pilot flying characteristics; integrating pilot control was to allow the pilot the opportunity to add to the reliability of the system. The "go-around" landing engine for air launch was to aid in the pilot training and development of landing techniques. The "twice-around" range and altitude of 300 nautical miles was to assure sizing the glider for growth to a useful military potential. The use of system redundancy by duplication was necessary to approach a survival reliability objective of 0.998.

The resulting configuration is shown in figure 6. Significant changes from the last configuration are:

- (1) Equipment is installed in a body with wings attached in lieu of a thick wing
- (2) The base area is reduced with resulting improvement in subsonic L/D to 4.25
- (3) Vertical fins are moved to the wing tips so that resulting control forces are acting more nearly through the center of gravity
- (4) The flat bottom is to improve stability characteristics and reduced local skin temperatures
- (5) The leading-edge sweep is reduced to 73° to provide some improvement in landing characteristics and to permit a better fixed equipment arrangement for the same wing area
- (6) The nose is bent up 4° to permit trimming at higher lift coefficient C_{T} hypersonically



- (7) The wing area is increased to 330 square feet to reduce the wing loading to help compensate for the increase in temperatures resulting from using turbulent flow in lieu of laminar flow
 - (8) Conventional elevons and a center elevator are used
- (9) The weight has increased to 9,200 pounds due principally to added systems for redundancy, larger wings, and a more detailed weight analysis
 - (10) The hypersonic L/D has increased to 1.95.

Subsequent analysis and testing of this configuration brought out some problems as follows:

L 1

1

- (1) The temperature of the lower surface was greater than predicted and about 500° F beyond the capability of super alloy materials. Structural temperature limits at this time were $4,000^{\circ}$ F for nose, $2,700^{\circ}$ F for leading edges, and $2,000^{\circ}$ F for all other surfaces.
- (2) The hypersonic L/D was below the expected value because of excessive body cross-section area.
- (3) The temperature of the lower leading edge of the vertical fins was excessive (about 3,700° F) and beyond a passive structure capability.

PHASE I CONFIGURATION OF APRIL 1959

These problems led to the next configuration of April 1959. The design objectives remain the same. The design approach, however, is becoming more specific as noted in figure 7. The 14,000-foot maneuver corridor was established to provide a safety margin of at least 6,000 feet as a minimum for pilot safety based on a 45° bank at all speeds. Equipment redundancy was virtually eliminated to obtain a lower wing loading to reduce lower-surface temperatures and to limit the amount of refractory-coated insulated panels, a new addition to the glider. The 500-pound payload limitation is another way of reducing the wing loading. The 2500-nautical-mile lateral turn was considered necessary to maintain the objective of potential military value. The air launch to a Mach number greater than 1.5 is a new requirement to explore the critical supersonic flight regime.

The resulting configuration is shown in figure 8. Significant changes from the previous configuration (fig. 6) are:

(1) The body cross section has been reduced





- (2) Molybdenum-insulated panels have been added to the forward part of the lower surface; the 2,000° F limit for surface temperature was abandoned
- (3) The lower leading edge of the vertical fins has been eliminated by elimination of the area below the wing
- (4) The weight has been reduced to 7,800 pounds, while a wing area of 330 square feet has been maintained. The hypersonic L/D has increased to 2.2 and the subsonic L/D to 4.5.

Problems subsequently determined were as follows:

- (1) Trim was not possible at low supersonic speeds because of the large camber in the wing upper surface
- (2) The leading edge and nose temperatures were higher than predicted so that the 14,000-foot maneuver corridor could not be obtained
- (3) The center elevator created booster interstage difficulties and interferences with the installation of the air launch liquid rocket engine.

PHASE ALPHA CONFIGURATION OF MARCH 1960

During the period through April 1959 the Air Force was conducting a phase I computation in which one of the items of work was to develop the glider design requirements. It was not until after the source selection of April 1959 that the Air Force published their design requirements to the winner of the competition. Based on these, the design objectoves remained unchanged; however, changes were reflected in the design approach as shown in figure 9.

The configuration resulting from these requirements is shown in figure 10. The significant differences from the previous configuration are:

- (1) The weight has been increased to 9,283 pounds, primarily because of the return of 1,000 pounds of payload and subsystem redundancies.
- (2) The entire lower surface has been covered with coated-molybdenum insulated panels because of higher temperatures due to the higher wing loading and because of a requirement that the temperature be based on a 100-percent equipment blocking of the inward radiated heat.





- (3) The radius of the leading edge and nose has been increased approximately 1 inch to recover the minimum maneuver safety margin of 6,000 feet
- (4) Retractable fin tip stabilizers have been added to reduce the aerodynamic center shift and thus to provide positive aerodynamic stability throughout the flight profile
- (5) The center elevator has been removed and the area added to the elevons
- (6) The wing upper surface camber has been removed to solve the subsonic trim problem
- (7) The nose gear has become a skid to save weight by eliminating the cooling system required to protect a normal type nose gear.

This configuration is one month old and three problems have appeared, as follows:

- (1) The escape capsule appears to be too complex and costly.
- (2) It is very desirable to reduce the temperature on the lower surface to limit the extent of molybdenum shielded panels.
- (3) The stability characteristics at hypersonic low angles of attack are unsatisfactory.

Solution to these problems is now in progress.

Figure 11 shows the current inboard profile for the ground-launch configuration.

Figure 12 shows the current inboard profile for the air-launch configuration. The pertinent equipment is identified.

SUMMARIZATION

Figure 13 compares the significant areas of change in the evolution of the Dyna-Soar gliders. The fluctuation of weight is due primarily to the choice made as to which of two influences was greatest at the time, the structural-material temperature capabilities or the aerodynamics-maneuver safety margin. As can be seen, aerodynamics is at present ahead.



From this review, one might conclude that the designers were in a "rut" in staying so closely to a given shape and size and simply making refinements. This is not true. Throughout the development period many "excursions" and trade studies were made. Consideration was given to a range of devices from a 3,000-pound unmanned vehicle to 15,000-pound vehicle with a two-man crew. Wing loadings from less than 20 to greater than 40 were studied. Leading-edge sweep was varied from 70° to 80°. In all of these excursions, the designers were always forced back to the configuration shown herein by three constraints or "road blocks." These are (1) the current ICBM booster capabilities, not only in the thrown weight but in the modifications required for winged, manned payloads: (2) the temperature limits created structural materials capabilities for long time exposure; and (3) the Dyna-Soar requirements of such things as pilot control, conventional landing, positive aerodynamic stability, hypersonic maneuverability, and orbital velocities. These constraints led the designers to return to a wing loading of 20 to 30 lb/sq ft, a weight of 8,500 to 9,500 pounds, a hypersonic L/D of 1.5 to 2.5 and a subsonic L/D of 4 to 5.

Ĺ

1

1

1

1

Whether subsequent work will remove any of these constraints to allow for a better compromise between structures, aerodynamics, and requirements will have to await decisions concerning the next configuration milestone, which as is shown in figure 1, is scheduled for early spring of 1961.





CONFIGURATION EVOLUTION

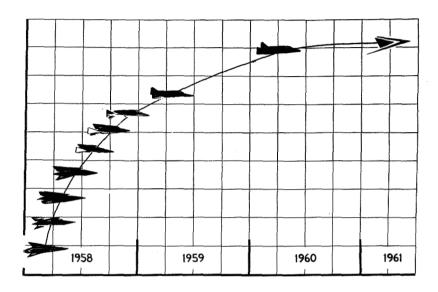


Figure 1

DESIGN OBJECTIVES MARCH, 1958

- CONCEPTUAL GLIDER DEVELOPMENT
 - SIGNIFICANTLY ADVANCING TECHNOLOGY
 - SUBSEQUENT MILITARY APPLICATION
 - DEMONSTRATING MANNED FLIGHT
 - HYPERSONIC BOOST GLIDE
 - ORBIT
 - RE-ENTRY
 - CONVENTIONAL LANDING

Figure 2





DESIGN APPROACH - MARCH 1958

- SMALL SIZE
- MAXIMUM USE OF EXISTING HARDWARE
- VERSATILE TEST STORES BAY
- SIMPLE PASSIVE STRUCTURE
- MANEUVERABLE IN GLIDING FLIGHT
- RELIABLE AND SAFE
- MILITARY POTENTIAL
- ICBM BOOSTERS
- RANGE "ONCE-AROUND"

Figure 3

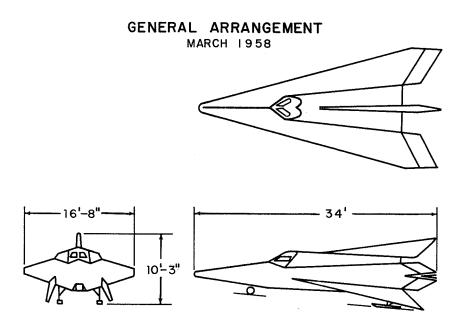


Figure 4





DESIGN APPROACH DECEMBER, 1958

- SAME AS MARCH, 1958, EXCEPT-
 - GOOD LANDING WITHOUT ENGINES
 - ESCAPE THROUGHOUT FLIGHT ENVELOPE
 - 3-AXIS-FULLTIME-STABILITY AUGMENTATION
 - INTEGRATED PILOT CONTROL
 - "GO-AROUND" LANDING ENGINE FOR AIRLAUNCH
 - RANGE "TWICE-AROUND"-ALTITUDE 300 N.M.
 - REDUNDANCY FOR ADDED SAFETY

Figure 5

GENERAL ARRANGEMENT DECEMBER 1958

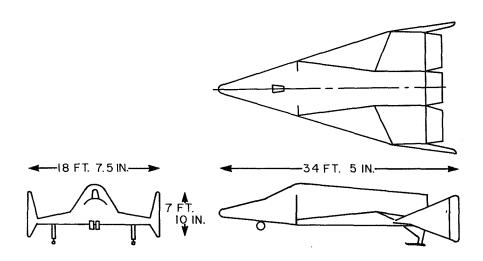


Figure 6





DESIGN APPROACH APRIL 1959

- SAME AS DECEMBER 1958 EXCEPT
 - 14,000 FT. MIN. BETWEEN MAX. L/D EQUILIBRIUM AND MAX.L/D HEAT LIMIT
 - LIMITED REDUNDANCY
 - 500 LB. PAYLOAD FOR MANNED FLIGHTS
 - 2500 N.MI. LATERAL TURN
 - AIR LAUNCH TO MACH 1.5 MINIMUM

Figure 7

GENERAL ARRANGEMENT APRIL 1959

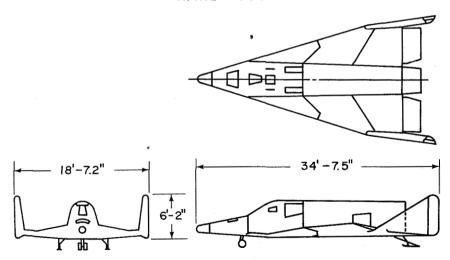


Figure 8





DESIGN APPROACH MARCH 1960

•	PAYLOAD	1000 LB & 75 CU. FT.
•	BOOSTER	MODIFIED TITAN ICBM
•	VELOCITY	26,000 FPS (INERTIAL) @ 400,000 FT. ALT.
•	LANDING	CONVENTIONAL
•	LATERAL RANGE	2000 NAUT. MI. (MIN.)
•	FLIGHT CORRIDOR	30,000 FT. (MIN.)
•	GLIDER LIFE	4 FLIGHTS (MIN)
•	STABILITY	NEUTRAL - LAUNCH TO LANDING

Figure 9

RELIABILITY

GENERAL ARRANGEMENT MARCH 1960

REDUNDANCY OF CRITICAL

COMPONENTS

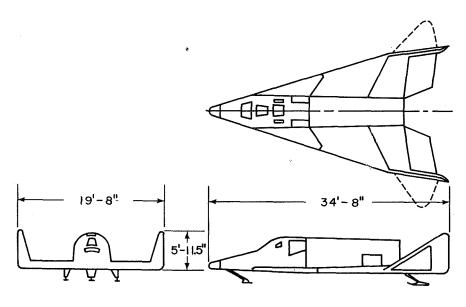


Figure 10





INBOARD PROFILE, GROUND LAUNCH

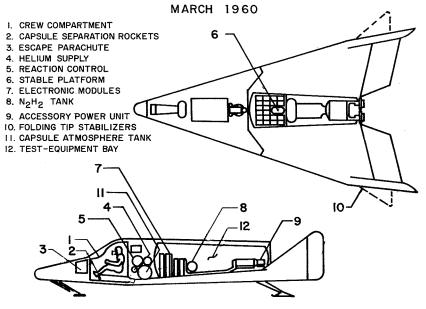


Figure 11

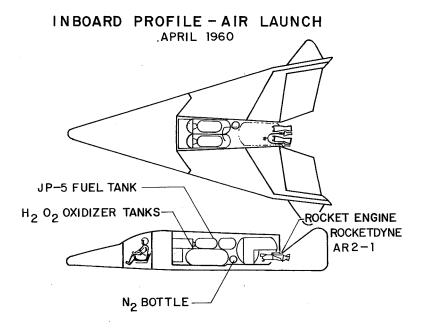


Figure 12



æ

40

94

DYNA-SOAR GLIDER DATA

MODEL	MAR. 58	DEC.'58	APR. 159	MAR!60
DESIGN LAUNCH WEIGHT, LB	8260	9200	7,800	9,283
PAYLOAD, LB	510	1130	500	1,000
WING AREA, SQ FT	250	330	330	330
(L/D) HYPERSONIC	1.85	1.95	2.2	2.2
(L/D) SUBSONIC	3 .25	4.25	4.7	4.5

Figure 13

DYNA-SOAR AERODYNAMIC PERFORMANCE

By James S. Lesko Boeing Airplane Company

SUMMARY

The aerodynamic performance capabilities of the Dyna-Soar vehicle are summarized below.

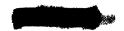
The piloted vehicle has a wing area of 330 square feet and weighs 9,720 pounds for the "once-around" mission. This weight includes the pilot and 1,000 pounds of payload.

A test mission has been defined for a "once-around" flight starting at Cape Canaveral and ending at Edwards Air Force Base. The vehicle is launched in a safety boost trajectory to an end-of-boost speed of 105 feet per second above satellite speed at an altitude of 300,000 feet with a flight-path angle of 0°. The vehicle is pitched to a nominal lift coefficient of 0.45 and is held at that lift coefficient to a velocity of Mach 4 at 130,000 feet. It then completes its glide into the landing area at a lower nominal lift coefficient. Range correction, if needed during flight, is made by variation of lift-drag ratio only. Maximum altitude reached is 430,000 feet. For the due East launch, a bank angle of -15° is held during equilibrium glide to cause the vehicle to deviate from its great circle path to proceed to Edwards Air Force Base. Total mission time is 110 minutes.

Energy management studies have been conducted to show an ability to overcome range errors that would have resulted from boost dispersion errors and errors in assumptions of drag coefficient and density.

The vehicle has large maneuver corridors. Even in a banked turn for maximum lateral offset, the vehicle operates with a temperature margin of over 200° F for its most temperature-critical areas.

The vehicle has a large lateral maneuver capability. For an end-of-boost speed of 23,000 feet per second (relative), the vehicle can fly 2,200 nautical miles to the side, down to a speed of 800 feet per second. This side displacement increases to 2,500 nautical miles for an end-of-boost speed of 24,100 feet per second. These values are based on turbulent-boundary-layer assumptions. Additional capability to 2,900 nautical miles would be available if the boundary layer were laminar.



A landing procedure has been devised to enable development of piloted, nonpowered landing capabilities. Subsonic maximum lift-drag ratio is 4.5. Speed brakes are provided to modulate subsonic aerodynamic characteristics. For down-range flights, a drag chute is provided. This drag chute and high-friction skids materially reduce runout distance.

INTRODUCTION

 \mathbf{L}

1

1

1

2

The name "Dyna-Soar" is an abbreviation of the words dynamic soaring which are used to describe an equilibrium-flight process wherein a large fraction of the weight of the vehicle is supported by the centrifugal acceleration of high subsatellite velocities. The amount of aerodynamic lift required to maintain equilibrium flight is a small fraction of the weight of the vehicle and this fact results in the following flight characteristics:

- 1. Equilibrium-flight trajectories take place at extremely high altitudes
 - 2. Vehicle longitudinal deceleration is a small fraction of a g
- 3. Extremely long ranges can be covered in unpowered gliding flight even when the vehicle has a small lift-drag ratio
- 4. The actual longitudinal range of the vehicle is directly dependent on its longitudinal deceleration which, in turn, depends directly on its lift-drag ratio. For good range control it is necessary for the vehicle to possess a wide range of lift-drag ratios.

Reliance on extreme speed to obtain longitudinal range imposes serious restrictions on the ability of the vehicle to maneuver in a lateral direction. Large lateral forces are required to make a heading change; however, the vehicle is limited in its ability to develop large lateral forces because of its high-altitude—low-dynamic-pressure glide trajectory.

The resulting ratio of lateral range to longitudinal range for the hypersonic glider is of the order of 1:5 as contrasted to a ratio of 1:1 which is the characteristic of subsonic or low supersonic airplanes. Although the range ratio as mentioned is small, the actual lateral-range capability of the Dyna-Soar is of the order of 2,500 nautical miles, a not inconsiderable amount.



Lateral maneuver control is also dependent directly on the range of lift-drag ratios possessed by the vehicle.

SYMBOLS

C_D drag coefficient

C_{T.} lift coefficient

 $C_{L,max}$ maximum trimmed lift coefficient

g gravitational acceleration

h altitude, ft

h rate of climb, fps

L lift

L/D lift-drag ratio

M Mach number

n maneuver factor, $\left(\frac{V^2}{rg} + \frac{L}{W} - 1\right)$

R radius

r flight-path radius of curvature

S wing area, sq ft

V inertial velocity, fps

V_i indicated airspeed, knots

W weight, lb

W/S wing loading, lb/sq ft

angle of attack, measured from lower surface center line

β sideslip angle, deg



- γ flight-path angle, deg
- Ø bank angle, deg

Subscripts:

- e equilibrium flight
- l structural limit

DISCUSSION

L

111

2

General Arrangement

The general arrangement of the Dyna-Soar glider is shown in figure 1. Some pertinent dimensions are as follows:

Wing area, sq ft	•	٠	•	•	•	•	•	•	•		•	•	•	٠	•	9		•	•	330
Fin area, each, sq ft							•			•	•	•	•				9	•	e	31
Elevon area, sq ft		•		۰	٠	•	•	•	•	•		•	•	•	•	•	•	•	•	34
Rudder area, each, sq ft .	•	•	•			•		•		•	•	•	•	•	•				•	10
Fold-out fin, each, sq ft			•			•			9			٠	•	•	•	•		•	•	9
Forward area uptilt		•						•	•	•	•		•	•			L 5	рe	erc	ent S
Angle of tilt, deg	۰		•	9			•	•		•	•	•	•	•	•	•	•	•		4

The weights and wing loadings of the Dyna-Soar are summarized as follows:

	St	cep I	Step IIA								
	Weight, lb	W/S, lb/sq ft	Weight, lb	W/S, lb/sq ft							
On launch pad Reentry Landing	9,280 9,190 8,890	28.1 27.8 27.0	9,720 9,450 9,060	29.4 28.7 27.5							

All weights include pilot plus 1,000 pounds of payload. The primary differences for the weights going from Step I to Step IIA are the increased expendable allowances and increased tank sizes to house those expendables.

The center of gravity is located at 63 percent of the reference root chord and varies less than 1/2 percent throughout the flight. The





reference root chord is 400 inches measured from the theoretical apex of the wing.

Flight Envelope

The flight envelope for the Dyna-Soar launched eastward is shown in figure 2. The recovery ceiling is the locus of points on the h-V diagram at $\gamma=0^{\circ}$, from which the glider could successfully reenter its flight corridor without violating its structural limits. It is of interest primarily to insure that a terminated boost trajectory would not place the glider into a regime from which it could not recover. The equilibrium glide trajectories are those for hypersonic values of $C_{L,max}$ of 0.69 and of C_{L} for $(L/D)_{max}$ of 0.15. The minimum flight-altitude line is that where the vehicle becomes structurally limited.

The overall flight corridor at 20,000 feet per second is 60,000 feet. For flight at this speed the dynamic pressure ranges from 15 pounds per square foot at $C_{L,max}$ to 120 pounds per square foot at the minimum flight altitude. Reynolds numbers at these conditions range from 0.2 to 1.2 \times 10⁶.

Maneuver Corridors

Maneuver corridors are shown in figure 3 as a function of velocity at three lift coefficients. The maneuver corridor is defined as the altitude difference between the altitude for equilibrium glide at a given lift coefficient and that at which the vehicle is limited structurally at the same lift coefficient.

Of pertinent interest is the fact that large corridors are available at all speeds and lift coefficients for vehicle operation. The smallest corridors are evident at a speed of 20,000 feet per second and this speed will be closely approached during Step I tests.

The importance of the corridor depth can be better understood when it is realized that the vehicle operates at temperatures 100° F lower than its limit for each 6,000 feet of corridor depth. Furthermore, its ability to generate aerodynamic lift doubles for 15,000 to 18,000 feet of depth.

Allowable Maneuver Factors

The maneuver factors available to the Dyna-Soar vehicle at a relative velocity of 20,700 feet per second and the limitations which



restrict these maneuver factors are shown in figure 4. The ordinate is the altitude and the abscissa is the maneuver factor, described as $\left(\frac{L}{\overline{W}} + \frac{V^2}{rg} - 1\right)$.

At 20,700 feet per second the value of $\frac{V^2}{rg}$ is approximately 0.73. This is the percent of vehicle weight that would be supported in the absence of aerodynamic lift. For flight at $C_{L,max}$, it is seen that there is no lift contribution to the maneuver factor at 400,000 feet due to extremely low dynamic pressure. For operation at a lower altitude, the aerodynamic lift becomes appreciable. At 258,000 feet, the lift provides equilibrium-flight capability. At still lower altitude the increased lift provides maneuver capability and would increase to very large values if there were no structural limitation imposed on the vehicle for flight at $C_{L,max}$. However, it can be seen that point 2 on the vehicle has met its temperature limit at the altitude of 241,000 feet. Similarly, for flight at $C_{T} = 0.14$ there is no contribution of lift at high altitudes, but for lower altitude operation the lift contribution again becomes appreciable. Equilibrium glide is established at h = 223,000 feet, and, as the vehicle is flown at lower altitudes, significant load factors are developed until the vehicle again becomes structurally limited (due to temperature) along the wing leading edge. The complete boundary of temperature limitations and the maneuver factors that are allowed at various lift coefficients are illustrated in this figure.

L

1

1

1

2

It can be seen that the nose limitation is imposed over a small portion of the h-n diagram and that the dorsal-fin limitation cuts off the low-lift-coefficient operation capability at approximately $C_L=0.09$ in equilibrium flight. This circumstance makes it possible to fly the vehicle at a lower altitude at $C_L=0.14$ than at the equilibrium altitude for $C_L=0.09$ because of temperature relief on the dorsal fin at the higher angle of attack. It can be seen that the maneuver factor required to fly in a 45° banked turn is easily accommodated within the allowable maneuver factors.

For this speed the maneuver factor allowed to the vehicle at $C_{\rm L,max}$ is 0.37; at $C_{\rm L}$ = 0.45, it is 0.6; and at $C_{\rm L}$ for $({\rm L/D})_{\rm max}$, it is 0.45.

It should be noted that there is an upper limit of ${\tt C}_{\tt L}$ that the vehicle cannot surpass when starting at any given ${\tt C}_{\tt L}$ in equilibrium glide. This restriction in attitude-change capability becomes important in longitudinal-range control capability, since the full range of





lift-drag ratios cannot always be applied. For instance, if the vehicle were in equilibrium at $C_L = 0.1^h$, the maximum C_L that could be "pulled" would be 0.5.

There is an approximate relationship between the shaded area to the right of the equilibrium line and the shaded area to the left of that line. The upper bound of the shaded area to the left of the equilibrium line is the recovery ceiling of the vehicle at this speed. This relationship follows from the consideration that the maximum vertical velocity of the vehicle attained by starting at the recovery ceiling at $\gamma = 0^{\circ}$ is given by the expression '

$$\dot{h} = -\sqrt{2 \int_{\text{hrecovery ceiling}}^{\text{he}} n(h) dh}$$

For the vehicle to recover, positive vertical acceleration acting over an altitude depth must be applied to decrease the vertical velocity to zero. The amount available within the bounds of the h-n diagram to the right of equilibrium flight is

$$\dot{h} = \sqrt{2 \int_{h_e}^{h_l} n(h) dh}$$

These two values of h must be equal and opposite in sign and they are defined by the shaded areas as previously mentioned.

The exact determination of the recovery ceiling is more complex since the horizontal velocity does not remain constant throughout the recovery maneuver.

Drag Polars

The trimmed drag polars for the Dyna-Soar in equilibrium flight are shown for speeds ranging from subsonic to a Mach number of 25 in figure 5. These values are based on turbulent skin friction. At a Mach number of 5, the percent of drag that is skin friction ranges from 15 at $(L/D)_{max}$ to less than 1 at $C_{L,max}$. At a Mach number of 20, this percent ranges from 30.5 at $(L/D)_{max}$ to less than 5 at $C_{L,max}$. There is a small decrease in $(L/D)_{max}$ with increasing hypersonic speed due to the reduction in Reynolds number in the flight corridor and a small reduction in the lift-curve slope. The lift coefficient



for $(L/D)_{max}$ is essentially constant for the hypersonic speed range as is the angle of attack for $(L/D)_{max}$ which is 15° .

At Mach number 20 the following relationships prevail:

CL	L/D	α, deg
0.15	2.18	15
.45	1.5	29
.69	.8	50

L 1 1

2

The ratio of maximum to minimum lift-drag ratios is 2.7, which is an index of equilibrium-glide range-control capability.

Mission Profile

For the once-around mission from Cape Canaveral to Edwards Air Force Base, the altitude, range, and time are shown in figure 6. The velocity at boost burnout is 105 feet per second above satellite speed at 300,000 feet. This speed is chosen for a nominal flight at $C_{\rm L}=0.45$ to be flown to the vicinity of the landing area. This value of $C_{\rm L}$ and the 300,000-foot injection altitude were chosen so that the vehicle could aerodynamically correct, prior to leaving the sensible atmosphere, boost dispersion errors and errors in the assumptions of vehicle drag coefficient and in density at that tape-line altitude. The nominal mission time is 110 minutes.

Range Control Capability

The range control capabilities during the once-around mission is shown as a function of velocity in figure 7. For a mission which required no range correction the value of C_L would be maintained at 0.45 to approximately 100 miles short of touchdown. In the event that an accumulation of errors requires range correction, there exists a capability to extend the range over 20,000 miles by flying at $(L/D)_{max}$ or to shorten the range by over 10,000 miles by flying at $C_{L,max}$. These range-correction capabilities are significantly greater than conceivable errors that could be made in assumptions in drag coefficient or air density. Most of the range-correction capability exists in the same speedaltitude regime where these errors would have significance. During equilibrium glide the vehicle flies at its proper density altitude;





consequently, there would be no error introduced by inaccurately known density at a given tape-line altitude. A range-correction capability of ±3,000 miles exists for equilibrium flight.

Lateral-Turn Capability

The maximum lateral-turn capability is shown as a function of velocity at the start of the turn in figure 8. Essentially no lateral-turn capability is available until the vehicle has begun equilibrium flight. The maximum capability is attained by flying at the lift coefficient for $(L/D)_{max}$ and at a bank angle of 45°. It can be seen in the figure that most of the lateral displacement is achieved through turns initiated at the higher velocities. Lateral-turn control extends from zero displacement to those displacements shown.

Terminal Flight Phase

A plan and profile view of the terminal flight phase is shown in figure 9. For the nominal glide trajectory at a little over 300 miles from the landing site, the vehicle is at a Mach number of 7, at 165,000 feet, and 10 minutes from touchdown. At this point the onboard inertial navigator will place the vehicle within an accuracy of ±2 miles in longitudinal range and ±6 miles in lateral displacement. The vehicle longitudinal— and lateral—range correction capabilities are ±100 miles and ±75 miles, respectively. The pilot receives radar—obtained data by radio and updates his inertial navigator readings. He makes range—to—go corrections and proceeds to line up with his landing site. At 30 miles to go he is in visual contact with the landing site at a Mach number of 2 and at 65,000 feet. At this point the vehicle can be landed within a radius of 10 miles of the assumed touchdown point. A pitot-static tube provides the pilot with indicated airspeed and altimeter information starting at a Mach number of 5.

Nominal Landing Profile

The nominal landing profile is shown in figure 10. Although the straight—in approach is pictured, the vehicle can land by using the circular approach developed at Edwards Air Force Base. The landing consists of a high-energy approach using an aiming point short of the runway and starting a moderate flare at an altitude of 1,100 feet. The flare ends 200 feet over the end of the runway and the vehicle decelerates to touchdown at a small rate of sink. Considerably less than the 8,000 feet of runway are used to perform the landing, which allows a high tolerance of touchdown point miss.



During the approach and flare the vehicle configuration is clean except for nominal setting of the speed brakes. At the end of flare, landing skids are extended and the speed brakes are full open. At touchdown a 10-square-foot drag chute is opened.

During the nominal approach the following conditions prevail:

$$\gamma = -22.5^{\circ}$$

$$\dot{h} = -180 \text{ fps}$$

$$V_1 = 280 \text{ knots}$$

L

1

1 2

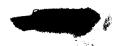
$$C_{T_{\star}} = 0.10$$

The flare takes place at n=1.5g over a 10-second interval with a speed loss of 50 knots. During deceleration the rate of sink is 25 feet per second and time to touchdown is 7 seconds. The velocity at touchdown is 175 knots.

A large tolerance in speed along the nominal glide path exists. The speed may be between 210 knots and 350 knots. Also, there exists a large tolerance in flight-path angle to the aiming point. It could be between -15° and -30° without altering the touchdown point.

CONCLUDING REMARKS

The vehicle designed to perform the Dyna-Soar mission is capable of exploring the effects of hypersonic environment over a wide range of attitudes in a safe manner and can therefore obtain information pertaining to the design of a wide range of possible reentry shapes. It possesses a large longitudinal-range and range control capability, a large lateral-range capability, and can land in a conventional manner, features which will aid in the overall system test and are potentially of military value.



GENERAL ARRANGEMENT

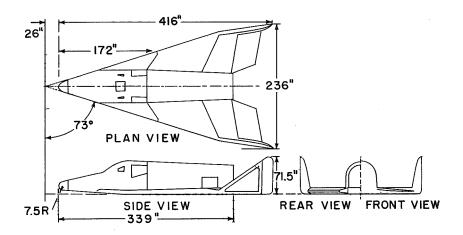


Figure 1

FLIGHT ENVELOPE W/S=29.0 PSF

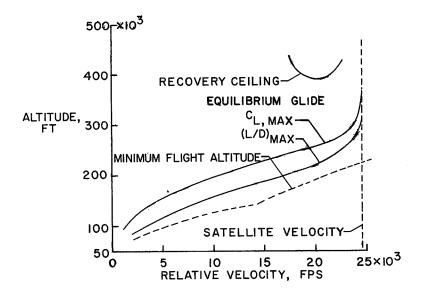


Figure 2

MANEUVER CORRIDORS W/S=29.0 PSI; β =0°; ϕ = 0°

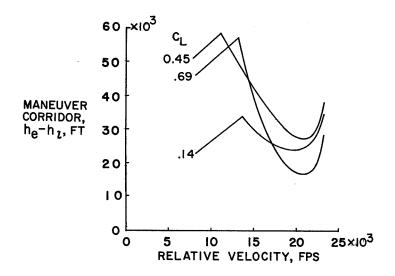


Figure 3

ALLOWABLE MANEUVER FACTOR RELATIVE VELOCITY, 20,700 FPS; W/S = 29

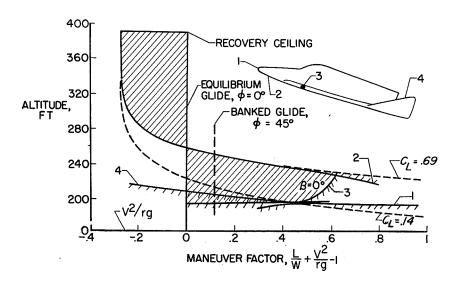


Figure 4



DRAG POLARS

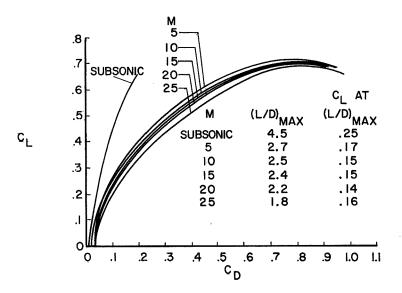


Figure 5

$\begin{array}{c} \text{ONCE-AROUND-MISSION PROFILE} \\ \text{C}_{\text{L}} = \text{0.45} \end{array}$

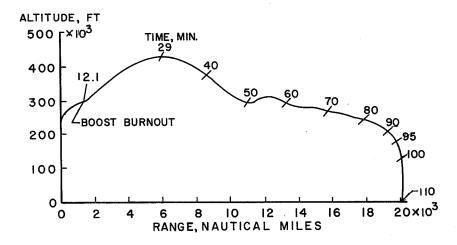
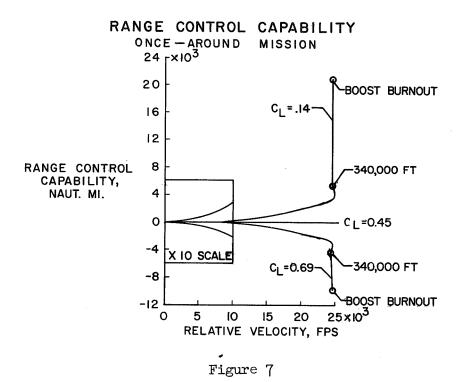


Figure 6







LATERAL TURN CAPABILITY (L/D) $_{\rm MAX}$ AT ϕ = 45°; TURBULENT SKIN FRICTION

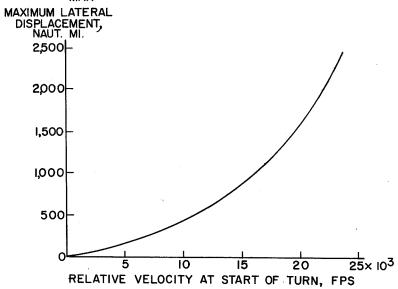


Figure 8



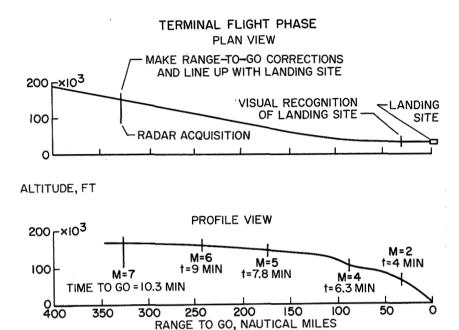


Figure 9

NOMINAL LANDING PROFILE

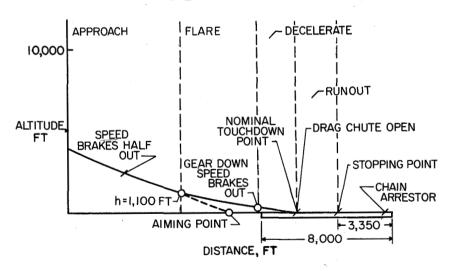


Figure 10

Page intentionally left blank

STABILITY, FLIGHT CONTROL, AND ENERGY MANAGEMENT

OF THE DYNA-SOAR GLIDER

By A. H. Lee and L. J. Mason Boeing Airplane Company

SUMMARY

This paper presents some of the stability and control characteristics of the Dyna-Soar glider based upon analysis and testing done during the phase I contract period. Flying qualities, with and without stability augmentation, and a method of outer loop control for energy management are described.

An adaptive control system is planned. The primary control mode is manual with pilot input commands through the stability-augmentation system. A second control mode is provided which couples the pilot directly with the actuation system, bypassing the stability-augmentation system. Flying qualities with stability augmentation correlate with the "desired response" region of the flying qualities requirements of reference 1. Unaugmented flying qualities satisfactory for emergency operation appear to be attainable.

Control of the vehicle vélocity as a function of range to go is shown to be a feasible method of energy management to achieve range control.

INTRODUCTION

The wide range of flight conditions encountered during reentry and glide create unusual stability and control problems. In order to perform its mission, the glider must be capable of trimmed flight to angles of attack of about 50° at hypersonic speeds and must be capable of a conventional landing. Flying qualities satisfactory for pilot control with and without stability augmentation are desired throughout the flight regime.

From experience and, more recently, from investigations by the NASA and Air Force funded projects involving variable-stability aircraft, the desired handling qualities for piloted control are reasonably well known.



9

Minimum required flying qualities for pilot control are not as well defined. Recent investigations by the NASA and by the Cornell Aeronautical Laboratory under WADD contract have provided data on minimum handling qualities at low speeds. Results from these investigations, and others, have been compiled in reference 1 as a preliminary statement of handling-qualities requirements for hypervelocity aircraft. These requirements have been considered in developing Dyna-Soar handling qualities, although it is recognized that further studies are required to confirm their applicability to hypersonic conditions.

For conventional low-speed aircraft, desired flying qualities can be provided by proper tailoring of the configuration. For vehicles similar to the Dyna-Soar glider, configuration tailoring is less satisfactory. However, through the use of stability augmentation, desired handling qualities can be provided. Without stability augmentation, handling qualities satisfactory for emergency operation appear obtainable. A self-adaptive control system is planned to achieve the desired system response over the flight range and to facilitate blending of aerodynamic and reaction control forces. A specific guidance and control system, and therefore the specific adaptive technique, has not been selected for Dyna-Soar, and the controlled vehicle characteristics should be regarded as typical of what can be attained by using adaptive methods.

L

1

1

1

3

SYMBOLS

Ъ	wing span, ft
c _{1/2}	number of cycles of oscillation to damp to half-amplitude
c_2	number of cycles of oscillation to double amplitude
$\mathtt{C}_{\mathtt{D}}$	drag coefficient, Drag/qS
$\mathtt{C}_{\mathbf{L}}$	lift coefficient, Lift/qS
$^{\mathrm{C}}_{\mathrm{L},\mathrm{MAX}}$	maximum lift coefficient
Cl	rolling-moment coefficient, Rolling moment/qSb
$C_{l_{\beta}} = \partial C_{l}$	/dβ per degree
c_n	yawing-moment coefficient, Yawing moment/qSb
$c_{n\beta} = \partial c_n$	/∂β per degree



$c_{\mathbf{r}}$	reference wing root chord, ft
fn	natural frequency, cps
h	altitude, ft
h	rate of change of altitude, ft/sec
I_{X} , I_{Z}	moments of inertia about conventional airplane X and Z body axes, respectively, slug-ft2
K	control-system gain
L/D	lift-drag ratio
(L/D) _{MAX}	maximum lift-drag ratio
M	Mach number
p	rolling velocity, radians/sec
q	pitching velocity, radians/sec; dynamic pressure, lb/sq ft
R	range, nautical miles
S	wing area, sq ft
s ·	Laplace transform operator
v_{M}	measured velocity, ft/sec
ν _o .	initial total velocity, ft/sec
v_P	programed velocity, ft/sec
v _e	equivalent velocity along conventional airplane Y body axis
α	angle of attack, deg
β	angle of sideslip, deg
′	



damping ratio of oscillatory mode of motion

initial flight-path angle, deg

 γ_{o}

ζ

∅ roll angle, deg

 $\omega_{\rm n}$ natural frequency of oscillatory motion, radians/sec

DISCUSSION

Vehicle Stability Characteristics Without Augmentation

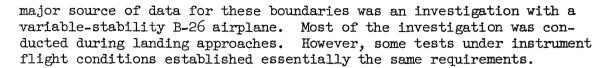
Longitudinal. - Aerodynamic-center estimates based on wind-tunnel tests during phase I are shown in figure 1 as functions of Mach number and lift coefficient. The center-of-gravity location, which is practically invariant during the flight, is 63 percent of the reference root chord. Positive stability is indicated for all normal flight conditions which are, in general, at lift coefficients above that for (L/D)_{MAX}. However, an instability is noted for lift coefficients below 0.08 at hypersonic speeds. Future studies will be directed toward improving this low-lift-coefficient stability. Possible means of improvement include a change in the forward body contour.

The unaugmented flying qualities of the glider are presented for representative speeds of the flight regime at maximum lift and maximum range conditions. These conditions are presented in figure 2 as $C_{L,MAX}$ and C_{L} for $(L/D)_{MAX}$ as a function of Mach number. At speeds below a Mach number of approximately 5, $C_{L,MAX}$ is limited by the angle of attack for neutral static stability. Above a Mach number of approximately 5, it is limited by the wing lift capability.

The glider's longitudinal flying qualities without stability augmentation are presented in figure 3. The reference boundaries were obtained from reference 1. Since normal operation of the Dyna-Soar glider is with stability augmentation, the boundaries of interest for flight without augmentation are nose to emergency operation. The



I 1 1



The unaugmented flying qualities of the glider are reasonably good during landing. In fact, the damping and frequency are adequate for normal operation at the angle of attack for maximum L/D. As speed increases, both frequency and damping are reduced. At hypervelocities - Mach 20 is an example - unaugmented damping is essentially nonexistent. This condition is fundamental for any practical configuration. However, frequencies are also very low, about 0.1 cps at Mach 20, as shown in figure 4. Therefore, a pilot can provide damping through the proper phasing of his control inputs. It is noted that the flying qualities for supersonic and hypersonic speeds fall in the "acceptable for short-time emergency operation" category. Since this category was derived principally during landings, future studies are required to define the degree of its applicability to the high-altitude flight of this class of vehicles.

Lateral-directional stability and control. Directional-stability and dihedral-effect derivatives, c_{n_β} and c_{l_β} , are presented in figure 5. The data are presented for conventional airplane body axes. Although this c_{n_β} is a good representation of a vehicle's directional stability at low angles of attack, it has been shown in the paper by John W. Paulson, Robert E. Shanks, and Joseph L. Johnson that it is not necessarily representative of stability for the high angles of attack associated with the Dyna-Soar glider. A better representation is $\left(c_{n_\beta}\right)_{dynamic}$. This parameter is defined as

$$(C_{n_{\beta}})_{\text{dynamic}} = C_{n_{\beta}} - \frac{I_{z}}{I_{x}} C_{l_{\beta}} \sin \alpha$$

For the glider, $\left({{{\text{C}}_{{n_\beta }}}} \right)_{dynamic}$ is significantly larger than ${{\text{C}}_{{n_\beta }}}$ at high angles of attack. The glider's directional stability and dihedral effect are positive except for a small negative dihedral effect for flight at maximum L/D at supersonic speeds.

The unaugmented lateral-directional flying qualities are presented in figure 6, correlated with handling qualities required for emergency operation. The boundaries were obtained from reference 1. Boundaries for emergency conditions were determined principally from tests with a variable-stability F-86 airplane making simulated landings at 10,000 feet.



As shown, lateral flying qualities for the glider are in the "acceptable (emergency)" category from landing through hypervelocity speeds. Low damping exists for all flight conditions. This is characteristic of aircraft with highly swept wings because of their high ratios of yaw moment of inertia to roll moment of inertia and their low roll damping. Lateral-oscillation frequencies during landing are approximately 0.3 cps. At Mach 20, the frequencies range from 0.3 cps at $\rm C_{L,MAX}$ to 0.2 cps at $\rm (L/D)_{MAX}$, as shown in figure 7. The higher frequency at $\rm C_{L,MAX}$ stems from the stabilizing effect of $\rm C_{\it l}_{\it b}$ at high angles of attack.

Vehicle Stability Characteristics With

Stability Augmentation

Longitudinal and lateral response and control-system gains for three representative flight conditions that cover the range of uncontrolled vehicle dynamics are shown in figure 8. The flight conditions are:

Condition	Mach number	q, lb/sq ft	$lpha_{ ext{trim}}$, deg
Reentry (near zero damping)	15	25	41
Landing (near neutral stability)	.25	167	7.5
Approach (high-dynamic pressure)	.85	200	5•5

With the indicated gains, both longitudinal and lateral responses are nearly constant (about 0.5 cps and a damping ratio of 0.5 to 0.7). Longitudinal response was selected on the basis of "desired" handling-qualities requirements from reference 1. Longitudinal response characteristics, with and without stability augmentation, are shown in figure 9 relative to the desired response. The selected response with augmentation, toward the low-frequency and low-damping-ratio boundaries, was purposeful. Much higher control-system gains were required to provide longitudinal response at the center of the desired response region. Problems with regard to control-surface deflection limits would result and pilot commands would be restricted to avoid rate saturation.

The approach taken to achieve the desired longitudinal response is shown by the diagram at the top of figure 8. The analysis included reasonable assumptions for instrument and actuation system characteristics. A control function was determined by using pitch angular



acceleration, pitch angular rate, and lagged angular-rate feedbacks. The control function was mechanized in such a manner that only the forward gain was varied; the gains associated with angular acceleration, angular rate, and lagged angular rate were each changed in the same proportion. These proportions remained fixed for the entire flight. The variable gain element in the forward control loop must be adaptive and must be adjusted as a function of a particular error criterion, depending upon the adaptive method used. Pitch-axis gain changes of the order of 10:1 were required for the range of flight conditions shown.

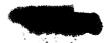
A similar approach was used in mechanizing the lateral-directional control. Yaw rate and yaw angular acceleration (not shown in fig. 8) were used for yaw control. Roll rate and lagged roll rate were used for roll control. Gain ratios were formed which remained constant during the flight and only the forward gain parameter was varied in each axis. Roll gain changes of about 20:1 were required. However, the selected gains were slightly high, since the desired damping for normal operation (from fig. 6) was about 0.3 to 0.5 rather than 0.5 to 0.7 as shown in figure 8.

Flight-Path Control

One area of outer loop control that has received considerable attention is energy management or range control. As defined here, the problem is concerned with:

- 1. Range control by proper management of energy to insure that the vehicle arrives at the landing site within permissible tolerances
- 2. Correction of errors in initial conditions and range errors resulting from deviations from expected atmospheric properties and aerodynamic parameters
- 3. Control of the flight path to maintain a safe margin above the reentry heating boundary

The Dyna-Soar will be landed manually with visual, voice, or radar contact with ground. Therefore, the problem of energy management is concerned with the period of flight from boost termination to a terminal position and velocity from which landing can be accomplished. In phase I studies, this was assumed to be a 100,000-foot altitude and a velocity of 4,000 ft/sec. Between these limits the stored energy is almost totally kinetic and some form of velocity control appears desirable. Velocity control as a function of range to go proved satisfactory. Control was achieved by varying the vehicle angle of attack to change lift and drag forces.



This range-control concept is illustrated in figure 10. The nominal flight path lies approximately midway between the trajectories for $^{\rm C}{\rm L}$,MAX and $^{\rm C}{\rm L}$ for $({\rm L/D})_{\rm MAX}.$ The angle of attack required for the nominal path is programed before the flight as a function of velocity or range to go. In figure 10, the vehicle is shown off the nominal path at a velocity less than the programed velocity. If the vehicle continued to fly the nominal angle-of-attack program, it would fall short of the desired terminal condition. Path corrections are made in the following manner. A change in angle of attack $\Delta\alpha$ is computed from comparison of the measured or actual velocity $V_{\rm M}$ and the programed velocity Vp, where Vp is a function of the range to go. For the condition shown in figure 10, the commanded angle of attack would be reduced from the nominal value. With this change, the vehicle would fly at a higher L/D to reduce the velocity error to zero.

Damping of the altitude oscillation is provided by a function of altitude rate ħ. Altitude rate, temperature rate, and forward acceleration are each a possible data source of the proper phase to provide the damping function. Altitude rate was selected because it is readily available from the inertial guidance system. Steady-state altitude rate signals would be filtered to avoid bias errors during the gliding descent. Since the vehicle seeks the right density for equilibrium glide, safe margin above the heating boundary at hypersonic speeds is inherent with this energy-management concept, provided altitude oscillations are adequately damped. Also, appropriate altitude limits relative to heating restrictions must be applied.

Flight-path stability and vehicle performance during reentry and glide, with velocity control used for energy management, are shown in figure 11. These examples were taken from analog simulation studies. Perfect guidance was assumed and trajectory calculations were based on a spherical earth. The terminal condition was an altitude of 100,000 feet and a velocity of 4,000 ft/sec. Controlled reentry trajectories with excessively large initial velocity errors of -300 and 200 ft/sec from the nominal initial velocity of 23,800 ft/sec are shown to indicate the control capability. In this series of tests the vehicle angle of attack was changed as a function of range error, that is, the difference between predicted range (based on the nominal programed path) and required range (based on knowledge of present position and destination).

The information in figure 11 is repeated in figure 12 in terms of velocity and altitude. It can be seen that the vehicle is controlled to a safe margin above the heating limit with altitude response well damped in spite of the very large initial velocity error. From these simulation tests, it was concluded that the controlled vehicle was





stable and could accommodate the range of reentry errors shown in table I with less than 2 percent error in velocity and altitude at zero range to go:

To this point the discussion has been of the reentry phase. Actually, range control must be continuous from launch. So far as the glider alone is concerned, range control must be initiated immediately after boost termination. As shown in the paper by James S. Lesko, the total range control available after boost termination (for the nominal once-around mission; launch at Cape Canaveral to landing at Edwards Air Force Base) was 21,000 nautical miles and -10,000 nautical miles. After reentry the range-control capability was reduced to about ±3,000 nautical miles. Range errors resulting from tolerances in end-of-boost conditions and possible deviations from standard atmospheric properties and expected aerodynamic drag are summarized in table II. The predominant error sources, air density and predicted vehicle drag coefficient, define the requirement for initiating glider range control immediately after boost termination since the possible error exceeds the control available after reentry. The effectiveness of the range control system, velocity controlled as a function of range to go, in minimizing range errors during flight from the end of boost to reentry is shown in table III. As in the study of the reentry phase, perfect guidance was assumed. Trajectory calculations are based on a spherical rotating earth.

CONCLUDING REMARKS

Desired handling qualities can be provided throughout the flight regime with stability augmentation. Handling qualities of the basic vehicle without stability augmentation appear satisfactory for emergency operation. However, additional work is required to define minimum handling-qualities requirements more precisely for hypervelocity gliders. As additional knowledge on the requirements is gained, it will be applied to the configuration development.

Flight control and guidance systems have not been selected for the Dyna-Soar vehicle. Controlled-vehicle characteristics have been presented as typical of those that can be attained by adaptive flight-control system.

The energy-management system in which velocity control is used as a function of range to go is shown to be feasible and must function from the end of boost for adequate range control. Perfect guidance accuracy was assumed in the data presented. A guidance error analysis has also





been made for the Dyna-Soar. Summarizing from the paper by James S. Lesko, the principal guidance errors are reflected in range errors of ± 2 nautical miles downrange and ± 6 nautical miles crossrange for the nominal once-around mission.

REFERENCE

1. Breuhaus, W. O., Reynolds, P. A., and Kidd, E. A.: Handling Qualities Requirements for Hyper-Velocity Aircraft. Rep. No. TC-1332-F-1 (Preliminary), Cornell Aero. Iab., Inc., Sept. 30, 1959.

L

l

1

13





TABLE I

RANGE CONTROL AFTER REENTRY

REENTRY CONDITION -TERMINAL CONDITION

ALTITUDE, FT

400,000 ± 100,000 100,000 ± 2,000

VELOCITY, FPS

23,800 + 200

4,000 ± 80

FLIGHT-PATH ANGLE, DEG 0 ± .5

TABLE I RANGE ERRORS ONCE-AROUND MISSION

ERROR SOURCE	3σ ERROR	RESULTING RANGE ERROR, NAUT. MI.	
DRAG COEFFICIENT DENSITY	-10% 10% -50%	2,100 6,000	-1,800
VELOCITY AT	50% -9FPS	800	-2,400
BOOST BURNOUT FLIGHT PATH ANGLE AT BOOST BURNOUT	9FPS 0I2° .0I2°	200	-800 -200
ALTITUDE AT BOOST BURNOUT	-1,000 FT 1,000 FT	400	- 400
OVERALL 30 RAI	6,400	-3,100	

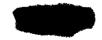


TABLE III.

RANGE CONTROL

END OF BOOST TO REENTRY (23,000 FPS)

CONDITION		Δ RANGE, NAUTICAL MILES		
		NO CONTROL	CONTROLLED	
ΔDENSITY, PERCEN	NT { 50 -50	-2,332 5,724	-16.3 O	
ΔC _D , PERCENT	{-10	-1,650 1,810	8.2 7	

TRIMMED AERODYNAMIC CENTERS

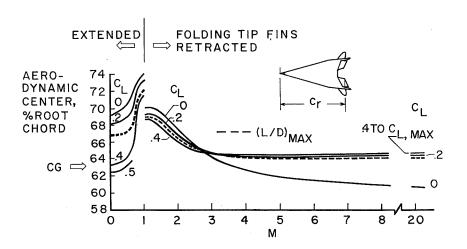


Figure 1

TRIMMED LIFT COEFFICIENT

$$\left(\frac{L}{D}\right)_{\text{MAX}}$$
 AND $C_{\text{L, MAX}}$

---- FOLDING TIPS EXTENDED
----- FOLDING TIPS RETRACTED

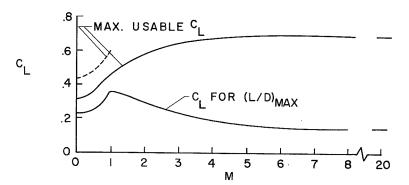


Figure 2





LONGITUDINAL SHORT-PERIOD FLYING QUALITIES NO STABILITY AUGMENTATION

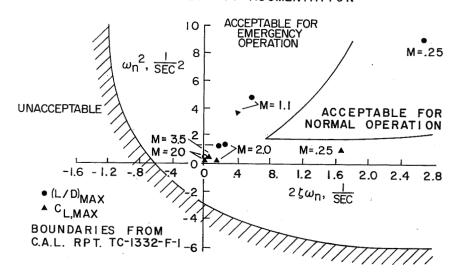


Figure 3

LONGITUDINAL SHORT-PERIOD DYNAMICS NO STABILITY AUGMENTATION

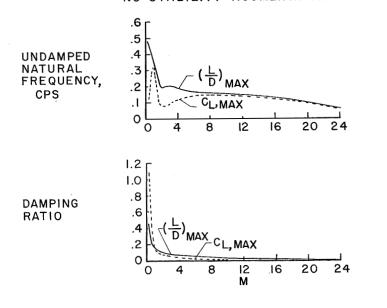
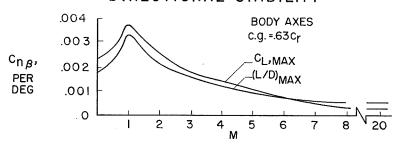


Figure 4



DIRECTIONAL STABILITY



DIHEDRAL EFFECT BODY AXES C.g. = .63C_r Cl_B, PER -.001 Cl_B, PER -.003 1 2 3 4 5 6 7 8 20

Figure 5

LATERAL-DIRECTIONAL FLYING QUALITIES NO STABILITY AUGMENTATION

BOUNDARIES FROM C.A.L. RPT. TC-1332-F-I

- $(\frac{L}{D})_{MAX}$ conditions
- ▲ C_{L, MAX} CONDITIONS

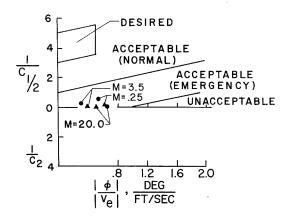
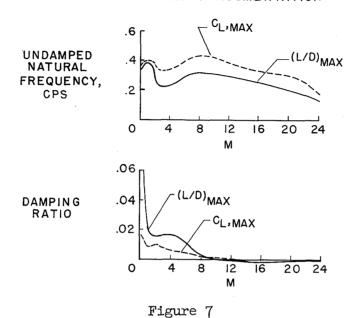


Figure 6

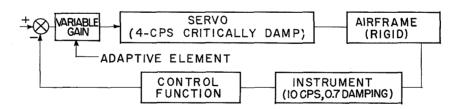




LATERAL OSCILLATION DYNAMICS NO STABILITY AUGMENTATION



LONGITUDINAL AND LATERAL HANDLING QUALITIES WITH AUGMENTATION



MODE	FLIGHT	RESPONSE			CONTROL FUNCTION
MODE	CONDITION	f _n ,	ζ	ELEMENT	SONTHOE TONGTON
		CPS			
LONGITUDINAL	REENTRY	0.46	0.49	5.0	$\frac{s^2}{10} + s + \frac{2s}{s + 0.3}$
	APPROACH	.52	.61	.3 .52	$\frac{10}{10} + 5 + \frac{1}{5} + 0.3$
	LANDING	.46	.58	.52	
				_	S + 1.9 S S + 0.3
LATERAL	REENTRY	0.5	0.5	2.1	
	APPROACH	.46	.68	.11	(RUDDER LOOP CLOSED)
	LANDING	.53	.63	.14	

मigure 8





LONGITUDINAL SHORT-PERIOD FLYING QUALITIES WITH STABILITY AUGMENTATION

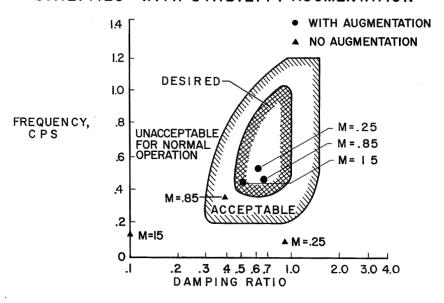


Figure 9

ENERGY-MANAGEMENT CONCEPT

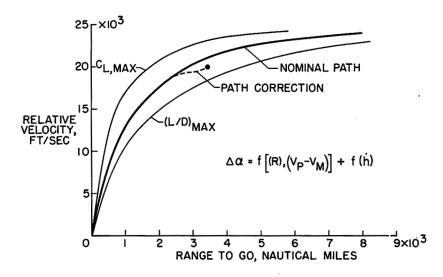


Figure 10





CONTROLLED GLIDER REENTRY

INITIAL CONDITIONS: h=400,000 FT; γ_0 =0°; α =44.3°

RANGE TO GO, NAUT. MI.

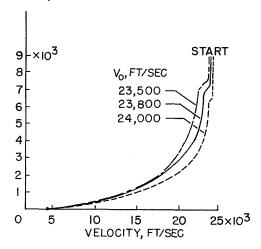


Figure 11

CONTROLLED GLIDER REENTRY

INITIAL CONDITIONS: h=400,000 FT; γ_0 =0°; α =44.3°

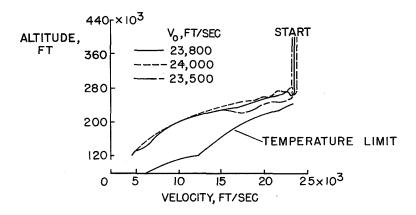


Figure 12



SELF-ADAPTIVE FLIGHT-CONTROL STUDIES

APPLICABLE TO DYNA-SOAR

By 1st Lt. Philip C. Gregory, USAF Wright Air Development Division

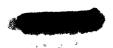
INTRODUCTION

This paper presents a summary of the requirements for, and the advantages to be obtained from, a self-adaptive flight-control system. A review of a research program to design and build a self-adaptive system for the X-15 is made. This program, while not directly connected with the Dyna-Soar program, will furnish information that will be of value in resolving Dyna-Soar flight-control design problems.

DISCUSSION

During the past several years there has been a growing realization that development programs were not producing optimum flight-control systems. This condition exists because of the greater extremes of environment through which aircraft are operating. These extremes cause changes in the aircraft-response characteristics, as shown in the previous paper by A. H. Lee and L. J. Mason, which must be compensated for by changes in the autopilot parameters if satisfactory response is to be maintained at all flight conditions.

Several methods are available to change these autopilot parameters. At present, in most operational supersonic aircraft, the required changes are made in a predetermined fashion based upon air-data measurements as shown in figure 1. Several inadequate features of these adjustments should be emphasized. First, accurate and detailed information about the aircraft stability derivatives is required for the entire flight regime. Second, the capability must exist for measuring air data for all flight conditions. Third, the calculation of the required adjustments is a long process and must be confirmed by flight-test data. Fourth, subsequent changes in airplane configuration, such as a change in vertical-tail area to improve performance, will require additional autopilot testing and adjustment. After flight test the autopilot will



work satisfactorily at the conditions at which it was tested provided degradation of components, such as the hydraulic servo valve, is held to a minimum.

When the flight profile is sufficiently well known, for instance, that of an ICBM, the changes in autopilot parameters can be made as a function of time and, thus, eliminate the need for accurate measurement of air data; however, because of unknown factors regarding the exact stability derivatives, the autopilot must be designed with some margin for stability. Thus, the system will not operate to its full capability at all flight conditions. In each of the systems described, there is no guarantee of true relationship between the changes in autopilot parameters and vehicle stability other than flight test.

L

1

1

Obvious problems concerning the design of flight-control systems for advanced vehicles arise. A vehicle such as the Dyna-Soar must perform satisfactorily on the first flight. The vehicle must operate through regions where air data are not available, and the flight profile cannot be predetermined for time-based parameter changes. Also, there is the problem of maintaining dynamic performance through unexpected changes in structure from hard-to-predict sources, such as aerodynamic heating.

In order to solve these problems, the Air Research and Development Command (ARDC) initiated a program in 1956 to determine methods of adjusting autopilots in a closed-loop fashion, which required no airdata measurements, by direct measurement of system performance. These systems have been called self-adaptive controllers. A self-adaptive system is defined as one which has the capability of changing its parameters through an internal process of measurement, evaluation, and adjustment to adapt to a changing environment, either external or internal to the vehicle under control (ref. 1).

Several self-adaptive techniques were studied under WADD contracts and some of these have been flight-tested in century-series aircraft to demonstrate their practicality. A flight test of one system developed by the Minneapolis-Honeywell Regulator Company has shown that the effect of aerodynamic-parameter changes on the performance of a flight-control system can be minimized by raising the loop gain to increase the system bandwidth. Figure 2 shows a technique for keeping the system gain at the highest possible value without incurring system instabilities. Note that this technique uses no air-data scheduling. Figure 3 illustrates how the gain controller operates. A nonlinear high-gain characteristic K_0 is furnished by a variable-gain amplifier with clipped outputs. The filter and lead network insure that the first element to become neutrally stable as the loop gain is increased will be the hydraulic servo. When the gain has been raised to its critical value, the servo will exhibit a



characteristic motion or limit cycle. This motion is picked up by the band pass filter, demodulated, and compared with a fixed reference. Any difference in these signals will cause the gain to be lowered or raised through the integrator gain control. In the absence of any input from the servo, the reference bias will slowly drive the loop gain up until limit cycling occurs. In this manner, the system can be operated at the highest gain possible for all flight conditions.

Because of the high loop gain the response of the flight-control system is much more rapid than that which A. H. Lee and L. J. Mason showed in the previous paper would be desired by the pilot; therefore, an electronic model or prefilter is inserted as shown in figure 2. This model is a simple second-order system which is set at the natural frequency and damping ratio desired by the pilot. Note that this system does not require the usual gain margin associated with conventional systems because the closed-loop gain-changing feature permits operation just below the critical level throughout the flight regime. Operation at a higher gain produces a significant improvement in dynamic performance and makes the control system far less sensitive to changes in vehicle characteristics.

L

1

1

1.

Since June 1959, the Minneapolis-Honeywell Regulator Company has been studying, under the sponsorship of WADD, some of the automatic flight-control problems associated with boost-glide weapon systems. The first phase of this effort was to determine and to define the type of pilot-assist modes which would be of value and how they would be used in a mission profile. The next phase is to design a self-adaptive autopilot employing the technique previously described to furnish those modes which could be flight-tested in an X-15. The last phase would be to build and flight test such a system in an X-15.

In previous research aircraft, such as the X-15, the flight-control philosophy has been to design a simple, reliable damper system to assist the pilot. In future military vehicles which will follow the Dyna-Soar, a system of this type falls far short of what is required. The pilot will have to perform duties other than flight control, such as energy management, navigation, and a military mission. In order to secure sufficient time for these other duties, an automatic flight-control system will be required. It is such a system which is now being designed and built for flight testing in the severest flight-control environment available, the X-15. Figures 4 to 6 are tentative block diagrams of the X-15 self-adaptive system now being designed.

The X-15 flight-control system is composed of three subsystems. The minimum-flight system (MFS) furnishes stability augmentation, includes the self-adaptive feature, integrates reaction and aerodynamic control in one stick, and permits the pilot to put mechanical inputs



into the flight-control system. The piloted-flight system (PFS) contains the pilot-assist modes, control-stick steering (CSS), angle of attack, altitude, and altitude holds. The basic stability loop utilizes a pitch-rate feedback, and normal acceleration is blended with this in the CSS mode. The proposed automatic-flight system (AFS) is being studied and designed under separate procurement and would include onboard computing equipment to provide such functions as energy management and automatic approach and landing.

Figure 7 shows the control modes and the control variable utilized throughout the different flight phases. For example, in the first phase of flight the MFS utilizes high-passed pitch rate, roll rate, and high-passed yaw rate plus lateral acceleration for stability augmentation. The pilot command mode of the PFS is accomplished with normal acceleration plus pitch rate and roll rate.

Ι

1

1

1

The flight-control system being designed for test in the X-15 must have more than good dynamic performance. It must demonstrate high reliability. A reliability analysis based on a 1-hour mission of the MFS pitch channel shows a mean time between failure (MTBF) of 515 hours for single-channel operation. If a redundant configuration such as the one shown in figure 8 is used, the MTBF is increased to 925 hours. reliability is in effect the reliability of the hydraulic servo which is a series element in the control system. This reliability figure is based on the premise that not more than one failure of the hard over or shorted type will occur in the triple redundant networks. It can be postulated that the gain changes will compensate for up to two open or "dead" type failures or one hard over failure with no loss in system performance. Most electrical failures are of the open or "dead" type (ref. 2). This capability is achieved because any one electrical network can provide the maximum required signal and because the gain changer will raise the gain of any remaining channel to compensate for failures. Even in the case of a single remaining channel or a nonredundant system, the self-adaptive feature will compensate for deterioration, to the point of failure, of components by raising the forward loop gain.

A three-axis self-adaptive system similar to the one described for the X-15 has been flight tested on an F-101. This system was built by the Minneapolis-Honeywell Regulator Company and is presently being flight evaluated by WADD, NASA, and AFFTC pilots. The WADD pilots have reported the system performance as excellent. It has given constant response at all flight conditions, and the pilots have not been able to detect the limit cycle operation. Figure 9 is a flight recording taken from this aircraft showing step commands into the roll axis. Note the operation of the roll and pitch gain as the limit cycle appears on the aileron and pitch servos and the difficulty of detecting the limit cycle from the system noise. Actually, amplitudes of the noise and limit cycle are almost identical;



however, the limit cycle can be detected by looking for its characteristic frequency of 4 cycles per second. Flight data have demonstrated the operation of the gain changer in compensating for the deterioration of components. Thus, one reason besides dynamic performance for the use of a self-adaptive technique would be increased reliability.

An important consideration in the design of any autopilot is the amount of attention required of the pilot for satisfactory performance in mission profiles. Figure 10 shows the pilot workload for an X-15 profile with self-adaptive stability augmentation only. Note that workload does not indicate the effort required of the pilot, either mental or physical, but rather the time spent in performing a function. The self-adaptive stability augmentation furnishes constant performance at all flight conditions and has blended aerodynamic and reaction control. Figure 11 shows the same mission profile flown with a complete autopilot including control-stick steering and altitude, attitude, and angle-of-attack hold functions. There is a sharp decrease in the amount of pilot workload required to accomplish the mission with the complete autopilot; thus the pilot is free to direct or oversee the operation of other equipment required for a military mission.

L

1

1

4

The results of the X-15 study and simulation and the F-101 flight test have shown that a self-adaptive flight-control system will provide the response required for mechanization of these outer loops without scheduling and will permit reduction of pilot workload.

Before initiating the program described, it was first necessary to establish that the range of dynamic conditions and the control problems encountered in the X-15 test vehicle would be comparable enough with the Dyna-Soar and other future vehicles to make the results of a test program of practical value.

A two-degree-of-freedom short-period comparison of the natural-frequency-and-damping ratio of the X-15 and a typical Dyna-Soar vehicle was made (ref. 3). The X-15 trajectory chosen for study is a typical maximum-altitude flight. The X-15 was boosted to a peak velocity of 6,400 ft/sec and an altitude of 250,000 feet. The boost phase of the Dyna-Soar trajectory was not studied, since differences in the two vehicle configurations do not permit sound comparisons. The Dyna-Soar trajectory used had a peak velocity of 2^4 ,000 ft/sec at an altitude of 250,000 feet and followed an $(L/D)_{MAX}$ trajectory, modified through the heating range to keep the temperature within specified limits. A 9,000-pound vehicle with a delta-wing area of about 330 square feet was used as a representative Dyna-Soar. Perfect lateral stability was assumed for both the X-15 and Dyna-Soar.

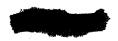


Figure 12 shows a comparison of dynamic-pressure variations with time for the X-15 and the Dyna-Soar at the critical reentry regions along the respective trajectories. It can be seen that the dynamic pressure of the X-15 changes much more rapidly than that of the Dyna-Soar and has a greater total variation.

Another important criteria affecting autopilot design is the product of ζ the damping ratio and ω_n the undamped short-period natural frequency. This product can be used to compare the speed of response of the airframes, and as shown in figure 13 the product varies over a wide range for both vehicles. The stability derivatives used to calculate ω_n and ζ time histories were estimated from data supplied by North American Aviation, Incorporated, and the Dyna-Soar contractors.

It can be seen from figures 12 and 13 that the total variations of two of the control parameters which are normally specified for autopilot design are greater for the X-15 than for the Dyna-Soar during reentry and change more rapidly for the X-15. This rate of change will be a factor in determining what type of self-adaptive autopilot technique should be selected. Since the rate of change of $\omega_n \zeta$ is much greater for the X-15, a self-adaptive technique capable of adjusting to the changing parameters of the X-15 should work for the Dyna-Soar.

In orders of magnitude of period and damping, the Dutch roll case is comparable to the longitudinal short-period mode and the same general conclusions are applicable at low angles of attack for both vehicles.

From this analysis, it was concluded that a self-adaptive control system was feasible for the X-15 and that flight test of such a system would gain data of value for use on later vehicles such as the Dyna-Soar.

The present schedule (fig. 14) calls for installation of the adaptive equipment in an X-15 in February of 1961 with flight test of the system starting in May of 1961. This airborne equipment will be supported by a complete set of ground-support equipment for checkout and maintenance. Presently, the system to go in the X-15 has been breadboarded and is being operated on the X-15 simulator. At the conclusion of these tests this month, design and fabrication of the airborne equipment will start.

The operation of this equipment during the summer of 1961 should provide timely information for confirming design techniques of a flight-control system which could be used in the Dyna-Soar.





CONCLUDING REMARKS

A self-adaptive control system has several advantages over a linear control system even when the design dynamic performance of both is acceptable.

A self-adaptive system furnishes more margin for error regarding the knowledge of stability derivatives and the effects of aerodynamic variations and structural heating not yet fully defined.

The system integrates aerodynamic and reaction control and provides the possibility of greater reliability through redundancy. It provides a stable, nonvarying inner loop which permits the design of outer loops without scheduling, which will relieve the pilot workload and permit operation of more sophisticated onboard computing systems.

A self-adaptive system requires less redesign and will adjust and operate correctly with less performance testing when vehicle configuration changes are made; thus it has greater growth potential.

A self-adaptive system designed and flight-tested in the X-15 will provide useful information for the Dyna-Soar program.

REFERENCES

- 1. Gregory, P. C., ed.: Proceedings of the Self Adaptive Flight Control Systems Symposium. WADC Tech. Rep. 59-49. ASTIA Doc. No. AD209389, U.S. Air Force, Mar. 1959.
- 2. Connors, A. J., and Ekern, H. O.: Comparison of Dyna-Soar and X-15 Longitudinal Dynamics. WADC TN 59-213, U.S. Air Force, June 1959.
- 3. Keyt, F. Gene: Electrical Primary Flight Control Systems. Paper No. 59-99, Inst. Aero. Sci., June 16-19, 1959.





LINEAR DAMPER

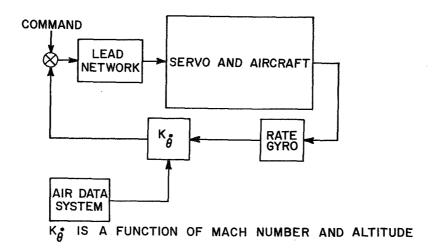
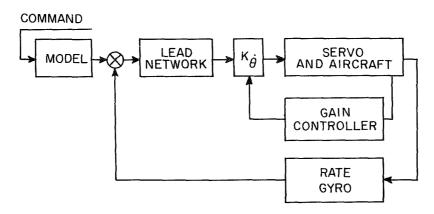


Figure 1

ADAPTIVE DAMPER



 $\kappa_{\dot{\theta}}$ is varied automatically as a function of system performance

Figure 2



 $^{2}\Delta_{\mathbf{A}^{\prime}}$



DIAGRAM OF ADAPTIVE LOOP

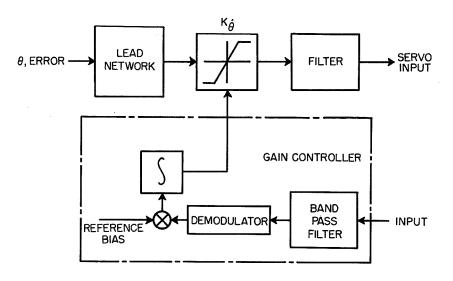


Figure 3

X-15 PITCH AXIS CONTROL SYSTEM

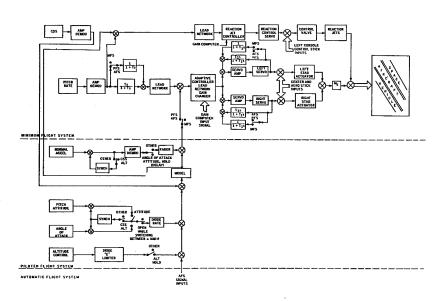


Figure 4



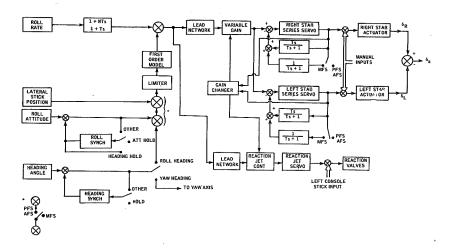


Figure 5

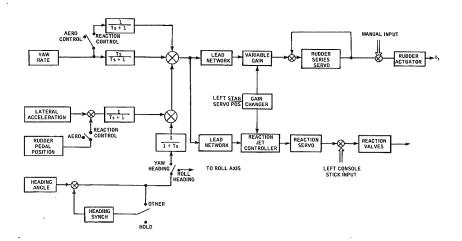


Figure 6



CONTROL MODES

θ _H - high-pass	pitch	rate
PH- high-pass	roll ro	ite

^гн - high-pass yaw rate

ay-lateral acceleration nz-normal acceleration

θ -pitch rate

P -roll rate

CSL command signal limiting (α, n)

θ - pitch attitude α -angle of attack

ø −roll attitude

y - yaw orientation

PHASE OF FLIGHT	MFS AUGMEN- TATION	PILOT COMMAND	S HOLD	AFS COMMAND GUIDANCE
PHASE I LAUNCH (TAKEOFF)	<i>θ</i> _H P	n _{z + $\dot{\theta}$}	O: or O Ø, W	AUTO NAVIGATION
EXIT (PULLOUT)	rH + a y			AUTO EXIT
BURNOUT		ALTITUDE	HOLD OPTI	ONAL CSL
PHASE I	ė	$n_Z + \theta$	ar a	
BALLISTIC	Р	P	ø	AUTO-NAVIGATION
SEMI-ORBITAL	r	r	ψ	ALTITUDE CONTROL
ORBITAL			CSL	
PHASE III	θH	nz + 0	Ocor O	
RE-ENTRY	P	P	φ. ψ	AUTO RE-ENTRY
CONSTANT g	rH + a4			
CONSTANT ∝				l
EQUILIBRIUM GLIDE	l .	AUTO DRAG	BRAKE - Q	LIMITING CSL
PHASE IX	θΉ	$n_z + \theta$	θ	AUTO APPROACH
DECELERATION	P	P	ø, ¥	
GLIDE	r _H + ay			AUTO FLARE-OUT
LAND		ALTITUDE	HOLD OPTIC	DNAL CSL

Figure 7

MECHANIZATION FOR RELIABILITY

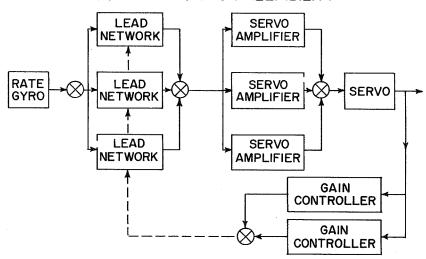


Figure 8



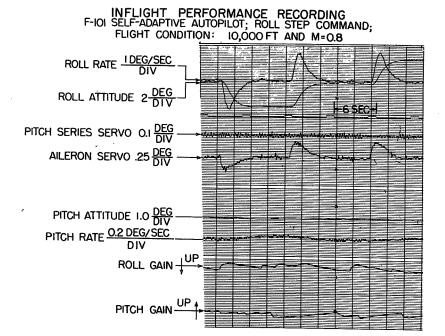


Figure 9

PILOT WORKLOAD WITH BASIC ADAPTIVE SYSTEM

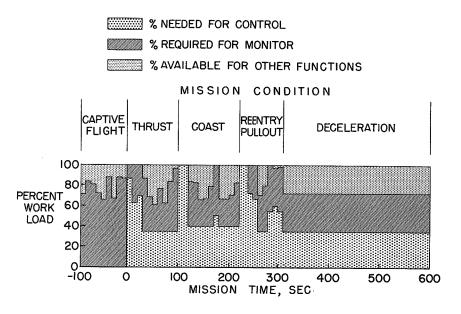
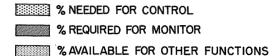


Figure 10



PILOT WORKLOAD WITH PILOT-ASSIST FUNCTIONS



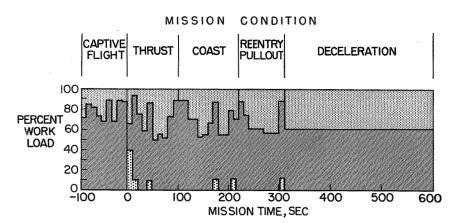


Figure 11

VARIATION OF DYNAMIC PRESSURE WITH TIME

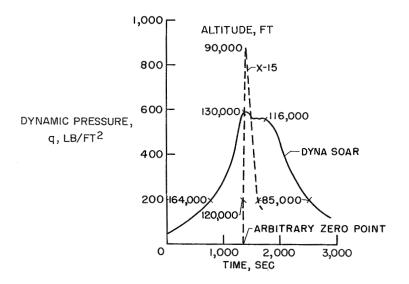


Figure 12





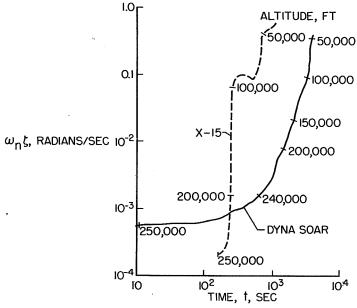


Figure 13

	SPACE FLIGHT CONTROL PROJECT SCHEDULE
	J J A S O N D J F M A M J J A S O N D J F M A M J
Р И (уляру) FCS	Prelim Ret 1st Prelim Ret Phese I
P H S I (STUDY) FCS GSE Use of X-15 6° Sim	Prelim. Rot. Ist Vr. Final Final Rot. Phose I
E Use of X-15 6° Sim. Use of WADD Enviro.	——————————————————————————————————————
7	Prelim Brut - Final Ret Final Ret - Phase II
71 (1961/1947)	
A II Superior GSE Use of X-15 6°Sim. Use of WADD Enviro.	Delivery FCS
P (GARRICATION) FCS	×
FABRICATION) FCS GSE Use of WADD Enviro.	Pretim Funding to arder \ Delivery 6SE big lead time Hems
	big lead time items
P (INSTALLATION) A III (& CHECK OUT)	
SE Use of X-15 6° Sim. Use of WADD Enviro.	
FUGHT TEST_	
ž (hirtiel Flight Test

Figure 14



ACCURACY OF AERODYNAMIC-HEATING PREDICTIONS

By A. L. Nagel and R. A. Hanks Boeing Airplane Company

INTRODUCTION

It has been shown in previous discussions that aerodynamic heating has a major role in determining the performance and safety of the Dyna-Soar vehicle. A careful examination of the methods which have been used to calculate aerodynamic heating rates during reentry, and a comparison of those same methods with test data is a necessary part of performance evaluation.

SYMBOLS

D	leading-edge or nose diameter
h	enthalpy
k	conductivity
$N_{\mathtt{Pr}}$	Prandtl number
$N_{ ext{Le}}$	Lewis number
р	pressure
q	heat flux
r	radius
R	Reynolds number
T	temperature
u	velocity
x	coordinate
Λ	sweep angle





μ	viscosity	98
ρ	density	
Subscript	s:	·*₹
D	fraction in dissociation; based on diameter	
EXP	experimental	
е	exterior condition	
r	recovery	
S	stagnation point or line value	
TH	theoretical value	مو
w	evaluated at wall temperature	
∞	free-stream value	ing.
0	stagnation condition	

DISCUSSION

The most severe heating rates on winged hypersonic vehicles will occur at the nose and leading edges. The areas involved are relatively small, however, and may admit structural solutions (local cooling or refractories) which are not practical for the remainder of the vehicle. In such a case, the lower-surface material at its most forward point may also become a critical heating point, and may be nearer its temperature limit than either the nose or the leading edge. Other points which would have high local heating rates would be protrusions below the lower surface, such as ventral fins or a dihedral ridge line. Some early Dyna-Soar configurations had such features and were eliminated for that reason. By the end of the Phase I studies, both the Boeing and the Martin-Bell teams had arrived at configurations having simple geometry in regions of high heat transfer. Upper surface complications are less important as the overall heating level for the upper surface is very much lower than for the lower surface. The present Dyna-Soar configuration has only four critical heating points. These are indicated in figure 1 as the nose, the leading edge, the lower surface just aft of the nose, and the dorsal leading edge of the fin, which is critical at low angles of attack.



Complete simulation of the reentry environment is not possible in any of the ground facilities which must be used to provide the bulk of heat-transfer test data. For this reason extrapolation of the test results to the flight condition by some theoretical method is necessary. The study of prediction accuracy cannot be limited to an examination of the data scatter, but must include an evaluation of the theoretical method as well. The combination of a rigorous theoretical approach and test data taken in facilities which simulate the important aspects of the flight environment allows a high degree of confidence in the prediction. In other cases, the theory may be too idealized to lend credence to extrapolations.

Heat-Transfer Equations

The equations used for calculating laminar heating rates both for the reentry condition and for the following comparisons with test data are:

$$q_s = Const. \frac{\sqrt{\rho_e \mu_e}}{N_{Pr} 0.6} \left(\frac{\rho_w \mu_w}{\rho_e \mu_e}\right)^{0.06} \sqrt{\frac{du_e}{dx}} \left[1 + \left(N_{Le}^{0.52} - 1\right) \frac{h_D}{h_e}\right] (h_r - h_w)$$
 (1)

$$q = \frac{q_s}{2} \frac{\left(\frac{p}{p_s}\right) \left(\frac{u_e}{u_\infty}\right) r \sqrt{\frac{u_\infty}{du_e/dx}}}{\left[\int_0^x \left(\frac{p}{p_s}\right) \left(\frac{u_e}{u_\infty}\right) r^2 dx\right]^{1/2}}$$
(2)

The constant in equation (1) is 0.793 for the axisymmetric stagnation point and 0.576 for the two-dimensional stagnation line. Equation (2) is used for calculating heat-transfer rates away from the stagnation point. Both equations (1) and (2) are from the work of Kemp, Rose, and Detra, (ref. 1) which is an extension of the earlier work of Fay and Riddell (ref. 2). These equations were selected as a basis for reentry-heating calculations because they are the most rigorously developed methods available, and because they are in good agreement with the test data, as will be shown. The expressions were originally obtained by numerically integrating the boundary-layer equations, using the real-gas equation of state and the Sutherland viscosity law. The cases specifically considered corresponded to the axisymmetric stagnation point, the unswept stagnation line, the flat plate, and a limiting pressure gradient case. Applying simple geometric corrections for flow pattern allows the results to be used for swept leading edges as well.



Calculations by Beckwith (ref. 3) have further shown that equation (1) also results from ideal-gas calculations for both the swept and unswept leading edges except that the Lewis number term is, of course, missing.

The velocity gradient used in applying equation (1) was based on the modified Newtonian pressure distribution, which is within a few percent of the best known values. Equilibrium dissociation was assumed and the values of viscosity calculated by Hansen (ref. 4) were used, and the Lewis number was taken as 1.4. Use of the higher viscosity values has been found to improve agreement with test data. Evaluated in this way heat-transfer rates are 5 to 15 percent higher than those obtained by the method of Fay and Riddell in reference 2.

L

1

1

5

Since the calculations on which equation (1) is based assumed the Sutherland law for viscosity, use of another viscosity law might appear to invalidate the equation. Recent unpublished calculations of Beckwith and Cohen at the Langley Research Center have shown, however, that the form of the equation does not depend on the viscosity law or even upon the equation of state. It appears then, that use of equation (1) with the best available fluid properties will provide the best estimate of heat transfer.

In the form shown here, the heat-transfer distribution function (eq. (2)) depends only on the local pressure and flow velocity. Simplifying assumptions first suggested by L. Lees (ref. 5) are required to eliminate the dependence on the local transport properties and the pressure gradient. The simplification has been found to be satisfactory for shapes without sharp corners, such as the present Dyna-Soar nose.

In the original development, equation (2) was intended for application to two-dimensional or axisymmetric bodies at zero angle of attack. Application to less simple shapes can be accomplished by replacing the radius terms with an equivalent radius which expresses both the body shape and the streamline pattern which occurs on it.

Equations (1) and (2) supply the required laminar flow heatingrate estimates at all the critical points. At the nose and forward
lower surface the Reynolds number is in the range for which laminarflow heating rates are higher than the turbulent flow rates. The
leading edge, however, is limiting in turbulent flow at velocities
less than about 19,000 ft/sec. It might appear at first that turbulent flow cannot exist at the leading-edge stagnation line. This is
not true for the swept leading edge, as the flow along the stagnation
line can become turbulent. The possibility of turbulent low leadingedge heating rates must therefore be considered in aerodynamic heating
calculations. The tendency of the boundary-layer secondary flow to



promote transition at very low Reynolds numbers makes it especially important to consider turbulent boundary-layer flow. The expression used to calculate turbulent leading-edge heat transfer for the reentry condition as well as for the comparisons with wind-tunnel data which follow is:

$$q_{s} = 0.1343 \frac{k_{\infty}}{D} (R_{\infty,D})^{0.8} (N_{Pr})^{1/3} \left(\frac{\mu_{w}}{\mu_{o}} \frac{T_{\infty}}{T_{w}} \frac{p_{e}}{p_{\infty}}\right)^{0.8} \left[\frac{\mu_{o}}{\mu_{\infty}} \left(\frac{D}{u_{\infty}} \frac{du_{e}}{dx}\right)\right]^{0.2} \times \sin \Lambda^{0.6} (h_{r} - h_{w})$$

$$(3)$$

This expression was developed by Beckwith and Gallagher (ref. 6). A similar expression can be obtained by applying geometric corrections to turbulent-flow flat-plate theory.

Experimental Comparisons

Stagnation point. The experimental data for hemispherical stagnation point available for comparison with the theory are presented in figure 2. Data are taken from shock-tube experiments (ref. 7), wind-tunnel tests (ref. 8), and free-flight tests (ref. 9) and have been divided by the theoretical value for the same conditions. A ratio of 1.00 therefore indicates perfect correlation of theory and experiment. The data are shown to scatter from 0.65 to 1.4 times the theory with the average very nearly 1.0 over the entire velocity range. It is believed that this large scatter reflects experimental errors rather than fluctuations in the actual heat-transfer rates. This view is supported by the random nature of the scatter.

The comparison of figure 3 lends further support to this explanation of the scatter. Heat-transfer data from an Atlas (ref. 10) reentry flight are compared with the theory as a function of time. The theory and experimental curves are of similar shape and with almost identical peak values, but with an offset of about 2 seconds in time. If plotted in figure 2, these data would have shown a scatter of about 50 percent around the theoretical curve. The heat-transfer rates shown in figure 3 are calculated from the temperature response of the skin as recorded by thermocouples installed in plugs in the skin. The same characteristic lag of experiment behind theory was observed in many flights. After several other explanations had been ruled out by the consistency of the lag, similar thermocouple installations were calibrated in ground tests. Lags in heating rate were found to occur which, when extrapolated to the flight conditions, are of the same order as those observed in flight. They cannot be said to be precisely the same, as no two thermocouple installations showed exactly the same lag. However, the thermocouple lag does seem to provide a reasonable explanation of the offset. Another





point worth mentioning is in the comparison of the theory of reference 2 with these same data, which is shown to be approximately 10 percent too low at peak heating. Equation (1) was originally selected in preference to the Fay and Riddell theory on the basis of the shock-tube data presented in figure 2. Although both theories fell well within the scatter of the data, the values from the Fay and Riddell method were about 10 percent below the average of the data at high speeds. Re-evaluating the theory to improve the agreement with the average of the shock-tube data brings it into almost exact agreement with the flight data.

Hot-gas radiation heating and variation in wall catalytic effect are two effects not reflected in these data. Calculations based on best available information show that the radiative heat-transfer rate is very small compared to the convective rate for nose radii of 1 foot or less. This result is consistent with the conclusions of previous papers in this conference. The effect of wall catalytic effect may be significantly favorable if nose coating materials can be developed which do not catalyze recombination at the wall. Reductions of over 50 percent are theoretically possible. Neglecting this effect is conservative, and appears to be most realistic at present, as noncatalytic materials have not been developed.

L

1

1

1

5

Laminar distribution. Nose hemisphere and afterbody data are compared with the theory in figure 4. The agreement is shown to be satisfactory for cones (ref. 11). Recent Langley data on delta wings at angle of attack presented by Bertram and others at this conference are also in good agreement. In making these comparisons equation (2) has been used with an effective radius to correct for nonaxisymmetric shape in the manner previously suggested. This correction requires a knowledge of the streamline patterns as well as the shape of the body. For the cone, the streamline pattern is based on values from the Kopal tables (refs. 12 and 13). For the delta wing, streamline patterns were calculated from a correlation previously made of oil flow patterns obtained in delta wing tests.

Laminar leading edge. Laminar leading edge data from several wind-tunnel tests (refs. 14 to 16 and unpublished Boeing and Langley test data) are presented in figure 5. The agreement is shown to be excellent over the entire range of sweep angles. None of the experimental leading-edge data shown are in the total temperature range for which real gas effects would be distinguishable. However, the theoretical expression indicates that for the highly swept leading edge the real-gas effect is much smaller than at the stagnation point, and even for that case the predicted (and experimentally supported) effect is only 15 percent at the velocity for maximum reentry heating.

Turbulent leading edge. Experimental data (ref. 6 and unpublished Boeing test data) for turbulent stagnation-line heat transfer are compared to theoretical values in figure 6. The data are predominantly



below the theory, indicating principally the difficulty of obtaining turbulent flow on the leading edge. The low points at 10°, 20°, and 75° sweep angles are apparently transitional. The low data points taken on delta wing at angles of attack of 30° and 34° are affected by the presence of the wing, which distorts the inviscid flow field. The rest of the data are in very good agreement with the theory.

Extrapolation to the flight condition is still somewhat uncertain because the theory has assumed ideal gas relations throughout. Some information regarding the validity of ideal gas heat-transfer calculations in a real gas environment is afforded by an examination of the effect in laminar flow, for which the theory is well developed. Comparisons of ideal-gas solutions for both the stagnation point and the zero pressure gradient flat plate have been found to be within 10 percent of rigorous real-gas solutions at speeds up to satellite velocity. A more significant comparison is presented in figure 7. Experimental turbulent heat-transfer data (refs. 10 and 17 to 20) in the real-gas temperature range are compared with the ideal-gas reference temperature method. The agreement of the theory and experiment is very good over the entire velocity range. The good agreement between the normalized heat transfer in free flight and in the shock tube tends to eliminate the possibility of fortuitous agreement. This agreement also indicates that the shock tube can provide fundamental information about real-gas effects in turbulent flow just as it has been used in the past to study laminar flow stagnation point heat transfer.

CONCLUDING REMARKS

It has been shown that there exists a unified theoretical method for laminar-flow heat transfer which is applicable to critical temperature locations on the Dyna-Soar vehicle. The method rigorously includes real-gas behavior and other phenomena having significant effects on heat transfer. Test data have been presented which confirm the ability of the method to account for such effects over a wide range of conditions.

In the turbulent-flow case no similar well developed theory exists. There is, however, a compensation for this deficiency in the relative insensitivity of the turbulent boundary layer to any influence other than local pressure and velocity. Some turbulent-flow heat-transfer data in the speed range corresponding to reentry maximum heating do exist, and these data are in agreement with semiempirical methods now in use.

From these comparisons it appears that existing methods will satisfactorily predict aerodynamic heating during reentry for the critical locations on the present configuration. Further testing is required to



substantiate this conclusion with the emphasis on data for the configuration specifically chosen. Further testing is also desirable to reduce the uncertainty caused by scatter in available data. These data appear to reflect experimental errors, rather than fluctuations in actual heating rates, so that a design based on these data alone would incorporate unneccessarily large margins in temperature capability, with corresponding weight and performance penalties.

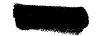
The methods used for theoretical calculations can be extended to other locations on the vehicle. As previously stated, the accuracy of calculations over the rest of the vehicle is less important, as one of the four points discussed will always be nearer its limit temperature. Future alterations of configuration or materials may cause other points to become critical.

I 1

1



42



REFERENCES

- 1. Kemp, Nelson H., Rose, Peter H., and Detra, Ralph W.: Laminar Heat Transfer Around Blunt Bodies in Dissociated Air. Res. Rep. 15, AVCO Res. Lab., May 1958.
- 2. Fay, J. A., and Riddell, F. R.: Theory of Stagnation Point Heat Transfer in Dissociated Air. Jour. Aero. Sci., vol. 25, no. 2, Feb. 1958, pp. 73-85, 121.
- 3. Beckwith, Ivan E.: Similar Solutions for the Compressible Boundary Layer on a Yawed Cylinder With Transpiration Cooling. NACA TN 4345, 1958.
- 4. Hansen, C. Frederick: Approximations for the Thermodynamic and Transport Properties of High-Temperature Air. NACA TN 4150, 1958.
- 5. Lees, Lester: Laminar Heat Transfer Over Blunt-Nosed Bodies at Hypersonic Flight Speeds. Jet Propulsion, vol. 26, no. 4, Apr. 1956, pp. 259-269.
- 6. Beckwith, Ivan E., and Gallagher, James J.: Local Heat Transfer and Recovery Temperatures on a Yawed Cylinder at a Mach Number of 4.15 and High Reynolds Numbers. NASA MEMO 2-27-59L, Apr. 1959.
- 7. Rose, P. H., and Stark, W. I.: Stagnation Point Heat-Transfer Measurements in Dissociated Air. Jour. Aero. Sci., vol. 25, no. 2, Feb. 1958, pp. 86-97.
- 8. Crawford, Davis H., and McCauley, William D.: Investigation of the Laminar Aerodynamic Heat-Transfer Characteristics of a Hemisphere-Cylinder in the Langley 11-Inch Hypersonic Tunnel at a Mach Number of 6.8. NACA Rep. 1323, 1957. (Supersedes NACA TN 3706.)
- 9. Pellet, D. M., and Hoshizaki, H.: Summary Analysis of X-17 RTV Program Aerodynamic Heating and Boundary Layer Transition. Rep. LSMD 2161, Lockheed Aircraft Corp., July 2, 1957.
- 10. Anon.: Aerothermodynamic Analysis of Mark 2 Flight Test Data Summary Report. Rep. 59SD743, Sept. 2, 1959.
- 11. Zakkay, Victor: Pressure and Laminar Heat Transfer Results in Three-Dimensional Hypersonic Flow. WADC TN 182, U.S. Air Force, Sept. 1958.





- 12. Staff of the Computing Section, Center of Analysis (Under Direction of Zdenek Kopal): Tables of Supersonic Flow Around Yawing Cones. Tech. Rep. No. 3 (NOrd Contract No. 9169), M.I.T., 1947.
- 13. Staff of the Computing Section, Center of Analysis (Under Direction of Zdenek Kopal): Tables of Supersonic Flow Around Cones at Large Yaw. Tech. Rep. No. 5, M.I.T., 1949.
- 14. Goodwin, Glen, Creager, Marcus O., and Winkler, Ernest L.: Investigation of Local Heat-Transfer and Pressure Drag Characteristics of a Yawed Circular Cylinder at Supersonic Speeds. NACA RM A55H31, 1956.
- 15. Feller, William V.: Investigation of Equilibrium Temperatures and Average Laminar Heat-Transfer Coefficients for the Front Half of Swept Circular Cylinders at a Mach Number 6.9. NACA RM L55F08a, 1955.
- 16. Cunningham, Bernard E., and Kraus, Samuel: Experimental Investigation of the Effect of Yaw on Rates of Heat Transfer to Transverse Circular Cylinders in a 6500-Foot-Per-Second Hypersonic Air Stream. NACA RM A58E19, 1958.
- 17. Rose, Peter H., Probstein, Ronald F., and Adams, Mac C.: Turbulent Heat Transfer Through a Highly Cooled Partially Dissociated Boundary Layer. Res. Rep. 14, AVCO Res. Lab., Jan. 1958.
- 18. Swanson, Andrew G., and Rumsey, Charles B.: Aerodynamic Heating of a Wing As Determined From a Free-Flight Rocket-Model Test to Mach Number 3.64. NACA RM L56Flla, 1956.
- 19. Krasnican, M. J., and Wisniewski, R. J.: Free-Flight Determination of Boundary-Layer Transition and Heat Transfer for a Hemisphere-Cylinder at Mach Numbers to 5.6. NACA RM E57FlO, 1957.
- 20. Buglia, James J.: Heat Transfer and Boundary-Layer Transition on a Highly Polished Hemisphere-Cone in Free Flight at Mach Numbers Up to 3.14 and Reynolds Numbers Up to 24×10^6 . NACA RM L57D05, 1957.





DYNA-SOAR REENTRY VEHICLE CRITICAL HEATING LOCATIONS

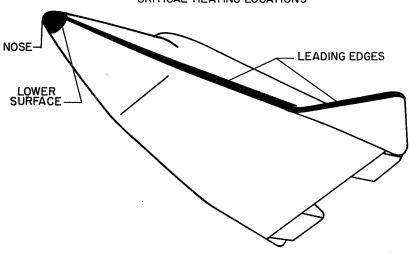


Figure 1

STAGNATION-POINT HEAT TRANSFER

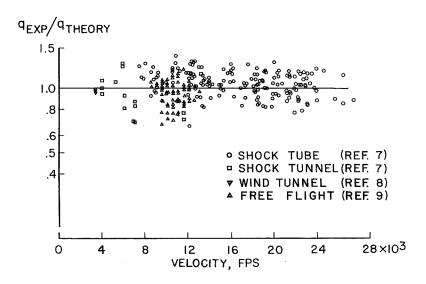


Figure 2





STAGNATION-POINT HEAT TRANSFER FLIGHT TEST DATA

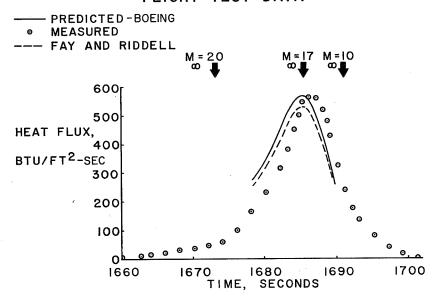


Figure 3

NOSE-AFTERBODY HEAT TRANSFER

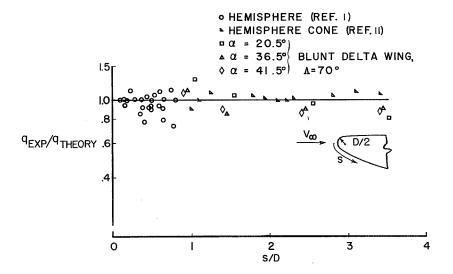


Figure 4





LEADING-EDGE LAMINAR FLOW

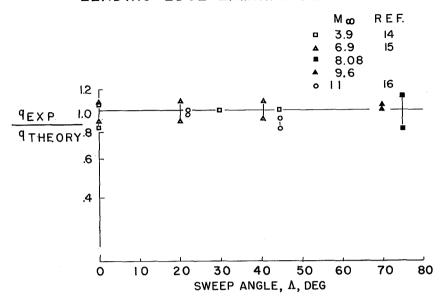


Figure 5

LEADING-EDGE TURBULENT FLOW

• SWEPT CYLINDER; $R_{\omega, D} = 10^6$; REF. 6

WING L.E.; $\Lambda = 75^\circ$; $R_{\omega, D} = 0.75 \times 10^6$; UNPUBLISHED α , DEG α , DEG

0 ∇ 23 Δ 15 \Leftrightarrow 30 D 20 D 34

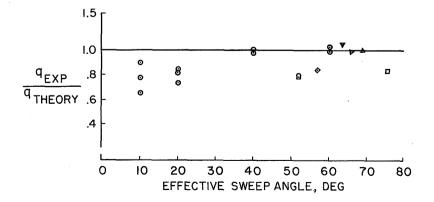


Figure 6



TURBULENT HEAT TRANSFER

- ⊾ SHOCK TUBE (REF. 17)
- FREE FLIGHT (REF. 20)
- ▲ FREE FLIGHT (REF. 19)
- FREE FLIGHT (REF. 18)
- ♦ FREE FLIGHT(REF. 10)

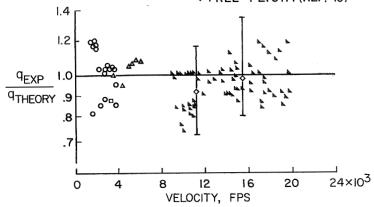


Figure 7



DYNA-SOAR-GLIDER FLIGHT-ENVELOPE STRUCTURAL PARAMETERS

By Edwin G. Czarnecki and Gordon N. Davison Boeing Airplane Company

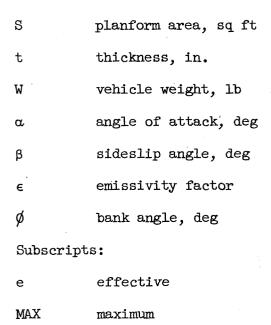
INTRODUCTION

The flight regime of the Dyna-Soar glider is established by both aerodynamic and structural parameters. The upper limit of equilibrium flight on a plot of altitude against velocity is established by maximum lift coefficient, and the lower limits by various structural parameters such as panel flutter, and combinations of loads and temperatures. The structural aspects of the boost phase, orbital flight, and reentry glide are reviewed in this paper.

SYMBOLS

а	panel width parallel to flow, in.
ъ	panel width perpendicular to flow, in.
$\mathtt{C}_{\mathtt{D}}$	drag coefficient
$\mathtt{C}_{\mathbf{L}}$	lift coefficient
D	hole diameter, in.
E	modulus of elasticity, psi
ı	length, in.
L/D	lift-drag ratio
M	Mach number
$n_{ m N}$	structural load factor, normal to vehicle longitudinal axis
q	dynamic pressure, psi





DISCUSSION

The variation of altitude with time for both a once-around and a twice-around mission is shown in figure 1. The boost phase is characterized by high dynamic pressures, wind shears, and gusts. The orbital phase is associated with low temperatures and micrometeorites. The reentry glide imposes combinations of high temperatures and maneuver loads. These three regions will now be discussed in greater detail.

The flight envelope of the boost phase (fig. 2) may be developed from the known, or expected, normal trajectory of the selected gliderbooster combination. The glider recovery ceiling may be defined as the maximum altitude and corresponding velocity from which the vehicle may be recovered if injected into the atmosphere at an entry angle of 0°. It is based on the temperature limits of the various components of the glider, as it operates through the range of lift coefficients from maximum to that at maximum lift-drag ratio. Glide trajectories for both maximum lift-drag ratio at 45° bank angle and maximum lift coefficient are included as reference boundaries for the glider reentry flight regime (shaded area) and will be discussed later with respect to temperatures and loads during the reentry glide. The recovery ceiling is established after the glider is designed for the reentry environment. The boost trajectories should be chosen so that, in the event of boost malfunction, the glider remains below the recovery ceiling.





The wind shear and gust loads occurring in the low-altitude flight regime are critical for the aft fuselage of the glider and are, of course, very important in the design of the booster-glider combination.

The booster and interstage structures have peak temperatures due to aerodynamic heating toward the ends of first- and second-stage boost burnout. The design criteria for these components must account for reasonable deviations from the standard atmosphere and for oscillatory motions of the booster-glider combination.

The panel-flutter placard is of particular interest since it represents a significant item of structural criteria for the glider designer for the boost-phase environment. In the work of reference 1,

Hedgepeth showed that $(\sqrt{M^2-1}\,\frac{E}{q})^{1/3}\,\frac{t}{l}$ is the governing panel-flutter parameter for isotropic panels. In reference 2, Sylvester presents the results of panel-flutter wind-tunnel tests in terms of this parameter for isotropic panels.

More recently work has been directed toward the skin-corrugation panel-flutter problem. It has been assumed that the same panel-flutter parameter applies with a geometric modification; that is, all geometric quantities are replaced with effective values as indicated in figure 3. These same data are presented by Eldon E. Kordes in a separate discussion of panel flutter, and are shown here for the purpose of completeness in this overall discussion of Dyna-Soar structural parameters.

The temperature history (fig. 4) for a particular point of interest on the lower surface of the glider nose skirt may be represented by a boost-phase peak, moderate cooling during orbit, and a subsequent hot soak during the long reentry glide for the "once-around" mission. The "twice-around" mission exhibits a perigee temperature peak at approximately 90 minutes after launch. This small peak is preceded and followed by moderately low temperature apogee cold soaks. The peak heating is the same for glide reentry from either type of mission, the major difference being the more severe cabin cooling requirements due to greater total heat input in the longer mission.

At altitudes above 250,000 feet, the possibility appears to exist that the glider may sustain slight damage from direct meteoric penetration of its steel surface. According to the latest available information, the daily influx of meteors into the earth's atmosphere is around 11,000 tons. The density of the particles ranges from that of dust to that of iron, but the distribution of density is unknown.

The mass of an individual particle may be estimated by correlation with its visual magnitude (according to M. Dubin of ARDC). The



assumption that all the meteoroids are iron will yield conservative analytical results. For a given mass the diameter of the particle may be determined.

A maximum meteoroid velocity of 250,000 fps and a penetration depth proportional to the particle were assumed, in consultation with the Rand Corporation, and the probability and depth of meteoric penetration were predicted. The relationship between hole diameter D and the probable number of penetrations larger than D per square foot per hour is shown in figure 5. It appears that for a single 0.01-inchthick skin there will be about 2 penetrations per square foot in 100 hours above 250,000 feet in altitude. Since the glider will spend about 75 minutes above 250,000 feet during a "once-around" mission, and has 330 square feet of planform area, there will be about 8 penetrations greater than 0.0014 inch in diameter per flight. Only one of these will be larger than 0.003 inch and the probability of much larger holes is very small.

Figure 6, the reentry temperature limits for $C_{L,MAX}$, is the first of four figures necessary to portray adequately the relationship of vehicle attitude in equilibrium glide to vehicle component temperature. For high lift coefficients, such as the one shown, there is an area of critical temperature just aft of the transition from nose-cap structure to flat lower surface. An emissivity factor of 0.9 has been used to calculate the 2,700° F temperature limit line for this point "F." There is altitude margin between the limit line and the glide path at the most narrow point around a velocity of 20,000 fps. The more critical of the three heating theories, laminar, turbulent, or transition, is used for design. The laminar theory was critical for this component. The 7.33 limit-load-factor line and the panel-flutter placard are shown as reference limits. The wing loading of 29 psf used in this example is a typical value for a Dyna-Soar glider with medium lift-drag ratio.

The temperature limits shown in figure 7 for an intermediate value of lift coefficient were calculated for the same wing loading as for the maximum-lift-coefficient chart, but involve a different critical glider component. The wing leading edge, swept back 73° and rounded to a 4-inch lower radius, is now the most critical relative to a limiting temperature of 2,700° F. The emissivity factor for this component is also 0.9. The laminar and turbulent limit lines are both shown, and it may be seen that the narrowest altitude margin now occurs at a velocity of around 20,000 fps. An additional design criterion was placed on these limits in that a sideslip angle of 5° was imposed.

The temperature limits shown in figure 8 are for a trajectory at maximum lift-drag ratio with 5° of yaw, and with a 45° bank angle





imposed to provide maximum lateral range. This is actually the critical high-temperature design condition since it has the minimum altitude margin of the three trajectories shown. The cusp usually formed between laminar and turbulent theory temperature limit lines is barely discernible here. The wing loading remains at 29 psf as before, and the leading-edge material is still most critical relative to a limiting temperature of $2,700^{\circ}$ F with an emissivity factor of 0.9. The above condition results in a 6,000-foot altitude margin. With a 5° yaw condition and 0° bank angle, the altitude margin is 15,000 feet. With 0° yaw and bank angle, the altitude margin is 21,000 feet.

The variation of glider-component criticality with respect to heating is shown in figure 9. The individual variation of each glider component is represented by the altitude margin between the bank lines shown as references and the lines of altitude plotted against glider angle of attack. The constant velocity of 20,700 fps used in this figure is a typical critical velocity taken from the previous three figures.

The stagnation temperature of the nose cap is invariant with angle of attack, which fact is represented by the horizontal straight line for a 192,500-foot altitude. The heating of the dorsal leading edge of the fin decreases with angle of attack and thus permits a lower operating altitude. The wing leading edge and point "F" exhibit the opposite effect, and thus require higher operating altitudes. The dashed portion of the wing-leading-edge curve is used to account for regions of uncertainty with respect to heating of a highly swept wing leading edge at high angles of attack.

The altitude margin shows the leading-edge structural components to be critical at low angles of attack and the flat plate at point "F" to be critical at high angles of attack.

The glider isotherms shown in figure 10 indicate the maximum upper-surface temperatures encountered during equilibrium glide at 0° bank angle for reentry at maximum lift coefficient and for reentry at maximum lift-drag ratio. The temperatures are based upon an insulated-plate radiation-equilibrium analysis with a surface emissivity factor of 0.9 except as follows: (a) the nose stagnation-point emissivity factor is 0.6 and (b) the leading-edge stagnation-line temperature is reduced 150° F from the insulated case by internal radiation around the leading-edge cell. Aerodynamic heating rates on the upper surfaces are low because of the separated flow conditions, except at the low-lift-coefficient attitude where the windshield cover, the dorsal-fin leading edges, and the forward sides of the fuselage experience high heating rates. Temperatures on the upper aft fuselage have been approximated from flat-plate zero-angle-of-attack conditions and are not affected by internal cross radiation.



The glider isotherms shown in figure 11 indicate the maximum lower-surface temperatures encountered during equilibrium glide for the same flight conditions as in figure 10. The lower-surface isotherms have been determined by using flat-plate equations modified by the three-dimensional delta-wing outflow effects. The outflow effect is responsible for the radical difference in the shape of the isotherms as the vehicle attitude changes from the low- to the high-lift-coefficient case. At low lift coefficient the isotherms are approximately parallel to the wing leading edge and exhibit maximum temperature gradients over the wing surface. At high lift coefficient the isotherms run approximately spanwise and low temperature gradients exist over the entire surface.

1

]

 ϵ

All of the lower surface is insulated, as required, to restrict the temperature of the instructure to 2,000° F. The inside face of the lower surface of the wing radiates to the upper wing surface. This is the major factor in determining wing upper-surface temperatures. The temperatures of the lower outer surface directly beneath the fuselage have been computed with no internal cross radiation. The internal cross radiation of an insulated panel does not appreciably affect the outer-surface temperature, but significantly reduces the temperature of the primary structure behind the insulation.

The maneuver capability of the Dyna-Soar glider may be portrayed as in figure 12. The wing loading is 29 psf and the equilibrium glide trajectories for the maximum lift coefficient and maximum lift-drag ratio at 45° bank angle are shown as references. The previous charts explained the criticality of structural heating, relative to vehicle attitude and environment, associated with equilibrium gliding flight at these high and low lift coefficients.

The glider will not sustain steady-state accelerated flight, as experienced in a pull-up maneuver, at altitudes higher than those shown for the various load-factor limits. This maneuver limit exists because the density variation with altitude and the velocity variation do not provide sufficient dynamic pressure. The interesting portion of the curves appears at the cusp points. The cusps are formed where the temperature limit line for the vehicle attitude at maximum lift coefficient, shown previously in figure 6, intersects the constantload-factor lines established by dynamic-pressure limitations. fore, at the cusp of any curve the maneuver capability of the vehicle is limited by temperature at this maximum angle-of-attack condition, but below the cusps, the curves are formed by temperature limits for various points on the vehicle at particular lower lift coefficients along the constant-load-factor lines. Therefore, the structural operational envelope extends between the upper and lower lines in figure 12, but maneuver capability varies with temperature at speeds approaching satellite velocity, dynamic pressure, and elevon system and surface load capacity in the regions of high dynamic pressure.



The load factor referred to in the preceding discussion is computed relative to the vehicle longitudinal axis. The equation used for the determination of this normal limit load factor is as follows:

$$n_{N} = \frac{C_{L}qS}{W} \cos \alpha + \frac{C_{D}qS}{W} \sin \alpha$$

CONCLUDING REMARKS

A description of the environmental factors which affect the design of the principal components of a Dyna-Soar glider has been given. These factors are panel flutter during the boost phase and reentry at low altitude, and aerodynamic heating and maneuver loads during the hypersonic reentry glide. The components are the skin panels, the nose cap and skirt, and the wing and dorsal-fin leading edges.

Altitude margin was shown to exist between the various equilibrium glide trajectories and the corresponding altitude-velocity relationships for the individual structural components at particular flight attitudes. The variation of these altitude margins with changes in flight attitude, for constant velocity, was also shown. The absolute margins are of course dependent upon the design criteria, such as bank angle, yaw angle, and material limits. The margins also may be changed by local, as well as overall, variations in external and internal configuration. Provision for internal cross radiation is an important aspect of configuration.

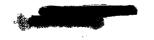
The variation of heating along the different glide trajectories was also shown in combination with the changing load-factor capability. A typical glider configuration, such as that designed for a medium lift-drag ratio used in this analysis, has the capability to maneuver to a limit load factor of 7.33 where there is sufficient dynamic pressure available.





REFERENCES

- 1. Hedgepeth, John M.: Flutter of Rectangular Simply Supported Panels at High Supersonic Speeds. Jour. Aero. Sci., vol. 24, no. 8, Aug. 1957, pp. 563-573, 586.
- 2. Sylvester, Maurice A.: Experimental Studies of Flutter of Buckled Rectangular Panels at Mach Numbers From 1.2 to 3.0 Including Effects of Pressure Differential and of Panel Width-Length Ratio. NACA RM L55130, 1955.





DESIGN AREAS

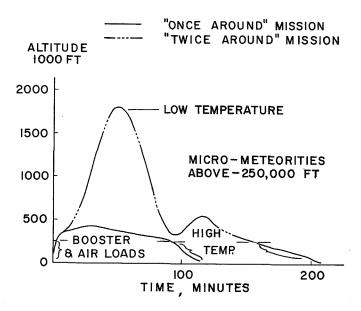


Figure 1

FLIGHT ENVELOPE, BOOST PHASE W/S = 29 PSF

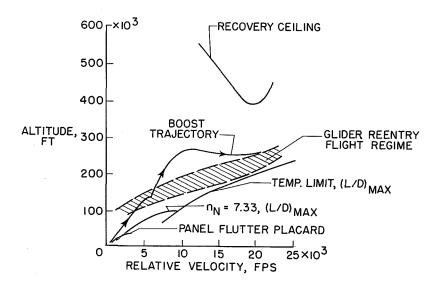


Figure 2





PANEL FLUTTER

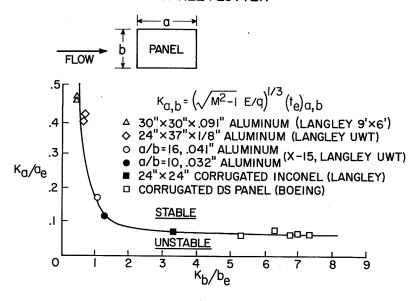


Figure 3

TEMPERATURE HISTORY

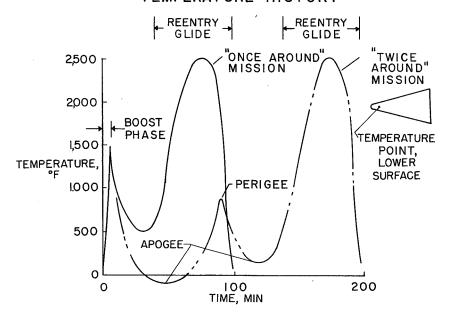


Figure 4





MICROMETEORITE PENETRATION ALTITUDE, 250,000 FT

NUMBER AND DIAMETER OF IRON PARTICLES PENETRATING A HORIZONTAL STEEL SURFACE IN ORBITAL FLIGHT

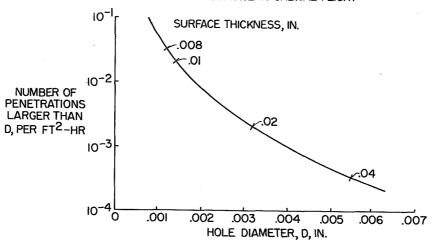


Figure 5

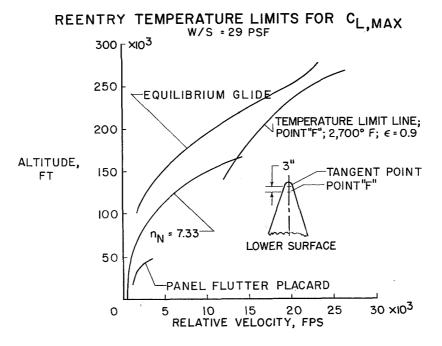


Figure 6





REENTRY TEMPERATURE LIMITS FOR C_L = 0.40 W/S = 29 PSF

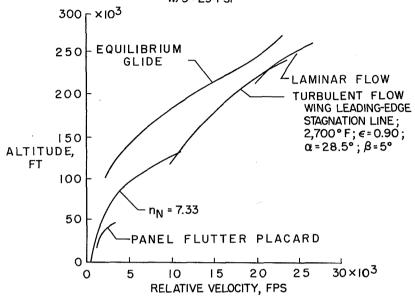


Figure 7

REENTRY TEMPERATURE LIMITS FOR (L/D)MAX

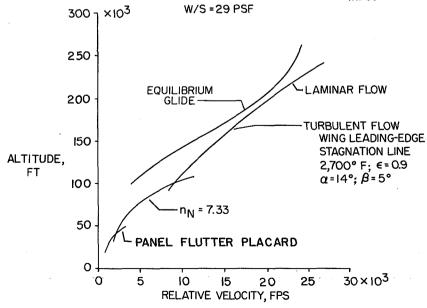


Figure 8





COMPONENT 'TEMPERATURE VARIATION WITH α W/S = 29 PSF; RELATIVE VELOCITY=20,700 FPS; ϵ = 0.9 (EXCEPT 0.6 ON NOSE)

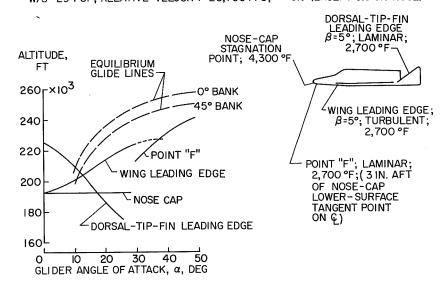
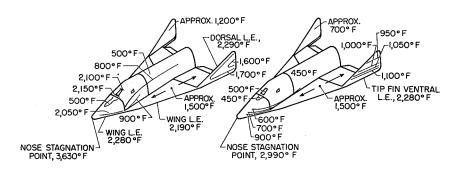


Figure 9

UPPER-SURFACE ISOTHERMS EQUILIBRIUM GLIDE; VELOCITY = 18,700 FPS; ϕ = 0°; β = 0°



(L/D)_{MAX} REENTRY

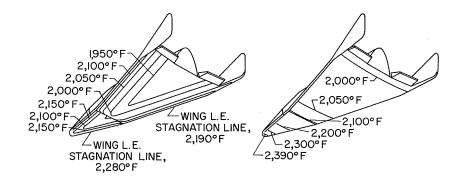
ALTITUDE = 207,000 FT ANGLE OF ATTACK = 14° C_{L,MAX} REENTRY

ALTITUDE = 246,000 FT ANGLE OF ATTACK = 51°

Figure 10







(L/D)_{MAX} REENTRY ALTITUDE = 207,000 FT ANGLE OF ATTACK = 14° C_{L,MAX} REENTRY ALTITUDE = 246,000 FT ANGLE OF ATTACK = 51°

Figure 11

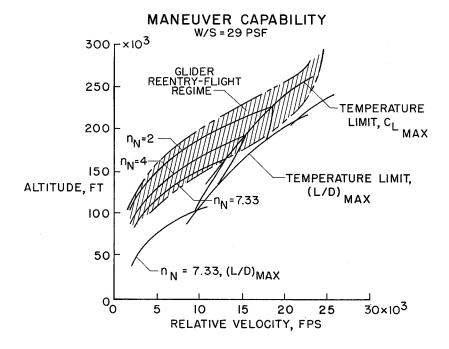


Figure 12





DEVELOPMENT OF TRUSS TYPE DYNA-SOAR GLIDER STRUCTURE

By Andrew K. Hepler, Bruce E. Landry, and Melvin A. Nelson Boeing Airplane Company

INTRODUCTION

This paper is concerned with the structural design evolution, construction, and testing of airframe components suitable for a delta-wing, glider-type reentry device. The structural design of a reentry vehicle is influenced by the configuration of the vehicle and the load and thermal input conditions associated with the flight trajectory. During reentry, the typical glide vehicle is capable of using a number of equilibrium glide paths, during which flight is maintained at essentially constant values of W/SC_{L} . The glide vehicle is also capable of performing high-load-factor maneuvers from the reentry glide path.

For the purposes of this paper, the structural temperature rise due to the thermal energy imparted during reentry is that rise which is associated with a radiation-cooled structure. The basic structural concept considered employs skin panels which transmit the external aerodynamic loads to the primary load-carrying structure. These panels also serve as an exterior protective heat shield such that the primary structure does not reach the temperatures experienced by the outer shell. The primary load-carrying structure is considered to be maintained at temperatures below 2,000° F; therefore, the use of superalloy construction materials is permitted.

The concept of cooling by thermal radiation leads to temperature differences in the various internal structural members. These temperature differences, or gradients, depend on the structural arrangement and the magnitude of the change in exterior skin temperature with time. For example, the temperature gradient between the upper and lower wing surface is greatest during high-load-factor maneuvers at hypersonic speeds. These temperature gradients produce differential changes in the lengths and orientation of the various internal structural components. High stresses can occur in a structural design in which the elongation and rotation of structural elements are restrained. Thermal stresses of this nature can be eliminated from the primary structure by utilizing a statically determinate trusswork employing pinned attachments.





Static room temperature and hot tests performed on various truss members and joints and on the forward structural section of a full-size vehicle have verified that the truss-type structure has the structural capability required of a typical Dyna-Soar reentry glider. This type of structure can be constructed by using the current state of the art in materials development and manufacturing methods.

SYMBOLS

L 1 1

$\mathtt{C}_{\mathtt{L}}$	lift coefficient
S	reference lifting area of the vehicle, sq ft
W	total weight of the vehicle, 1b
T_0T_3	local structural temperatures, ^O F

DISCUSSION

Structural Arrangement

The structural arrangement shown in figure 1 is representative of the truss-type structure developed for a typical Dyna-Soar reentry glider. This particular reentry vehicle component is currently being fabricated for structural testing which will duplicate typical reentry environmental conditions. The structure is 10.5 feet long and is a full-size representation of the forward section of the vehicle. René 41. a nickel-base superalloy material, is used throughout the structure with the exception of the lower surface skin panels which are made of HS-25, a cobalt-base superalloy. The body is composed of two main longitudinal trusses joined together with four cross frames. Diagonal bracing between the longerons of the main trusses has the capability of reacting asymmetrical loading conditions. The primary wing structure is made up of wing-spar trusses and leading-edge beams. The wing-spar trusses are perpendicular to the leading edge of the vehicle and are attached to the main body trusses at the lower longerons and vertical body truss members. Air loads are transmitted to this primary truss structure by means of corrugated skin panels. These panels transfer the applied air loads to the leading-edge beams, intercostals, longerons, and keel beam by simple beam action. In order to understand this airframe development more fully, it is necessary to investigate the conditions and basic concepts which affect the structural design.



L 1 1

Structural Design Conditions

The flight trajectory of a hypersonic glider reentry vehicle is composed of three phases: boost, orbit, and reentry. High wind shear conditions and rapid heating rates can exist during the boost phase. During this phase, the internal primary structure is cool and, consequently, these conditions do not affect the design of most of the structural members. During the orbital phase of the flight, the substructure likewise is cool and loads due to activation of reaction controls are small. It develops that the principal design conditions for the primary structure occur for combinations of temperature and aerodynamic loads during the reentry phase of the trajectory. For approximately 30 minutes after initiation of reentry, the heating rate of the external surfaces is gradual and the overall vehicle structural temperatures tend to approach equilibrium conditions. This phase of the reentry is characterized by high temperatures and relatively low structural loads. Figure 2 shows typical temperatures for the inner surface of the lower skin and lower chord of a wing-spar truss during the final 50 minutes of reentry. Equilibrium temperature conditions are shown for one factor flight and uninsulated skin panels in an area away from leading-edge effects. For this case, the maximum temperature of the internal primary structure is 1,530° F. This condition occurs when the maximum skin temperature is 1,780° F.

Transient structural temperatures are illustrated for a high-load-factor maneuver condition. The curves show that the internal structural temperatures during this severe maneuver will be somewhat lower than those at maximum equilibrium conditions. However, the aerodynamic loading combined with the temperatures during this type of maneuver can be the designing condition for the primary load-carrying structure.

Structural temperatures experienced during a severe pull-up maneuver are shown in figure 3. Transient temperatures are shown for the inner surface of the lower skin and the lower and upper chords of a wing-spar truss. After initiation of maneuver, the temperatures increase until the maneuver load factor is decreased. With a reduction in flight load factor, the skin temperature decreases rapidly and after a short time lag the internal structural temperatures also peak and decrease. Even though thin materials are used for construction, internal structural heating rates are small immediately after maneuver initiation. For a representative maneuver time of 30 seconds, the transient temperatures of the lower and upper spar chords are 300° F and 330° F below their respective equilibrium temperatures based on a skin temperature of 2,000° F. At this time, the temperature gradient between lower and upper spar chords is approximately 390° F. High-load-factor maneuver conditions of this type, combined with the associated structuraltemperature differences, usually constitute the principal design conditions for the primary structure of the vehicle.





Structural Concept

The effect of temperature gradients between members of a typical truss bay is shown in figure 4. With truss joints in the fixed condition, the changes in member lengths due to differential thermal expansions produce stresses from end moments and shears. If all joints are pinned, there is no resistance to changes in relative member orientation. Bending of the truss members is thereby eliminated and the structure becomes free of this type of thermal stress.

L

1

1

1

Multiple-bay truss deflection caused by differential temperatures must be considered since this deflection will modify the aerodynamics of the glider. Calculations indicate that multiple-bay truss deflections due to temperature gradients across the truss are not significantly changed by varying the positions of the truss verticals and diagonals. As a result, the design of a truss-type structure is primarily based on optimum weight considerations.

Structural Design and Construction

Air loads are carried by the skin panels in simple beam bending. The method of reacting the loads from these panels is shown in figure 5. Shear forces from the panels result in nearly uniform loads carried in bending by the leading-edge beams, intercostals, longerons, and the keel beam. The end shear forces from these members are reacted at the joints of the wing spars and body trusses. With this arrangement, the primary stresses in the truss elements are due to axial loads.

The weight of structural joints represents a significant portion of the total weight of the structure. When a truss structure is designed for axial forces, pinned connections are heavier than fixed joints. However, the lighter fixed joints introduce moments and shears into the members because of the temperature distributions previously discussed. These additional loads require the truss members to be heavier. In figure 6 the weight of truss-type structure for a typical wing spar with three different conditions of joint fixity is shown. For the fully pinned condition the weight of the joints approaches 30 percent of the total truss weight. Although joint weight decreases in the fully fixed case, the weight of the total structure is approximately 130 percent of an equivalent pinned joint truss. A design where only certain joints are fixed results in the lightest structure. Thermal stresses are present in some of the members in this latter arrangement but they are of small magnitude. The advantage of incorporating some fixed joints becomes apparent at connections between many members in more than one plane.



7



A typical wing spar in which this design technique has been utilized is illustrated in figure 7. This wing spar is used on a structure currently being fabricated for test. All truss material is René 41 superalloy. Tubular members have been swaged where there are space limitations on the sizes of connections. Pinned connections are formed by bolting through tabs or fittings which have been fusion welded in tube end slots. Fixed connections are formed by fusion welding the members to fittings or gussets.

A typical joint for the intersection of wing and body truss elements for current test structure is shown in figure 8. Longeron loads are transmitted through a bolted connection. A fitting is used to attach the wing and body truss tubes to the longeron. Wing-spar members are fusion welded to a lug which is bolted to this fitting. A similar arrangement is used for the body cross-frame elements. The bolted connection between the fitting and longeron allows independent rotation of the vertical-diagonal assembly in the main truss plane.

Superalloys were selected for the construction of the primary structure since the temperature environment does not exceed 2,000° F. Materials evaluated have included M-252, René 41, and HS-25 superalloys. The structural design conditions and the desirable material properties of René 41 at elevated temperatures have led to the selection of this material for the trusswork. René 41 is a precipitation hardenable material. After solution treating at 1,975° F the material is aged at 1,400° F for 16 hours. This process increases the strength of René 41 at temperatures below 1,600° F. Conditions which produce high stresses in the primary structure occur at temperatures below the range where the creep of René 41 becomes significant.

The longeron shown is formed from sheet stock and consists of a close-out plate spot-welded to a hat section. Beads are incorporated in the hat-section design to increase crippling strength.

Swaged-tube manufacture has been developed by starting with a tube size intermediate between the basic section required and the swaged end. Tube ends are swaged by a succession of cold-draw operations with the use of intermediate anneals. With the material in the annealed condition, fluid forming is utilized to increase the basic section to the diameter required. Final treatment of René 41 assemblies consists of solution treatment and aging.

Tests Results

Structural testing conducted by the Boeing Airplane Company has included elevated-temperature tests on structural elements and components





of various cross sections and materials. A full-scale structural assembly representing an earlier design version of a truss-type structural arrangement has been built and tested to prove this structural concept for a reentry glide vehicle.

Element tests.- Five substructure elements have been life-tested. These elements are shown in figure 9. They represent two designs typical of the glider structure. These components were subjected to a continuous program of 20 minutes at $1,200^{\circ}$ F, 20 minutes at $1,400^{\circ}$ F, 10 minutes at $1,600^{\circ}$ F, and 4 minutes at $1,800^{\circ}$ F, with approximately 50 percent of the ultimate compression design load applied at each corresponding temperature level. This program represented the cumulative time at predominant temperatures and stresses for 10 glider reentries. After this program the specimens were tested to failure in compression at $1,800^{\circ}$ F.

The materials used for element construction were the superalloys René 41, HS-25, and Hastelloy X. The René 41 specimen was age-hardened after welding.

All the capped-hat sections were constructed with identical sheet gages and weld patterns. The overall length of the hat-section specimens was 43.92 inches with a distance of 40.00 inches between support-bolt center lines. The basic section of square-capped-hat design, 3.0 inches on a side, extended for 12.80 inches at midspan. This section was of 0.040 gage with each side beaded to increase crippling strength.

Swaged tube elements were 16.9 inches long with an overall length of 19.70 inches including end tabs. The distance between support pins was 18.00 inches. The basic section of the tubes was 1.50 inches in diameter with 0.014-inch-thick wall. The section is swaged over a distance of 3.0 inches to 0.50-inch diameter with an 0.027-inch-thick wall. The reduced sections were 0.40 inches long and slotted to receive the end tabs. Stiffener rings of 0.020 gage were fusion plug welded to the specimens at the junction of the basic section and swaged end in order to increase the strength in the transition area.

Because of the lengths and section properties of the specimens, the elements were critical in crippling. Life testing was accomplished for the elements and the failure stresses at $1,800^{\circ}$ F are shown as a ratio of the corresponding predicted crippling stresses. The test results compare favorably with analytically predicted strengths for the two structural shapes manufactured from the three basic materials.

A view of the test facility used for these tests is shown in figure 10. The elements were heated by air-cooled high-density radiant heat lamps with ceramic reflectors mounted on aluminum manifolds. Power





to the lamps was regulated by control thermocouples mounted on the specimens and the use of ignitron controller carts. Load was applied to the specimens by a hydraulically operated test machine. Thermal expansion of the machine during testing was reduced by wrapping all exposed parts in aluminum foil.

Structural-concept model tests. This test structure was a full-size vehicle forward section approximately 6.5 feet long. Its primary purpose was to verify the structural integrity of the truss-type design concept. In addition, the heat transfer through the structure and the deflections of the model due to heat and load were evaluated throughout the tests. This test specimen was subjected to seven simulated reentry flight trajectories, including maneuvers, which an actual reentry vehicle would encounter. A view of the specimen is illustrated in figure 11.

The test specimen was fabricated from M-252 superalloy sheet stock and, consequently, the design was restricted to parts which could be fabricated in the sheet metal shops. All parts were spot-welded together with the exception of the bolted-member connections. For example, the tube members were constructed of two hat sections spot-welded together. The specimen was built around two fore-and-aft full-depth trusses. The second and fourth verticals from the forward end employed pinned ends whereas the diagonal members were connected by short tabs at the joints. These main trusses were connected by three cross frames. A leading-edge beam was attached to the outboard ends of the cross frames. The exterior skin panels were made of corrugated sheet spot-welded to a flat external skin.

An overall view of this structural-concept model during testing is shown in figure 12. Instrumentation on the concept model consisted of 327 thermocouples, 28 high-temperature strain gages, 12 deflection indicators, and 1 dynamometer-bar load indicator. Thermocouples were installed to measure temperature distributions on the external skin and throughout the joints and members of the trusswork. The test specimen was cantilevered from the reaction jig by extensions of the main trusses. Load was applied by one hydraulic jack acting through a fulcrum beam to an evener system. The evener system was attached at 22 load points on the specimen. All points were at the intersections of main truss members and along the leading-edge beams. Heat was applied to the specimen from radiant heat lamps. The lamps were fixed to a jig which surrounded the specimen. This lamp jig was hinged at the reaction support and counterbalanced to rise with the model as it deflected.

The first test run was a load-only test to check the load distribution and room-temperature deflections of the model. The model was subsequently tested with a maximum lower surface skin temperature of 500° F to check the heating facility and to investigate the effects of moderate temperatures on the specimen. A total of seven simulated



reentry tests were conducted on this specimen. The first two reentry tests reached maximum lower surface skin temperatures of 1,600° F and 1,800° F. Two other tests reached a maximum temperature of 1,900° F and three tests imposed a maximum of 2,000° F. Test loads simulated one-factor flight conditions and two maneuver conditions to the maximum aerodynamic capability of the vehicle represented. The heating rate of the lower skin surface was maintained at 3° F per second during the maneuver conditions.

The first high-temperature reentry to 1,900° F verified the structural concept. The specimen survived all testing with no damage to the primary structural members. Deflection readings taken during the tests indicated that the specimen behaved elastically. No measurable creep or permanent deformation occurred to the primary structural components. Some minor cracks and spot-welded failures on the skin panels and skin expansion joints occurred. The corrugated sections of the skin panels did not experience damage. The damage to the outer surface skins was apparently the result of the skin-support structure being too rigid and not allowing freedom of movement of the panel corners.

Numerous data were obtained on heat transfer throughout the structure. Representative of the numerous temperature results were the measurements of temperatures of truss structure attached to the lower surface skin panels. As shown in figure 13, the temperatures and thermal gradients of elements attached directly to the skin are high. These measurements were taken on the lower chord of the main truss. A substantial decrease in member temperatures and thermal gradients is obtained by attaching skins a small distance away from the primary truss elements by means of clip angles. This arrangement was used between the skin panels and cross frames. Current designs of skin panel to truss component attachments utilize this method.

Even though the programed model surface isotherms were difficult to obtain during testing, the variation of skin-panel temperatures along the main truss chords were close to those required. Figure 14 shows the temperatures through the body truss structure for the most critical reentry test. The results show that temperature differences between the lower chord and diagonal members are much higher than those between the diagonal and upper chord members. This high gradient has been decreased in current truss-type structural design by not attaching chord members directly to the skin panels.

The complexity of truss joint structure does not readily lend itself to analytical solution. The maximum temperatures attained near a representative concept model joint are shown in figure 15.





CONCLUDING REMARKS

In conclusion, it can be stated that, although the concept of structural cooling by thermal radiation leads to differential member temperatures, thermal stresses are essentially eliminated in the trusswork by the use of pinned joints. Structural design is improved from the standpoint of weight by employing fixed joints where the truss members will not be adversely affected.

Fabrication capability has been demonstrated by the manufacture of airframe components using superalloy materials of construction. The testing of these components at their design temperatures has confirmed the analytically predicted strengths.

Testing of a full-size vehicle forward section by repeated heat and load programs simulating reentry trajectories has indicated that pinned-joint structure is not adversely affected by large differences in component temperatures. Temperature data have led to a better understanding of heat transfer between internal structural elements. This information has been utilized to improve the design of current truss-type airframes. These tests have verified that a radiation-cooled primary structure, employing a trusswork design, has the structural capability required for a typical Dyna-Soar reentry glider.





STRUCTURAL ARRANGEMENT FOR A TYPICAL GLIDE VEHICLE

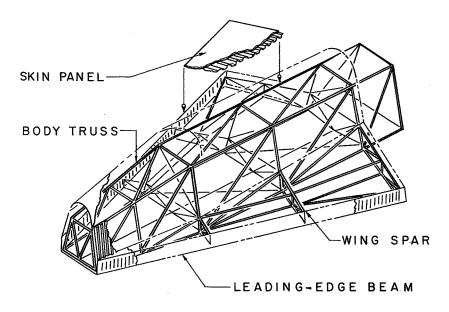


Figure 1

TYPICAL STRUCTURAL TEMPERATURES DURING REENTRY

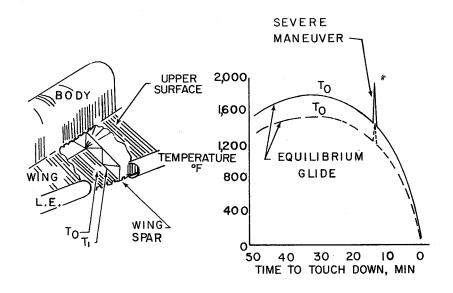
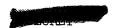


Figure 2





TYPICAL STRUCTURAL TEMPERATURES DURING SEVERE REENTRY MANEUVER

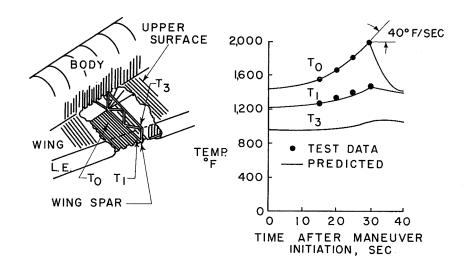


Figure 3

SINGLE-BAY TRUSS DEFLECTION DUE TO DIFFERENCE IN STRUCTURAL TEMPERATURES

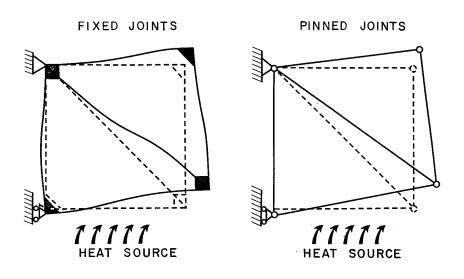


Figure 4



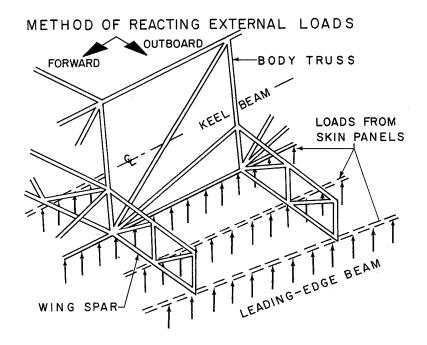


Figure 5

EFFECT OF JOINT FIXITY ON TYPICAL WING SPAR TRUSS

Figure 6





TYPICAL WING-SPAR DETAIL

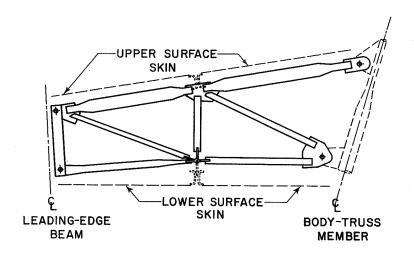


Figure 7

TYPICAL JOINT DETAIL

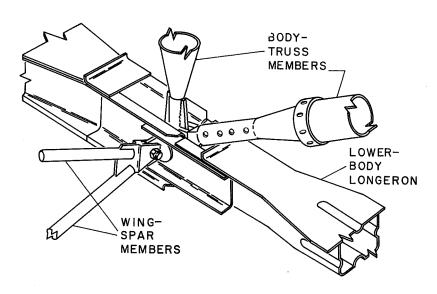


Figure 8







COMPRESSION CRIPPLING

TESTS OF TRUSS ELEMENTS; 1,800° F TEST TEMPERATURE

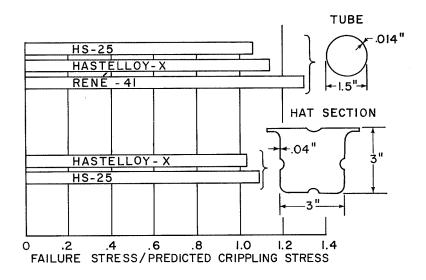


Figure 9

TEST FACILITY FOR COMPRESSION CRIPPLING TESTS OF TRUSS ELEMENTS

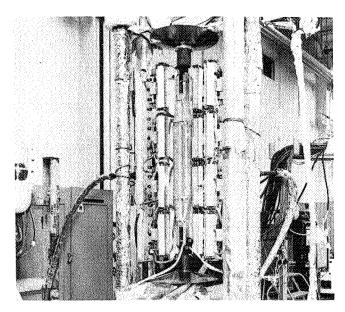


Figure 10





STRUCTURAL-CONCEPT MODEL

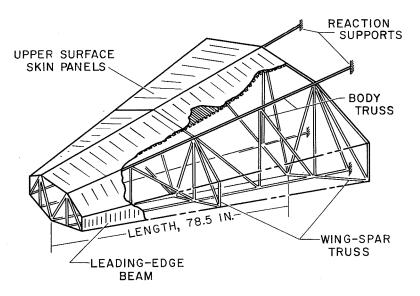


Figure 11

TEST FACILITY FOR STRUCTURAL-CONCEPT MODEL

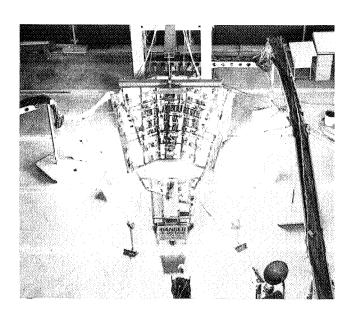


Figure 12





EFFECT OF TRUSS-TO-SKIN ATTACHMENT ON LOCAL TEMPERATURES

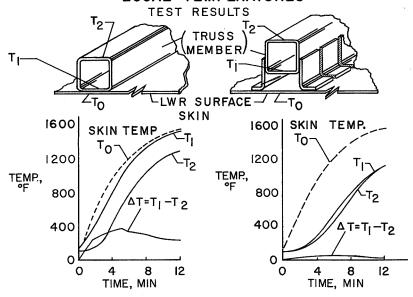


Figure 13

TYPICAL BODY-TRUSS TEMPERATURE DATA TEST RESULTS

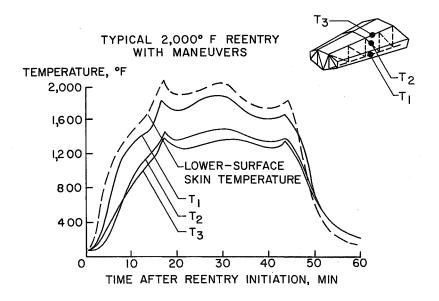


Figure 14



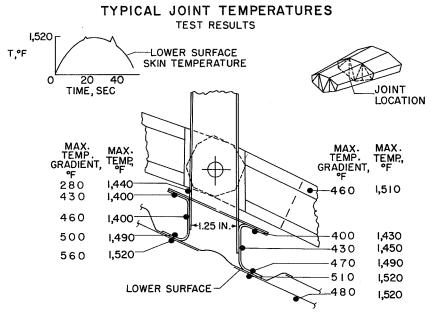


Figure 15



Page intentionally left blank



DYNA-SOAR SKIN PANEL DEVELOPMENT

By Andrew K. Hepler, Walter E. Backus, and George B. Smith Boeing Airplane Company

INTRODUCTION

Reentry from orbital velocity by glider-type vehicles imposes new and severe requirements for external surfaces. The relatively long heating period coupled with the requirements of maintaining aerodynamic shape at high equilibrium temperatures and minimum weight create major design and development problems. This paper presents certain aspects of the analysis and development testing of external panels for use at temperatures as high as 2,700° F.

The surface panels to be reviewed are shown in the vehicle cross section in figure 1. The cross section and structural arrangement are representative of a reentry, radiation-cooled, glide vehicle. In general, the operating temperature of the upper surface is less than 2,000° F while the lower surface equals or exceeds this number. The only structural purpose of the panels under discussion is to transfer the external airloads to the internal primary load-carrying structure. Thermal gradients through the airframe structure require that the external surfaces absorb thermal deformations, either through flexing or movement of the panel supports or by deformations, such as buckling, of the panel itself.

A typical reentry heat and load environment for the external surfaces is shown in figure 2. The maximum lower surface temperature attained was $2,700^{\circ}$ F for panel A, with pressure loadings in the vicinity of 1 to $1\frac{1}{4}$ psi. Panel B, on the upper wing surface, reaches a temperature of $2,000^{\circ}$ F. The simultaneous increase of load and temperature during maneuvers is due to increased heating with increased angle of attack. In addition to temperature and aerodynamic loads, such items as airstream erosive effects and stiffness requirements to prevent flutter also influence the panel design.



SYMBOLS

- to thermal gradient (OF/in.) in a given material, Btu-in.

 gradient of the material of the mat
- ρ density of material, lb/cu ft
- q air pressure on outer surface of glider, lb/sq ft

DESIGN APPROACH

With the environment established, a design approach can be formulated as outlined in figure 3. First a basic material is selected suitable for the required operating temperatures. For temperatures up to $2,000^{\circ}$ F, the superalloys such as René 41, a nickel-base alloy, are available. These materials may be used with a high degree of structural confidence up to $2,000^{\circ}$ F. For temperature in excess of $2,000^{\circ}$ F, refractory materials such as the molybdenum alloys or niobium alloys must be considered for external covering if a conventional sheet-metal construction is to be used. In the area of insulation, recent developments of both alumina and zirconia fibers have shown promise of a relatively efficient insulation for use up to $2,900^{\circ}$ F.

These material limitations are fundamental in establishing panel configuration. For temperatures to 2,000° F a conventional design utilizing the superalloys is possible. For areas where the temperature exceeds 2,000° F, the use of the superalloys in the panel structure is only possible if an insulating heat shield is used to protect them from the high-temperature airstream. The use of refractory alloys for the primary panel structure is not considered satisfactory at this time.

Surface panel development has been divided into two types - noninsulated panels for use to $2,000^{\circ}$ F and insulated panels for use to $2,700^{\circ}$ F.

Verification of the structural integrity of the panels employs, in general, the following testing:

Simulated environment
Load and temperature
Sonic (with and without heat)
Plasma tunnel (erosive and thermal shock)

Actual environment (free flight)



I]]]



NONINGULATED PANELS

For structural temperatures up to 2,000°F, development of the superalloys permits the use of conventional sheet-metal designs for the external surface. In keeping with the design philosophy of minimizing thermally induced stresses, a skin panel has been developed which utilizes a flat skin spot-welded to a corrugation. A typical panel is shown in figure 4. This type of surface panel is currently being evaluated both analytically and experimentally at the Boeing Airplane Company.

The structural environments are being simulated in the laboratory, as practical, as either singularly applied or combined test conditions. Testing has been confined to heat, surface pressure load, sonic excitation, and panel flutter. Three superalloys were used for this panel development program.

Heat and Load Testing

Panels 71 by 22 inches have been fabricated from 0.010-gage sheet metal. The cross sections of the panels are shown in figure 4. Two panels of René 41, two of Hastelloy X and two of Haynes Stellite 25 were tested. One of each pair of panels employed a "Z-edge" design at the corrugation ends, and the other a "creased-edge" design. These edge treatments are illustrated in figure 5.

The test setup of the panel is shown in figure 6. The bank of heat lamps can be seen above the panel. The panel was mounted as the top of a flat box on the test table. Load was applied to the top of the panel by pulling vacuum in the box. A beaded pressure seal was used between the panel edges and the vacuum box. The beading permits unrestrained longitudinal growth of the panel, and flexing of an adjacent unbeaded area permits lateral growth.

Each panel was subjected to 10 heat-load cycles representative of a typical reentry. Maximum loadings of 0.8 psi at 2,000° F were included in the testing. After these environmental tests, the panels were heated to 2,000° F, soaked for 10 minutes, and loaded to failure. The pressure loading was applied in finite steps, with the load held constant for 5 minutes at each step. Deflection to 1/2 inch at the center of the panel was considered the failure point. Test results are summarized in figure 7. All of the Z-edge panels supported a loading of 2 psi for at least 1 minute. The creased-edge panels supported only about 50 percent as much load due to the weakness of the short nonstiffened length just inside the edge of the panel.





Sonic Testing

Structural verification of these panels by sonic testing is also required. The skin panels of a typical boost-glide vehicle are subjected to rocket-engine and aerodynamic noise during the boost and reentry glide phases of the flight. A maximum overall noise level during launch of 145 decibels is anticipated. During the boost and reentry phases the glider will be exposed to an overall level of 135 decibels due to aerodynamic noise. The maximum temperature at which significant noise levels occur will not exceed 500° F. At this temperature the mechanical properties of the structural materials used are not significantly different from those at room temperature. For this reason sonic testing has been conducted at room temperature.

A series of superalloy panels were sonic tested at the Boeing Airplane Company. These tests were conducted in the Boeing progressive wave sonic test chamber. The sonic generator is the siren type which produces a sinusoidal wave form of a given single frequency and intensity. Panels are mounted in this facility in such a way that sonic waves move parallel to the surface of the panel, thus minimizing the standing wave effect. Pressure levels are adjusted directly from a microphone reading with the panel in place.

Figure 8 shows results of a series of sonic tests for panels of three superalloys (René 41, Hastelloy X, and Haynes Stellite 25). The panels were constructed of an 0.010-gage skin spot-welded to an 0.010-gage corrugation and had the Z edge shown in figure 5. The panels were simply supported on two edges with the distance between supports being 22 inches.

An approach to reducing the scatter in sonic test data is shown in the lower plot. The equivalent static uniform pressure load is calculated (utilizing uniform-load simple-support equations) based on the measured deflection during sonic testing. Time to failure from the upper plot is converted to cycles to failure. This is possible inasmuch as all testing was at a single resonant frequency. The values for equivalent pressure and cycles to failure are then plotted as shown in figure 8 to show relative life of the test panels. This approach essentially corrects for tolerances in measuring sound levels and for the variation in the damping of the panel to the test-jig bolted joint. This joint contributes the major portion of the overall test-installation damping.

In the lower load, high life region, all curves of figure 8 are drawn through test points where no failure occurred. Similar sonic tests were made to evaluate the effect of both the beaded edge and creased edge shown in figure 5.





Initial failure of the Z-edge panels occurred at the spotwelds and adjacent material connecting the Z-angle to the inner nodes of the corrugations. This was followed by failures in the spotwelds connecting the outer nodes of the corrugation to the doubler and skin. With the edge of the panel in this flexible condition, cracks appeared in the skin, doubler, and corrugation. Initial failure of the beaded- and creased-edge panels occurred at the spotwelds connecting the corrugations to the doubler and skin.

Conclusions from this program were that the Z-edge configuration was superior for all materials, that René 41 panels provided the longest fatigue life, and that all test panels demonstrated the capability of withstanding the noise environment anticipated during the flight of a typical boost-glide vehicle.

Flutter Testing

Flutter characteristics of typical corrugated skin panels have been evaluated in the Langley Unitary Plan wind tunnel. The effects of panel surface heating were investigated during these tests as well as variations in corrugation geometry.

Heating of the panels was investigated to determine the effect of skin buckling on inducing flutter of the panel. In general, it was found that heating the panel enough to cause buckling tends to decrease the response amplitude of the panel and to increase the critical flutter dynamic pressure.

One technique developed to increase the stiffness of the panel was the addition of flat straps attached to the back of the panel as shown in figure 9. The straps were placed normal to the corrugations and spaced 5.1 inches. The straps were terminated at the edges of the panel on the last full corrugation. There was no indication of flutter of the stiffened panel at the test Mach numbers and dynamic pressures. The straps proved to be a simple and lightweight method of increasing the flutter capability of the corrugated panel.

INSULATED PANELS

For the surface areas of a hypersonic boost-glide vehicle where skin temperatures are too high for the superalloys, that is, approximately 2,000° F, insulated panels are required. A typical insulated panel designed to operate in the temperature range from 2,000° F to 2,700° F is shown in figure 10. The panel consists of an airload-carrying, corrugated inner panel of superalloy, a layer of insulation,





and a hard outer surface for protection of the insulation from high-velocity airstream erosion.

This panel design is such that the erosion shield is secondary structure only. It transmits the local aerodynamic pressures through supporting clips to the superalloy corrugated inner panel. This design arrangement has been adopted due to a lack of a reliable structural material for load beaming in a 2,700° F environment.

Insulation Properties

Several promising insulations with various high-temperature capabilities are compared in figure 11. A measure of insulating efficiency as applied to airframe design is the factor kp; that is, the product of thermal conductivity times the density of the insulation. For high insulating efficiency, low values of kp are desired. The data presented as solid lines are based on test experience at the temperature indicated and represent the current limit of conductivity data. Testing of these insulations at higher temperatures is required to establish the insulating properties which are predicted by the dashed portion of the curves. The dashed curves do not extend beyond the maximum hot wall temperature to which the material is known to have been successfully submitted. It will be noted that there is a serious lack of data above 2,000° F, the temperature range currently of interest. The aluminaand zirconia-fiber insulations have shown promise for satisfactory performance at temperatures in the range from 2,000° F to 3,000° F. The data are based on sea-level atmospheric pressure with the exception of the bottom curve which is included for comparison of altitude effect.

Insulated Panel Testing

Insulated panels incorporating various insulations, erosion shields, attachments, and assembly techniques have been fabricated and thermally tested at the Boeing Airplane Company. These insulated panels have included either a metal or a ceramic erosion shield. Some of the ceramic shields were reinforced by a wire grid.

Testing to date has been limited to a maximum temperature of 2,000° F. However, these tests, coupled with those of higher temperature evaluation of materials, have established the foundation for insulated panel designs to operate up to $2,700^{\circ}$ F.

The thermal response of certain types of insulated panels as determined by testing is shown in figure 12. The outer surface of each panel was heated to the test temperature by radiant lamps. After heat flow



1

8



had stabilized, the temperatures were measured at various locations. The lowest curve shows the characteristics of a panel which was partly insulated by the erosion shield. The erosion shield was made from 4- by 6-inch tiles of foamed silicon carbide. The tiles were 1/8 inch thick, and pairs of tile were cemented together for a total thickness of 1/4 inch. The upper curve shows the characteristics of a similar panel with less insulating thickness. These panels survived the test without damage, but the tiles are fragile and several were cracked during fabrication.

The remaining data points show the characteristics of panels with noninsulating erosion shields. Four different insulations were tested in conjunction with this type of shield. Two insulations were load-carrying types and two were non-load-carrying types.

The non-load-carrying types of insulation included Q-felt (silica fiber) at a density of 3 lb/cu ft and Fiberfrax (aluminum silicate) fibers at a density of 8 lb/cu ft. The load-carrying types included Fiberfrax fibers in a board form at a density of 20 lb/cu ft and a ceramic honeycomb in which cells were filled with Fiberfrax at a density of 8 lb/cu ft.

The erosion shields on the load-carrying type of panels included metal, alumina, and alumina reinforced with wire grid. The alumina shielding broke apart during the test, but the wire-grid reinforcement was able to retain the pieces in place; however, the extensive cracking of alumina indicates a probable failure in reentry environment. All of the metal erosion shields survived the tests.

Five different designs were used for supporting the erosion shield in the test panels:

- (1) A load-bearing board type of insulation for compression, and wires at 3-inch intervals for tension loads (A formed sheet-metal part in the center of the panel similar to those shown in figure 10 provided shear transfer.)
- (2) Ceramic spacers at 3-inch intervals for compression and shear, and a wire through each spacer for tension.
- (3) Studs at 3-inch intervals, reaching through the insulation and carrying all types of load.
- (4) Formed sheet-metal parts similar to those shown in figure 10. (The spacing of posts in one test panel was less than that shown so that the posts along each inner panel corrugation were simply 1/2-inch strips of corrugation. In another panel these strips of corrugation were replaced by a continuous sheet of corrugations.)





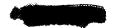
(5) Formed metal channels nested in pairs so that a space between the outer flanges supported the edges of erosion-shield panels.

The wire tension members were sewn through the reinforcing grids in the reinforced alumina shield, and through small formed sheet-metal fittings on the metal shield parts. The studs were attached to the metal parts by speed nuts and to the ceramic shield by ceramic cementing of an imbedded head or sheet-metal fitting. The formed sheet-metal parts were attached by either spotwelding or riveting, depending on the similarity of the metals.

All of these supporting schemes survived the tests without failure with the exception of the alumina erosion shields. The continuous corrugated sheet used for the inner support structure was found to be undesirable for two reasons. First, the thermal response was poor due to excessive heat paths which short circuited the insulation. Second, the free thermal growth of the shield was restrained by the relatively cool valleys of the corrugations. Resulting thermal stresses were found to cause cracking of the shield after several reentry heat-plus-load cycles.

CONCLUDING REMARKS

Development to date has shown that the design and fabrication of structurally sound external surface panels for use to 2,700° F on reentry vehicles are possible. For temperatures to 2,000° F, environmental testing of noninsulated panels has established the capability of these structures to survive the reentry environments. For temperatures between 2,000° F and 2,700° F there are still questions to be answered; however, sufficient work has been accomplished to indicate that these questions will be resolved through a normal design-development program.



SURFACE PANELS IN GLIDER STRUCTURE

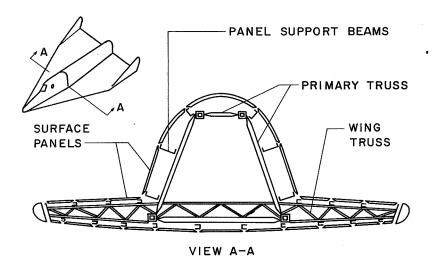


Figure 1

PANEL ENVIRONMENT DURING REENTRY

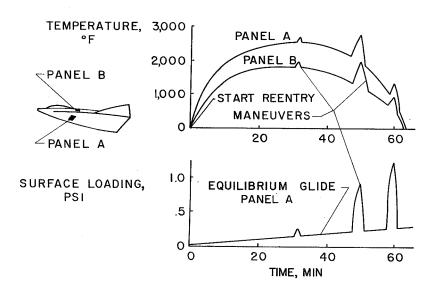


Figure 2





DESIGN APPROACH

- MATERIAL
 - (1) SUPERALLOYS (2,000 °F MAXIMUM)
 - (2) REFRACTORY ALLOYS (OVER 2000°F)
 - (3) INSULATION (OVER 2,000°F)
 - (4) CERAMICS
- CONFIGURATION
 - (I) NONINSULATED (UP TO 2,000°F)
 - (2) INSULATED (ABOVE 2,000°F)
 - (3)"THERMAL RESTRAINT FREE "SUPPORT
- TEST
 - (1) SIMULATED ENVIRONMENT
 - (2) ACTUAL ENVIRONMENT

Figure 3

NONINSULATED PANEL (USE LIMITED TO MAXIMUM TEMPERATURE OF 2,000 °F)

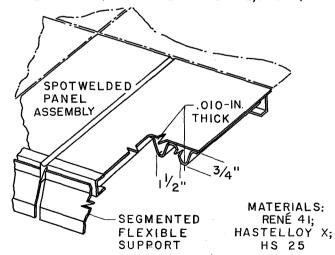


Figure 4



PANEL-EDGE CONFIGURATION

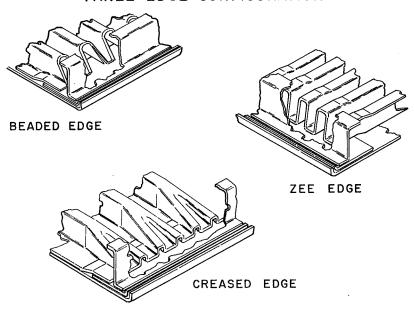


Figure 5

HEAT AND LOAD TEST SETUP

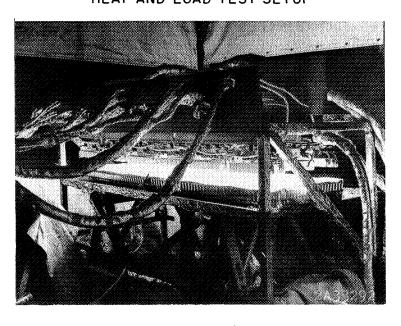


Figure 6

ULTIMATE PANEL TESTS AT 2,000°F

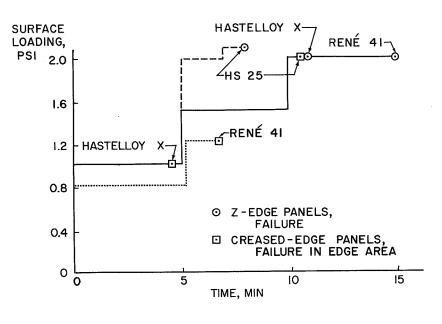


Figure 7

SONIC TEST RESULTS, NONINSULATED PANELS

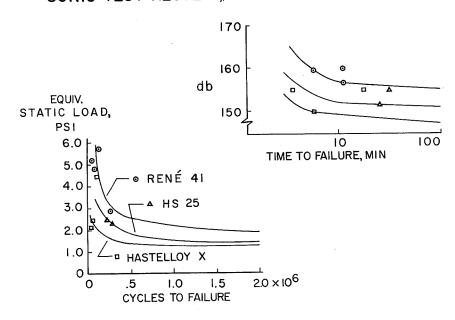


Figure 8



EFFECT OF INCREASING PANEL STIFFNESS

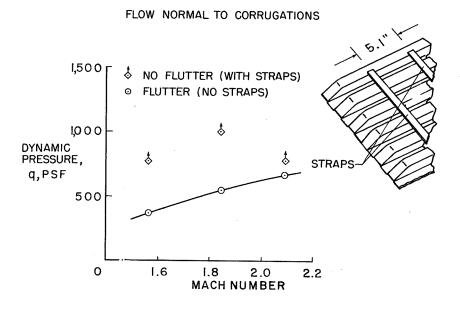


Figure 9

INSULATED PANEL (FOR USE ABOVE 2,000°F)

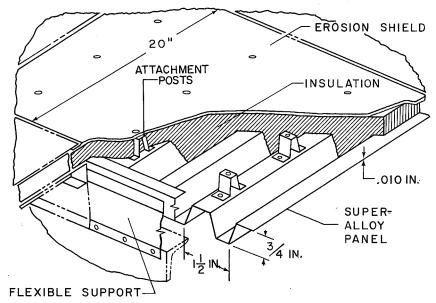


Figure 10





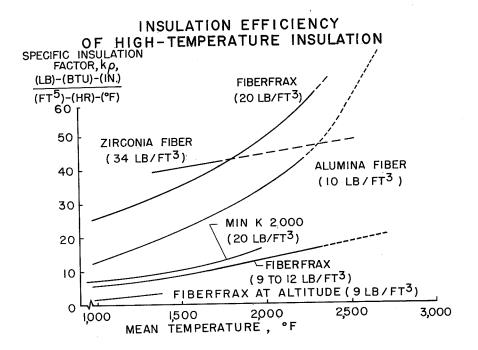


Figure 11

THERMAL RESPONSE OF INSULATED PANELS

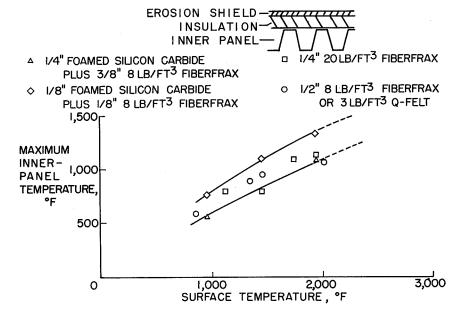


Figure 12



15

CURRENT STATUS OF REFRACTORY METALS FOR

STRUCTURAL APPLICATIONS

By T. Sgt. Jesse C. Ingram, Jr., USAF Wright Air Development Division

TNTRODUCTION

This paper is essentially a report on applied research programs which cover the use of refractory materials as load-carrying primary structural members. The Dyna-Soar glider employs refractory materials in leading edges and heat-shield applications. In order to provide growth capability in the Dyna-Soar glider, higher temperature load-carrying structures would be desirable. This paper is a status report on efforts to achieve this goal. In recent months the Wright Air Development Division (WADD) has been cognizant of an urgent need for immediate development in refractory materials for both structural and heat-shield applications and, since no one had really explored the state of the art in refractory metals structural technology, it was decided that fairly comprehensive programs in this area should be initiated. Figure 1 depicts a nominal trajectory including transient conditions for a typical skip reentry mission.

DISCUSSION

WADD began a number of research and development efforts including a contract with McDonnell Aircraft Corporation for the design, fabrication, and test of a representative, refractory metal, load-carrying, structural component capable of efficient operation in the temperature range of 1,800° F to 2,500° F. The General Electric Company, Flight Propulsion Laboratory Division (Evendale, Ohio), was subsequently selected as the main subcontractor. There are two other subcontractors, that is, Hughes Tool Company (Culver City, Calif.), and Temco (Dallas, Texas). This program was aimed at determining the state of the art and demonstrating the feasibility of a refractory metal structure.

It is widely known that one of the primary requirements to produce a refractory metallic end item, having high integrity, is to begin with closely controlled extraction, refinement, melting, and ingot casting practices. Even if the ore is extracted and refined carefully and a



high purity sponge or other metallic form is obtained many problems remain. An example of one of these problems is conversion of the metal to a powder with which to make ingots for further processing. All refractory metals have an affinity for one or more elements which adversely affect the base metal properties. As a rule undesirable oxides, hydrides, nitrides, etc., may be formed and more often than not, it is necessary to vacuum-arc melt the powder ingot (billet) to purify it. Naturally, the impurity problem does not end here.

Another serious problem is segregation. Because of wide differences in resistivity, conductivity, constituent melting points, and vapor pressures, intolerable differences in chemistry, density, etc., may exist from section to section within the same ingot. This problem has not yet been overcome by powder metallurgy, but it is believed that a properly conducted program on prealloying of powder can greatly alleviate this problem. Also, the undesirable large grain size that is characteristic of cast ingots can be somewhat overcome, initially, through powder metallurgy techniques.

I

1

1

1

9

Next, before the ingot can be processed into bar for machining, or still further processed into sheet, the cast structure must be broken down and the ingot partially homogenized by hot work. Here, again, problems are faced of an entirely different nature. As has been the experience with Al, Mg, Ti, and steel, in order to achieve the ultimate in physical and mechanical properties, hot work or "hot processing" of the material above the recrystallization temperature must be possible and should be started with the basic ingot. In order to accomplish this with arc cast molybdenum (Mo), efficient controlled atmosphere furnaces capable of reaching and maintaining equilibrium temperatures of 3,500° F to 3,600° F are required. The best furnaces available will yield temperatures between 2,700° F and 2,900° F and the capacity of any such furnace is fairly small. In general, the higher capability furnaces are smaller, cylindrical, induction-heated apparatus and therefore are not very conducive to the processing of plate and sheet.

After the ingot is partially warm or hot-cold worked by extrusion and maybe by further swaging into sheet bar, the recrystallization temperature begins to lower. However, the problem of impurities still exists and now, in particular, oxidation and nitriding of the material may occur.

Mo does not exhibit a high degree of oxygen penetration since, at the temperatures under consideration, the oxide product (MoO₃) is volatile and, in processing, this problem could be overcome by either a good vacuum or a reducing atmosphere such as high-purity dry hydrogen. Cracked ammonia will severely nitride and embrittle Mo and commercially available argon contains sufficient amounts of impurities to be quite deleterious. With niobium (Nb), it is different in that the oxide product is both





stable and porous and, therefore, oxygen will continue to penetrate. Here, either a good vacuum or high-purity inert atmosphere is required.

Now, when an attempt is made to roll the sheet bar into sheet, especially thinner gages, the aforementioned problems are magnified. There are essentially no facilities available with necessary atmospheric control. An exception to this statement is the Inert Fabrication (INFAB) facility at Universal Cyclops Steel which is sponsored by the Navy. This facility is a self-contained room with a minimum amount of necessary processing equipment which will be operated in an atmosphere of argon under slight pressure. At present, necessary, reliable, and adequate quality control is almost nonexistent. This is an area that needs very close attention; with it many of our problems, both present and future, can be alleviated or even eliminated.

Consider joining for a moment. (See fig. 2.) It is generally conceded that Mo is very brittle and, therefore, susceptible to fracture in the cast state. This property makes welding a problem and so far no welds, either fusion or resistance, have been seen that did not exhibit severe grain growth and resultant brittle-type fractures. No is more amenable to welding, if in the pure state or even alloyed with certain elements. However, when the alloys which are most attractive for the reentry temperatures involved are considered, problems arise. On the USAF contract with McDonnell Aircraft Corporation the General Electric developed F48 alloy was chosen to fabricate the end item which is a fin and rudder with necessary hinge fittings and attachments but without a leading edge. As of today, it is highly questionable as to whether it is possible to weld it successfully either by fusion or resistance It should be added, however, that at least one of the experiments conducted by the General Electric Company has shown promise in spot welding the F48 alloy. With a thin titanium foil (about 1 mil) inserted between the two sheets and by closely controlling the welding cycle, the notch sensitivity around the shoulder of the nugget has been noticeably reduced. Weld shear values have been increased and fractures are apparently less brittle.

Reasonable success has been realized in riveting both Mo and Nb. Marquardt Aircraft has been riveting and bolting Mo ramjet assemblies for some time but, in general, the detail parts were not coated prior to assembly. In fabricating the small test items under the McDonnell Aircraft Corporation contract, it was deemed necessary to multiple coat in some cases because of the configuration complexity. Figure 3 shows a W2 coated $Mol_{\overline{2}}$ rivet after squeezing. This condition meant using coated rivets, if possible, and this has been done. Even though it is still essentially a hand operation, Mo rivets can be manufactured easily, coated with a W2 or Durak MG type coating, and squeezed successfully by torch heating to 1,600° F or slightly above. Figure 4 shows some of the





more easily manufactured fasteners other than rivets. Driving the rivets by impacting appears to be risky at present. Many other fastener configurations are being investigated and evaluated including blind-mechanical and explosive types. All the refractory metals which may be candidates for structural applications at present and in the foreseeable future are susceptible to oxidation, which can be catastrophic, at the temperatures involved. Molybdenum, which is under serious consideration, reacts violently with oxygen above 1,500° F to 1,600° F; therefore, it must be protected. So far, the only work or development in this area of any great import has been the cementation pack process which has produced a disilicide (or variation thereof) type of coating. This is the best of known available coatings for Mo. However, even though this may be suitable for short-time applications such as ramjet engines, it is not considered at this time to be uniform, entirely reproducible, or wholly reliable for long-time, multiple-mission structural applications. static oxidation tests rather encouraging results have been realized at temperatures up to 2,500° F, but patching or repairing any kind of break or defect appears to be impossible.

The potential of Nb is somewhat more encouraging than Mo up to about 2,500°F, in that the oxide product is stable and not volatile and that Nb is inherently more oxidation-resistant than Mo but it still needs to be protected. However, if a coating failure occurs, the end product should not be as catastrophic as that with Mo. Figure 5 is a time-temperature static oxidation comparison between Nb and Mo alloys. From a relative viewpoint and under a given set of conditions, alloyed Nb can be 100 times as oxidation-resistant as Mo. Incidentally, so far, alloying Mo has not enhanced its oxidation resistance. Again, work on the McDonnell Aircraft Corporation - General Electric Company contract has proven a need for a Nb coating, and a fair amount of effort has been expended in this direction. At present, it appears that an aluminum base cold slurry dip, with subsequent heat treatment, may prove to be the best for this program which of necessity must be limited in scope of coating development.

At this point, it is appropriate to mention some more of the perverse characteristics of promising coatings for structural applications which could possibly offer us the needed protection. First, they are all brittle; at room temperature their impact value is essentially zero. Second, as a rule, their coefficient of expansion is very low, and, therefore, radically different and usually incompatible with the substrate. These two inherent characteristics generally cause, at one time or another, cracking, spalling, crazing, etc. The General Electric Company is investigating the possibility of a glass-like material for an overlay, on the Nb dip coating, which would become viscous at the temperatures under consideration and, thereby, fill and heal any cracks that may have developed.





Production problems should be pointed out which have been encountered in procurement. An order can be placed for a lot of thin gage (below 0.020) material, having a given chemistry, exhibiting reasonable T bend and elongation characteristics at room temperature, and being free from scales, slivers, laminations, gouges, etc. With present technology, the chemistry requirements would probably be met except for a few undesirable segregations and possibly excessive amounts of contaminants. Thin-gage material has been ordered with a promised delivery of 8 weeks and 8 months later the complete order has not been received. Figure 6 is an ultrasonic trace recording of Mo sheet which has been fusion buttwelded. Notice the discontinuities in the weld zone and also the parent metal laminations. At present all material must be accepted on a bestefforts, consigned basis. This year material has been shipped as "supposedly acceptable" and, in the MoZr, more than a half-dozen surface scales and slivers were evident in 1 square foot. Also, Month has been shipped as 0.010 gage in which the thickness varied from 0.0065 at one end to 0.0105 at the other in a 10-inch by 28-inch piece. This is not indicative of quality, quality control, reproducibility, or assurance that the material needed can be obtained today. However, as the gage thickness increases, problems decrease. For gage thicknesses of 0.050 up, either the MokTi, MokZr, or the TZM alloy could be made available in reasonable quantity and with reasonable quality, provided that necessary process control is exercised. Inspection techniques and/or establishment of acceptance standards and limits must still be optimized for these alloys.

Another matter for consideration is expected or calculated yield. The program at McDonnell - General Electric was initiated with material basic cost being estimated at approximately \$60 per pound for Mo sheet and \$120 per pound for Nb sheet. First, with the more attractive alloys, such as the Nb base F48 and Mo base TZC, no more than a 10- to 20-percent yield from the ingot to thin-gage material has been realized. Second, if desired quality requirements were imposed, probably 90 percent of the yield would be rejected. Because of breakage, waste, rejections, etc., our original cost estimates have increased by factors of 5 for the thin-gage material and the material which is ultimately desired for fabrication into usable and reliable structures has not been obtained. Figure 7 does show that with careful processing techniques it is possible to hand fabricate small detailed parts.

CONCLUDING REMARKS

For structural applications other than heat shield and leading-edge elements, problems associated with ingot production, sheet quality control,



available assembly, coating, and material cost have been presented. Because of these problems our confidence in structural applications of refractory materials is poor; however, it is hoped that, at the conclusion of the McDonnell - General Electric program in September, a satisfactory test of component hardware will be accomplished and the program will have indicated the steps which industry as well as the USAF must take to assure reliable efficient refractory structures. The creep and rupture properties shown in figure 8 are a very real reason why these refractory metals are so attractive for elevated-temperature structural and heat-shield applications.

COLET

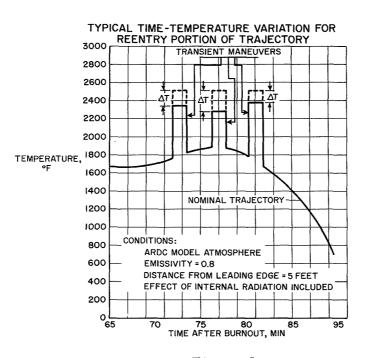


Figure 1

MOLYBDENUM ALLOY WELDING PROBLEMS

- I. LOW DUCTILITY OF WELD DEPOSIT
 - a. LARGE GRAIN SIZE IN WELD AREA
 - b. CRATER CRACKING (OXYGEN)
 - c. GRAIN BOUNDARY CONSTITUENTS
- 2. POROSITY IN WELD DEPOSITS
- 3. ELECTRODE STICKING (RESISTANCE WELDING)
- 4. TENSILE PROPERTIES OF WELDS
- 5. POST WELD CRACKING (RESIDUAL STRESSES)

Figure 2



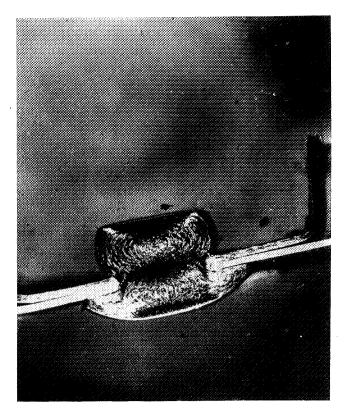


Figure 3

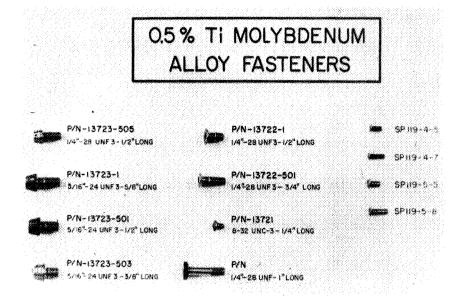


Figure 4





2300°F OXIDATION

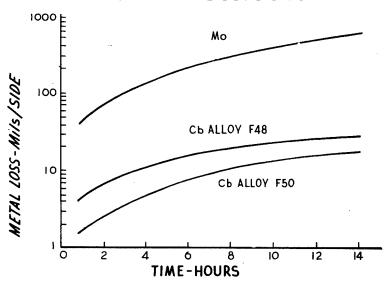


Figure 5

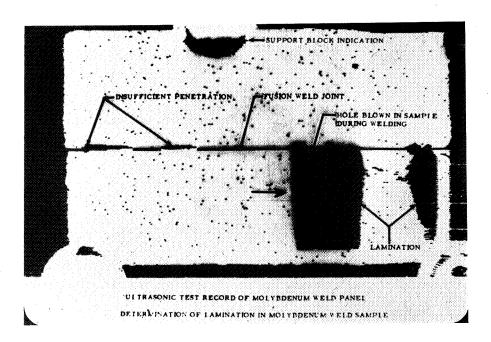


Figure 6





CREEP AND RUPTURE STRENGTH OF MOLYBDENUM ALLOYS 100-HR. EXPOSURE

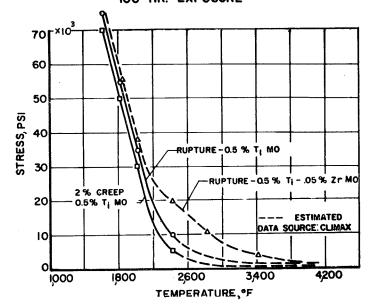


Figure 7

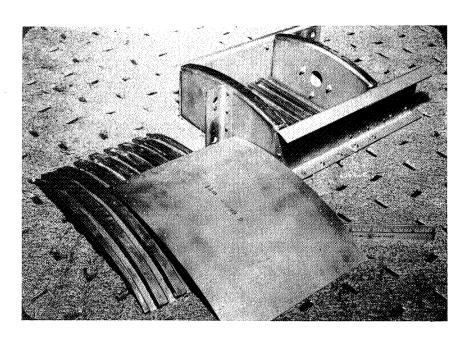


Figure 8



HOT-GAS TESTS FOR DYNA-SOAR STRUCTURES AND

MATERIALS DEVELOPMENT

By E. L. Kaminsky and H. W. Klopfenstein Boeing Airplane Company

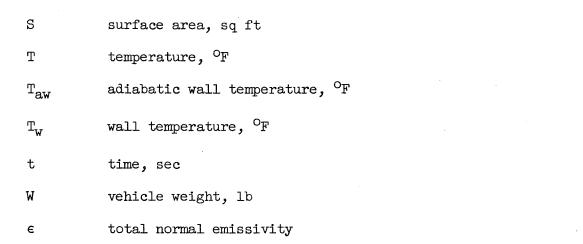
INTRODUCTION

During Phase I of the Dyna-Soar study, a considerable number of hot-gas tests were performed for purposes of developing materials and full-scale structural components intended for application to the Dyna-Soar reentry glider. The tests on full-scale components were feasibility tests, not proof tests. Proof testing of the Dyna-Soar vehicle will take place during actual flight of the vehicle. Prior to actual flight, preliminary flight tests like those of Pilotless Aircraft Research Division (PARD, now Applied Materials and Physics Division) of NASA and the Hyper Environmental Test System (HETS) of BMD, USAF, are contemplated, but hot-gas tests in ground facilities will be used as aids in the final choice of materials and structural designs. Resorting to hot-gas tests means becoming involved in the problem of simulating, in a ground facility, the reentry environment. This discussion deals primarily with this simulation problem; that is, with the types of tests performed, the degree of simulation obtained, the limitations of the facilities, and the results of the tests. The present investigation is restricted to tests on full-scale components.

SYMBOLS

$c_{\mathbf{L}}$	lift coefficient
$\mathbf{c}_{\mathbf{p}}$	specific heat at constant pressure, Btu/(lb)(OF)
h	heat-transfer coefficient, Btu/(sq ft)(sec)(OF)
m	mass, 1b
ģ	heat flux, Btu/(sq ft)(sec)

σ.



DISCUSSION AND RESULTS

Stefan-Boltzmann constant, 0.4759 x 10-12 Btu/(sq ft)(sec)(oR)4

Calibration Tests

The purpose of the hot-gas tests was to determine whether full-scale structural components fabricated from various materials could survive exposure to test conditions intended to simulate the vehicle flight environment. In order to illustrate the nature of this environment, the conditions encountered by the nose cap of the Dyna-Soar glider during a typical reentry are discussed herein.

The heat flux shown by the dotted line in figure 1 is anticipated for the environment at the stagnation point on the glider nose cap. The maximum value reached is 178 Btu/(sq ft)(sec), and the corresponding radiation-equilibrium temperature, based on an emissivity of 0.9, is 4,060° F. The stagnation point is subjected to high heat fluxes for relatively long periods of time. For example, the time of exposure to heat fluxes in excess of 170 Btu/(sq ft)(sec) is 12 minutes; in excess of 160 Btu/(sq ft)(sec), 17 minutes; and in excess of 150 Btu/(sq ft)(sec), 20 minutes. Maximum values of other flight parameters, such as stagnation-point pressure, total enthalpy of the stream, relative stream velocity, and stream mass-flow rate for the same reentry trajectory, are tabulated in the second column of table I. Complicating the problem is the presence of an oxidation and erosion environment.

No present ground test facility can duplicate all flight parameters simultaneously; consequently, the question arose concerning which parameters should be simulated. Since some of the structural components on the Dyna-Soar glider are radiation-cooled designs fabricated from





refractory metals, which oxidize catastrophically if protective coatings fail, and refractory nonmetals, which can fail due to thermal stresses, oxidation, or erosion, it was decided that the heat flux, maximum surface temperature of the component, amount of oxygen in the gas stream, and time of exposure to high temperature were the important parameters. The importance of the parameters for these structural components is in contrast with those for ablating components, for example, where stagnation enthalpy is the most important quantity. In order to eliminate scale effects, it was also decided that tests would be performed on full-scale components.

The next problem to be resolved concerned the kind of test facility The practical choices were ram jet, rocket exhaust, or plasma jet. Early tests were conducted using ram-jet facilities for both leading-edge and nose-cap tests; however, these facilities were incapable of producing the maximum design heat flux and stagnation temperature of the nose cap. Also, the combustion products of the fuel used did not provide simulation of gas chemistry. Rocket-motor facilities will simulate maximum design heat flux and temperature. These facilities operate at pressures considerably higher than flight values and have the same problem as ram jets with regard to gas chemistry. The gas-stabilized-arc plasma jet at Chicago Midway Laboratories (CML) of the University of Chicago was selected because it met all requirements except time of exposure and because the facility was available on a schedule demanded by the test program. The compromise adopted concerning time of exposure is illustrated by the solid line in figure 1 for the nose cap. A single exposure in this facility is limited to $2\frac{1}{2}$ minutes. Hence, the component being tested was first heated to 2,700° F in a furnace, swung into the gas stream for $2\frac{1}{2}$ minutes, returned to the furnace for about 30 seconds while the cathode on the arc unit was being changed, and then swung back into the stream. This process was repeated until a total of four $2\frac{1}{2}$ - minute exposures had been run. At the end of the second exposure, the anode was replaced. The simulation of flight environment conditions obtained in the CML facility is shown in table I. Stagnation pressure and mass flow are higher than the corresponding values for the vehicle, and enthalpy and stream velocity are lower. The gas used in the facility was nitrogen, but sufficient air was entrained to provide an ample supply of oxygen at the component. Stagnation-point heat flux and equilibrium temperature were simulated.

In calibrating the CML test facility, two specimens for each type of structural component were used: a high-temperature specimen and a low-temperature specimen. The high-temperature specimen for nose caps is shown in figure 2. The specimen was fabricated from AGR graphite, and slots and grooves were machined into it to reduce heat flow by conduction



from the stagnation-point region. The base diameter of the specimen was smaller than that of the actual cap, but the nose radius was full scale. The specimen location required for simulation of heat flux and radiation-equilibrium temperature was found by the following procedure: After being placed at a selected distance downstream from the orifice of the arc unit, the specimen was subjected to a $2\frac{1}{2}$ -minute exposure in the

plasma flow, and the arc unit was then turned off. At that instant, the heat flux being emitted from the stagnation point of the specimen was measured by a recording radiation pyrometer, which had been calibrated previously. Measurements of heat flux were made at sufficient specimen positions in the stream to establish where the design heat flux of 178 Btu/(sq ft)(sec) occurred. Assuming that the emissivity of the graphite specimen was 0.9, the radiation-equilibrium temperature of 4.060° F is computed from the formula

$$\dot{\mathbf{q}} = \epsilon \sigma \left(\mathbf{T}_{\mathbf{W}} + 460 \right)^{1/4} \tag{1}$$

The calibration of the test setup with the high-temperature specimen does not make available a means for evaluating the effect of difference in emissivity of a component from the calibration specimen, nor does it provide a means for obtaining the heat flux at points other than the stagnation point.

A low-temperature copper specimen, shown in figure 3, was used in the second step of the calibration. Built into the specimen were copper calorimeters, each containing a thermocouple. The specimen was first located in the apparatus at the position occupied previously by the high-temperature specimen, and a Transite shield was placed between the specimen and the arc unit. The arc unit was turned on and brought to full operating condition, and the Transite shield was removed. The temperature-time history for the thermocouple in each calorimeter was then recorded, and the test continued until incipient melting of the specimen was detected. Since the specific heat and mass of the copper calorimeter were known, it was possible to compute the net heat flux delivered to the calorimeter from the equation

$$\dot{q}_{\text{net}} = c_{\text{p}} \frac{m}{S} \frac{dT}{dt}$$
 (2)

Since

$$\dot{q}_{\text{net}} = h \left(T_{\text{aw}} - T_{\text{w}} \right) - \epsilon \sigma \left(T_{\text{w}} + 460 \right)^{1/4}$$
 (3)



Z



and since the emissivity of copper is well known, the convective heat flux, which is:

$$\dot{q} = h \left(T_{aw} - T_{w} \right) \tag{4}$$

can be computed.

For convenience, the slope of the temperature-time curve was evaluated at a temperature of 800° F. The use of a number of calorimeters made it possible to obtain the heat-flux distribution over the specimen.

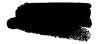
From these tests performed on the calibration specimens, two points were obtained for the variation of heat flux with surface temperature at the stagnation point shown in figure 4.

If it is assumed that the dependence of the heat-transfer coefficient on the wall temperature is weak, the heat flux is a linear function of the wall temperature, and a straight line can be drawn connecting the two points mentioned previously. The line for the nose-cap calibration in the plasma jet is shown in figure 4, and for comparison a line is also plotted for the vehicle with the assumption that the heat flux is constant. Plots of equation (1) for various values of emissivity are also shown in this figure. The intersection of an emissivity curve with the calibration line represents the heat flux and radiation-equilibrium temperature for the emissivity selected. With these curves, it was possible to estimate the actual emissivity and temperature of a nose-cap material based on measured heat flux. First, the heat flux was measured by the radiation pyrometer. With this value as an ordinate in figure 4, a horizontal line was drawn to the calibration line, and the radiationequilibrium temperature and emissivity determined. The intersection of the emissivity curve with the vehicle line represents what the heat flux and temperature would be in flight.

The comparison between computed heat-flux distribution and the distribution measured on the low-temperature specimen is shown in figure 5. The discrepancy is partly due to the variation of temperature through the cross section of the jet issuing from the arc unit.

Test Results

Tests were performed at Chicago Midway Laboratories on full-scale nose caps and leading edges and on small, insulated skin panels and antenna-cover materials. The nose caps were provided under subcontract from Chance Vought Aircraft, Incorporated. The nose caps were constructed of hemispherical segments of ATJ graphite. Additional thermal capability was provided in the tip through the use of zirconia rods. Incipient





melting of the nose cap and oxidation and erosion of the graphite adapter occurred, but the nose-cap specimen survived the test.

The following summary of 6-inch-diameter leading-edge components tested in the CML facility includes the test conditions and results:

- 1. A composite segment fabricated of phosphate-bonded chromia-alumina reinforced with molybdenum wire was tested under unknown environmental conditions since the radiation pyrometer was not connected during the test. A small, shallow crack formed in the component parallel to and about 2 inches from the stagnation line, but the component survived the test.
- 2. A flame-sprayed multilayer laminate of alumina and molybdenum was tested at a recorded heat flux of 34 Btu/(sq ft)(sec), and emissivity of 0.4, and a radiation-equilibrium temperature of $3,150^{\circ}$ F. The component smoked badly in the preheat furnace and delaminated in the plasma jet.
- 3. A circumferentially and longitudinally stiffened, welded columbium shell protected by Chromalloy N-l coating was tested at a recorded heat flux of 32 Btu/(sq ft)(sec), an emissivity of 0.37, and a radiation-equilibrium temperature of $3,200^{\circ}$ F. The outer layer of the coating melted and flowed. Three small holes approximately 1/8 to 1/4 inch in diameter appeared near the stagnation line, possibly due to impact of graphite against the specimen when a piece of the anode broke off in the arc unit and moved downstream.
- 4. A circumferentially and longitudinally stiffened, welded 33-percent-tantalum—columbium shell protected by Chromalloy N-1 coating was tested at the same environmental conditions as those for the previous specimen. Again, the outer layer of the coating melted and flowed, but the intermediate layer remained intact, and the substrate was protected. The component passed the test.
- 5. A circumferentially and longitudinally stiffened, welded 0.5-percent-titanium—molybdenum shell protected by Chromalloy W-2 coating was tested at a measured heat flux of 43 Btu/(sq ft)(sec), an emissivity of 0.7, and a radiation-equilibrium temperature of 2,900° F. There was a slight glassy discoloration of the surface, but the component passed the test.
- 6. A circumferentially and longitudinally stiffened, riveted 0.5-percent titanium—molybdenum shell protected by Chromalloy W-2 coating was tested at the same environmental conditions as those for the previous specimen. The same glassy discoloration appeared, but the component passed the test.





For all of these leading-edge tests, the component was preheated to 2,300°F before exposure to the plasma jet.

In addition to the CML tests, preliminary evaluation tests were performed in a ram-jet exhaust by the Marquardt Aircraft Company on 4-inch-diameter leading edges. Two designs were tested: a longitudinally stiffened 0.5-percent-titanium—molybdenum shell protected by Chromalloy W-2 coating and a phosphate-bonded alumina component reinforced with molybdenum wire mesh. The components were not preheated for these tests. The component, at room temperature, was swung into the exhaust gases of the ram-jet burner, held there approximately 20 minutes, and then swung out and allowed to cool to room temperature. On the typical molybdenum specimen, the maximum temperature reached during the first two tests was $3,025^{\circ}$ F, and the component was unaffected after several test runs with a cumulative test time of $43\frac{1}{2}$ minutes at $2,800^{\circ}$ F or higher. During the

first test on the alumina component, the maximum temperature reached slightly exceeded $3,000^{\circ}$ F, and two hairline cracks appeared during the cooling cycle. In the second test, the maximum temperature was $3,150^{\circ}$ F. A slight change in shape occurred in the hottest area. The maximum temperature reached during the third test was about $3,200^{\circ}$ F. There were no additional cracks and no further shrinkage.

Tests on full-scale graphite nose sections and molybdenum skirts were conducted in the ram-jet facility at Chance Vought Aircraft, Incorporated. The graphite was siliconized ATJ with and without a further multilayer coating of molybdenum, zirconia, and alumina. Welded and riveted skirt designs were tested. The molybdenum was chromized and also protected by the multilayer coating. In general, the tests indicated unsatisfactory performance of both cap and skirt. It was not possible to reach a stagnation-point temperature of 4,000° F in the ram-jet facility. The multilayer coating failed at the stagnation point and flaked off in some regions of the skirt. Based on the results of these tests, the design of the nose was changed. The tip was subsequently constructed from zirconia rods inserted into a siliconized graphite nose as described previously for the CML tests. The coating on the molybdenum skirt was changed to Chromalloy W-2.

CONCLUSIONS

1. Through the use of a gas-stabilized-arc plasma jet, it is possible to simulate, on full-scale structural components, the most severe heating conditions encountered during reentry of a hypersonic glider, but because of the short operating time of the plasma jet, it was not possible to simulate uninterrupted time of exposure to heating.





- 2. The plasma jet appears to be the only ground test facility which can approximate the gas chemistry during heating. The ram jet and rocket exhaust cannot provide this simulation. Also, the ram-jet and rocket-exhaust facilities are limited to lower enthalpies than plasma jets.
- 3. The plasma-jet facilities provided partial correction for possible errors in predicting emissivity of test parts. Plasma-jet facilities with enthalpy equal to flight conditions can provide essentially complete correction for errors in emissivity prediction.
- 4. Although testing with a plasma jet is limited to relatively small components compared with radiant-heat-lamp testing, it has the following advantages:
 - (a) Radiant-heat facilities cannot simulate nose-cap temperatures.
 - (b) Heat flux rather than controlled temperature is applied by plasma jet.
 - (c) It is possible to simulate environmental parameters such as oxidation and erosion with a distributed airload in a plasma jet.
 - (d) It is possible to avoid off-design thermal gradients such as those which occur when part of a radiant-heat setup fails.

TABLE I

COMPARISON OF CML ENVIRONMENT
WITH VEHICLE NOSE ENVIRONMENT

,	CML	VEHICLE
STAGNATION POINT PRESSURE, LB/FT ²	2,116	350
ENTHALPY OF STREAM, BTU/LB	2,300	10,000
STREAM VELOCITY, FT/SEC	2,500	24,000
HEAT FLUX (== 0.9), BTU/FT 2 SEC	178	178
STREAM MASS FLOW RATE, LB/FT ² SEC	16.4	0.432
STAGNATION POINT EQUILIBRIUM TEMPERATURE («=0.9), °F	4,060	4,060
CHEMICAL SPECIES OF BOUNDARY LAYER	N& AIR, PART, ATOMIC& IONIZED	AIR, PART. ATOMIC & IONIZED



PLASMA JET SIMULATION OF VEHICLE STAGNATION POINT HEAT FLUX VERSUS TIME

$$\frac{W}{SC_1} = 311 \quad \frac{LB}{FT}2$$

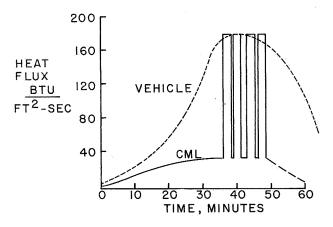


Figure 1

CML HIGH-TEMPERATURE CALIBRATION MODEL (NOSE CAP) AND INSTRUMENTATION

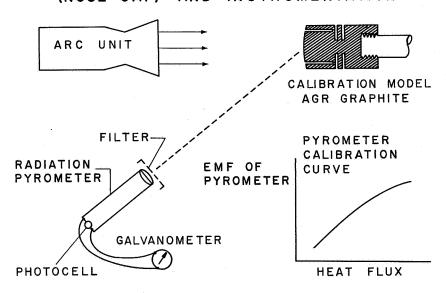


Figure 2





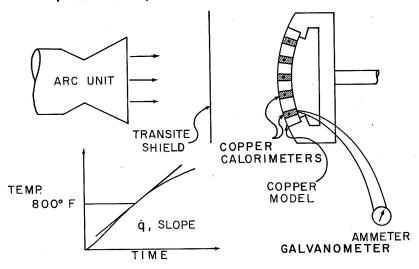


Figure 3

COMPARISON OF PLASMA JET AND VEHICLE STAGNATION POINT HEAT FLUX

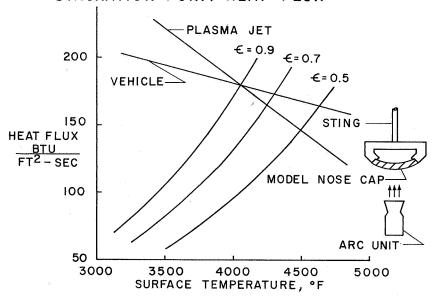


Figure 4



NOSE CAP HEAT FLUX DISTRIBUTION

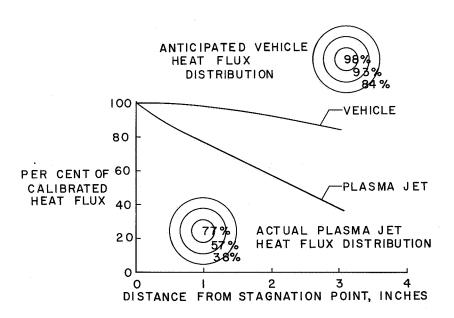


Figure 5



BOOSTER-STRUCTURE-MODIFICATION STUDIES FOR

WINGED DYNA-SOAR VEHICLES

By R. M. Haynes, R. T. Boll, and M. T. Braun Boeing Airplane Company

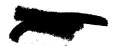
TNTRODUCTION

The utilization of booster systems based on those utilized in current ICBM's (Intercontinental Ballistic Missiles) for boosting manned winged payloads to orbital or near orbital speeds requires modifications of the booster structure and an increase in the engine deflection limits, or the addition of large stabilizing fins. These changes and modifications are required in part because of the addition of the lifting surface on the front of the booster and in part because of the design criteria which are unique to manned winged Dyna-Soar type vehicles.

This paper discusses some of the implications as to effects of these items on the booster structural requirements, touches on the aeroservo-elastic stability characteristics, and finally illustrates several potential load-reduction schemes which have been considered.

SYMBOLS

q	dynamic pressure, lb/sq ft
$\mathtt{C}^{\mathbf{L}^{\alpha}}$	lift-curve slope, per deg
s	reference area, sq ft
P_{eq}	equivalent end load, 1b
Paxial	axial load, 1b
M_{b}	bending moment, in-lb
R	radius, in.





R ₁	pitch-fin area ratio, S/S _O
Z	stiffness parameter, $(\omega/\omega_0)^2$
κ_{θ}	pitch attitude gain, deg/deg
Кė	pitch rate gain, deg/deg/sec
$\kappa_{oldsymbol{eta}}$	control-surface gain, deg/deg
L	normalized body length
α	angle of attack, deg
θ	local pitch angle at booster-glider transition, deg
ė	local pitch rate at booster interstage, deg/sec
ω	frequency of first bending mode, radians/sec
$\delta_{ m T}$	thrust deflection from center line, deg
Subscript	• • • • • • • • • • • • • • • • • • •
o ·	nominal value representative of design value

L 1 2

UNIQUE CRITERIA

Four major unique criteria which have directly influenced structural design and structural weight in the Dyna-Soar Phase Alpha studies are listed in figure 1. The significance of these criteria is explained as follows:

- (1) The criterion to provide at least neutral aerodynamic stability during first-stage boost reflects directly in the design and attachment problem of the stabilizing fin and also influences the aeroelastic behavior of the vehicle.
- (2) The influence of a factor of safety of 1.4 is somewhat obvious since the standard missile structural factor of safety is 1.25.
- (3) The third criterion, pilot safety from hazardous malfunction conditions, establishes that adequate time must be allowed for the pilot





to escape from the booster before the occurrence of major structural failure due to engine or autopilot servo failures.

1 1

4.3

(4) The 5° angle-of-attack capability during boost has been selected to provide a margin for pilot and control-system tolerance and lag during flight through the lower altitude wind profiles.

PARAMETRIC STUDIES

Application of these criteria to one of the Phase Alpha winged configurations, in conjunction with the usual design wind criteria, for example, wind shear-turbulence and ground wind, results in the design bending moments shown in figure 2. The requirement for $5^{\rm O}$ angle-of-attack capability is most severe when the aerodynamic loading is highest (maximum $qC_{\rm L}_{\rm C}$) and actually results in the most critical loading condition over most of the booster.

The pilot-safety criterion, which requires that structural integrity following a malfunction be maintained for something on the order of 1 second, results in the condition shown in figure 2 as engines hard-over. The loads resulting from this condition are not critical for this particular configuration, but such is not always the case.

In general, it may be assumed that storm turbulence and wind-shear conditions do not occur simultaneously. However, there is a distinct possibility of nonstorm turbulence in the vicinity of the tropopause, and the loads resulting from this turbulence must be combined in some manner with the wind-shear loads. The exact correlation between wind shear and gust loads is not known, but it is probably positive. The loads which would result from such turbulence were approximated by determining the response to a 12 ft/sec discrete gust. These loads were combined directly with the load response for flight through a synthetic 1-percent wind-shear profile for Patrick Air Force Base. The resulting bending moments are not critical for this configuration.

The ground-wind condition, which was based on a 60 ft/sec steady wind plus a 30 ft/sec gust, is critical on the aft end of the booster.

The effect of variation in reentry-device weight is to change the relationship between the $5^{\rm O}$ condition and the wind-shear response. A comparison of the severity of the $5^{\rm O}$ trim condition at maximum $q^{\rm C}L_{\rm C}$ with that of the wind-shear-plus-gust condition is shown in figure 3. This comparison illustrates the point that for the range of reentry-device weight studied, the $5^{\rm O}$ trim condition is the critical condition. It should be pointed out, however, that this figure is based on an area of 250 square feet for the reentry device and that an increase in reentry-device area would cause an increase in the bending-moment ratio. That is,

the 5° trim condition becomes more severe relative to the wind-shear-plus-gust condition as the reentry-device area is increased.

·...

7

The variation of booster loads during first-stage burn time for the 5° trim and engines hard-over conditions is presented in figure 4 for a winged reentry device. Equivalent end load $\left(P_{\text{eq}} = P_{\text{axial}} + \frac{2M_{\text{b}}}{R}\right)$ for a particular booster station is shown plotted against first-stage burn time for a reentry-device area of 330 square feet and weight of 9,283 pounds. The 5° trim condition essentially increases with increasing dynamic pressure, reaching a maximum value at maximum qCL, and then decaying as burn time increases. The contribution of bending moment is illustrated by the difference between the axial-load-alone curve and the total-end-load curve. The end load due to engines hardover increases with burn time, primarily as the axial load increases since the contribution due to bending moment is practically constant with burn time. The end load due to ground wind is also shown for comparison. As may be seen from figure 4, the critical condition varies from ground wind at time zero to the 50 trim condition, with the engineshard-over condition becoming critical near first-stage burnout. The design condition at this particular station is, of course, the 5° trim condition. A similar variation of equivalent end load is shown in figure 5 for a ballistic reentry device with an area of 54.5 sq ft and a weight of 7,221 pounds. The condition of engines hard-over is seen to be critical throughout the range of first-stage burn time. A comparison of this figure with figure 4 illustrates the effect of reentry-device area on booster design.

It should be pointed out that the remainder of the parametric data presented is based on strength-designed boosters and, therefore, is based on a booster stiffness obtained from the design of a booster for the particular reentry-device area and weight for which the parameters $SC_{L_{\gamma_{1}}}$ and weight are being read. The data presented are based on the Titan Lot "J" ICBM modified to meet the appropriate strength requirements. The effect of reentry-device area and weight on booster maximum bending moments is further emphasized in figure 6. These data are based on the 50 trim condition at maximum dynamic pressure. For the 9,000-pound reentry-device weight, an increase in $SC_{L_{re}}$ from 1.20 to 15.0 increases the maximum bending moment by 1,320 percent. Since the value of SCL, of 1.20 is representative of a ballistic device, these increases in booster bending moment emphasize again the effect that winged reentry devices have on booster design. The reduction in maximum bending moment due to increasing the reentry-device weight is, of course, due to the increase in inertia relief. At a value of $SC_{L_{rx}}$ of 7.50, an increase of reentrydevice weight from 6,000 pounds to 12,000 pounds decreases the maximum bending moment by 20 percent.





The effect of these bending moments on the booster structural material required for strength-designed boosters is shown in figure 7, where cross-sectional area is plotted against body station for $\mathrm{SC}_{L_{\alpha}}$ values of 1.2, 7.50, and 15.0. Once again, since the value of 1.20 for $\mathrm{SC}_{L_{\alpha}}$ is representative of a ballistic device, the difference in area required between this curve and the other values of $\mathrm{SC}_{L_{\alpha}}$ emphasizes the effect of winged reentry devices on booster design. It should also be noted that this difference increases toward the forward end of the booster.

Because of flexibility in the structure, the angle of attack at the reentry device will be greater than the angle of attack at the vehicle center of gravity, and the angle of attack at the fins will be less than the angle of attack at the vehicle center of gravity. The ratio of the angle of attack at the reentry device to the angle of attack at the fins is a measure of the amount of structural deformation present. The effects of the reentry device $\mathrm{SC}_{L_{\mathrm{CL}}}$ and weight on this flexibility ratio are shown in figure 8. This flexibility effect is directly related to the pitch-fin-area requirements, as illustrated in figure 9. Here the effect of the reentry device $\mathrm{SC}_{L_{\mathrm{CL}}}$ and weight are related to the pitch fin $\mathrm{SC}_{L_{\mathrm{CL}}}$ required for neutral aerodynamic stability at the maximum dynamic pressure 5^{O} trim condition. The effects of structural deformation, which are included in these requirements result in from 2 percent to 73 percent more fin than would be required from rigid-body considerations.

1.0

Conversion of the pitch-fin-area requirement from figure 9 and the structural-material-area requirements from figure 7 directly into weight results in a structural weight requirement as a function of the reentry-device area (fig. 10). It is seen that for a 9,000-pound reentry device and an $\mathrm{SC}_{L_{\alpha}}=9.8$ (representative of a 330-sq-ft glider), approximately 65 percent of the weight added to the ICBM booster system is directly attributable to the fins and booster modification required for their installation. This weight is a direct result of the requirement for neutral aerodynamic stability. Of the remaining 35 percent of added weight, which is necessary because of the air loads resulting from the winged device on the front of the booster, the contribution of the second stage is the largest and that of the first stage is the least.

Comparing the data for other reentry-device weights with the 9,000-pound data gives the results shown in figure 11. The conclusions are, as would be expected from the trends shown previously (figs. 6, 7, and 9), that the heavier the reentry device, the smaller the structural-weight penalty to the booster; and the greater the reentry-device area, the greater the structural-weight penalty to the booster.





AEROSERVOELASTIC CONSIDERATIONS

The interaction between the elastic structure and the automatic control system is always of some concern for flexible missiles. This problem is potentially intensified by the addition of the glider on the front of the booster and the attendant destabilizing effect of the wing. The rigorous treatment of this problem would require a very detailed analysis and an extensive knowledge of the structure and the flight control system of the configuration. Such an analysis was not suitable, nor warranted, for a study such as that conducted for Dyna-Soar Phase Alpha. However, a preliminary study of this problem was conducted for a 7,800-pound, 330-square-foot glider on a modified Titan ICBM. Rigid-body pitch, rigid-body translation, and the first body-bending mode were considered as degrees of freedom. The system analyzed was assumed to have a thrust-vectoring control system governed by a simple linear control law expressed as follows:

$$\delta_{\mathbf{T}} = K_{\theta}\theta + K_{\theta}^{\bullet}\dot{\theta}$$

Nominal values of K_{θ} and $K_{\dot{\theta}}$ (1.0 and 0.5, respectively), which resulted in a rigid-body pitch frequency of 0.3 cps with approximately 0.7 critical damping for the system with the nominal stability fins, were chosen. Figure 12 illustrates the effect of pitch-fin area ratio R₁, as a function of booster-bending-stiffness parameter Z, on the aeroservoelastic characteristics of the system. The nominal configuration is indicated. For small pitch-fin areas the system is unstable in the pitch mode, as illustrated by the area below the stable portion of the curve. As fin area is increased, the system first becomes stable and ultimately again becomes unstable in the first elastic mode. The pitch-fin area required to cause this modal instability is a function of the bending stiffness, as indicated. The nominal configuration is well within the stable region. However, this figure has illustrated only one effect. Adjustment of the attitude gain K_{θ} can result in a considerable change in the stability characteristics, as illustrated in figure 13. The effect of fin area is reflected in the position of the stability boundary in this figure. For the configuration without stabilizing fins $(R_1 = 0)$, it is apparent that, although unstable at the nominal gain and stiffness, the system can be gain stabilized. This effect is also apparent for the case where the pitch-fin area is twice the nominal value $(R_1 = 2)$. For $R_1 = 0.5$ and 1.0, gain changes do not affect the stability characteristics appreciably. As shown in figure 12 and again in figure 13, it is of significance that a large static stability margin can result in a modal instability. The approximate stability margins resulting from the tail (pitchfin) areas considered in this study are:



Tail area ratio	Stability margin, percent body length
0	-4O
y •5	+1
1.0	+12
2.0	+20
l s	

*Nominal tail area = 425 sq ft.

Figures 12 and 13 have shown to some extent how control gain, bending stiffness, and static stability (pitch-fin area) can influence the aeroservoelastic stability problem and, potentially, how they might influence a stiffness requirement for the vehicle. The structural-load response to atmospheric disturbances is not insensitive to these same parameters. Figure 14 indicates some of the trends in maximum bending-moment response to a wind-shear profile which results from variation of one of these parameters, with all others held at their nominal value. These trends become particularly significant if wind-shear considerations are critical from the design-load standpoint. Fortunately, from the load analysis point of view, wind shear was not a critical condition for the Phase Alpha studies.

BENDING-MOMENT-REDUCTION DEVICES

It has been shown previously in figures 4 and 5 that the booster loads associated with a forward-mounted lifting device are quite large in comparison with those incurred by a ballistic device. Consideration of the use of existing ICBM's as potential boosters for the Dyna-Soar glider has resulted in considerable thought as to how existing boosters could be utilized with a minimum of modification and the least possible loss in performance. Alleviation of the large glider-induced bending moments is potentially one means of minimizing this modification.

Three different "forward flying" schemes for load alleviation which have been investigated at Boeing are shown in figure 15. The first involves use of the existing glider elevons. Proper actuation and phasing of the glider elevons during boost reduces the net aerodynamic load on the glider and thereby also reduces the booster bending moments and the thrust force required for pitch trim. The second scheme requires the addition of a set of "flippers" just aft of the glider. These flippers serve essentially the same purpose as the elevons. That is, by proper actuation, the flipper load can be made to cancel the glider aerodynamic load so that the booster bending moments are reduced. The third scheme requires the glider to be supported, free in pitch, at the glider center of gravity. Since the aerodynamic center of the glider is aft of



the pivot point, the glider will seek a zero angle-of-attack position, so that the glider aerodynamic loads and the booster bending moments are reduced.

In figure 16 the magnitude of bending-moment reduction which can be achieved by one of these schemes is illustrated. The bending-moment response of a typical system with geared elevons to a sharp-edge-gust disturbance is shown as a function of the body-length ratio L/L_0 . An elevon control gain K_{B} of 6.0 (that is, 6° of elevon angle per degree of engine thrust deflection) results in a 60-percent reduction in applied bending moment. Figure 17 illustrates, comparatively, the typical reductions which can be achieved by each of these three schemes. Although the load distribution varies somewhat, the reductions are of the same order of magnitude. These results were obtained from preliminary dynamic analyses, and although these systems appear to have promise as far as the required modification to the booster structure is concerned, additional work must be done to prove their full feasibility. Some other considerations which must be included in a complete feasibility study would be the loss in performance due to additional drag, the power-system requirements to drive the control surfaces, the complication of the aeroservoelastic problem, the weight penalties, and the decrease in total system reliability.

It must be pointed out that reduction of bending moment can be carried past the point of no return. The data of figure 4 show that if the moment is reduced to the point where the total end load, at the maximum air load point (t=65 seconds), is less than the total end load resulting at first-stage burnout (t=136 seconds), the air load is no longer the critical design condition. It could very well be that the loads at first-stage burnout are in excess of those incurred in the ballistic missile application of the same booster. In such case, modification of the missile is required anyway, and in essence, the price of admission may have already been paid.

CONCLUDING REMARKS

Results presented have shown that the addition of a winged reentry device to an existing ICBM can result in large structural weight penalties to the booster. Similarly, it has been shown that criteria unique to the particular system also have a significant influence on the final booster structural weight. The influence of certain control-system and stability parameters on aeroservoelastic stability has been illustrated. Several methods for load alleviation have been illustrated, and the structural benefits and limitations of these methods have been described.





At the present time the approach being used to handle the structural modification problem on the Dyna-Soar boost system is that of the simple straightforward approach of structural "beefup."



DESIGN CRITERIA UNIQUE TO DYNA-SOAR BOOSTER SYSTEM

- I. NEUTRAL AERODYNAMIC STABILITY
- 2. SAFETY FACTOR, 1.4
- 3. PILOT SAFETY FROM HAZARDOUS MALFUNCTION CONDITIONS
- 4. 5° ANGLE OF ATTACK CAPABILITY

Figure 1

BENDING - MOMENT COMPARISON 330-FT2, 9,283-LB REENTRY DEVICE, MODIFIED TITAN LOT "J"

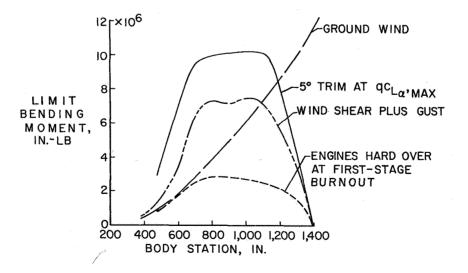
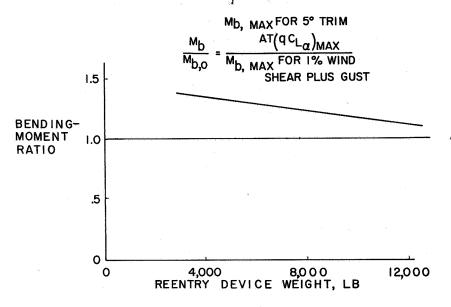


Figure 2





BENDING - MOMENT RATIO 250 SQ FT REENTRY DEVICE, MODIFIED TITAN LOT "J"



K 084

Figure 3

VARIATION OF EQUIVALENT END LOAD WITH TIME MANNED WINGED REENTRY DEVICE

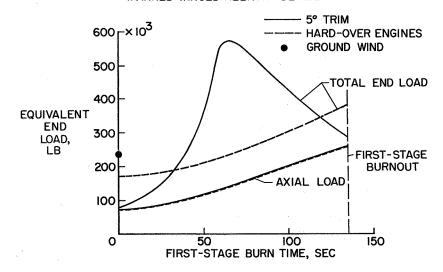


Figure 4





VARIATION OF EQUIVALENT END LOAD

MANNED BALLISTIC REENTRY DEVISE

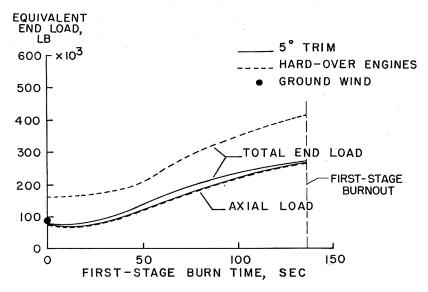


Figure 5

EFFECT OF REENTRY DEVICE ON MAXIMUM BENDING MOMENT

MODIFIED TITAN LOT "J"

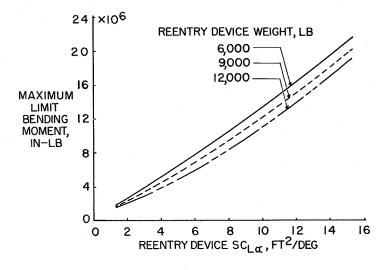


Figure 6





EFFECT OF REENTRY DEVICE ON STRUCTURAL MATERIAL REQUIREMENT

REENTRY DEVICE WEIGHT, 9,000 LB; MODIFIED TITAN LOT "J"

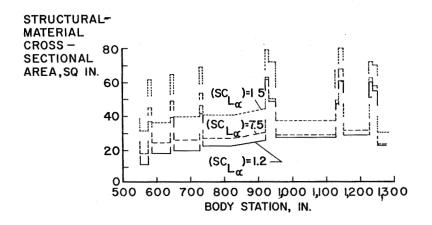


Figure 7

EFFECT OF REENTRY DEVICE ON FLEXIBILITY RATIO

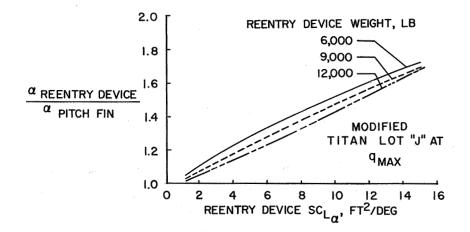


Figure 8





EFFECT OF REENTRY DEVICE ON PITCH FIN REQUIREMENTS

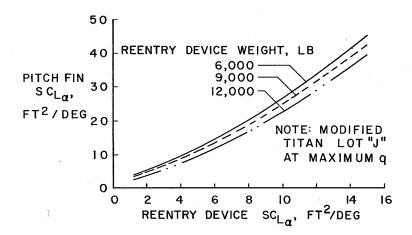


Figure 9

EFFECT OF REENTRY DEVICE ON STRUCTURAL COMPONENT WEIGHT REENTRY DEVICE, 9,000 LB; MODIFIED TITAN LOT "J" 9 -**103 8 - //

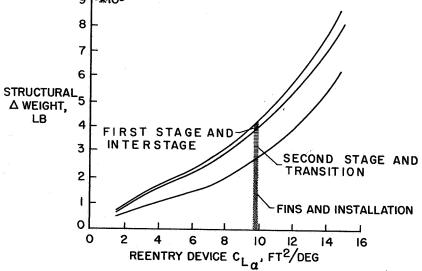


Figure 10





ON STRUCTURAL WEIGHT MODIFIED TITAN LOT "J"

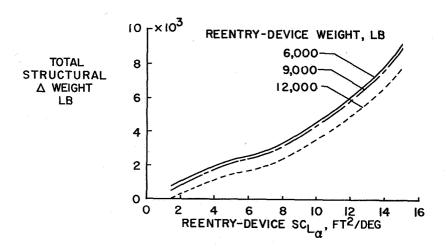


Figure 11

EFFECTS OF PITCH FIN AREA AND VEHICLE FLEXIBILITY ON AERO-SERVO-ELASTIC STABILITY

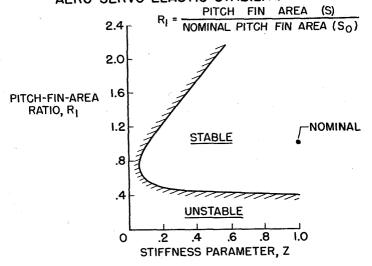


Figure 12



EFFECTS OF PITCH ATTITUDE GAIN AND VEHICLE FLEXIBILITY ON AERO-SERVO-ELASTIC STABILITY $\delta_{T} = \kappa_{\theta} \, \theta + \kappa_{\dot{\theta}} \, \dot{\theta}$

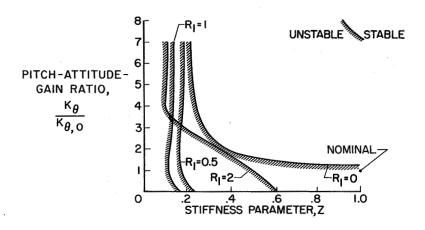


Figure 13

EFFECT OF DESIGN PARAMETERS WIND SHEAR LOAD

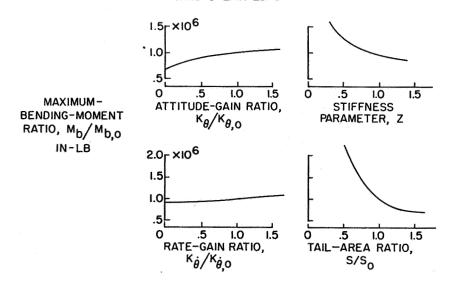


Figure 14





LOAD REDUCTION DEVICES

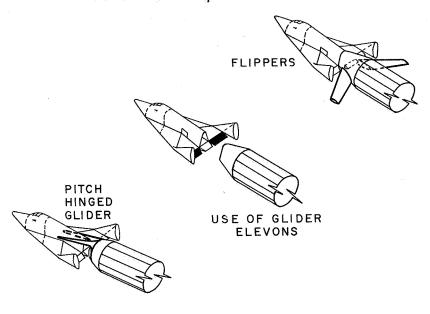


Figure 15

BENDING-MOMENT REDUCTION DUE TO GEARED ELEVON SHARP-EDGE GUST

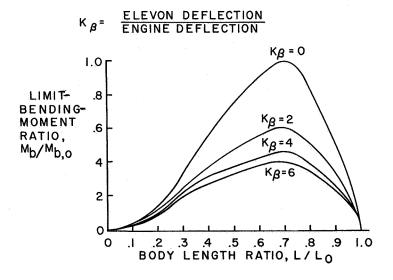


Figure 16



BENDING-MOMENT-REDUCTION DEVICES SHARP-EDGE GUST

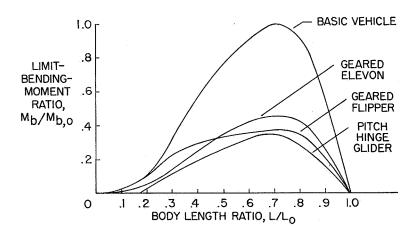


Figure 17

1

18

DESIGN CONSIDERATIONS FOR THE TRANSPARENT VISION AREAS

IN ORBITAL GLIDE VEHICLES

By Kennerly H. Digges Wright Air Development Division

INTRODUCTION

This paper presents a summary of the characteristics of three high-temperature glasses and indicates the considerations required in applying these materials to the design of transparent vision areas for orbital glide vehicles. The three glasses discussed are Corning Glass Works 1723 alumino-silicate, 7900 96-percent silica, and 7940 fused silica.

DISCUSSION

General Characteristics of Glass

For almost 5,000 years men have been using glass. Soda-lime glass, which is widely used in automobiles, aircraft, and home windows, has been in use for 500 years. With such a background to draw upon, one might expect structural design with glass to be a highly developed science. Unfortunately, it is closer to a black art.

In order to understand a few of the idiosyncrasies peculiar to glass, some of its more interesting properties will be discussed.

The atomic structure of glass is random. It lacks the uniform lattice structure which is characteristic of the individual crystals in most solids. There is evidence of some tendency for glasses to form crystals at and below an experimentally determined crystallization temperature. However, the viscosity of the material is sufficiently high throughout this temperature range to preclude crystal formation. Glass is therefore called a high-viscosity liquid.

Because of its liquid-like structure, glass has no distinct melting point. Instead, its viscosity decreases continuously with increasing temperature. At ordinary temperatures, glass is so viscous that it may be considered an elastic material. Its modulus of elasticity, approximately 10 million psi, is comparable to that of aluminum. It obeys Hook's law and the theories of elastic solids to the point of failure.





At elevated temperatures, its characteristics are quite different. Such plastic properties as creep under load, a phenomenon completely unknown at low temperatures, may be observed.

The transformation from elastic behavior to plastic behavior takes place slowly over a wide temperature range. Throughout this transformation range, the properties of glass are dependent upon both the temperature and the time of exposure. Thus, glass may be used at temperatures well into the transformation range, provided the time is sufficiently short and the load is sufficiently low to maintain elastic behavior.

In order to provide reference temperatures to which the transformation range and other properties may be related, a number of points on the smooth temperature-viscosity curve have been selected. Three of these points are of interest to engineers. These points are shown on the temperature-viscosity curve for soda-lime glass in figure 1.

The softening point defines the temperature at which the glass will deform under its own weight. The viscosity at this temperature will range from $10^{7.5}$ to 10^{8} poises. Obviously, this establishes the absolute maximum exposure temperature for glass even for a short time and under no load.

The annealing point defines the center of the transformation range. The transformation range extends for about 250° F above and below this point. The viscosity at the annealing point is 10^{13} poises.

The most important point to engineers is the strain point. This point defines the maximum practical service temperature for annealed glass. The viscosity at this point is $10^{14.5}$ poises.

Failure in glass always occurs as a result of the tensile components rather than the compressive or shear components of a force. The stress at failure depends significantly upon the condition of the surface and edges. Incipient cracks and flaws in the surface may introduce stress concentration of 100 to 1,000 times the average. Since the glass structure does not permit stress relief through local yielding, the breaking stress is reduced by a proportionate factor. The average breaking stress for a severely sandblasted glass specimen may be 2,000 psi or below. However, if the surface is properly treated and protected, strengths above 250,000 psi are not uncommon. It is apparent that tests of glass specimens indicate relative quality of the surface rather than the actual strength of the glass.

Because of the wide scatter in breaking stresses for seemingly identical specimens, there has been considerable disagreement among engineers as to the design strength of glass. This problem has been





resolved somewhat by the recent work of Matthew Kerper of the National Bureau of Standards. (See ref. 1.) Working under Wright Air Development Division contract, Kerper has obtained repeatable results by applying beam loading to sandblasted glass specimens. These results have provided excellent data upon which to base the design of glass for high-temperature applications. However, the difficulty of translating the characteristics of small specimens to full-scale designs still exists, and extensive testing of the final configuration is mandatory.

The "notch sensitivity" and tensile weakness of glass can be mitigated somewhat by a strengthening process known as tempering. Tempering is accomplished by heating glass to the neighborhood of the softening point and then rapidly chilling the surface. The surface contracts and becomes rigid, leaving the interior semimolten. As the interior cools and shrinks, compressive stresses are induced at the surface. The resulting stress distribution is shown in figure 2. The tempering process may increase the average breaking strength by a factor of $2\frac{1}{2}$ to $3\frac{1}{2}$.

Unfortunately, the maximum long-time temperature exposure for tempered glass is considerably below that of annealed glass. At the strain point, the tempering stresses will be essentially relieved in a period of 4 hours. Due to this slow stress release at temperatures approaching the strain point, the maximum long-time temperature exposure for tempered glass must be reduced to about 400° F below the strain point.

In selecting a glass for the high-temperature applications of orbital glide vehicles, two factors are prime requisites. First, a low coefficient of expansion is required to provide resistance to thermal shock and, second, a high strain point is required to provide strength at elevated temperatures.

Thermomechanical Properties of High-Temperature Glasses

Figure 3 compares the expansion coefficients of three high-temperature glasses with that of soda-lime glass. The 96-percent-silica and fused-silica glasses have extremely low expansion coefficients and exhibit excellent thermal shock resistance. However, there is a paradox here. The expansion coefficient of these glasses is so low that it is almost impossible to strengthen them by tempering. This paradox is one of the reasons why the alumino-silicate glass is of interest. Its expansion coefficient is sufficiently high to allow tempering yet is low enough to provide considerable resistance to thermal shock.

The temperature limits of the four glasses are shown in figure 4. Since tempering of the high-silica glasses is not presently feasible, the tempered use range has been excluded for these glasses. The maximum

long-time temperature of the annealed glasses is defined by the strain point. Use of the glass above the strain point will depend upon the loading, temperature, and time of exposure.

Figure 5 illustrates the effect of temperature and time on the breaking strength of tempered and annealed alumino-silicate glass (ref. 1). In the annealed state, alumino-silicate glass reaches its maximum strength at approximately 50° C below the strain point. The increased strength elevated temperature is the result of some stress reduction through local yielding permitted by the reduced viscosity. The drop in strength in the 400° F to 700° F range may be attributed to the deleterious effects of surface chemical attach which are more influential than the healing effects of annealing.

Ι

1

1

The curves for tempered alumino-silicate glass in figure 5 illustrate the influence of time and temperature on the loss of temper. A short time exposure of 1 hour at 1,150° F causes only a 25-percent loss in temper. A 500-hour exposure at 1,150° F results in almost complete loss of temper.

The center curves in figure 5 provide a comparison of the temperature-strength properties of fused silica with alumino-silicate. Fused silica is extremely resistant to atmospheric chemical attack. Consequently, its strength increases continuously with increasing temperature to above $1,700^{\circ}$ F. The 500-hour exposure at temperature has little influence on the strength of this glass below $1,700^{\circ}$ F.

Design Applications

At this point, the application of each high-temperature glass becomes apparent. Window designs for orbital glide vehicles will probably require a composite of several glasses to utilize the best properties of each material. The superior strength of tempered aluminosilicate may be used for the cooler interior layers to withstand pressurization and structural loads. The high-silica glasses may be used for the outer layers which require resistance to high temperature and thermal shock.

The problem of attaching these materials to the vehicle frame now arises. Figure 6 compares the expansion coefficients of some metals proposed for orbital glide vehicles with those of the glasses. It may be noted that a frame of either 0.5-percent titanium molybdenum, kovar, or tungsten would be reasonably compatible with alumino-silicate glass. However, these metals have an expansion coefficient 10 times that of the high-silica glasses. Any edge attachment for the high-silica materials must be designed to compensate for differential thermal expansion. Since





relative movement and low clamping pressures are required, sealing between the glass and frame at high temperatures will be difficult.

Figure 7 illustrates the type of glass configuration which might be used in orbital glide vehicles. The maximum long-time temperature limit of the configuration is around 1,800° F, the strain point of fused silica. Short time exposures to 2,400° F may be tolerated. However, at these temperatures, the material exhibits properties which vary with time, loading, and size of specimen. The maximum thermal limits can be determined only through testing the design configuration. If, as in the Dyna-Soar windshield, the maximum temperature is above the limits of fused silica, a removable external heat shield is mandatory.

The outer panels of high-silica glass will be isolated as much as possible from structural loads and vibrations. An inorganic cushion between the glass edges and the frame will be required to permit relative movement and to provide some measure of sealing.

Absolute sealing of the inner alumino-silicate panel may be accomplished by bonding a metallic foil directly to the glass. Compartment pressure loads may be transmitted through a heavier framing member which would back up the foil. This attachment has been developed by Narmco, Inc., under Wright Air Development Division contract. (See refs. 2 and 3.) Its temperature is limited by the bonding material to 600° F.

A second higher temperature seal is presently under investigation. This seal consists of a fused bond between alumino-silicate glass and siliconized 0.5-percent titanium molybdenum. No deleterious effects on this seal have been noted over the -90° F to $+900^{\circ}$ F range. Investigation of the upper temperature limit is now underway. An upper temperature of $1,200^{\circ}$ F is anticipated.

A third type of seal for the inner panel might be accomplished through the use of an interlayer. This seal would be similar to the type used in current aircraft and would be limited by the interlayer to a temperature of approximately 350° F.

No discussion of transparency design would be complete without a word about optics. Two definitions relative to optical properties are illustrated in figure 8. The angle of incidence is the angle between the line of sight and a perpendicular to the glass surface. The deviation is the distance between the image and the point where the image appears when viewed through the glass.

As the angle of incidence increases above 60°, the optical qualities of a panel deteriorate rapidly. This point is illustrated in figure 9 (ref. 4). It may be noted that the deviation increases and the light





transmission decreases rapidly above 60° . The increase in deviation gives an indication of the relative difficulty of maintaining optical quality at large angles of incidence. The decrease in light transmission points up another problem - that of maintaining visibility. Additional glass panels separated by air spaces will reduce the light transmission by a proportionate amount. Three panels each with 70-percent transmission would reduce the overall transmission to around 34 percent.

The light transmission at large angles of incidence may be increased by the use of reflection-reducing coatings. However, a coating is not a panacea. Light transmission at nonoptimum angles of incidence and of nonoptimum wavelengths will be reduced. Also, these coatings may reduce the temperature limit of the high-silica glass or may tend to glow at elevated temperatures. In view of the optical difficulties which arise, the angle of incidence should be kept below 60° , if possible.

L

12

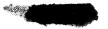
2

The need for transparent materials having higher temperature ranges is illustrated by the requirements for a shield on the Dyna-Soar wind-shield. There is a good possibility that future materials will extend the temperature range past the present limitations of fused silica. The most promising materials appear to be single crystals grown from metallic oxides. Aluminum oxide crystals, known as synthetic sapphire, are available in small sizes. The materials laboratory at the Wright Air Development Division is currently evaluating this material. A temperature extension into the 2,000° F range appears feasible. As crystalgrowing techniques improve, larger and higher temperature transparent materials may be expected.

CONCLUDING REMARKS

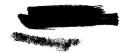
Transparent areas for orbital glide vehicles will require a composite structure of several different glasses. The low-expansion high-silica glasses will provide heat shields for the alumino-silicate structural glasses. Edge attachments must be designed to isolate the glazing, compensate for differential expansion, and provide a seal between the glazing and the frame. The angle of incidence, number of glass panes, and type of glass coating must be chosen so that the optical quality of the overall transparency is maintained. The work of Kerper and Partain provides background data upon which to base the design of glass and edge attachments at elevated temperatures. However, due to the pecularities of the material, extensive testing of the design configuration is required.





REFERENCES

- 1. Kerper, M. J., Diller, C. C., and Eimer, E. H.: Properties of Glasses at Elevated Temperatures, Part III. WADC Tech. Rep. 56-645, Pt. III, U.S. Air Force, Oct. 1959.
- 2. Partain, Gerald K., and Kantner, Richard D.: Development of an Integrally Bonded Edge Attachment System for Aircraft Glass Assemblies. WADC Tech. Rep. 57-19, ASTIA Doc. No. AD 110709, U.S. Air Force, Dec. 1956.
- 3. Partain, G. K., Piscopo, F. A., and Wilson, R. E.: Research of Techniques and Methods on Which to Base Development of High Temperature Glazing Attachments. WADD Tech. Rep. 60-119, U.S. Air Force, Mar. 1960.
- 4. Anon.: Handbook of Instruction for Aircraft Designers. Vol. I Piloted Aircraft, pt. B, ch. 2, sec. 3.2. ARDCM 80-1, U.S. Air Force, pp. 2-4 2-6.





TEMPERATURE-VISCOSITY CURVE FOR SODA-LIME GLASS

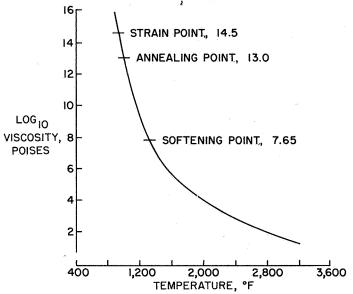


Figure 1

RESIDUAL STRESSES IN A PLATE OF TEMPERED GLASS

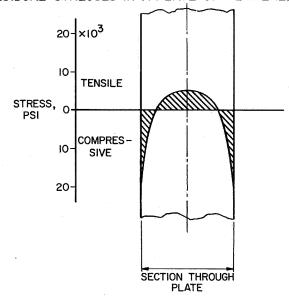


Figure 2





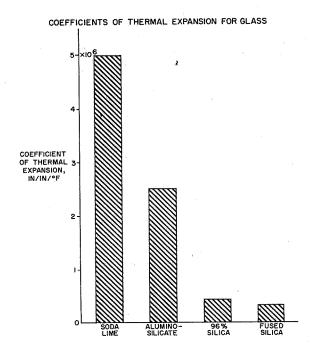


Figure 3

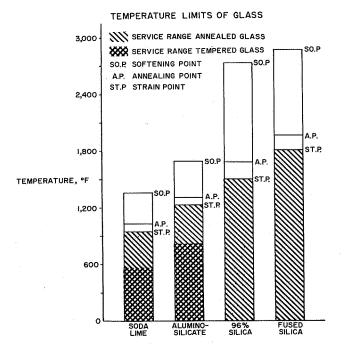


Figure 4





AVERAGE MODULUS OF SANDBLASTED SPECIMENS AT DIFFERENT TEMPERATURES

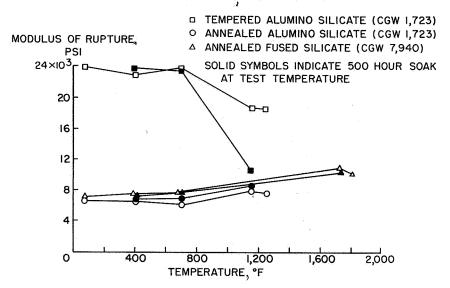


Figure 5

VARIATION OF COEFFICIENT OF THERMAL EXPANSION WITH TEMPERATURE

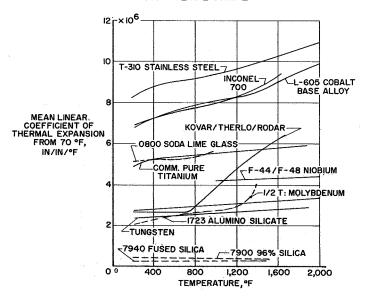


Figure 6





GLASS CONFIGURATION FOR ORBITAL GLIDE VEHICLES

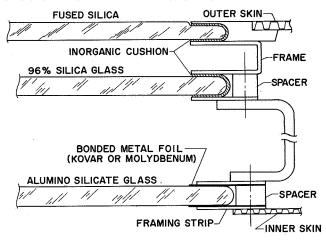


Figure 7

ILLUSTRATION OF ANGLE OF INCIDENCE AND DEVIATION

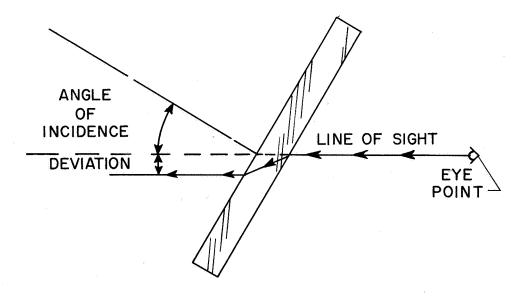


Figure 8





EFFECT OF ANGLE OF INCIDENCE ON LIGHT TRANSMISSION AND DEVIATION

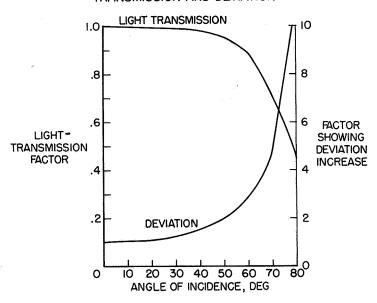


Figure 9





DYNA-SOAR PILOT FUNCTIONS, UTILIZATION,

INFORMATION, AND DISPLAY

By Harold E. Bamford, Jr. Boeing Airplane Company

SUMMARY

Considerations of crew utilization and crew station design are placed in the context of total system development. A model of the development process is presented in which the relations ideally existing between the different phases are clarified. Special attention is given to the functions, design, and crew performance phases as they relate to the development of cockpit indicator displays.

The objective of the functions phase is to define the functional requirements of man and machine. The functions allocated to the pilot constitute the information output which is required of him. The parameters of those functions are his input information requirements, and their indication in cockpit displays is a functional requirement of the machine.

The definition of these functional requirements is accomplished through analysis of the system's mission, within the constraints of the technological and human resources which are available for the accomplishment of that mission. The resulting performance specifications must also be taken into account as they become available. Functions are defined on each of the system's output variables. These functions are then allocated between man and machine, subsidiary functions being defined where necessary. Requirements are established separately for each longitudinal segment of the mission which exhibits a distinct functional organization.

The objective of design is to specify equipment (e.g., indicator displays) which will satisfy the machine-allocated functional requirements developed in the functions phase. The design specifications are constrained in the first instance by the available human and technological resources, and subsequently by the feedback of performance specifications.

In the crew performance phase there is a synthesis of equipment design specifications with the pilot-allocated functional requirements.



The resulting specification of pilot performance is fed back to the design and functions phases, where account must be taken of the task's difficulty level. Excessive task difficulty necessitates redesign of equipment and/or reallocation of functions between man and machine. The development process is thus seen to be an iterative one, continuing until functional requirements and design specifications combine to specify performance whose realization is feasible.

Two general approaches to crew task definition are possible: simulation and rational synthesis. Simulation is particularly attractive because of the increase in confidence which must attend a demonstration of feasibility in simulated operation. Rational synthesis must also be employed, however, because of the impossibility of fully simulating operational conditions.

INTRODUCTION

In designing an aircraft cockpit, it used to be possible to rely upon a vast background of successful experience in the operational environment. Instrument systems which had proved themselves in earlier vehicles were simply taken over, with their indicator displays intact. Minor adaptations may have been necessitated by the somewhat more exacting requirements of the new vehicle. But little or no deliberate attention was paid to the pilot's role in the man-machine system, or to the implications of that role for equipment design.

This approach to cockpit design was not systematic in the sense of proceeding from a clearcut statement of requirements to a system which would satisfy those requirements. But it worked. Whatever the requirements were, they could usually be solved by minor adaptations of established techniques. This was true because the problems were but minor variations on familiar problems.

But this casual approach to crew station design is not possible in the case of Dyna-Soar. The experience which served so well in the past simply does not apply to the problems of boost, orbit, reentry, and hypersonic glide. A systematic approach to the pilot's role and to cockpit design is indispensable if we are to deal competently with these problems. It is the purpose of this paper to describe such a systematic approach and to illustrate its application to Dyna-Soar.

The diagram in figure 1 is an idealized model of the development process. It will serve to place considerations of crew utilization and crew station design within the context of total system development. The boxes in the diagram represent phases which would ideally occur in the development of any complex man-machine system. The arrows connecting





Y

them represent the relations which would ideally exist between the phases. Three of these developmental phases lie within the scope of the present paper. They are the functions, design, and crew performance phases.

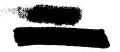
In the functions phase of system development, an analysis of the system's mission is carried out. The mission has previously been defined, as the diagram indicates, through operations research. The output of the functions phase is a set of functional requirements, allocated between the system's crew and the residual system. These requirements, represented in the diagram by hollow arrows, are defined and allocated subject to constraints imposed by the resources, both human and technological, which are available for mission accomplishment.

The functional requirements which are allocated to the residual system constitute the input to the design phase. The design output consists of specifications for equipment. These are represented in the diagram by solid black arrows. The use of solid arrows to symbolize the output of design, in contrast with the use of hollow arrows for its input, signifies that abstract functional requirements are given a concrete interpretation in the design phase. As the diagram indicates, this interpretation is constrained by the available human and technological resources.

Finally, in the crew performance phase, there is a synthesis of equipment design with the crew-allocated functional requirements. The result is a specification of the tasks to be performed by the crew. The performance specifications are represented in the diagram by striped arrows, since they are determined jointly by functional requirements and equipment specifications. As the diagram indicates, they are fed back to the functions and design phases, where their feasibility is evaluated.

If the tasks to be performed by the crew are found upon evaluation to be excessively difficult, the functional requirements may be reallocated between crew and residual system, or the equipment may be redesigned, or both. In any case, new crew performance specifications are defined and fed back to the functions and design phases for evaluation. This iterative process continues until all crew performance specifications are found to be feasible.

While this process is going on, a similar process leading to a feasible set of machine performance specifications is simultaneously going to completion. This complementary process is indicated at the top of the diagram. When both processes are complete, equipment specifications are released to production and crew performance specifications to training and organization. The ensuing events, which are indicated in the diagram, are beyond the scope of this paper.





THE FUNCTIONS PHASE

In considering the functions phase of system development, one point is worthy of emphasis. Functional requirements are abstract. They are not specifications of crew performance, nor do they specify equipment. Functional requirements allocated to the machine may be interpreted in a variety of designs. Similarly, there are various ways to interpret crew-allocated functions as crew performance.

The mission which is analyzed in the functions phase is a general statement of what the system must be to achieve its operational objectives in its operational environment. The functional requirements which are defined in this phase are the detailed logical consequences of the mission and of the available resources. The mission which has been assumed as a point of departure for our studies was defined in Phase I. As development proceeds, changes in this mission will be fed into the functions phase. The functional requirements which have been defined will then be modified appropriately.

The definition and allocation of functional requirements, as previously mentioned, are subject to certain constraints. These constraints are imposed by the resources which are available, or expected to be available, for the accomplishment of the system's mission. The major part of this symposium has been concerned with the resources of inanimate technology. But there is a different class of resources - the potential utility of the pilot. Just what is this potential utility? The pilot's contribution to mission accomplishment consists, in general, of satisfying certain of the system's functional requirements which may be allocated to him.

Two steps are involved in the functions phase of system development: First, the required performance of the system must be specified and, second, the responsibility for realizing the required performance must be allocated between man and machine.

Specification of Required Performance

In order to specify the required performance of the system, a set of variables must be chosen. These variables are termed "outputs." The required value of each output can then be defined as a function of one or more parameters. The functions so defined, called "output functions," are the required performance of the system. The parameters, called "input parameters," constitute the system's requirement for input information.





S 40

4

. 13

In order for the required value of an output to be realized, two things are necessary. First, the output must be programed - i.e., a series of decisions must be made as to its required value. And second, the decisions must be implemented - the values decided upon must be brought about. These things are represented diagrammatically in figure 2. In that figure, output functions are represented by double vertical lines. Since the required value of an output is a function of one or more parameters, programing may be conceived as a functional linkage between parameter and function. Such a linkage is diagramed on the left-hand side of each function symbol. Thus, if required velocity is a function of actual position, the programing of velocity is symbolized by the arrow linking actual position to required velocity. The implementation of a decision respecting the required value of an output is diagramed as a functional linkage on the right-hand side of the function symbol. In this case, a decision as to required velocity is implemented through an acceleration program. The implementation of decisions respecting required acceleration is not represented in this figure.

It will be noticed that in the figure required acceleration is linked on the left to both required and actual velocity. This implies that required acceleration is a function of both parameters. Decisions respecting required acceleration must be based on information as to both actual and required velocity.

The pattern of functional linkages between the various output functions of the system and their input parameters is the basis of the system's functional organization. Diagrams such as these are of great utility in defining functional requirements and in allocating them between man and machine. Their useful interpretation, however, demands that they be supplemented by a more detailed statement of the functions involved. The range and domain of each function, the form of each function's dependence upon its parameters, and the allowable variation of each output about its required value must all be explicitly defined.

In the analytical work which has been completed to date, the required performance of the system has been specified with respect to 15 outputs (fig. 3). Of these, two define the vehicle's position in space, three define its velocity vector, five are the factors which control its acceleration vector, and five are the changes or rates of change of those factors. The required value of each of these outputs has been expressed as a function of one or more input parameters. This has been done only for normal, or nonemergency, conditions. The analysis is presently being extended to the case in which one or more of the outputs of the system or of its subsystems is out of tolerance.





Allocation of Functional Requirements

A pattern of relations such as are diagramed in figure 2 is the basis of the system's functional organization. A complete diagram of that organization, however, must also represent the allocation between the man and machine of the responsibility for realizing the required outputs. It is a simple matter to incorporate this additional information. Functional linkages allocated to the pilot for realization are represented in figure 4 by broken arrows, while solid arrows symbolize those whose realization is allocated to the machine. In this figure there appear a number of single vertical lines. These symbolize the outputs required of various subsystems in support of the system's output functions. Such required subsystem outputs are referred to as subsidiary functions, or simply subfunctions. Subfunction symbols lying between solid and broken arrows represent man-machine interfaces. An interface is a display indication if the solid arrow lies on the left of its symbol, and a control action if the solid arrow is to the right. Besides the interfaces, another kind of subfunction is represented in figure 4. This is the interpretation which the pilot must make of his sensory input. Such subfunctions as these are implicit responses required of the pilot.

Now what does this diagram tell us? Briefly, it makes six statements:

- (1) Actual position is indicated to the pilot in a display.
- (2) The pilot determines required velocity on the basis of that display indication.
 - (3) Actual velocity is indicated to the pilot in a display.
- (4) The pilot reads that display indication and interprets it as a sign of actual velocity.
- (5) The pilot correlates actual and required velocity and transmits the result as a control action.
- (6) The machine determines the required acceleration on the basis of the pilot's control action.

This diagram is a comprehensive way of presenting the functional organization of the man-machine system. Once again, however, its useful interpretation requires supplementary information. Besides the detailed statements of the output functions there must be similar statements of the subsidiary functions. Over what range must a parameter be indicated, with what precision, and with what rates of change? With what precision must the





pilot read and interpret the indication, and as a sign of what? What must the pilot correlate, how often, and what is the form of the correlation?

100

5

8

1

An initial allocation has been made of the responsibility for realizing our fifteen output functions under nonemergency conditions. This trial allocation was guided by a policy of maximum pilot utilization. Under this policy, any functional requirement which is not clearly beyond human capability is allocated to the pilot. The resulting functional organization represents the maximum work load which can be imposed upon the pilot insofar as the normal guidance and control of the vehicle is concerned. Emergency operations and the management of subsystems can of course increase his workload above this level. This policy was adopted to establish a baseline from which pilot utilization can be reduced as may appear desirable and feasible in the ensuing studies.

Segmentation of Mission

In this discussion of the system's functional organization, there is one question which must have occurred to all of you. Doesn't the functional organization change during the course of the mission? It certainly does. For this reason it has been necessary to divide the mission into a series of longitudinal segments, each characterized by a particular functional organization.

The process of segmentation is an iterative one. It begins with a set of trial segments. An attempt is made to define the system's functional organization in each. If analysis discloses a change in organization during any of these, it is immediately divided into two or more new trial segments. Analysis may also show two or more trial segments to have the same organization. Such trial segments are combined. This process continues until a set of mission segments is defined whose elements taken serially constitute a restatement of the system's mission.

Like the overall mission, each segment is characterized by certain objectives. The initial conditions necessary for the accomplishment of each segment must be among the objectives of the segment which precedes it. To insure that this would be the case, the initial trial segments were defined in reverse order. The process began with the vehicle safely at rest, its mission completed, and worked backward to launch.

The mission segments which finally resulted are presented in figure 5. Their objectives are not given for reasons of security. Time does not permit any detailed consideration of these segments and their functional organizations. However, a quick look at a typical organization diagram may be of interest. Figure 6 is presented to illustrate the general



appearance of these diagrams. The functions represented there are defined in detail in the report from which this figure was taken.

The Functional Requirements

The mission has been divided into seven longitudinal segments, and the functional organization characterizing each segment has been diagramed. In these diagrams are indicated the allocation of functional requirements between man and machine. Just what are these requirements? In a word, they are for information. An information output is required of the pilot, and he in turn requires input information of the machine.

In figure 4 the pilot's information output is shown to be transmitted as a control action. In order to determine the required control action under the functional organization shown here, he must do two kinds of things. He must interpret display indications, and he must correlate the interpretations. One display indication is interpreted as a sign of required velocity, the other as a sign of actual velocity. The correlation of these interpretations, transmitted to the machine as a control action, selects an acceleration which will tend to reduce their discrepancy. Correlation and interpretation, then, are the functional requirements allocated to the pilot. A full definition of these functional requirements would, as we have said, include a statement as to the form of the relations between the required responses and their parameters, or independent variables, and the allowable variation of the responses about their required values.

If the pilot is not able to determine the parameters of his required responses with sufficient precision, they must be indicated to him by the machine. Twenty-two functional requirements for display indication are symbolized in figure 6. These are the requirements for input information which must be satisfied by the machine under the functional organization diagramed here. Once again, their full definition must include a statement as to the range of the required display indications and the allowable error of indication.

THE DESIGN PHASE

The functional requirements for display indication are among the inputs to the design phase. They are the only such inputs which will be considered in this paper.

The design phase, like the functions phase, is constrained by the available resources. The sensing, computing, and indicating technologies impose practical limits on the displays which can be specified. Further



limits are imposed by the ability of a man to read a display indication within given tolerances of time and error. Subject to these constraints, displays are designed so as to facilitate the pilot's required responses of interpreting and correlating.

3.78

The outputs of the design phase, as far as this paper is concerned, are specifications for indicator displays. Displays are designed to satisfy the given functional requirements subject to the given constraints. The concern of this paper, let it be noted, is with indicator displays, not with indicators. By this is meant that these specifications are for what the pilot actually sees, and not for the mechanism of the indicator, which is hidden from him.

In the design phase, display specifications were developed in three steps. First, the functional requirements were summarized. Second, a panel concept was defined to integrate the functional requirements. And third, the panel concept was elaborated in concrete detail.

In the seven functional organization diagrams to emerge from the functions phase, there are denoted no less than 95 different requirements for display indication. For each of these a summary sheet was prepared. On that sheet was entered the parameter to be indicated, its maximum expected rate of change, and the required range of indication. information was then supplemented on each summary sheet with data respecting the responses required of the pilot - viz., his interpretations and correlations. Error tolerances were associated with each required response. (The reading tolerances are implicit in the allowable error of interpretation.) These summary sheets contain a complete statement of the functional requirements for display indication; but although there were 95 distinct requirements, many of them were so nearly identical that they could be considered the same requirement. Accordingly, the summary sheets were collected into essentially homogeneous clusters. In this way, the number of functional requirements was reduced to some twenty, a much more manageable number.

The integration of these requirements into an organic panel concept came next. In the definition of that concept these things were considered:

- (1) The presentation to the pilot of his required input information. This, of course, is the functional requirement to be satisfied.
- (2) The facilitation of the pilot's required responses of interpretation and correlation. The demands upon the pilot for these responses must not exceed his ability to make them within the given error tolerances. The difficulty of his task is importantly influenced by the organization of the instrument panel.



(3) The state of the instrumentation art. This consideration is recognizable as the technological resources which constrain the design phase of development.

The general concept which was defined and adopted for further elaboration is depicted in figure 7. The information needed by the pilot can be acquired from the displays denoted in that figure.

It is interesting that so complex a welter of requirements for display indication can be satisfied by an instrument panel so simple in conception. The design of such a panel is possible only on the basis of the exact functional requirements for display indication. Such a basis allows the conception of an uncluttered, starkly functional panel.

L

1

1 2 3

The individual displays were designed and arranged so as to facilitate the required interpretations and correlations. And the demands imposed by the display specifications upon the state of the art have been held to a minimum.

The third and final step was elaboration of the panel concept. In this step exact specifications were defined for the panel and for the individual displays. The dimensions and operating characteristics of the displays were specified. The scales and indices were designed in detail, and the use of color to facilitate interpretation, particularly in check reading, was explored.

In presenting these specifications, great attention is being given to their rationale. The method by which they were developed lends itself to such documentation. The indication of any parameter on this instrument panel is justified by reference to the functional requirements which are thereby satisfied. The particular form of the display in which it is indicated and the relation between that display and the rest of the panel are justified as attempts to facilitate the responses required of the pilot. Along with the specifications for indicator displays, suggestions for the instrumentation of those displays are being prepared. These suggestions include possible data sources and possible indicator mechanisms.

THE CREW PERFORMANCE PHASE

As noted in figure 1, it is in the crew performance phase that functional requirements join with equipment design to define the pilot's task. It will be clear from what has been said that both inputs are required to specify the performance required of the pilot. For given functional requirements his task will vary with the design of the

30



indicator displays with which he is provided. And a given instrument panel may be used to satisfy a variety of functional requirements.

Since both inputs are needed to specify the pilot's task, it is also clear that a definitive statement that the task is feasible cannot be made on the basis of either input alone. Just as the pilot's task changes with variation in either his functional requirements or his displays, so does the difficulty of that task. It is for this reason that his performance specifications are fed back to the functions and design phases.

These specifications provide the basis for modifying the original design specifications and the functional requirements originally allocated to the pilot. If the initial performance specifications are not feasible - i.e., if their demands exceed the available human resources - they must be modified. And the performance required of the pilot can be modified only by modifying either his functional requirements or the design of his equipment.

Two general approaches to the definition of performance requirements are available: rational synthesis and simulation. There are advantages and disadvantages to each method.

The method of rational synthesis may also be called the armchair method. It assumes various forms. For example, a detailed series of concrete interactions of man and machine may be specified. These consist chiefly of the actuation of controls and the discrimination of display indications. The equipment and operational conditions are examined to determine whether these interactions are feasible, given the nature of the crew member. In this form the armchair method has been called "task analysis." Being independent of the laboratory, it can be carried out quickly and is useful for rough estimates of a task's feasibility. It does not often lend itself to exact statements, however, and does not inspire great confidence when applied to complex systems of any novelty.

Simulation of the man-machine system, on the other hand, permits the study of a concrete analog of the system to which inference is made. Although this method is comparatively slow, being dependent on apparatus, it does lend itself to exact measurements. In this method the performance required of the pilot is demonstrated physically as the behavior of the experimental subject in a successful simulated operation. And the confidence in the feasibility of the pilot's task which is inspired by such a demonstration is limited only by the fidelity of simulation. This fidelity is of course not perfect. Indeed, there is no practical way of simulating certain of the stresses which the operational system must be expected to encounter. About the only way of dealing with this



problem is to supplement the method of simulation with rational synthesis. The feasibility of the pilot's task is demonstrated in operations simulated under favorable conditions. Estimates are then made of the extent to which his performance will be degraded under operational stress. The paper by Euclid C. Holleman deals with some of the empirical bases upon which estimates of this kind may be made.



DEVELOPMENT OF A MAN-MACHINE SYSTEM

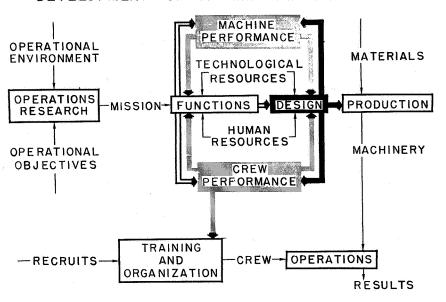


Figure 1

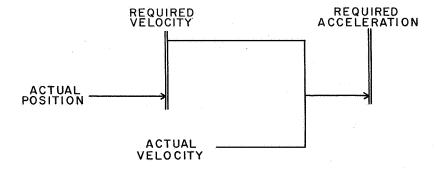


Figure 2

4



OUTPUTS

POSITION GROUND POSITION ALTITUDE

VELOCITY TRACK VELOCITY FLIGHT-PATH ANGLE

ACCELERATION ROLL ANGLE OF ATTACK DRAG CONFIGURATION THRUST SIDESLIP

ACCELERATION CHANGE CHANGE OF DRAG CONFIGURATION THRUST CUTOFF SIDESLIP ANGULAR RATE

Figure 3

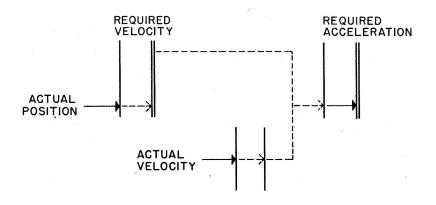


Figure 4



MISSION SEGMENTS

- TERMINATION
- SUPERSONIC GLIDE
- HYPERSONIC GLIDE
- REENTRY
- ORBIT
- COAST
- BOOST

Figure 5

FUNCTIONAL ORGANIZATION OF THE SYSTEM IN HYPERSONIC GLIDE

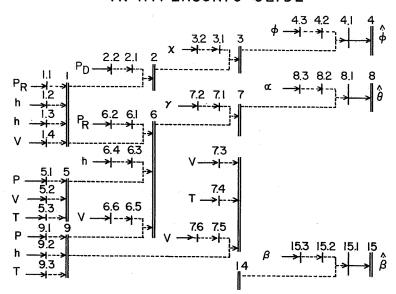


Figure 6





PANEL

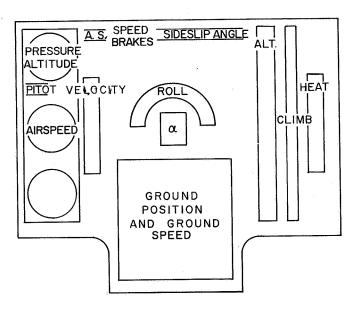


Figure 7





UTILIZATION OF THE PILOT DURING BOOST PHASE

OF THE STEP I MISSION

By Euclid C. Holleman Flight Research Center

SUMMARY

Some of the capabilities of the human pilot for controlling the Step I Dyna-Soar launch have been assessed by requiring the pilot to control the simulated launch. The piloting task was well within the capability of the human pilot. With only rudimentary presentation, the pilot could control the launch to within acceptable limits of the desired velocity and altitude. As the primary controller of the launch, it is believed that the pilot can add materially to the reliability and flexibility of the launch.

INTRODUCTION

The role of the pilot in the launch of a multistaged vehicle with orbital capability has been examined extensively during the past year (for example, ref. 1). Generally, these studies used launch simulations in which the pilot, presentation, controller, and analog computer formed a closed-loop system. In one study the effects of the launch-acceleration environment on the performance of the pilot was investigated, and the human centrifuge was used to close the launch-acceleration loops in normal and longitudinal acceleration. The results of these studies were generally encouraging and showed that the use of the pilot as the primary controller of the launch of multistaged vehicles holds promise.

It is the purpose of this paper to indicate some of the capabilities of the pilot for controlling the Step I Dyna-Soar launch based on a fixed-base simulation program and on the results of previous investigations at the Flight Research Center.



SYMBOLS

	and the state of the
a _x	longitudinal acceleration, g units
g	acceleration due to gravity, ft/sec ²
h	altitude, ft
Δh	altitude error, ft
I _Y	vehicle moment of inertia in pitch, slug-ft ²
q	dynamic pressure, lb/sq ft
R	range, nautical miles
S	reference area, sq ft
V	relative velocity, ft/sec
ΔV	velocity error, ft/sec
α	angle of attack, deg
γ	flight-path angle, deg
Δγ	flight-path error, deg
$\delta_{ m h}$	stabilizer position (X-15), deg
$\delta_{\mathbf{n}}$	nozzle position (Dyna-Soar), deg
ζ	damping ratio
ω_n	vehicle undamped natural frequency, radians/sec

LAUNCH SIMULATIONS

In figure 1 is shown the nominal Step I Dyna-Soar mission. The two-stage launch to a velocity of 19,000 ft/sec with a range capability for the lifting glider of 3,000 to 4,000 miles is shown. This study investigated primarily the boost phase of the mission but did consider briefly the effects that piloting errors at burnout would have on the range capability of the glider.



Control, presentation, and guidance similar to that which proved satisfactory during previous launch programs was used to enable the pilot to control the desired boost trajectory. For pilot's control, the Flight Research Center's three-axis controller was used by virtue of its generally satisfactory performance during previous fixed-base and centrifuge investigations. The previous paper by Brent Y. Creer, Harald A. Smedal, and Rodney C. Wingrove showed that more conventional controllers, for instance, a two-axis controller with toe pedals, would have been satisfactory at the level of acceleration (about 5g) expected for this vehicle. It was determined during the Flight Research Center's centrifuge boost program that longitudinal staging accelerations up to 9g had very little effect on the ability of the pilot to perform the boost control task. In fact, at this level of acceleration the pilots estimated that only 30 to 40 percent of their physical effort was required for the control task. There was some loss in peripheral vision due to the normal component of the acceleration environment, but actual data show no deterioration in performance at this acceleration level. Since the Dyna-Soar launch is not expected to require an acceleration higher than 6g, little effect of the acceleration environment on the pilot's performance would be expected. However, a good support system, such as the molded seat used during the centrifuge program (ref. 1), is vital for the pilot's comfort and for fixing the pilot-controller position during acceleration.

For the present study, no new presentation concepts were developed. Rather, known required quantities were presented to the pilot on conventional instruments as is shown in figure 2. Primary control quantities were angle of attack, angle of sideslip, angle of bank, altitude, and velocity. No vernier rockets were used for control of final velocity, but a sensitive presentation of the final thousand feet per second proved useful for indicating when to cut off thrust. Other useful quantities were pitch attitude, pitch and yaw program errors, and remaining burning time. A stage warning light was useful, especially for controlling vehicles with unstable aerodynamics. A card of the desired attitudealtitude provided alternate guidance.

RESULTS AND DISCUSSION

Figure 3 shows a typical piloted launch from the fixed-base Step I simulation. The performance quantities are shown in the upper half of the figure, and the control quantities are shown in the lower half. The control task was initiated 20 seconds after ground launch with the vehicle at an initial angle of 87° . In order to accelerate the 9,000-pound glider to the desired end conditions of about h = 250,000 feet and V = 19,000 ft/sec, two stages of about 5g each were required.





Typical mass and aerodynamic characteristics for the finned vehicle were assumed. For this launch the vehicle longitudinal stability was statically stable for the first stage and unstable for the second stage; however, several levels of stability - both stable and unstable - were investigated. Representative characteristics for the lateral and directional modes were assumed, but primary emphasis was placed on the longitudinal modes of motion. Titan (Lot J) missile weight and inertia characteristics were used (table I), as were the Titan nozzle-deflection and rate limitations.

For primary guidance, flight-path error was presented to the pilot. This error was controlled by controlling angle of attack through nozzle angle. Shown also in figure 3 is the vehicle first-stage structural limit of $\alpha q = 3,750$ considered during the study. Only small values of α were required to correct flight-path error during the first stage, but considerably higher values were required during the second stage where aerodynamic lift was small. Of interest also was the absence of disturbances during staging where a limit of $\alpha q = 350$ was used.

Reference 1 has also shown that a control problem could exist at staging for vehicles of this type. Figure 4 orients the assumed Dyna-Soar vehicle aerodynamic characteristics in pitch relative to previous investigations. The crosshatched region shows the scope of previous investigations of static stability and damping. Included is the piloted controllability limit for zero-time thrust delay between stages. Indicated are points investigated in considerable detail under the acceleration environment during the Flight Research Center's centrifuge program and the two levels of damping at which the piloting controllability limits were verified during closed-loop centrifuge operation. Shown also in figure 4 are the first- and second-stage Dyna-Soar longitudinal aerodynamic characteristics representing the basic unaugmented configuration. The Dyna-Soar vehicle appears to be easily controllable, but lightly damped. With reference to figure 3, which illustrates the control task with the basic configuration, it can be seen that the control motions are characterized by small precisely timed inputs. The pilots commented that even stable static stability is not appreciated without damping.

For staging, the "fire-in-the-hole" technique (or firing of the second stage before separation of the first stage) proposed for the Dyna-Soar vehicle proved very beneficial during thrust delays, but second-stage unstable aerodynamics can result in a control problem if staging occurs at an angle of attack.

Figure 5 shows the results of an investigation of the control of the second stage of the Dyna-Soar vehicle. Shown is the ratio of angle-of-attack excursions to the staging angle of attack for various levels of second-stage instability. These data indicated that for the basic level of instability ($\omega_n^2 = -2.5 \text{ radians}^2/\text{sec}^2$), an excursion in α of



approximately 2.5° can be expected for each degree of staging angle of attack. Staging up to about 1.5° could be tolerated to restrict the α excursions to the assumed αq limit. However, it was relatively easy to control staging angle of attack to low values.

In order to determine the effect of vehicle aerodynamic characteristics on the pilot's performance, launches were made at several levels of vehicle stability and damping. The performance of one pilot is summarized in figure 6, which shows a typical launch as a function of velocity and altitude. Also indicated in this figure is the spread in altitude and velocity at first staging and also at the final cutoff velocity of 19,000 ft/sec. Shown in the left inset is a typical set of second-stage end velocities and altitudes for the basic vehicle and two other levels of vehicle stability and damping. No variation in performance with stability or damping was indicated. However, it was indicated that the pilot can control the final velocity and altitude for this mission with the simple presentation used to within about 20 to 30 ft/sec in velocity and 3,000 to 4,000 feet in altitude.

The ability of the pilot to adjust to more demanding control tasks during the launch was investigated by unexpectedly failing augmentation loops and guidance during the launch. The results of these simulated emergencies are shown in the other insets as final incremental altitude and velocity about the desired quantity. It can be seen in figure 6 that the pilot has the capability of performing this launch control task even with limited presentation.

A heading change has been proposed during the Dyna-Soar launch to avoid dropping the first-stage booster in a restricted area. To determine the effect that this more complex piloting task might have on the pilot's performance, heading changes of $10^{\rm O}$ and $20^{\rm O}$ were made during the second stage.

A comparison of the pilot's performance with and without the heading-change task is shown in figure 7. Also shown is the variation in altitude and velocity for the two tasks. It is apparent that the addition of heading-change task had little effect on the ability of the pilot to control the vehicle burnout altitude and velocity. Figure 8 shows the effect of piloting errors in velocity and heading at burnout on the range capability of the lifting glider. The crosshatched region shows the range resulting from errors in velocity of 50 ft/sec and in heading of 2°. It can be seen that the expected piloting errors are insignificant compared to the maneuvering envelope of the vehicle for the 19,000 ft/sec mission.

Since the North American X-15 is a rocket-powered vehicle and is designed to be piloted to 250,000 feet, a brief comparison will be drawn between the piloting requirements for the X-15 design altitude





mission and the piloted Dyna-Soar launch. Typical launches are compared in figure 9. Shown in this figure are the longitudinal acceleration, velocity, altitude, angle of attack, and pilot's control position.

The launch accelerations during boost are quite similar and the piloting tasks are similar once the X-15 is rotated to the proper attitude angle of 31° . The X-15 launch requires constant pitch attitude to burnout, whereas the Dyna-Soar ideally requires constant angle of attack (zero).

Piloting the X-15 during the launch would serve to delineate the piloting problems of the Dyna-Soar vehicle. Based on simulator investigations of the control task and of the effects of acceleration environments, both control tasks appear to be well within the capability of the human pilot.

CONCLUDING REMARKS

In summary, it appears that the human pilot is capable of controlling the launch of the unaugmented Dyna-Soar vehicle. The launch acceleration environment anticipated will have a negligible effect on the performance of the pilot. With augmented damping, some negative stability could be controlled by the pilot. With only rudimentary presentation, the pilot can control the vehicle to within acceptable limits of the desired velocity and altitude. The inclusion of the turn task had little effect on the pilot's control of final altitude and velocity. As the primary controller of the launch, it is believed that the pilot can add materially to the reliability and flexibility of the launch maneuver.

REFERENCE

1. Holleman, Euclid C., Armstrong, Neil A., and Andrews, William H.: Utilization of the Pilot in the Launch and Injection of a Multistage Orbital Vehicle. Paper No. 60-16, Inst. Aero. Sci., Jan. 25-27, 1960.





L

TABLE I.- TITAN MISSILE CHARACTERISTICS

Stage I (at launch):																				
Weight, lb											•		•		•					232,400
Thrust at sea level,	1	b				٠					•			•	•			•	, 6	300,000
Iy, slug-ft 2				•				•	•				•	•		•		•		3,310,000
Control arm, ft																				42
Burning time, sec .	•	•	.•		٠	•	•	•	•	•	•	•	•	•	•	•		•	:•	138.5
Stage II:																				
Weight, lb						•				٠.						•	•			54,500
Thrust, lb																				80,000
Iy, slug-ft ²																				221,000
Control arm, ft																				21
Burning time, sec .	•		•	•		•	•	•		. •		.•	٠.	•	•	•	•	•	.•	157.5
Glider:																				
Weight, lb																				9,000
Wing area, sq ft					٠		•	•		•	٠	•	•	٠	•	٠	.•	•	•	330





TYPICAL DYNA SOAR-LAUNCHES

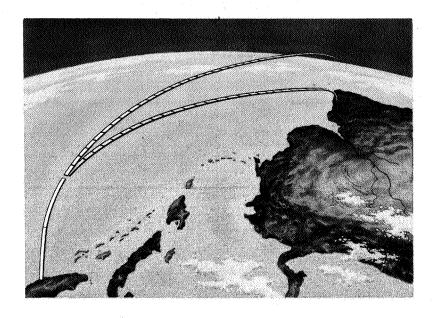


Figure 1

PILOT'S PANEL

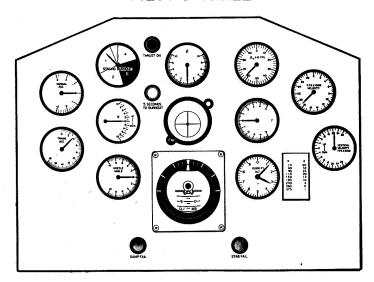


Figure 2





TYPICAL PILOTED LAUNCH

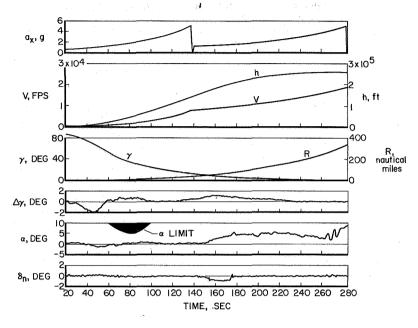


Figure 3

VEHICLE CONTROLLABILITY

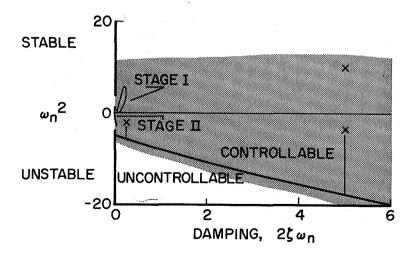


Figure 4



70

14

STAGING CONTROL PROBLEM

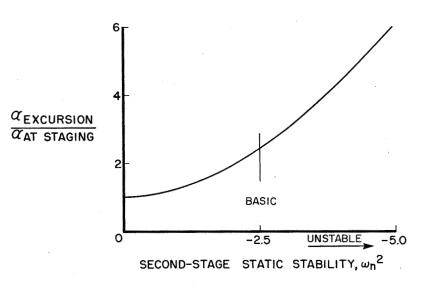


Figure 5

PILOT'S CONTROL OF FINAL VELOCITY AND ALTITUDE

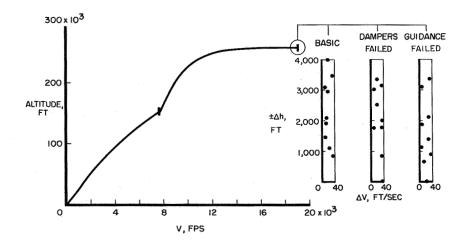


Figure 6





EFFECT OF HEADING-CHANGE TASK

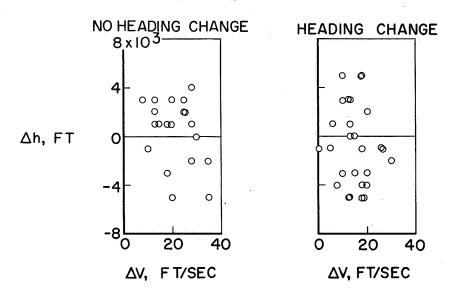


Figure 7

PILOTING ACCURACY

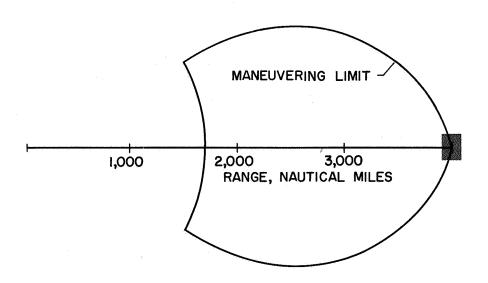


Figure 8



COMPARISON OF X-15 AND DYNA-SOAR LAUNCHES

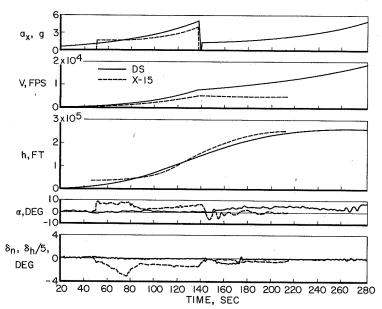


Figure 9

1 1



PILOT FACTORS INFLUENCING DYNA-SOAR GLIDER DESIGN

By Robert L. Campbell and Herbert G. Shepler Boeing Airplane Company

INTRODUCTION

One of the objectives of the Dyna-Soar program is piloted exploration of the hypersonic reentry regime. From an engineering standpoint, the end results of piloted Dyna-Soar flight are a weight and volume increase over that which would be required for nonpiloted flight. The weight and volume requirements for piloted flight are compensated for primarily in two ways:

- (1) The increase in mission reliability due to paralleling pilot and equipment functions and
- (2) The very important, but nonquantitative, aspects dealing with assessment of situations, alternative reaction capability, and reasoning capability beyond that of any known machine.

DISCUSSION

Some of the factors which influence the design of the Dyna-Soar reentry glider due to piloted flight are breathable atmosphere, protective devices and survival equipment, vision requirements, heat-sink temperature, temperature tolerance, g tolerance, and design margins. All of these factors exist for present piloted vehicles; however, each represents special design considerations due to the environments of the Dyna-Soar vehicle. The atmosphere for breathing must be carried within the glider since the flight altitudes are above those where outside air can be used. High accelerations create the need for protective devices. Survival equipment is needed for emergency conditions, particularly water landings. Direct-vision capability creates a problem in the use of high-temperature transparent materials. Heat-sink temperature and temperature tolerances are important from a weight-saving standpoint. In general, design margins are increased over those which would be used for unmanned flight. Some of these are the 1.4 factor (1.25 for unmanned vehicles) applied to the booster structure and the 10 percent reserve capacity for all expendables.





There has been much discussion of the Dyna-Soar pilot's functions and utilization. This paper presents some of the measures taken to provide the capability to perform those functions and a review of some of the tests conducted to verify the adequacy of the provisions for the pilot.

Figure 1 is a sketch of that portion of the Dyna-Soar vehicle which is specifically concerned with the pilot. The glider height and width in this area are determined by the requirements for the pilot. The cockpit volume is based on a 75 percentile man (this would be a man 70.7 inches tall). The weight associated with the pilot and his ventilated pressure suit is 194 pounds (162 for the man and 32 for the suit). No assessment has been made in this paper for structural weight due to piloted flight because it has been assumed that this compartment would be used for additional payload equipment for unmanned flights. Cooling provisions for equipment in unmanned flight would be provided from the environmental control system provided for the aft equipment bay. The automatic landing system is shown as a reference weight for unmanned flight.

L

1

5

The requirement for a breathable atmosphere is not unique to the Dyna-Soar vehicle. Submarines and high-altitude balloons have had to carry the atmosphere for breathing. Weight trade studies have resulted in providing the breathable atmosphere for the Dyna-Soar glider through the storage of a cryogenic (liquid) mixture of oxygen and nitrogen which is the first application of this technique. Results of tests (unpublished) have shown that removal of the mixture from the storage container as a liquid and then vaporized maintains a constant partial pressure of oxygen in the discharge. Where the mixture is taken off the top as a vapor, the discharge is first nitrogen rich and then becomes oxygen rich as the quantity in the tank decreases with time.

An emergency atmosphere is provided for the pilot in the event of malfunction of the normal supply. The supply is sufficient to cover the longest time period for escape which occurs at the end of the second-stage boost. After landing, there is sufficient emergency atmosphere for a 72-hour breathing demand.

The survival kit includes those items necessary for a 72-hour period after landing in the emergency mode. Other items shown in figure 1 are the sonic insulation, instrument panel, windows, and communications and electronic equipment. Some of this equipment is discussed subsequently.

Piloted flight has always created the need for escape; the Dyna-Soar reentry glider is no exception. Figure 2 shows a few of the considerations leading up to the selection of the Dyna-Soar escape system. This figure indicates how the weight varies with pilot safety when



1.00

L

L

several types of escape systems are considered. It can be seen that the weight increases sharply with increased pilot safety systems. The selection of the forward section of the yehicle as the escape system was based upon maximum pilot safety throughout the complete flight regime. The parts of the flight regime of interest for escape system design and selection are off the launch pad, the high q region of boost, the end of boost, during weightless flight, during reentry, and the landing phase. Escape from anywhere in the flight profile dictated the selection of the system. However sensitive the subject of pilot losses may be, there always remains the engineering trade between vehicle performance as affected by weight and the degree of pilot safety afforded. As long as requirements exist for escape throughout the complete profile. or even throughout the complete boost profile or the reentry mode, the escape system appears to be somewhat complex and heavy. It is difficult to generate specific numbers of losses per thousand missions without the benefit of many actual flights. Data such as these are used to establish trends upon which design decisions can be based.

The weight of the equipment provided to accomplish escape is presented in the following table:

Capsule trim surface, lb				•	١				. *										86
Capsule parachute, lb .									,		•						• ,		196
Escape rocket and separat	ion	pro	ivc	sic	ns,	11)												222
Capsule reaction control																			
Battery, inverter, etc.,																			
Electronic apparatus, 1b	,· •	•		•			•	•	•	٠	٠	.•	•	•	•	•		•	27
Total weight lb		_																	720

The capsule trim surfaces assist in producing the proper angle of attack after capsule separation. Both a deceleration parachute and a cluster of three recovery parachutes are used. The escape rocket applies a 25,000-pound thrust for 1 second to the capsule after separation. The reaction control system can be used for capsule orientation for reentry, for stability augmentation, and for maintaining proper attitude in conjunction with the trim surfaces. The battery and other electronic and electrical equipment supply power and control during emergency conditions. These items total 729 pounds.

Figure 3 shows a partial inboard profile wherein the escape provisions have been combined with the equipment provided for normal flight to give a total weight of about 1,400 pounds due to piloted flight. This total weight is about eight times greater than the weight of the pilot alone. The normal-cooling-system weight is less than the emergency-cooling-system weight because the emergency cooling system must cool those electronic devices necessary for pilot escape, whereas the normal cooling system is only chargeable to pilot cooling.

Protective devices which are peculiar to the pilot include the seat and restraint devices, the ventilated pressure suit, and the sonic insulation covering the inside surface of the capsule walls. It has been estimated that the noise level inside the pilot's compartment may be as high as 140 decibels during boost. The helmet will reduce this level by a minimum of 20 decibels. The allowable level is about 135 decibels for 10 seconds. One of the early tasks will be to obtain more definitive data on noise levels through tests. The pilot's seat is positioned forward 15° during the boost phase and 10° back during free flight. The peak acceleration during the Titan-Centaur boost is about 7g and is reached about 3 minutes after take-off. The pilot can easily withstand the boost-acceleration profile.

1

1

The design of the Dyna-Soar glider is not affected by solar radiation. Ultraviolet rays are absorbed strongly by the glass in the side windows. Visible light will be handled by suitable diffusers. The planned apogee (300 nautical miles) is well below the strong Van Allen radiation belt. The glider will experience a maximum of about 100 milliroentgens per week. The allowable value established by the Atomic Energy Commission is about 300 milliroentgens per week. The principal hazard of the nuclei particles is when they stabilize by suddenly giving off their energy in a small amount of tissue, which creates an intense ionization for 1 or 2 centimeters of tissue depth. The probability of hits by such particles is extremely low for the Dyna-Soar mission.

The extreme temperature environment encountered during the reentry phase dictates the requirements for cooling systems for both the pilot and equipment. One of the most important parameters in environmental control systems is the temperature to which heat is transferred which is called the heat-sink temperature. It is axiomatic to environmentalcontrol engineers that the weight cost for cooling systems decreases as the heat-sink temperature is raised. Thus, it is possible to get a 150° F heat-sink-temperature cooling system for less weight than a 0° F heat-sink-temperature cooling system for the same heat rejection. The curve on the left-hand side of figure 4 shows this trend of decreasing cooling-system weight as heat-sink temperature for equipment is increased. The curve presented is not for one particular cooling system but may represent several systems at different parts of the curve. On the righthand side of figure 4 are shown the temperature limitations for man as a function of time. It can be seen that, as the effective temperature surrounding the pilot is increased, the time duration of his tolerance to this temperature decreases. The effective temperature includes the effects of wall radiant temperature and ambient gas temperature. The curves for man are plotted for specific values of humidity and pressure and would shift as these parameters change. The significant feature of these curves is that the weight penalty for cooling the man may be higher on a long time basis than that for equipment but man can stand higher temperatures for short time periods than most electronic equipment.



For the Dyna-Soar glider, this feature is very important since water is used as a heat sink. During the later stages of the reentry at low altitude, the heat-sink temperature rises and the equipment temperature rises accordingly. It is necessary to shut off the equipment at touchdown in order to prevent overheating of the equipment. The pilot experiences the same heat-sink-temperature rise but his capability for withstanding high temperatures for short time periods allows for a system design which does not require extra provisions or special operational techniques.

Some of the test work which assisted in the design of the Dyna-Soar vehicle for piloted flight included vision capability, reaction-control simulation, cockpit-characteristics simulation, and centrifuge tests simulating the boost phase of flight.

Vision is one of the ground rules for piloted flight. The degree and type of vision provided will vary with the mission requirements. but all will agree that direct vision is the best way to do the job. Since the weight per square foot of window is about five times the weight per square foot of capsule wall, it is necessary in the design stages to make careful trades between window area and pilot vision requirements. The forward window on the vehicle is covered during most of the reentry because the materials cannot withstand the temperatures. The side windows are not subjected to as high temperatures and are not covered. Figure 5 shows a North American F-86 airplane used in checking out the capability of the pilot to use the side and forward windows of the Dyna-Soar vehicle. The canopy was covered over except for the portions simulating the windows on the Dyna-Soar vehicle. The pilot was positioned in the cockpit with respect to these windows as he would be in the Dyna-Soar cockpit. This was one of the ways in which direct pilot contact with proposed designs was used to select a configuration. Figure 6 shows the altitude and ground track of the vehicle during a 3600 landing approach. This is just one of several landing techniques being evaluated. This particular pattern is more critical for sizing the side window than others and was used to size the present side windows. Present efforts have been directed toward increasing side-vision capability along with a reduction in the weight of the window.

The centrifuge at Johnsville, Pa., was used extensively to check the pilot's capability to withstand the accelerations experienced during the boost phase of the Dyna-Soar flight. There are two major differences between piloted flight in the Dyna-Soar glider and in other aircraft. These differences are the operation in a high-acceleration field and the high degree of accuracy required in controlling pitch of the vehicle during boost in order to establish a successful orbit.

1

Figure 7 shows a comparison between the theoretical boost acceleration of a four-stage solid-propellant ICBM booster, which consisted of





clusters of the Minuteman booster, and the capability of the centrifuge. It can be seen that the maximum acceleration attained was about 8g at the end of the second-stage boost. The total boost period was about 300 seconds, 60 seconds of which were a coast period between the third-and fourth-stage boost. Later developments in the Dyna-Soar program resulted in the consideration of either the Atlas-Centaur or the Titan-Centaur booster in place of the clustered Minuteman booster. The boost-profile accelerations for the Titan-Centaur are shown for comparative purposes. It can be seen that selection of this booster would result in lower magnitudes of accelerations but a longer duration of boost. The maximum value of acceleration would be about 7g and the total boost period would be about 500 seconds. Either of the boost profiles shown would be well within the tolerance limits for a pilot. Onset accelerations are also within human tolerances.

Four pilots were used in a total of 100 runs in the centrifuge. The cockpit was fitted with a proper seat and a three-axis side-stick controller developed for the glider. Variables were wind shear, acceleration, and uneven stage termination. The tracking task was a closed-loop simulation of the vehicle dynamics. Figure 8 shows the result of a tracking exercise on the centrifuge. The four-stage boost profile was used. The ID-249 A/ARW cross point indicator was used by the pilot to attempt to follow the theoretical boost profile shown. Tolerances on his track were the lower limits of glider capability and the upper limit which was the recovery ceiling. Approximately 12 to 14 runs had to be made by each pilot before his proficiency was up to that indicated by this curve which was representative of the runs being made after 20 trials. The run was considered a success if at the end of boost the pilot's track equaled the theoretical track which establishes successful orbit at the altitude and speed shown.

Another simulator was used to obtain pilot reactions to other portions of the mission profile. This was a six-degree-of-freedom cockpit characteristics simulator which was used for simulating orbit, reentry, and glide to Mach 1.5 flight. Some of the cockpit instruments used were the side-stick controller and indicators for horizontal and vertical situation, range-to-go, inertial altitude and velocity, and vehicle temperature.

A reaction control simulator was constructed to check out various methods of controlling the vehicle during orbital flight. Figure 9 is a photograph of this simulator which utilized a large air bearing for almost frictionless support. Small nozzles located on the extremities of the simulator discharged nitrogen gas to provide the thrust necessary to move the simulator.

Most of the foregoing discussion has been directed toward those factors which directly influence the design of the Dyna-Soar vehicle



مِدُ أ

L 1

ĺ

2

5

due to piloted flight. The pilots of existing flight vehicles have added to the overall reliability of mission success and the Dyna-Soar is no exception. Figure 10 shows in a qualitative manner that the pilot contributes significantly to the attainment of a successful mission. The figure presents the weight increase as a function of failures (aborts) per 1,000 missions. The plot does not take into account the boost phase of flight. The solid-line curve includes various combinations of the following systems: flight control, guidance, secondary power, and environmental control. At 28 failures per 1,000 missions, it has been assumed that there is no redundancy in these systems. As systems are dualized, the weight increases with an attendant decrease in mission failures. The solid-line curve assumes no effect on mission success due to the pilot. The dashed-line curves show the effect on mission success when the pilot can act to various degrees in parallel with these subsystems. The percentage figures indicate the degree to which the pilot is in parallel with these subsystems. The pilot cannot act completely in parallel with any of these systems but he does have a partial paralleling capability. Although a pilot task and subsystem capability analysis has not been made at this time, it is felt that the Dyna-Soar pilot will be able to contribute to increased mission success through proper integration of man and machine.

CONCLUDING REMARKS

Some of the factors which have influenced piloted flight of the Dyna-Soar glider have been discussed. Because of the design, the pilot can contribute to mission success and will not be adversely affected by the mission profile environments. The attainment of the Dyna-Soar goals cannot be met without man and the price in weight is small compared with the achievement of the Dyna-Soar system objectives.

1





PROVISIONS FOR PILOT

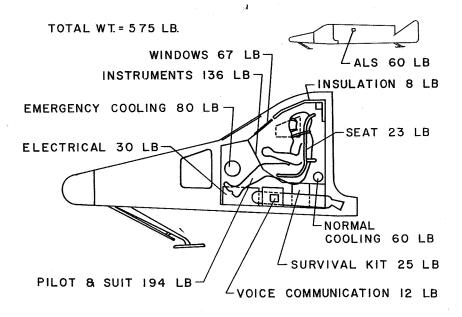


Figure 1

WEIGHT VS SURVIVAL

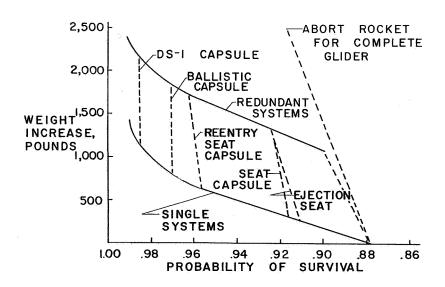
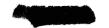


Figure 2



1



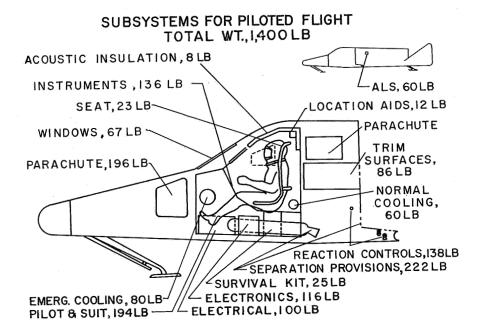


Figure 3

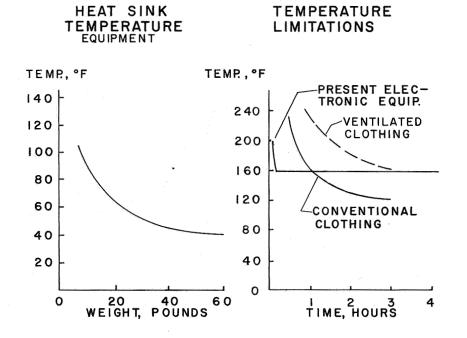


Figure 4





Figure 5

SIDE VISION ON APPROACH

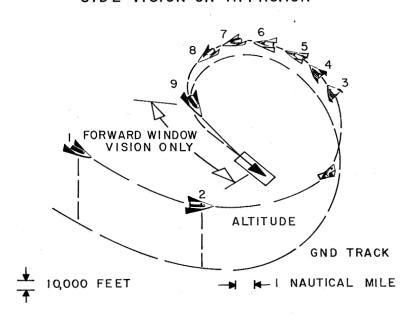


Figure 6



BOOST ACCELERATION

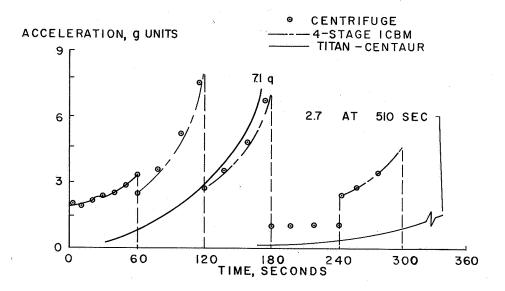


Figure 7

TRACKING EXERCISE

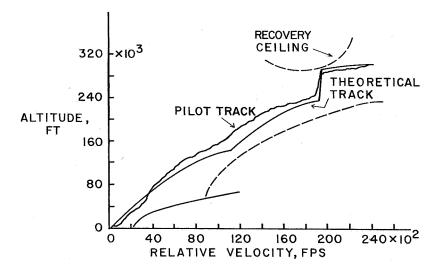


Figure 8



REACTION CONTROL SIMULATOR

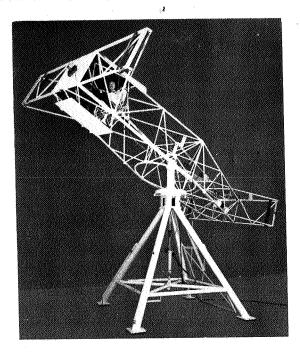


Figure 9

PILOT'S EFFECT ON MISSION SUCCESS

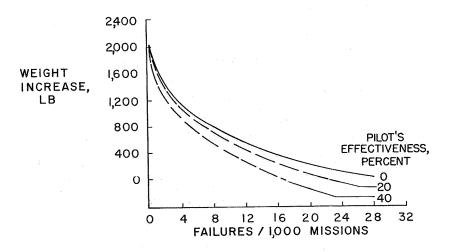


Figure 10





L 1 2 6



SECONDARY POWER AND ENVIRONMENTAL CONTROL FOR DYNA-SOAR

By Earl M. Donnen Boeing Airplane Company

INTRODUCTION

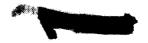
Secondary power is the term applied to all nonpropulsive power used on the Dyna-Soar flight vehicle. It includes electrical power needed for electrical and electronic equipment, power for moving aerodynamic control surfaces while the vehicle is within the atmosphere, and power for attitude control while the vehicle is at altitudes where aerodynamic control surfaces are ineffective. The term environmental control is applied to the provision of properly controlled cooling, heating, pressurization, and atmosphere necessary for the efficient operation of the pilot and the airborne equipment. This discussion will be limited to secondary power and environmental control as applied to (1) the glider portion of the airborne vehicle, and (2) the normal systems as contrasted to emergency systems.

SYMBOLS

I_{sp}	specific impulse, sec
p ₁	pressure upstream of nozzle, lb/sq in.
p ₂	pressure at nozzle exhaust, lb/sq in.
γ	ratio of specific heats
SFC	specific fuel consumption, lb fuel/lb thrust/hr
$T_1 \dots T_5$	local temperature, OF

SECONDARY POWER

The selection of the main power source is of primary interest in secondary power. Since all energy must be carried aboard the vehicle,



weight and volume requirements must be considered on the basis of total energy requirements for the design missions as well as peak-load and transient-load requirements. A total power requirement of 35 horsepower hours is typical of a 2-hour Dyna-Soar flight. Peak horsepower requirements for aerodynamic controls might be as high as 16 horsepower, and electrical requirements as high as 9 kilowatts at various times during the flight. The peak hydraulic loads will occur during the reentry phase, and the highest electrical loads are expected prior to reentry. The types of power sources considered for Dyna-Soar were: (1) open-cycle propellant prime movers, (2) batteries, (3) solar cells, (4) fuel cells, (5) thermionic devices, (6) thermoelectric devices, and (7) nuclear devices. Only the open-cycle propellant prime mover (usually termed an accessory power unit, or APU, when associated with its driven equipment) and batteries of various types were found to be applicable to the Dyna-Soar missions and time scale.

A typical monopropellant APU system is shown in figure 1. Here, two hydrazine-fueled prime movers, usually turbines, each drive an a-c generator, a hydraulic pump, a fuel pump, and a cooling-system blower. Only one APU is loaded. The other is run at no-load as a standby unit. Thus, a-c electrical power is provided directly from the generator, d-c power being furnished through a transformer rectifier unit. In this particular representation, dual prime movers are supplied from a single fuel system. This same system supplies fuel for the reaction-control gas generator. System integration is represented by the use of the turbine exhaust heat to keep the reaction-control gas generator heated, and use of the fuel as heat sink for part of the hydraulic-system cooling load. Water heat exchangers cool the gas from the blower before it is distributed to cool the electronic equipment as well as to remove that hydraulic oil heat which is above the heat-sink capacity of the hydrazine.

A battery system for Dyna-Soar is not illustrated. However, in a typical system, a multiple-cell battery supplies d-c power directly to the equipment and a-c power through a static inverter. Hydraulic-pump and cooling-blower power is provided by electric motors. Power for the reaction controls must be provided from a separate system.

The results of a weight-trade study of battery and hydrazine APU systems are shown in figure 2. The effect of mission duration on the two systems for the given power level is very apparent. For mission times greater than approximately 30 minutes, the APU system offers a significant weight advantage, even when dual APU prime movers are compared with a single battery. The basic weight, or 100 percent point, is that for a dual APU system on a 2-hour flight. For the same flight, the battery system is approximately 140 percent of the hydrazine APU system weight. Additional significance of the weight-time difference is realized when the design objective of a 4-hour flight is considered.



3

At this point the battery system is over 200 percent of the hydrazine system weight. For this particular illustration, two-stage turbines, each with a specific fuel consumption of 5.0 lb/hp/hr, and a secondary type, silver-oxide—zinc battery rated at 22 lb/kw-hr (including case and mounting provisions) were used. These values are considered to be representative of equipment which will meet performance, timing, and reliability requirements for Dyna-Soar. The selection of these systems was based on battery and APU investigations which will not be discussed here.

In general, the lower the specific fuel consumption of an APU system, the lower the system weight. For that reason alone, a hydrogenoxygen bipropellant APU system deserves special consideration. Because of the much higher energy content of the hydrogen-oxygen fuel, the specific fuel consumption obtainable may be 30 to 40 percent of that for hydrazine. In addition, if liquid or very cold hydrogen is used, its heat-sink capability (approximately 2,000 Btu/lb) may be used rather than that of water to absorb waste heat from the power-generating and power-using equipment, as well as aerodynamic heat. A typical system using cold hydrogen and oxygen is illustrated in figure 3. This system is very similar to the hydrazine-fueled system; the main differences are the use of bipropellants instead of a monopropellant, the replacement of water heat exchangers with hydrogen heat exchangers, and the control of fuel flow to satisfy both power and cooling demands. This last difference will require careful system analysis and design to prevent interacting effects between the power and cooling control loops.

The largest drawback to the use of liquid hydrogen is the large heavy tank required because of the low-density extremely cold fluid involved. A development holding much promise for lighter weight and simpler storage is the storage of hydrogen in insulated thin-wall tanks at pressures above critical pressure and at temperatures initially below critical temperature. A vacuum-jacketed Dewar type tank is not required. The hydrogen temperature is increased by heat transfer into the storage tank from ambient air and/or by the controlled addition of heat from electric heaters. The heat input is so controlled that, as fluid is withdrawn, the remaining hydrogen is maintained at a constant pressure. The critical pressure of hydrogen is about 13 atmospheres. Therefore, to be conservative, the hydrogen is stored well above critical pressure at approximately 20 atmospheres (300 lb/sq in. abs). Theoretically, the fluid, which can be called "supercritical," stays as a homogeneous material and will have no liquid-vapor interface. A small fan might be used within the tank to handle any temperature stratification. Thus, the fluid should be expellable in a predictable and consistent condition. Not only does this type of tankage allow controlled expulsion of the fluid, but dense storage as well. A tank volume not much greater than that ired for liquid storage should



result. This system should be almost as simple as a high-pressure ambient-temperature gaseous storage system and be just as controllable. In addition, the system has a heat-sink capability almost as great as that for liquid storage but does not have the complexity of a helium pressurizing medium and/or a pump system.

A weight comparison of the hydrogen-oxygen system, using super-critical storage, and the hydrazine system indicates that, for a 2-hour typical mission, weight savings of approximately 180 pounds can be achieved when the savings in the secondary power system and in the equipment cooling system are considered. The crew compartment cooling system is not included. Although the oxygen is required only for power generation, if it is stored as a liquid or in a "supercritical" state, some heat-sink capacity is provided. This heat-sink capability is relatively small, however, and has not been considered in the weight comparison given.

ENVIRONMENTAL CONTROL

The two main considerations for environmental control are the pilot and the equipment. The pilot must be provided with a breathable atmosphere controlled to pressures and temperatures which will allow him to perform efficiently. No less important is the provision of a pressurized atmosphere and a temperature-controlled environment for the equipment - upon whose satisfactory operation the pilot and vehicle are so dependent.

In figure 4 is shown a block diagram of one approach to crew compartment environmental control. It represents an atmosphere supply carried in vacuum-jacketed and insulated tanks as a mixture of liquid oxygen and liquid nitrogen. This mixture is in the ratio of 40 percent oxygen and 60 percent nitrogen by weight. In a total pressure of 7.35 pounds per square inch absolute (18,000 feet), the oxygen partial pressure will be 2.6 pounds per square inch absolute (5,000 feet). This mixture is expelled from the tanks as a liquid and is passed through cold-plate cooled electronic equipment where it cools the equipment and is changed to a gas in the process. The proper ratio of oxygen and nitrogen in the gas is thus assured. As breathable atmosphere, it is ducted through essentially two loops - one is through the pilot's pressure or ventilation suit and the other is through the cabin. pressure suit is not required under normal system operation but is included as a precaution against cabin decompression. A blower circulates the air through the equipment and around the compartment. A





water-boiler heat exchanger is in the circuit to remove heat. A back-pressure control on an overboard steam vent regulates the water boiling temperature. In addition, carbon dioxide and water absorbers are shown, since a very low leakage cabin is assumed. Most of the external heat is removed in the water-wall panels on the outside of the pressure shell. This provides a near isothermal boundary around the compartment. The water-wick wall panel is discussed more thoroughly in a subsequent section.

In figure 5 is shown a block diagram of the equipment-compartment environmental control. Liquid nitrogen is vaporized to provide an atmosphere pressurized to 10 pounds per square inch gage in an open-cycle low-leakage rate system. One blower, driven by an APU, circulates the nitrogen through the equipment and around the compartment. The other blower is unloaded to reduce power consumption. The heat picked up from the equipment and that which enters through the exterior insulation is removed by a water-boiler heat exchanger. A combination of water-boiler and hydrazine heat exchanger is used to cool the hydraulicsystem oil as it returns from the control-surface actuators and before it enters the hydraulic pump. The water boiling temperature is regulated by a simple orifice in the overboard vent line; therefore, temperature actually varies somewhat with load on the boiler. An investigation of the equipment-compartment cylindrical pressure shell indicated little structural weight penalty in pressurizing to 30 pounds per square inch gage. However, 10 pounds per square inch gage is used as a favorable compromise of compartment leakage rate, blower power required, and cooling effectiveness. The use of hydrogen as a heat sink instead of water is an alternate approach for equipment cooling which was discussed in the section on secondary power.

In order to determine the environmental control systems as illustrated in figures 4 and 5, pilot and equipment requirements are determined and system design approaches studied. For the pilot, the partial pressure of oxygen required, breathing requirements, pressure—or ventilation—suit requirements, allowable temperature range for ambient air and cabin wall surfaces, pressurization requirements, moisture and carbon dioxide concentration limitations, and potential fire hazard are among the more important items to be determined. For the equipment, cooling, pressurization, and temperature range allowable are determined. In addition, an analysis to determine the air temperatures which will surround the crew and equipment compartments is made for the range of flight conditions contemplated. The temperature range and rate of change of temperature have considerable effect on the selection of the environmental control system and a particularly significant effect on the thermal insulation needed for the compartments.

The more important of the crew-compartment studies are studies of (1) system cycle, that is, open as compared with closed, (2) cryogenic





cooling as compared with cryogenic plus water cooling, (3) wall cooling as compared with no wall cooling, (4) internal wall cooling as compared with external wall cooling, (5) cabin atmosphere and pressure, (6) crew-compartment humidity, and (7) crew-compartment carbon dioxide.

The determining factor in the selection of the type of cycle to be used for the crew-compartment environmental control system is the compartment leakage rate. The minimum system weight for either open or closed system occurs at a leakage rate of 0.15 to 0.25 pounds per minute. At lower leakage rates, the controls required for humidity, carbon dioxide, and partial pressure of oxygen increase the weight. At higher leakage rates, the penalty is due to the greater atmosphere supply which must be carried.

The primary factors in the study of cryogenic cooling as compared with cryogenic and water cooling are leakage rates and heat load. Water has approximately five times the heat sink of an equal weight of oxygen and nitrogen mixture. The heat loads which can be carried by the cryogenic mixture will depend on the flow rate to meet leakage requirements.

A study of heat transfer through the cabin walls will determine the necessity of removing heat at the walls to keep the inside wall and compartment temperature at tolerable levels for the pilot and equipment. If wall cooling is necessary, several approaches can be used; for example, (1) cabin air can be circulated through wall panels and then through a water-boiler heat exchanger for cooling, (2) internally or externally located panels can be filled with water, or (3) water can be circulated through wall panels or tubing. Careful consideration particularly must be given not only to the heat-removing capability and weight, but also to the reliability.

Cabin atmosphere and pressure level are determined primarily from consideration of human factors, structural weight, and fire hazard.

Similar studies are made for equipment-compartment environmental control. Without the pilot's requirements to consider, however, the results are often very different, particularly in regard to atmosphere composition, temperature, and pressure level.

EFFECT OF UTILIZATION SYSTEMS

The secondary power and environmental control systems perform essentially service functions; that is, they exist only to enable other systems, such as flight control, communications, guidance, and data acquisition, to perform their assigned jobs. Because of this service

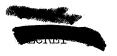




role, their size and cost, in addition to the efficiency of their particular design, are greatly dependent upon the demands of the utilization systems and upon the efficiency with which the utilization equipment makes use of these services. The following are a few examples. These examples actually represent good "horse-sense" design consideration but illustrate the point and are too frequently given inadequate attention.

- (1) The flight control system requires that hydraulic fluid be provided at flow rates and pressures which will actuate the control surfaces to meet vehicle stability and control requirements. If, however, hydraulic power is requested which represents maximum control surface rate and hinge moment at highest "q" conditions and for maximum "g" maneuver and is represented as a continuous demand on the hydraulic system, even though not actually required, the hydraulic system installed to meet this demand would be considerably oversized for actual flight requirements. Not only would the hydraulic pumps, transmission lines, accumulators, reservoirs, and the control-surface actuators be overly large, but also a larger APU and fuel system, a larger heat exchanger, and more water for cooling would be required. All this is in addition to structural provisions for the greater than necessary volume and weight which result.
- (2) In electronic equipment, emphasis is usually given to compact packaging and efficient arrangement of components for electronic reasons. Too often, however, the benefits of this packaging are lost to the vehicle because of prohibitively high cooling requirements. To be more specific, certain items of electronic equipment can be adequately cooled with an airflow rate of 4 pounds per minute per kilowatt at an inlet temperature of 70° F. Other equipment of the same type requires as high as 10 to 12 pounds per minute per kilowatt at 70° F. This requirement naturally is reflected back into blower, heat exchanger, and ducting size as well as additional fuel to provide for additional power. A detailed check of some of these packaging practices has shown that cooling requirements can be greatly reduced by simple rearrangement of components with the aim of more efficient heat transfer and still not impair the performance of the component.
- (3) Other items which can unfavorably affect the overall vehicle in terms of excessive secondary-power and environmental-control provisions are (a) excessively close frequency and voltage control for electrical supply system, (b) too low temperature and too high pressure-drop requirements of electronic equipment, and (c) greater than needed attitude resolution for reaction control at high altitude.

On a conventional jet airplane (such as the Boeing B-52 or the Boeing 707) where secondary power is extracted from the main engines (either by a shaft or by compressor bleed air) and pressurized air for



breathing and cooling are also extracted from the engine by bleed air or by ram air, the preceding considerations are also valid. However, the penalty of additional power extracted from the main engines, additional ram air, and additional weight is a minor reduction in range. The effect of added secondary power and environmental-control weight has added significance on Dyna-Soar, however, where weight is the determining factor in whether the vehicle can be boosted into the desired flight trajectory with a given booster.

DEVELOPMENT TESTS

Two development tests of special interest in secondary power and environmental control for Dyna-Soar are (1) a hot-gas system for reaction controls, in which hydrazine is decomposed in a centrally located gas generator, and (2) passive water-wick panels for providing a heat barrier around crew and equipment compartments. Both of these developments are of a feasible or exploratory nature and are not developments of completed flight hardware.

HOT-GAS SYSTEM

Development studies of reaction-control-system requirements indicated the need for a system with very rapid response characteristics. These requirements, in conjunction with vehicle considerations for low weight, low fuel consumption, and compatibility with the high temperature environment associated with a radiation-cooled structure, pointed up the attractiveness of a hot-gas reaction control system. The feasibility of an on-off gas type of reaction control system was demonstrated on a three-degree-of-freedom flight simulator. Compressed nitrogen gas was used for these tests, pending the development of a hot-gas supply system. A central hot-gas system using a monopropellant showed promise of meeting the basic requirements with a minimum weight penalty.

The purpose of these hot-gas development tests was twofold: (1) to establish the feasibility of maintaining hot-gas supply pressure and temperature under simulated operating conditions using hydrazine and (2) to obtain gas-supply-system design parameters for future system designs.

An operational mockup of a hot-gas reaction control system was set up. (See fig. 6.) It initially contained a pressurized fuel supply, a gas generator, relief valve, and three combination on-off valves and thrust nozzles; that is, one nozzle each for pitch, yaw, and roll. A



volume of distribution piping equivalent to that required for supplying gas to an additional 3 nozzles was provided. A fuel-metering valve was later added to provide a constant system gas pressure regardless of demand. The injector for the gas generator in this system mockup was water-cooled. This cooling prevented the heat "soak-back" from the gas generator from causing premature decomposition of the hydrazine in the

fuel line. The equipment used does not represent flight hardware but rather development hardware for demonstrating feasibility of approach.

Tests in which the valves were cycled manually for various reaction jet pulse lengths and also in which the valves were cycled automatically in conjunction with a computer program which simulated flight operation conditions were made. Computer studies of the reaction control system have shown that "thrust" demand will be short in relation to "no thrust" demand. Since the gas system will thus be dead-ended for a large percentage of time, the temperature of the gas at the nozzle will be considerably less than at the gas generator. Low ambient temperatures at the nozzle plus the dissociation of the ammonia in the gas reduce the temperature. In order to pursue the effect of temperature reduction on specific impulse, tests were made with insulated piping at a regulated gas-generator pressure of 160 pounds per square inch gage. Under full flow condition, this pressure represented a nozzle inlet pressure averaging 120 pounds per square inch gage. Oscillograph traces of pressure show this drop from a system pressure of 160 pounds per square inch gage to 120 pounds per square inch gage to be almost instantaneous with the valve opening. In figure 7, the average nozzleexhaust temperature after system warm-up is plotted against duty cycle. Pulse durations of 0.020 and 0.400 second were used. Good agreement of temperature data was obtained for the same duty cycle for different pulse durations. Duty cycles are not expected to approach the 40 percent mark except for a brief period required for vehicle stabilization at separation from the booster, and for a brief period for orienting the vehicle for reentry. A duty cycle of less than 1 percent would be typical of most of the high-altitude flights.

Figure 8 illustrates the effect of the previous temperature data on the effective specific impulse $\rm I_{sp}$ at the nozzle. Since reduced specific impulse means more fuel for a given total impulse, it seems to indicate that adequate consideration of temperature drop in a system must be given along with duty cycle to minimize fuel requirements for various flights. However, as shown in figure 9, when the same basic data are plotted in terms of specific fuel consumption (SFC), or pounds of fuel used per pound of thrust in one hour of operation, a somewhat different impression is obtained. For the longer duty cycles, higher temperatures at the nozzle and, therefore, higher effective $\rm I_{sp}$ are

maintained. For the shorter duty cycles, the temperature at the nozzle





and the effective $I_{\rm sp}$ are reduced. At these shorter duty cycles, the difference in SFC is so small as to make questionable the payment of the weight penalty for duct insulation. This curve also illustrates the desirability of a short duty cycle to achieve minimum fuel consumption.

In addition to design data obtained, the important conclusions which were reached as a result of this testing were:

- (1) A central hot-gas system using hydrazine is technically feasible
- (2) The hydrazine-gas generator can be operated in a selfsustaining manner for substantial periods of time with no gas being exhausted from the system. The operation is self-sustaining without the use of oxidizers or external heat
- (3) A simple fuel-metering system to maintain a constant system gas pressure can be built as flight hardware
- (4) A hot-gas valve with adequately fast response time can be built as flight hardware
- (5) Careful consideration must be given to fuel-injector cooling, or possibly the elimination of the need for injection cooling, in the design of flight hardware.

WATER WICK PANELS

If, for a particular vehicle design, it is determined that cooling of a cabin or equipment compartment wall is necessary, it is desirable that the cooling means be a passive system, that is, be independent of pumps, blowers, or other active devices. For pilot protection in particular, it is necessary that the wall cooling be also independent of cabin pressurization. One promising approach to satisfying this requirement is the use of the water wick panel.

In figure 10 are illustrated two approaches to the water wick panels - each intended to serve as a nonstructural heat barrier between the outer skin and the cabin. The first is the tube-type panel where a water-absorbent or wicking material is placed in tubes and the tubes are filled with water. The tubes are placed next to the cabin shell with a layer of aluminum foil next to the tubes and 2 inches of insulation on the outside of the foil. The insulation is held in place with a thin sheet of steel. The steam exhaust is collected in a manifold and vented overboard. In a flight configuration, the back pressure would



be regulated to control the boiling point at high altitude to approximately 70° F.

An earlier tube panel configuration did not include the aluminum foil over the tubes. However, a computer analysis showed that an appreciable amount of heat would flow around the tubes and cause severe temperature gradients in the cabin pressure shell. The addition of the foil causes a short which shunts the heat through the water-filled tubes and practically eliminates the temperature gradient in the pressure shell. At the same time, the percentage of aerodynamic heat allowed to flow to the cabin is reduced from approximately 30 percent to 2 percent.

The second configuration shown is termed a vapor-cooled insulation type. In this configuration, the wicking material is held against the pressure shell by a semipermeable membrane. This membrane will pass water vapor but not water at the design operation conditions. The water vapor passes through the insulation layer and out through the perforated steel retention sheet. The steam is vented overboard from the space between the outside skin and the panel.

Several materials were tested for suitability as a wick. One of the better materials is fiber glass in a mat of unbonded "B" fibers. Figure 11 illustrates the water-retention capability of three samples of varying height. The significant point of these data is that, for this material, the practical water wicking limit is approximately 8 inches. The average wetness ratio, or pounds of water per pound of wick, drops off rapidly above this wick height.

Another important consideration in choice of wick height is the water-retention ability of the wick under acceleration loads. Centrifuge tests of a saturated wick showed that water retention is markedly affected above an acceleration of 4g. Individual panel design must, therefore, account for boost accelerations and provide panel sizes which will permit the wicking action to redistribute the water in a reasonable time. More testing will be required to establish the specific sizes required.

The next illustration (fig. 12) shows the test results at 140,000 feet of a vapor-cooled-insulation type of panel. Heat lamps were used to raise the temperature of the perforated steel shield to 1,600° F. The temperatures at various points through the panel at its center are plotted against time. The wick material reached 100° F in 53 minutes when the water had been almost expended. In figure 12 is shown the temperature distribution in the water wick at 140,000 feet over a 12-inch by 18-inch panel. The significance of wick height is again illustrated. Those temperatures measured in the lower half of the panel are considerably lower than those measured at the top of



the panel because the water-retention capability of the wick is reduced at these upper locations, as previously shown in figure 11.

The exhausting of steam through the insulation has two main advantages: (1) the weight of a steam-collecting manifold is eliminated, and (2) the superheating of the steam as it passes through the insulation lowers the insulation temperature and, therefore, reduces the insulation conductivity. An analysis indicates that approximately 20 percent less water is required for a given heat input because of the vapor-cooled insulation.

Tests were made at sea level to establish the feasibility of the tube-type panels. Test panels were constructed with two rows of 8-inch water tubes. Heat lamps were used to raise the temperature of the outside steel sheet to $2,000^{\circ}$ F. (See fig. 13.) After 22 minutes of operation, the temperature on the inside surface of the acoustical insulation had not exceeded 105° F, even though the water boiled at 212° F, as compared with 70° F to 80° F boiling temperature at high altitude.

There are other approaches to the application of water to passively cooled panels. However, these tests firmly establish that the water-wick configurations described here are feasible designs directly applicable to Dyna-Soar.

CONCLUDING REMARKS

Feasible systems and two significant developments in secondary power and environment control for the Dyna-Soar vehicle have been presented. Additional studies and developments along with the latest vehicle requirements will establish the actual systems configurations.



SECONDARY POWER SYSTEM HYDRAZINE APU

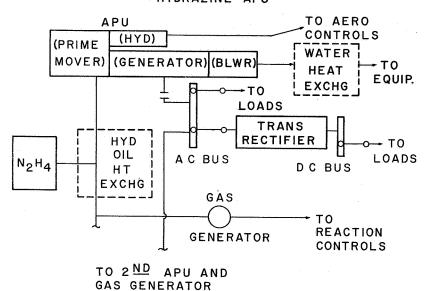


Figure 1

SECONDARY POWER SYSTEM WEIGHT COMPARISON HYDRAZINE APU AND BATTERY

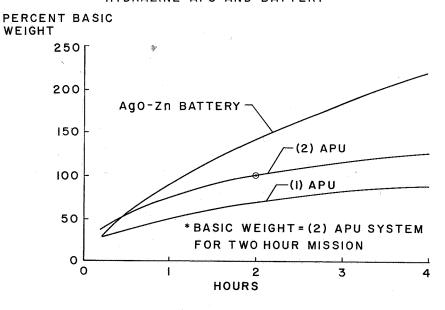


Figure 2





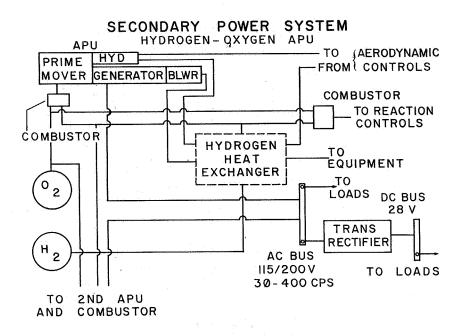


Figure 3

ENVIRONMENTAL CONTROL SYSTEM

CREW COMPARTMENT WATER-WALL CABIN BLOWER EQUIPMENT WATER SUIT HEAT BOILER FLOW **EXCHANGERS** CONTROL TEMP SENSOR VALVE

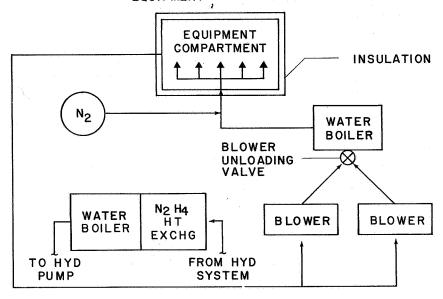
Figure 4

CO2 H2O ABSORBER ABSORBER

INSTR & EQUIP

PANEL

ENVIRONMENTAL CONTROL SYSTEM EQUIPMENT COMPARTMENT



1

3

Figure 5

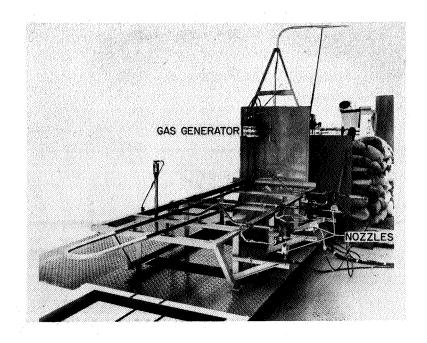


Figure 6





EXHAUST GAS TEMPERATURE AT NOZZLE REACTION CONTROLS

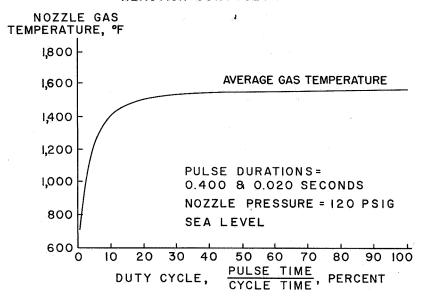


Figure 7

SPECIFIC IMPULSE OF NOZZLE EXHAUST GAS HYDRAZINE FUEL

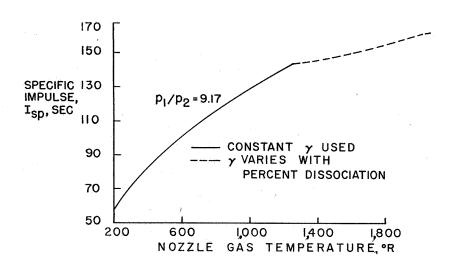


Figure 8







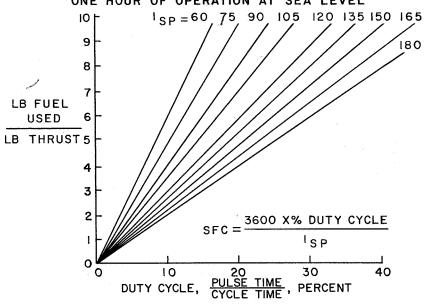


Figure 9

WATER WALL CONFIGURATIONS

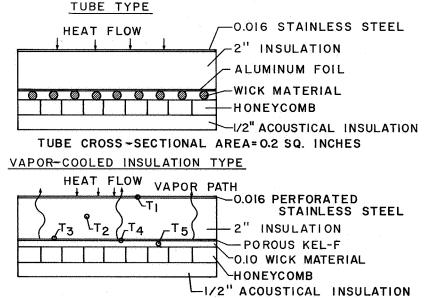


Figure 10





MOISTURE DISTRIBUTION IN SATURATED WICKS VERTICALLY ORIENTED SAMPLES

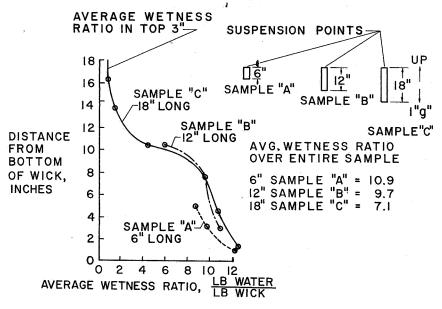


Figure 11

TEMPERATURE VARIATION IN WICK LAYER VERTICALLY MOUNTED PANEL

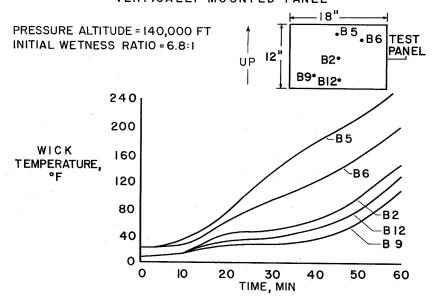


Figure 12



14

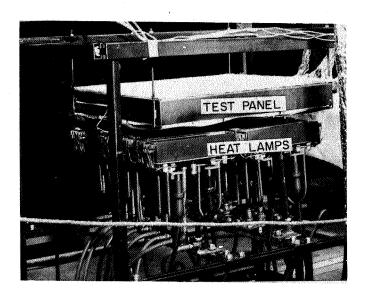


Figure 13

Page intentionally left blank



CONTRIBUTIONS OF FREE-FLIGHT MODEL TESTING TO THE

DEVELOPMENT OF BOOST-GLIDE VEHICLES

By Tung-Sheng Liu Wright Air Development Division

INTRODUCTION

L

1 1 2

7

During the last fifteen years, with the advancement of the ballistic missiles, rocket-boosted test vehicles using mostly solid propellants have achieved great capabilities. The primary purpose of the development of these rocket-powered test vehicles was for vertical probes. At the present time these test vehicles have attained a capability of probing into great altitudes, several thousands of miles up, at velocities beyond the earth-orbiting velocity. In combination with other available missile boosters, solid or liquid, these test vehicles can probe into the deep space at velocities exceeding the earth escape velocity.

In the development of lifting boost-glide and reentry vehicles, it is desirable to conduct some free-flight tests with these test vehicles. The question has often been asked what can be gained by these tests that can not be obtained from other ground experiments or tests. • It is the purpose of this paper to critically examine the capability of presently available test vehicles, their major contributions to the development of lift boost-glide reentry vehicles, and the problems remaining to be solved before free-flight tests can be reasonably assured of success.

CAPABILITY OF AVAILABLE TEST ROCKETS

Table I shows the capability of presently available rocket-powered test vehicles, their maximum payload and maximum attainable velocity. These rocket-powered test vehicles were primarily developed for probing the geophysical and gasdynamic environments. The requirements here are simply velocity, altitude, and reasonable payload capability for instrumentation. Their trajectories are mostly near vertical ballistic trajectories except those for the "over the top" firings at the NASA Wallops Station. But the requirement for lifting boost-glide testing is for a small reentry angle or near horizontal attitude at burnout for larger payloads. The NASA Scout and the Air Force Hyper Environment



Testing System (609A) are designed for this mission. The 609A and the Scout can send a payload of about 150 pounds into a 300-mile orbit and can carry much heavier payloads at suborbital velocities. Figure 1 shows the Scout or the 609A payload capability superimposed on a familiar flight corridor chart. It is seen that the Scout or the 609A vehicle is able to reach the critical heating region within the corridor at velocities between 18,000 and 22,000 feet per second with a substantial payload. The X-15 and X-17 capabilities are also indicated for comparison. The X-17 points are, of course, the maximum velocity at those altitudes on its ballistic trajectory. It is important to note that the major modification to the basic Scout is for the strengthening of the rocket casing and interstages and the stabilization of the last stages compatible with winged lifting reentry models.

L

1

1 2 7

LIMITATIONS OF GROUND TEST FACILITIES

Much of the present lifting reentry glider design is based on theoretical analyses and extrapolations which necessitate the employment of certain assumptions. Whenever there are assumptions, there are uncertainties. These uncertainties must be cleared up and the assumptions must be verified by experiments before a sound design can be achieved. Many experiments in the hypersonic regime have been conducted in ground facilities but these ground test facilities have limitations.

Present hypersonic wind tunnels are often limited in the Mach number and Reynolds number ranges due to the nozzle construction and physical plant. Shock tube, shock tunnel, and arc-heated tunnels all have similar limitations. Their temperature and pressure environments are quite satisfactory but the true environments encountered in actual flight are rarely simulated simultaneously. The chemical state of the gas in a test facility before and after the shock wave is beyond the control of the facility operators. Furthermore, the ground facilities are usually small; they can accommodate only small-scale models. This not only creates serious scaling problems but the data obtainable are also limited. It is therefore concluded that the present hypersonic ground test facilities can furnish some qualitative information or trends but are certainly not sufficient to produce truely simulated design data for the entire Mach and Reynolds number ranges. In figure 1 it was shown that a free-flight test vehicle can boost a model to the desired velocity and altitude and that the model will fly under the exact environments along its own glide path.





DATA FROM FREE-FLIGHT MODEL TESTS

From free-flight model tests the following data are obtained: tracking and accelerometer, pressure and skin friction, heat transfer and temperature, control effectiveness, survival of structures and materials, and the effectiveness of the cooling methods - namely, radiation, internal radiation, internal fluid cooling, film cooling, and ablation. It should be pointed out that these tests should not be treated as scaled model tests in the usual manner because of the model scaling problems involved. They provide local information on flow conditions and verification of theoretical predictions and design concepts.

CONTRIBUTIONS OF FREE-FLIGHT MODEL TESTS

L

(

The contribution of free-flight model tests can be described in two categories: (1) The comparison of different configurations and design concepts derived from the overall performances and (2) The increase of the degree of confidence of analytical methods from the local data. The comparative testing will result in a better selection of configuration and design concept, whereas the local data will aid in the removal of the uncertainties in the establishment of a reliable analytical design procedure as to the chemical state of the gas, the low density effects, and the interference effects.

Figure 2 shows the estimated region of flow conditions from theoretical studies made at the Flight Science Laboratory, AVCO, and the Wright Air Development Division Aircraft Laboratory. The dividing boundaries lie in the most critical region of the equilibrium flight corridor of a lifting reentry vehicle. If any confirmation of these theoretical studies can be obtained in determining more accurately the state of the flow, these tests will contribute greatly to the development of boost-glide reentry vehicles through the removal of many of the uncertainties. Even when the exterior configuration is decided, this information is still needed to finalize the detailed design.

PROBLEMS

Free-flight model testing still has some unsolved problems. The ground tracking and model-survival information can be obtained without data transmission. But, it is certainly most desirable to have both telemetered data and recovered records for all other information. The ionized sheath is known to cause considerable attenuation on standard





telemetering. However, many programs are in progress for the development in this area of means to overcome this difficulty and the Atlantic missile range already has higher frequency equipment in operation.

Model scaling is a basic problem in the theory of dynamic similitude. The NASA, the University of Minnesota, and other laboratories have studied this problem for some time. The general conclusion is to recommend to test full scale especially when some structural data are desired. If the objectives of a free-flight test are aimed at the verification of a design method or the comparison of design concepts and configurations, the model scaling difficulty becomes of secondary importance since the primary objective is to compare the test data with the design method of the test model itself without reference to any prototype vehicles. Consequently, the real problem is the design of the experiments. One must efficiently design the model, the sensors, and the instrumentation to give maximum useful information within the capability of the test vehicle.

CONCLUDING REMARKS

Test vehicles such as the Scout and system 609A are available now at relatively low cost. It is even more economical by incorporating many experiments in a single firing. The application of these test vehicles yielding information to verify the design analyses, structural concepts, and material application would contribute greatly towards better design as well as to the progress of present and future generations of lifting hypervelocity and reentry vehicles.

TABLE I.- CAPABILITY OF SEVERAL ROCKET-POWERED TEST VEHICLES

	I	3/		/	
Rocket	Maximum velocity, ft/sec, of vehicle with payload of -				
	15 lb	50 lb	150 lb	500 1ъ	800 1ъ
HTV-1	7,000				
HTV-2	12,000		·		
HTV-3	16,000			,	
Jason		13,500			
Javelin	·	15,000	13,000		
Journeyman		22,000			
Aerobee-Hi	: 		7,000		
Nike-Cajon		5,700			
Exos		10,000			
X-17			13,000 t	0 7,000	
Scout and 609A		·	30,000; orbiting	20,000	17,000



TEST VEHICLE CAPABILITY

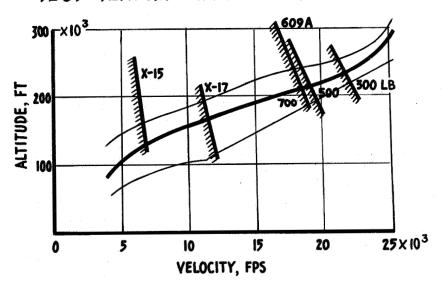


Figure 1

ESTIMATED FLOW CONDITIONS

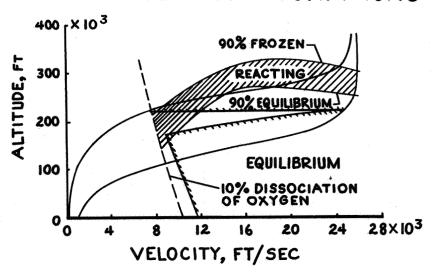
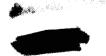


Figure 2



1

L

28

寶



DYNA-SOAR STEP I FLIGHT TEST PROGRAM

By Lt. Col. Harold G. Russell, USAF, and B. Lyle Schofield Air Force Flight Test Center

> and Thomas F. Baker Flight Research Center

INTRODUCTION

The objectives of the Dyna-Soar project have been stated to be the development of a piloted, maneuverable, hypersonic glider capable of a controlled landing following reentry from orbital flight. The Step I flight-test objectives of Dyna-Soar, as shown in figure 1, are twofold: exploration of the flight regime of the glider and development of satisfactory subsystems and vehicle.

Development and verification of the operational concepts and requirements for a Dyna-Soar type vehicle are significantly important from military, astronautical, and possibly commercial standpoints. Verification of the vehicle and subsystems design and modification and development of the hardware as problems arise is the historic role of flight testing and constitutes a primary objective of the Dyna-Soar flight-test program.

The cost, effort, and complexity of conducting ground-launched flights of the Dyna-Soar will be nearly an order of magnitude higher than those on previous airplanes, including the North American X-15. As a consequence, the number of flights that can be expended in developing a satisfactory vehicle and in exploring the flight regimes must be held to the absolute minimum.

FLIGHT REGIME

The general configuration contemplated for Dyna-Soar was described in a previous paper by R. L. Rotelli as being a winged glider with a hypersonic lift-drag ratio on the order of 2. The flight envelope of the Dyna-Soar glider is shown in figure 2 in terms of altitude and velocity. The equilibrium glide corridor is the primary regime to be explored

during the flight tests, although some semiballistic flights above the corridor will be performed. The booster currently planned for Step I of the Dyna-Soar program is a modified Titan ICBM which will limit the maximum Step I velocity to about 19,000 feet per second. For comparison, the design flight envelope of the X-15 is shown at the left in figure 2, and the nominal reentry trajectory of the Project Mercury capsule is indicated by the heavy line.

Within its relatively limited envelope, the X-15 will provide very valuable information on aerodynamic heating, flight control at high altitude, atmospheric reentry, piloting techniques, and terminal guidance. Project Mercury experience in utilizing an ICBM for boosting a manned vehicle, developing man's capabilities in a space environment, operating a global range, and developing recovery techniques will, likewise, be of much value. As may be seen, however, the flight regime of the Dyna-Soar is a tremendous extension of the X-15 envelope and there is a basic conceptual difference between the lifting-vehicle Dyna-Soar glider and the ballistic-vehicle Project Mercury capsule. Additionally, as the flight regime extends to higher velocities, the capabilities of wind tunnels and rocket models to support the design and development of the vehicle become substantially reduced. To reiterate, exploration of the hypersonic-glide corridor is the primary objective of the Dyna-Soar flight test.

L

1

1

2

8

....

DATA OBJECTIVES

The general flight-test areas of interest and the data objectives are shown in figure 3. In each area, onboard instrumentation will provide data by which the conduct of the flight and operation of the systems may be monitored to either confirm the design or provide information to correct deficiencies.

The aerodynamics area is perhaps the most important in that it encompasses aerodynamic heating, flow characteristics, performance, and stability and control. Adequate aerodynamic-heating information for progressive conduct of the flight test can be obtained from a knowledge of the temperatures that exist throughout the skin and airframe during the flight, the flight conditions, and the structural properties (fig. 4). A large number of temperature sensors will be located to provide for determination of experimental heat-transfer characteristics and verification of the structural design.

Detailed analysis of experimental heat-transfer data requires a knowledge of free-stream and local-flow conditions and local gas properties. Use of the nondimensional heat-transfer coefficient, Stanton



number S_{T} , is convenient in comparing experimental results and theory and is given in the following expression:

$$S_{T} = \frac{h}{\rho C_{p}V} = f(R_{e}, P_{r}, T_{s}, T_{w}, M_{\infty}, \alpha . . .)$$

where

h heat-transfer coefficient

ρ density

C_n specific heat of fluid

V free-stream velocity

Re Reynolds number

Pr Prandtl number

T_S stagnation temperature

 T_{W} wall temperature

 M_{∞} Mach number

α angle of attack

Some measurements of both free-stream local-flow characteristics pertinent to heat-transfer analysis are planned for a few specific locations. As shown in figure 5, the required free-stream data consist of total pressure $P_{\rm T}$, total temperature $T_{\rm T}$, angle of attack α , and angle of sideslip β .

Local-flow conditions will be determined primarily from surface-pressure measurements, together with such measurements of surface and boundary-layer temperatures, boundary-layer pressures, dissociation, and gas composition as are possible. The extent of the flow-characteristics measurements obtained during Dyna-Soar flight tests and the quality of information that can be attained depend to a large extent on successful development of both transducers and flight-measuring techniques.



Acquisition of accurate performance data is essential to the conduct of the Dyna-Soar flight program and can only be obtained during flight of the full-scale glider. Performance measurements during gliding flight require vehicle velocities, accelerations and attitudes, and a measure of the atmospheric environment. Ground-tracking trajectory information will be utilized as backup for onboard data.

Aerodynamic stability and control considerations are virtually inseparable from the vehicle's flight-control and guidance systems. These areas are considered under the general heading "Flight Controls" in figure 6. The flight-controls test objectives are determination of stability derivatives and control effectiveness parameters throughout the flight corridor. Such information is essential for the flight-program buildup discussed subsequently and also is of general research interest. Also, development of an adequate flight-control system is mandatory, and full-scale flight testing is required for final development and evaluation. A description of the flight-control system envisioned for the Dyna-Soar was presented in a previous paper by Alan H. Lee and Leroy J. Mason. The automatic and redundant features of the primary flight-control system, the guidance and navigation system, and cockpit-display equipment will require development in the course of the flight-test program.

One of the basic concepts of the Dyna-Soar flight-control system is to provide for maximum pilot utilization. Also of considerable interest is the determination of desirable handling qualities of hypersonic vehicles. The information gained from the Dyna-Soar flight-test program will be directly applicable to the verification of man's role and capabilities in piloting space and reentry vehicles and in the establishment of design guidelines for hypersonic handling qualities.

The data requirements in the area of flight controls for the Dyna-Soar flight-test program will be much like those of the X-15. Basically, it is necessary to establish the flight conditions, determine the control motions, and measure the vehicle response. The analysis procedure to be used for data evaluation will take various forms. Where possible, as with the trim evaluation, analysis will be made directly from the flight records. For maneuvering or dynamic analyses, where changes in flight conditions are appreciable or glider response is altered by spurious control inputs, a data-matching procedure utilizing analog computer synthesis methods will be used. It is anticipated that the X-15 flight-research program will develop new techniques and methods in this area of stability analysis which can be utilized in the Dyna-Soar program.

In the areas of dynamics, loads, structures, and materials, the objective, and subsequent contribution, of the Dyna-Soar flight-test



program is primarily one of demonstration. The usual accelerations, noise measurements, and strains required to verify the integrity of the vehicle will be obtained. Additionally, some measure of the distortion of the external shape of the glider will be made. The structural and aerodynamic measurements, when analyzed together, will provide useful design information on aerodynamic and heating loads.

The human-factor aspects of reentry from orbital and near-orbital speeds and altitudes will continue to be of importance. Reentry flight times during Step I testing will require up to 30 minutes, wherein longitudinal decelerations of from 0.3g to 2.0g will be experienced. Physiological effects of decelerations, time, and cockpit environment on pilot operation of the glider during reentry will be studied.

Development of reliable and efficient subsystems, such as environmental control and secondary power, and demonstration of their operation in the Dyna-Soar flight environment is no less an objective than exploration of the flight corridor. Adequate monitoring sensors will be included in the instrumentation package to assure acquisition of significant subsystem operating data.

The areas of military applications and geophysical research are additional flight-test objectives. The suitability of the Dyna-Soar type vehicle for military applications will be determined during the course of exploring its flight corridor, as will its suitability as a platform for conducting geophysical experiments.

FLIGHT-TEST PROCEDURE

The flight-test procedure to be utilized in developing the Dyna-Soar I and in exploring the hypersonic flight regime has been developed to stay within cost limitations but, at the same time, maintain a high degree of confidence in extending the flight envelope. The resulting flight-test program (fig. 7) consists of manned air-launch flights covering the subsonic and supersonic flight regimes, unmanned ground-launch flights for investigation of conditions from launch to hypersonic speeds, and the main test-program objective - manned exploration of the hypersonic flight corridor.

The air-launch phase of the test program, utilizing the Boeing B-52 for air drop, will provide the first opportunity to evaluate the test article under actual flight conditions. There are several important objectives (fig. 8) which must be accomplished during this phase before the test program can proceed to the manned ground-launch tests.



The first of these objectives is systems checkout and demonstration. Some systems development, including data-acquisition systems, will be most easily accomplished during the air-launch flights. Aerodynamic and structural verification, including investigation of stability and control characteristics, will be accomplished throughout the attainable speed and lift-coefficient range. Another objective is pilot familiarization with the low-speed flight and landing characteristics of the Dyna-Soar, together with the development of optimum approach and landing techniques. The maximum velocity that can be achieved during the air-launch phase utilizing a rocket-boosted glider is uncertain. Attainment of a supersonic Mach number of about 7 is highly desirable, but, because of technical and economic factors, the maximum feasible velocity for the air-launch phase may be a Mach number of about 2.

The unmanned ground-launch test phase will be conducted on the Atlantic Missile Range, with launch from Cape Canaveral. Although there will have been approximately 40 Titan firings prior to this time, modifications for Dyna-Soar - such as the addition of first-stage stabilizing fins, structural beef-up, and any booster-subsystems changes - will require flight testing. The prime requirements of unmanned tests are demonstration of the booster-glider combination and glider separation from the booster. Some assessment of the reliability of both the first and second stages of the booster is necessary before the manned portion of the test program can be initiated, and each of the unmanned test flights will be carried through ignition and separation of the second stage. Escape system tests will also be accomplished during this phase.

The third and major phase of the flight-test program consists of a manned systematic expansion of the Dyna-Soar flight envelope, with launch at Cape Canaveral down the Atlantic Missile Range utilizing down-range islands as intermediate landing sites. Improved landing strips, 8 to 10,000 feet in length, have been specified as landing-site runway requirements. The locations of the landing sites must be compatible with the glider range and maneuverability, desired burnout velocities, and test objectives. A summary of the results of the landing-site study is shown in figure 9. The limits of injection velocity for each landing site are determined from the lift coefficient (or lift-drag ratio), angle of bank, and the permissible launch azimuths of Cape Canaveral.

The first manned ground-launch flight has been planned for an injection velocity of approximately 9,000 feet per second. Selection of this speed was dictated by economic and geographical considerations as well as the knowledge that flight environment up to speeds of approximately 7,000 feet per second will have already been investigated during the X-15 program. The landing sites which would permit the most comprehensive coverage of injection velocities from 9,000 feet per second





to approximately 19,000 feet per second are Mayaguana, Santa Lucia, and Fortaleza, Brazil.

The test-flight tracks down the Atlantic Missile Range for maximum and minimum burnout velocities with landings at Mayaguana, Santa Lucia, and Fortaleza are indicated in figure 10. It should be noted that all the possible landing sites lie at approximately 130° azimuth from Cape Canaveral, but, since a maximum launch azimuth of 110° must be observed during boost, turning flight must be performed to arrive at the high key point over each of the landing sites.

The step-by-step expansion of the hypersonic flight regime during the manned test phase will provide a reasonable degree of confidence in exploring the unknown flight regime and attainment of test results. This test phase will commence with a glider injection at an optimum lift coefficient and a velocity of approximately 9,000 feet per second. Each successive flight in the speed range above 9,000 feet per second is a moderate extension in both speed and lift coefficient over the previous flights. Data obtained from each flight will be analyzed sufficiently to reveal possible danger areas so that they may be cautiously approached or avoided during follow-on test missions.

A typical flight for the systematic exapnsion of the Dyna-Soar flight envelope is presented in figure 11. The clear area denotes that portion of the flight envelope which has previously been explored, and the grey area denotes the unexplored regions of flight. The cross-hatched areas indicate the portion of the flight envelope which will be expanded by this particular test mission. It should be noted that the vehicle injection takes place at a mid lift coefficient and that the lift coefficient is increased as velocity decreases. A similar technique will be utilized for investigation of the lower lift coefficients. Testing at any particular lift coefficient and velocity combination will be a moderate extension in speed or lift coefficient, or both, over a previous test mission. Once the flight envelope has been extended, the remainder of the flight will be devoted to both data fill-in and energy-management requirements for arrival over the landing site.

The test flight outlined in figure 11 was simulated on an analog computer, and a time history of pertinent trajectory parameters is presented in figure 12. Although the simulation was limited, in that it was only a three-degree-of-freedom point mass simulation, it does provide an insight into the times which will be available for flight testing. As can be noted, something less than 5 minutes is available for testing during the flight-envelope expansion, while the remainder of the flight will provide for data fill-in and energy management.



Extensive use of six-degree-of-freedom flight simulation is a prerequisite to all Dyna-Soar flight planning. It is also necessary that the pilot fly each proposed mission on the simulator, including the higher probability boost-abort situations. All flights will be planned to allow maximum assurance of a successful landing of the glider in case of a boost abort.

CONCLUDING REMARKS

In summary, the Dyna-Soar flight-test program will consist of three phases: (1) air-launched tests using a powered glider to checkout and demonstrate the operating characteristics of the vehicle; (2) unmanned ground-launched tests to demonstrate the integrity of the booster-glider combination; and (3) the major phase, ground-launched manned exploration of the hypersonic flight regime.

Development and verification of the Dyna-Soar design and its operational concepts and requirements will be accomplished during the flight-test program which will be conducted as a joint operation by an Air Force - NASA - contractor team. This program will provide aerodynamic data from the reentry flight corridor, will verify the design requirements of reentry vehicles, and define their operational capabilities in this flight regime. These results, which must be timely for proper military exploitation of the aerospace medium, will provide valuable contributions to other astronautical ventures.

It is readily admitted that there are many unknowns to be discovered in this program. One thing is certain, however, this will be one of the greatest testing efforts that the free world has ever known.

DYNA-SOAR I STEP I FLIGHT TEST. OBJECTIVES

EXPLORE FLIGHT REGIME
TO M ≈ 20

DEVELOP VEHICLE AND
SUB-SYSTEMS

- definition and solution of problems
- ♦ development of operational concepts
- verification of design

Figure 1

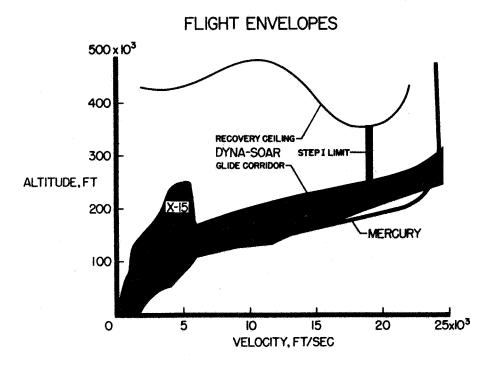


Figure 2



FLIGHT TEST DATA **OBJECTIVES**

aerodynamics control and guidance dynamics and loads structures and materials human factors vehicle subsystems

> military applications geophysics

MONITOR **CONFIRM DEVELOP** RESEARCH

Figure 3

AERODYNAMIC HEATING

FLIGHT TEST:

ANALYSIS:

$$S_{T} = \frac{h}{\rho C_{P}V} = f(R_{e}, P_{r}, T_{s}, T_{w}, M_{\infty}, \ll \cdots)$$

$$= f \begin{cases} free-stream conditions \\ local flow conditions \\ local gas properties \end{cases}$$

FLOW CHARACTERISTICS

- FREE-STREAM CONDITIONS, P_{τ} , T_{τ} , \prec , β .
- LOCAL FLOW CONDITIONS,

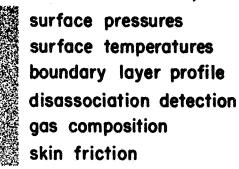


Figure 5

FLIGHT CONTROLS

7

FLIGHT TEST OBJECTIVES:

- determine stability derivatives
- develop flight control and energy management systems
- verify pilot's role and desirable handling qualities

DATA REQUIREMENTS:

- flight conditions
- control motions
- vehicle responses

Figure 6





DYNA-SOAR I FLIGHT TEST

TEST PHASE	FLIGHT REGIME COVERAGE	PRIME TEST INTERESTS
air launch manned	landing > supersonic	glider
ground launch unmanned	launch > hypersonic	booster-glider
ground launch manned	supersonic -> hypersonic	pilot-booster-glider

E.

Figure 7

AIR-LAUNCH FLIGHT TEST

sub systems checkout and demonstration aerodynamics and structural verification

pilot checkout and training landing characteristics and requirements

LANDING SITE REQUIREMENT

7

3

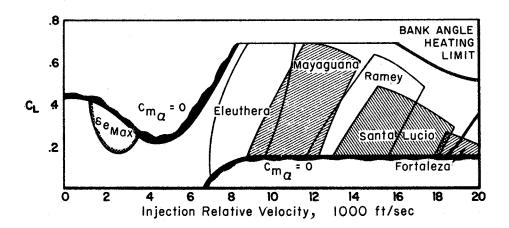


Figure 9

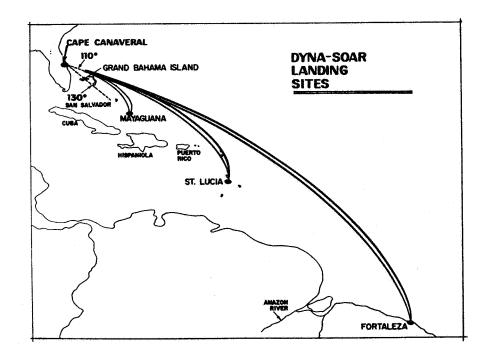


Figure 10



FLIGHT ENVELOPE EXPANSION

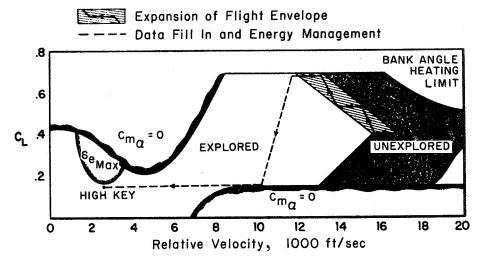


Figure 11

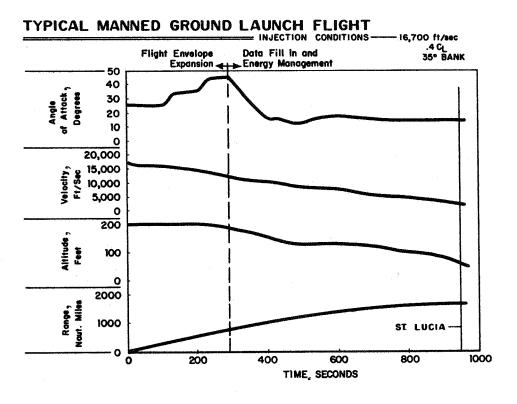


Figure 12

1



1

25

INSTRUMENTATION AND COMMUNICATIONS CONSIDERATIONS

FOR DYNA-SOAR

By Gerald M. Truszynski Flight Research Center

and Paul O. Lindfors
Air Force Flight Test Center

INTRODUCTION

The Dyna-Soar vehicle, when considered in terms of the regime of flight to be traversed and the length of test time available at extreme velocities while still within the atmosphere, becomes a research facility of unique value. Many of the flight conditions to be encountered are extremely difficult to duplicate satisfactorily in ground test facilities and, as a consequence, the vehicle itself becomes a primary means of obtaining the information required in validating hypersonic aerodynamic theory and the correctness of the vehicle design approach.

The previous paper by Harold G. Russell, B. Lyle Schofield, and Thomas F. Baker, has indicated a number of areas wherein research investigations will be conducted during flight tests of the Dyna-Soar glider. This paper discusses some of the measurements required in conducting the investigations, the possible general approaches to be taken in obtaining these measurements, and the system planned for the main data acquisition. Finally, the electromagnetic transmission problem is discussed as it directly affects the Dyna-Soar Step I tests.

DISCUSSION

Some of the measurements required to conduct the desired investigations with the Dyna-Soar vehicle and the general approach which will be taken in obtaining these measurements are shown in figures 1 and 2. Many of the measurements can be obtained by the extension of techniques presently in use, and, although a number of installation problems concerned with local internal environmental conditions in various parts of the vehicle, such as low pressure, acceleration levels, and high structural temperatures, will be encountered, it is felt that these problems



can be adequately solved during the course of development of the specific vehicle. However, some measurements - those noted in figure 2 - present difficulties mainly because of the external environmental conditions surrounding the Dyna-Soar vehicle at hypersonic velocity and extreme altitudes.

The measurement of skin and internal structural temperatures is required for verification of the structural and thermal design approaches and to obtain heat-transfer data for the vehicle. Thermocouple materials capable of withstanding a temperature environment of the order of 3,500° F are available which will be sufficient for all but a few of the very forward locations on the vehicle. These materials consist of iridium-rhodium sensing wire and utilize magnesium oxide and beryllium oxide insulating material, all enclosed in a metal sheath capable of withstanding the local temperature environments. Platinum sheathing will be required at the higher temperature locations. Thermocouples utilizing these materials have, with a proper preconditioning procedure, provided temperature measurements to 3,500° F and have maintained calibration through repeated exposures to these temperatures. For temperatures above 3,500° F and as a means of rapidly viewing broad structural areas, the adaptation of infrared detection methods to the measurement of temperature appears feasible and will be investigated for specific application to the Dyna-Soar vehicle.

L

1

2

9

The area of measurement encompassing static structural strains on the Dyna-Soar vehicle is one which presents formidable temperature problems, particularly if these measurements are to be made during the entire flight regime. Weldable-type strain gages are available which allow static strain measurements to the order of 800° F. However, even in this temperature range, careful consideration must be given to the problem of compensation of the gage outputs for the effects of thermal expansion of the airframe if reasonable accuracy is to be obtained. Studies indicate that temperature levels above 1,000° F will exist during portions of the flight trajectory on structural members where strain measurements would be desirable. The outlook for static strain measurements above 800° F is pessimistic unless suitable developments can be realized in the near future. Dynamic strain measurements appear to be feasible to the order of $1,500^{\circ}$ F for short time durations.

The measurement of angles of attack and sideslip is a very important requirement, both for proper control of the vehicle in the flight corridor and for interpretation of the flight data. These quantities can be derived from the stable platform and associated computer to be installed in the vehicle to perform the energy management and navigation function. However, an aerodynamic means of measurement is felt to be extremely important, both as the primary approach to assure measurement of this basic parameter and as a means of evaluating the platform's capability during the buildup flights. On the X-15 research airplane, this



*

measurement is obtained through the use of a null-seeking servo nose sphere. Figure 3 illustrates this particular device, which is constructed of Inconel and incorporates internal liquid nitrogen cooling. The device has satisfactorily undergone thermal shock tests to a stagnation temperature of 3,400° F and an impact pressure of 2,000 pounds per square foot. Investigations indicate that flow problems would not limit the use of this approach to the measurement of flow angles at hypersonic velocity and that sufficient sensitivity of the differential pressure obtained is maintained through the operational altitude and velocity range of the Dyna-Soar vehicle. The primary problem of extending this technique to higher velocities is, of course, that of maintaining structural integrity at the elevated temperatures which will be encountered. It appears that a suitable design, utilizing a ceramic nose-cap material such as beryllium oxide or alumina and cooled through the use of expendable coolant, may be possible for the Dyna-Soar vehicle even at the extreme flight conditions. In any event, the use of a servo nose sphere is desirable through as high a velocity range as possible during the buildup flights.

Surface pressure distribution will be measured by utilizing two types of transducers; this procedure was necessitated by the extreme variation of the range of pressure encountered during the altitude excursions of the Dyna-Soar. The range, limitations, and problem areas for these measurements are shown in the following table:

Approach	Range, mm Hg.	Limitations	Problem areas
Standard transducer	10 to 20	Low range	Temperature environment
Heat conducting transducer			Temperature environment, outgassing, pressure equilibrium

Standard transducers can be utilized down to the order of 10 to 20 millimeters of mercury full scale. Below this pressure range and down to the order of 10⁻³ millimeters of mercury full scale, which corresponds to the static-pressure level at 260,000 feet, a heat-conducting transducer can be utilized. This type has been constructed in thermocouple, thermistor, and wire-resistance, or Pirani configurations. Figure 4 illustrates a small Pirani gage which has been used by the National Aeronautics and Space Administration for low-range pressure measurements in hypersonic tunnels and are adaptable to flight use. The internal volume of this instrument is extremely small and internal



lag is of the order of 0.25 second at pressure levels of 2 millimeters of mercury. The structural temperature levels to be encountered on the vehicle will require the installation of pressure transducers in a protected environment and the use of tubing leading from the measurement orifice to the transducer; under these conditions, lag will be experienced. Representative values for these lag factors in a typical Dyna-Soar installation are about 5 seconds at pressure levels of 0.1 millimeter of mercury and about 7 seconds at pressure levels of 0.01 millimeter of mercury. These lag values are not considered to be unduly restrictive in terms of the investigations contemplated.

The use of heat-conducting, extremely low-range pressure transducers, however, presents some specialized problems. Their principle of operation requires a knowledge of the specific heat of the gas of which the pressure is being measured; hence, if large variations in the real-gas properties are experienced, the calibration will be affected. Also, at pressure levels where the mean free path becomes of the order of the size of the measuring apparatus, pressure equilibrium is not established and temperature measurements of the environment at the orifice and transducer locations must be made so that proper corrections can be applied. Finally, outgassing problems at extremely low-pressure levels will require a critical monitoring of all materials used in the pressure-measurement subsystem.

 \mathbf{L}

1

1

2

9

3

The measurement of shock-layer ionization levels is extremely desirable in order to correlate the analytical investigations of the problem of electromagnetic transmission through an ionized layer. Flush-mounted ionization probes can probably be installed to provide some information on the ionization level directly at the aircraft surface. Experimental determination of the degree of ionization within this layer is a more desirable measurement, but the problem of design of a probe which will withstand near-stagnation temperature and also minimize the effect of the probe itself on the desired measurement remains to be The Dyna-Soar vehicle does, however, provide a good means for the investigation of the overall effects of the ionized shock layer on the various communication systems in terms of total attenuation, noise, antenna breakdown and mismatch, and signal distortion and refraction. Multifrequency transmitting and receiving equipment properly instrumented for measurements of these effects will be installed to perform research tests in this specific area of interest.

The range of flight latitudes traversed by the Dyna-Soar vehicle and the duration of flight at extreme altitudes while still within the atmosphere make it a valuable means of obtaining a variety of geophysical measurements such as atmospheric density, composition, and lower ionospheric properties. Equipment is under development by the Air Force Cambridge Research Center (AFCRC) to obtain these measurements and will be integrated in the Dyna-Soar vehicle as part of the overall research program.



The number of areas of developmental and research interest to be investigated with the Dyna-Soar vehicle, coupled with the relatively small number of flights contemplated, demands a maximum return of recorded data for each flight. For the program presently planned, the instrumentation system must be capable of recording on the order of 800 individual channels of information. Most of the parameters to be recorded are quasi-static in nature, although a requirement exists for a small number of high-frequency information channels for specialized purposes.

It is planned to use a dual data-acquisition system in the Dyna-Soar vehicle: a pulse code modulation (PCM) system as the main high-capacity data system, and a frequency modulation (FM-FM) system to provide the required high-frequency capability. (See fig. 5.) Both systems will record on a single onboard magnetic tape which will be the primary recording medium. All information will also be telemetered to the ground to provide for real-time monitoring of certain critical vehicle and pilot reaction quantities and for data assurance in the event of loss of the vehicle during the boost or recovery phases of the flight.

Since much of the data to be acquired on Dyna-Soar flights will be utilized for research purposes, the accuracy provided by the instrumentation system is of importance. The pulse code modulation system, by analog-to-digital conversion of all data at their source, provides higher data-acquisition accuracy by eliminating many intermediate modulation-demodulation links found in other conventional tape systems. In addition, the digital form of the data minimizes degradation during the subsequent processing cycle. In order to satisfy the multitude of data requirements, the instrumentation system must be flexible and easily modified to meet specific requirements on each flight. The PCM system will be designed with versatility as one of the prime criteria to allow for rapid and relatively simple expansion or contraction of the number of parameters sampled and the sampling rates, or both.

The problem of electromagnetic transmission through the ionized shock layer surrounding the Dyna-Soar vehicle affects three primary functions: (1) voice communications to and from the vehicle, (2) transmission of research and operational information from the vehicle to the ground through the telemetry system, and (3) tracking the vehicle with precision ground radar equipment utilizing a beacon transponder. Although the vehicle itself provides the best means of performing detailed investigations of the problem over broad frequency ranges, the immediate problem for the Dyna-Soar is the determination of the frequencies of transmission which will allow satisfactory conduct of the Step I tests in light of these three functions. In terms of program cost, it would be desirable to utilize, where possible, equipment and systems which are already installed or programed for the Atlantic Missile Range where the Step I tests will be conducted. At present, voice communications and telemetry functions are generally conducted



in the UHF band (225 to 260 megacycles), whereas instrumentation radar tracking equipment operates on the S and C bands, at approximately 3,000 and 5,500 megacycles, respectively. It is desirable to examine the specific Dyna-Soar Step I flight program to determine where transmission difficulty in these frequency bands will occur and whether, from an operational standpoint, these "blackout" areas are tolerable. Figure 6 illustrates a Dyna-Soar trajectory in which the most severe conditions, from an ionization standpoint, at a rearward antenna location will occur. These conditions are for a vehicle with a wing loading of 27 pounds per square foot. Indicated on the trajectory are the calculated areas of blackout which are expected to occur on the UHF, S, and C bands. As noted, a very small gap appears on the C band and a large area of blackout on the UHF bands. Operationally, it is believed that it is extremely important to maintain continuous radar tracking over the entire trajectory, and this capability appears to be feasible with the existing C band equipment. Since all data are being recorded onboard, a telemetry gap of the extent indicated may possibly be tolerated, depending on the final requirement for real-time monitoring; however, a voice-communication blackout of this same extent is not acceptable and communications equipment operating in at least the C band is indicated. It is planned to obtain verification of these analytical results through the use of free-flight rocket-model tests to be conducted by the NASA Langley Research Center. These tests are required to provide the necessary level of confidence to proceed with the procurement of equipment for the Dyna-Soar Step I tests.

L

1

1

2

à

CONCLUDING REMARKS

In summary, it is felt that most of the measurements required for the developmental and research investigations contemplated with the Dyna-Soar vehicle can be accomplished. Specific installation problems will require continuing development of wire and insulating materials capable of withstanding higher temperature environments. A strong development effort is also required to obtain strain-measuring devices suitable for use at higher temperatures. Effort toward the practical adaptation of present infrared-sensing techniques to the measurement of high-level structural temperatures is necessary. Finally, research must continue into practical methods of obtaining in-flight measurements of ionization and dissociation levels necessary for a better understanding of the shock-layer phenomena to be encountered on this and subsequent hypervelocity vehicles.





- 1. Altitude, velocity, attitude.
- 2. Accelerations, angular velocity, control positions, forces, moments.
- 3. Vibration
- 4. Structural deformation.

APPROACH

Stable platform.

Standard transducer methods.

Strain gages and Accelerometers.

Cameras.

Figure 1

MEASUREMENT

- 1. Temperature,
- 2. Structural strain.
- 3. Angle of attack, Angle of sideslip.
- 4. Surface pressure.
- 5. Electromagnetic transmission phenomena.

APPROACH

Thermocouples, Infra-red.

Strain gages.

Stable platform, Nose sphere.

Specialized transducers.

Total attenuation, noise, antenna effects, refraction.

Figure 2



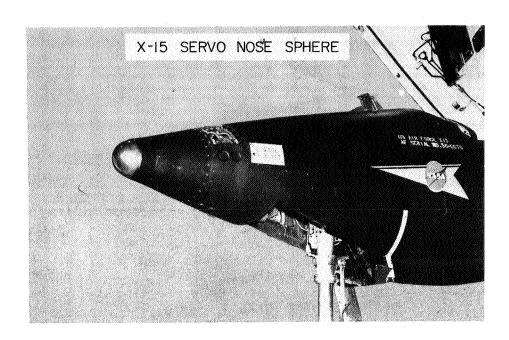


Figure 3

PIRANI PRESSURE TRANSDUCER

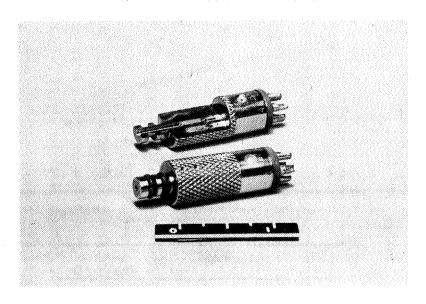


Figure 4



DATA ACQUISITION SYSTEM

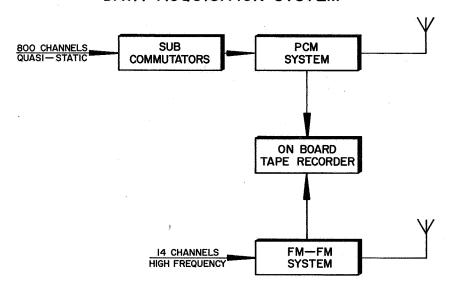


Figure 5

TRANSMISSION BLACKOUT AREAS

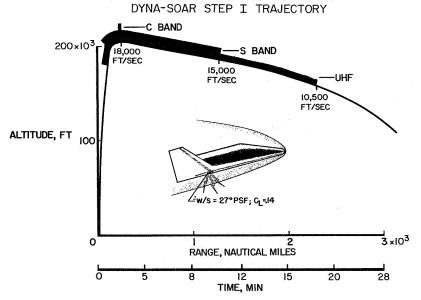
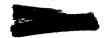


Figure 6

3



Page intentionally left blank



THE EFFECT OF REAL-AIR PROPERTIES UPON AERODYNAMIC FORCES,

MOMENTS, AND HEAT-TRANSFER RATES FOR REENTRY VEHICLES

By Nathaniel B. Cohen, Ivan E. Beckwith, and Robert L. Trimpi Langley Research Center

SUMMARY

The effects of the dependence of inviscid flow forces and moments and of aerodynamic heat-transfer rates upon the properties of real air in chemical equilibrium are investigated. It is concluded that equilibrium real-gas effects in general are small except for inviscid forces and moments on some unswept two-dimensional shapes having discontinuities in surface slope and at small angles of attack, and for swept flat plates near the shock detachment angle. Thus, for highly swept configurations at relatively high angles of attack, perfect-gas tests used in conjunction with those analytic studies which are possible should provide useful design data for flight conditions where equilibrium real-gas behavior is expected.

INTRODUCTION

When flight velocities of aircraft and missiles remained below about 3,000 to 4,000 ft/sec in the atmosphere it was permissible to determine aerodynamic and thermodynamic performance by assuming that the air was a perfect gas with constant specific heats. The attainment of considerably higher velocities in the last decade requires the more correct treatment of air as a real gas. The complex chemistry involved in the dissociation and recombination reactions makes simulation of the hypersonic environment more difficult than the low-speed environment, and though shock tubes, shock tunnels, and ballistic ranges have provided much useful data, analytic studies and flight tests must be relied upon to provide much of the necessary information for the determination of real-gas effects at this time. The purpose of the present report is to examine and illustrate the real-gas effects on the inviscid flow forces and moments and upon the aerodynamic heat-transfer rates for some simple shapes in a continuum flow of air in chemical equilibrium. Some comments regarding nonequilibrium flows are included.

The large body of experimental data on the Mark II and III nose cones and the numerical solutions of Gravalos were made available through the



26

courtesy of the General Electric Missile and Space Vehicle Department.

SYMBOLS

A	constant		
$c_{ m D}$	drag coefficient		
$\mathtt{c}_\mathtt{L}$	lift coefficient		
C _m	pitching-moment coefficient		
Ср	pressure coefficient		
D	drag		
H	total enthalpy		
h	static enthalpy		
$h_{\overline{D}}$	enthalpy in dissociation		
L	lift		
M	Mach number		
m	constant		
N_{Le}	Lewis number		
N _{Nu}	Nusselt number		
N_{Pr}	Prandtl number		
N_{Re}	Reynolds number		
N _{St}	Stanton number		
р	pressure		
α.	hest transfer rate		



*	,	R	nose radius		
		$R_{\mathbf{b}}$	base radius		
r r			enthalpy recovery factor		
		T	temperature		
,		t	thickness		
L 1 0 5		u	velocity in x-direction		
		v	velocity in y-direction		
0)	x	surface coordinate in direction of inviscid flow (chordwise coordinate for yawed infinite cylinder)		
*		У	spanwise surface coordinate for yawed infinite cylinder		
		α	angle of attack		
準	ķ	γ	ratio of specific heats or polytropic exponent		
		γ_{e}	effective specific-heat ratio		
		Λ	sweep or yaw angle		
		μ	viscosity		
		Ę	axial length		
		ρ	density		
		σ	hemisphere angular coordinate, x/R		
		Subscript	5 s:		
		aw	adiabatic wall		
		е	local external to boundary layer		
		XAM	maximum value		
à	•	s	stagnation point or line		





v local wall

free stream

INVISCID FLOW OF EQUILIBRIUM AIR

Inviscid flow will be discussed first. Equilibrium thermodynamic properties of air have been extensively and accurately calculated to temperatures of about 15,000° K. (See refs. 1 to 5.) With the aid of these results, the inviscid flow forces and moments for a body in an equilibrium real-air flow can be predicted with considerable confidence if the corresponding perfect-gas case is amenable to calculation. However, even the perfect-gas theoretical calculations are limited to comparatively simple shapes at present. Typical of these shapes is the blunt body of revolution, investigated thoroughly in connection with the development of heat-sink types of ballistic missiles.

L

1

0 5 0

3

Blunt-Body Pressure Distributions

As yet, no analytic solutions of the subsonic flow field between the body and the shock have been achieved, but a number of numerical procedures for computing the subsonic and transonic portions of this flow have been derived. These fall into two categories; namely, direct, in which the body shape is given and the shock shape and flow are computed (e.g., refs. 6 and 7), and inverse, in which the shock shape is assumed, and the flow field and body shape are computed (e.g., refs. 8 and 9). Any downstream supersonic flow is computed by the method of characteristics.

The simplest blunt shape, one extensively tested, is the hemisphere. A comparison of experimental pressure-distribution data with predicted distributions is shown for the perfect-gas case in figure 1(a) at Mach numbers near 5. The data were obtained from references 10 to 14, at Mach numbers of 4.15 to 6.80. Predictions shown are the modified Newtonian-Prandtl-Meyer distribution and three of the numerical procedures; namely, those of Gravalos, Edelfelt, and Emmons, $M_{\infty} = 5.0$ (ref. 6), Belotserkovskii, $M_{\infty} = 5.8$ (ref. 7) and Van Dyke, $M_{\infty} = 5.8$ (ref. 8). The three numerical solutions are indistinguishable from one another on this figure and fall slightly lower than the Newtonian-Prandtl-Meyer approximation. Agreement between theory and data is very good, and the modified Newtonian-Prandtl-Meyer distribution appears to be a useful, relatively simple approximation for this shape.



1



To investigate some of the real-gas effects, the predicted distribution of pressure coefficient over a hemisphere for atmospheric flight at a Mach number of 15 is shown in figure 1(b). The perfect-gas numerical solution up to $x/R\approx 1$ was obtained from the distribution on the blunt portion of a spherically blunted 30° half-angle cone given in reference 6. The remainder of the curve, to $\frac{x}{R}=\frac{\pi}{2}$, was estimated on the basis of other high Mach number perfect-gas solutions. The real-gas curve for $M_{\infty}=15$ at an altitude of 100,000 feet was computed by the Gravalos method. At this Mach number the predicted real- and perfectair pressure-coefficient distributions are only slightly different. However, the normalizing real- and perfect-air values of $C_{p,MAX}$, tabulated in the figure, differ by about 3 percent, and this difference is felt in the drag coefficients, which differ by about 2 percent.

Shown also in figure 1(b) are data at $M_{\infty}=12$ from X-17 flights R-22 and R-26 (refs. 15 and 16, respectively). These data are compared with the modified Newtonian-Prandtl-Meyer prediction with $M_{\infty}=12$ and $\gamma=1.195$, approximating a real-air distribution (this value of γ is the stagnation-point polytropic exponent for this flight condition). The limited amount of data and this prediction are in good agreement.

The G. E. Mark II nose cone represents another blunt shape on which extensive flight tests have been carried out. This shape has a nearly spherical nose with a conical skirt of $51\frac{1}{2}^{0}$ half-angle. Shown in figure 2 are experimental data for Mach numbers from 11.1 to 16.7 at altitudes of from 74,000 to 102,000 feet, plotted as $C_p/C_{p,MAX}$ against x/R_b . Real-air predictions by Gravalos' method at $M_{\infty}=14.6$ and 270,000 feet and at $M_{\infty}=10.5$ and about 90,000 feet are shown along with the perfect-gas prediction for $M_{\infty}=15$. The experimental data tend to follow the trend of the theoretical predictions but are somewhat lower. The perfect- and real-air predictions at comparable Mach numbers (15 and 14.6, respectively) indicate a significant real-gas effect on the skirt. Elsewhere, predicted real-gas effects on the pressure-coefficient distribution are small.

Downstream Pressures on Blunt Bodies

The requirement for vehicles with better performance than that given by the blunt heat sink led to the second-generation ICBM's, which are relatively slender blunted bodies. To illustrate the real-gas effects upon pressure distribution downstream of the nose regions, figure 3 shows the distribution of $C_{\rm p}/C_{\rm p,MAX}$ plotted against axial length



for the G. E. Mark III at a Mach number of 20. This missile consists of a spherically blunted 24° half-angle cone followed by an almost cylindrical section (1° converging cone) and a biconic flare. Shown are real-air predictions of Gravalos at 200,000 and 60,430 feet of altitude, the perfect-gas distribution (computed only through the first flare shock), and experimental data at $M_{\infty}=20$ and an altitude of 62,000 feet. The data, obtained during violent pitching oscillations, generally bracket the prediction.

On the spherical nose the real-gas effects are small, just as on the hemisphere shown earlier, but less noticeable because the abscissa is now axial length rather than surface distance. Downstream, there are more pronounced differences between the distributions, of the order of 20 percent on the main body and 40 percent on the flare. The main difference in pressures, between the real air at 200,000 feet and the real air at 60,000 feet as well as between the real air and perfect air, appears to occur after abrupt body-surface deflections, which on the three-dimensional body surface are still locally two-dimensional Prandtl-Meyer or oblique shock flows. Reflection of waves back onto the body causes a significant part of the pressure differences to disappear.

L

1

0

5

0

Inviscid Forces and Moments on Reentry Vehicles

Lifting reentry vehicles fall generally into two categories, winged vehicles and lifting bodies. Because the inviscid flow fields about these configurations at angles of attack are difficult to compute accurately, simple flows will again be used for illustrative purposes.

The forces and moments on a winged vehicle at positive angles of attack arise mainly from the pressure field on the lower surface. Shown in figure 4 is the ratio of perfect-air to real-air pressure on a swept flat plate plotted against angle of attack up to the perfect-air detachment angle and simulating part of a swept wing at $M_{\infty} = 20$ and an altitude of 200,000 feet. It is evident that real-gas effects are small at small angles of attack, increasing to the order of 20 percent near the perfect-air detachment angles for each sweep. Beyond the detachment angles the pressures cannot be accurately calculated, but measurements indicate that beyond the detachment angles the surface pressures monotonically approach the modified Newtonian predictions. Thus, the ratio would be expected to decrease beyond detachment for each PPERFECT/PREAL value of sweep, reaching the perfect- to real-air stagnation-pressure ratio at an angle of attack of 90° for all sweeps. For the flight conditions of figure 4, this value is 0.95 (shown at the right margin).

The aerodynamic characteristics of a blunted half-cone typify those of a lifting-body configuration. Shown in figure 5 are the characteristics of a spherically blunted 30° half-cone with a bluntness ratio

 R/R_b of 0.3 at $M_\infty = 15$ and an altitude of 85,000 feet. The pressure distributions, shown plotted as p/ps against dimensionless axial length, were obtained for the complete cone at zero angle of attack by Gravalos (ref. 6), and were assumed to apply to the lower half of this half-cone. The real- and perfect-air curves at a Mach number of 15 may be seen to be little different. With free-stream pressure assumed to be acting on the top surface and with zero base pressure, the aerodynamic characteristics were computed from the pressure distributions with the top surface alined with the stream $(\alpha = 0)$. The results are tabulated in figure 5, from which it is seen that the real-gas effects are generally about 1 percent. Shown also are nose (modified Newtonian-Prandtl-Meyer) and sharp-cone pressures for the same configuration at $M_{\infty} = 20$ and 200,000 feet of altitude. Though the performance coefficients were not computed because the pressure distribution is incomplete, the pressures shown indicate real-gas effects of the same order as those shown at $M_{\infty} = 15$.

L

1

つ う

> The real-gas effect on pressure distribution was shown earlier (in connection with the Mark III vehicle, fig. 3) to be larger just behind abrupt body-surface deflections than farther downstream. The resulting effect upon forces and moments at angles of attack cannot be computed accurately for such a body of revolution, but in order to investigate this phenomenon, a computation was performed for a similar two-dimensional body for which the results would be expected to show real-gas effects qualitatively like, but much larger than, those experienced by an axisymmetric body. The configuration, shown in figure 6(a), has a wedge nose with a 300 half-angle, a slab 10 thicknesses in length, and a terminal 20° flare 5/4 of the thickness in length. The pressure distributions for $M_{\infty} = 20$ and a 200,000-foot altitude were computed by the method of characteristics for angles of attack up to the detachment angles of the nose shock for helium, perfect air, and real air. The real-air distribution was approximated by that for a perfect gas with an effective specific-heat ratio γ_e defined so that the Rankine-Hugoniot equations across the strongest shock wave in the flow field yielded the correct (real air) pressure and density. This procedure also requires use of an effective Mach number equal to $\sqrt{\frac{\gamma_{\infty}}{\gamma_{c}}} M_{\infty}$.

Also shown in figure 6(a) are the pressure distributions p/p_{∞} plotted against ξ/t for zero angle of attack. Flare pressures were assumed to be constant at their initial values. Note the large differences in pressures just rearward of the shoulder and persisting until the first waves are reflected from the shock back to the body. Farther downstream, pressure differences between the various gases decrease, as shown in figure 3 for the Mark III body of revolution.

An example of the results obtained is shown in figure 6(b), a plot of pitching-moment coefficient (based upon overall length) against angle of attack. For the range of angle of attack shown, the configuration exhibits a positive pitching moment in all three gases; the largest values at given α are for helium up to 5° , and the smallest values are for real air. Significant real-gas effects on C_m are apparent for $5^{\circ} \le \alpha \le 15^{\circ}$. However, at very large angles of attack the real-gas effect should be rather small, since Newtonian pressures should be applicable. These differ for the gases only by the stagnation-pressure ratio, about a 5-percent difference between real and perfect air in this case. Flight data on the Mark III with a single-element flare showed a pitching-moment coefficient at small angles of attack qualitatively like that in figure 6(b) for real air.

Shown also in figure 6(b) is a table of static margin $\left(dC_m/dC_L\right)_{\alpha=0}$, as a fraction of body length, for the three cases. The shift in static margin from real air to perfect air is one-half of 1 percent of the body length.

L

1

0

50

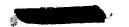
4

It is important to note that the moment is highly dependent upon the flare location and geometry. (See fig. 6(a).) For example, if the flare of the configuration investigated were placed where the real-gas pressure was a maximum, $\xi/t\approx 7$, the flare effectiveness near $\alpha=0$ would be little changed from the original location for the real air but much enhanced for the perfect-air and helium cases, changing the curve of C_m against α significantly.

To summarize for the inviscid flow of equilibrium air, the difference between real- and perfect-air pressure distributions and drag is at most a few percent in blunt-body nose regions, though downstream pressures on relatively slender blunted bodies may differ considerably. Because lift and moments depend on pressure differences, caution must be exercised in the interpretation of perfect-gas tests as applying to the real-gas conditions, especially for bodies having abrupt changes in surface slope and at small angles of attack. For blunt bodies of continuous slope real-gas effects are greatly reduced. Also, since sweep reduces the maximum flow-field temperatures and consequently the degree of gaseous imperfection, real-gas effects would be expected to be small for highly swept wings except at angles of attack near detachment of the wing shock.

AERODYNAMIC HEAT TRANSFER FOR EQUILIBRIUM AIR

Whereas the inviscid flow of equilibrium real air is a function of the well-tabulated thermodynamic properties and may be calculated with



*

some certainty, the viscous flow depends also upon the transport properties (viscosity, thermal conductivity, etc.) for which only approximations are available (e.g., refs., 17 to 19). These estimates differ, for example, by as much as 50 percent in viscosity for fully dissociated air. An important question to be considered, then, is how much are heat-transfer predictions affected by these different estimates? These predictions are limited to simple shapes where the differential equations are applicable. Because of the highly empirical nature of transitionand turbulent-flow analyses even for the perfect gas, the present discussion is limited to laminar flow.

Stagnation Flows

The stagnation boundary layers for a body of revolution and for a yawed infinite cylinder are members of the class for which exact solutions of the boundary-layer equations are possible. Correlations for the heat-transfer parameter have generally been found to be of the form

$$\left(\frac{N_{\text{Nu,w}}}{\left(N_{\text{Pr,w}}\right)^{\text{O.4}}\sqrt{N_{\text{Re,w}}}}\right)_{\text{S}} = A\left(\frac{\rho_{\text{e}}\mu_{\text{e}}}{\rho_{\text{w}}\mu_{\text{w}}}\right)_{\text{S}}^{\text{m}} \tag{1}$$

independent of the stagnation temperature or enthalpy level. The constants A and m depend upon the fluid properties used in solving the boundary-layer equations and the type of flow, and are listed in tables I and II for the axisymmetric stagnation point and yawed infinite cylinder, respectively. It is noteworthy that the small amount of variation in A and m shown in the tables represents solutions with fluid properties ranging from constant (incompressible fluid) to those for dissociated air computed by the present authors with the transport properties of Hansen (ref. 17). Thus the boundary-layer dimensionless parameters are hardly affected by real-gas properties.

From the definitions of the Nusselt and Reynolds numbers, the aerodynamic heat-transfer rate, using equation (1), is

$$-q_{w,s} = A(N_{Pr,w})_s^{-.6} \left(h_{aw} - h_w\right)_s \left(\rho_e \mu_e\right)_s^m \left(\rho_w \mu_w\right)_s^{\frac{1}{2}-m} \sqrt{\frac{du_e}{dx}}_s$$
 (2)



where for the axisymmetric case,

$$h_{aw} = H_e \tag{3a}$$

and for the yawed infinite cylinder,

$$h_{aw} = H_e - (1 - r) \frac{v_e^2}{2}$$
 (3b)

and where r is the enthalpy recovery factor. Although the constants A and m are little influenced by gas properties, as shown in tables I and II, the absolute heat-transfer rate, on the other hand, may be very much influenced by the gas properties, as can be seen from equation (2). The most important factors influencing the heat-transfer rate are the stagnation-point or stagnation-line density and viscosity outside the boundary layer, $\rho_{\text{e,s}}$ and $\mu_{\text{e,s}}$, respectively. For a known real-air inviscid flow (known $\rho_{\text{e,s}}$) the uncertainty in viscosity $\mu_{\text{e,s}}$ creates the major uncertainty in heat-transfer rate. As pointed out earlier, the viscosity for fully dissociated air may be uncertain by as much as 50 percent, but because the exponent m is near 1/2, the uncertainty in heat-transfer rate is at most about 25 percent for fully dissociated air, and even considerably less for only partial dissociation.

Up to this point, the discussion has used the assumption of unit Lewis number. For dissociating air with a constant Lewis number not equal to unity, Fay and Riddell (ref. 20) predict an effect of Lewis number given by

$$\frac{\left(N_{\text{Nu,w}}/\sqrt{N_{\text{Re,w}}}\right)_{\text{s,NLe}}}{\left(N_{\text{Nu,w}}/\sqrt{N_{\text{Re,w}}}\right)_{\text{s,NLe}} = 1 + \left(N_{\text{Le}}^{\text{0.52}} - 1\right)\left(\frac{h_{\text{D}}}{h_{\text{e}}}\right)_{\text{s}}$$
(4)

which, for $N_{\rm Le}=1.4$, ranges from 1 for no dissociation to about 1.15 for fully dissociated air. The more recent solutions of the present authors using Hansen's transport properties (ref. 17), including variable Lewis number, give a correction factor of

$$0.98 \leq \frac{\left(N_{\text{Nu}, w} / \sqrt{N_{\text{Re}, w}}\right)_{\text{s,NLe}}}{\left(N_{\text{Nu}, w} / \sqrt{N_{\text{Re}, w}}\right)_{\text{s,NLe}=1}} \leq 1.05$$
(5)

which is considered here a negligible correction.



Experimental data exist on a variety of axisymmetric nose shapes at hypersonic speeds during reentry flight tests. Shown in figure 7 are results for two shapes; the hemisphere (X-17 flights) with data obtained from references 15, 16, 21, 22, 23, and 24, and the G. E. Mark II nose cone (Atlas flights). Plotted is the ratio of experimental to theoretical real-air heat-transfer rates against flight velocity. The reference theory is that of the present authors for real air (A = 0.767, M = 0.45), but uses the more recent viscosity prediction of Bauer and Zlotnick (ref. 18) for the absolute viscosity in equation (2).

L

1

Ö

0

The X-17 hemisphere data scatter about the theoretical value (1.0) from 0.7 to 1.4 and the three Mark II points (three different flights, each data point at the peak heating value) scatter from 0.8 to 1.2. Shown also is a curve representing the predicted values obtained by using Fay and Riddell's correlations (A = 0.76, $\,m=0.4$) with the Sutherland viscosity and unit Lewis number. This prediction appears low by 10 to 20 percent, but this is mainly caused by use of the Sutherland viscosity law in computing $\mu_{\text{e,s}}$ from equation (2). A correction for Lewis number effects (eq. (5)) with $N_{\text{Le}}=1.4$, used in conjunction with the Sutherland viscosity, would bring Fay and Riddell's prediction into essential agreement with the authors'. Use of Hansen's or Bauer and Zlotnick's viscosity law for $\mu_{\text{e,s}}$ in conjunction with $N_{\text{Le}}=1$ and Fay and Riddell's solution would also yield very good agreement, as evidenced by the small differences in A and m.

Flat-Plate Flow

Another exact similar solution for the laminar flow of equilibrium air exists for flat-plate boundary layers. Shown in figure 8(a) are correlations of a few of the solutions obtained by the authors with Hansen's transport property approximations for real air. Plotted here are curves of the heat-transfer parameter $N_{\rm St}/N_{\rm Re}$ against the ratio of local external $\rho\mu$ to the local wall $\rho\mu$. The parameter is the ratio of the static enthalpy to total enthalpy outside the boundary layer; the corresponding perfect-gas (γ = 1.4) external Mach numbers are also shown. As for the stagnation flow, these correlations are independent of the enthalpy level of the external flow. Plotted in the figure are some corresponding perfect-gas values (taken from Van Driest, ref. 25, and adjusted to $N_{\rm Pr}$ = 0.7), and it is seen that the real-gas effect on this parameter is at most 5 to 10 percent. As in the stagnation case, however, the absolute heat-transfer rates can be influenced by the real-gas transport properties even though the dimensionless parameters are little affected.

In the absence of flat-plate data obtained during hypersonic atmospheric flight, shock-tube data obtained on a 10° wedge by Jones (ref. 26)





are shown in figure 8(b) compared with real-air theory. Plotted is the ratio of experimental to theoretical real-air heat-transfer rate against equivalent flight velocity for the same stagnation enthalpy as in the shock-tube test. The data tend to scatter about the theory within ±20 percent. For comparison, incompressible theory (based upon real-air inviscid shock-tube conditions) is also shown and is about 10 percent lower than real-gas theory.

Laminar Heat-Transfer Distribution

The laminar heat-transfer distribution (the ratio q_w/q_w ,s) has been shown by Lees (ref. 27) to be a function only of the inviscid flow for moderately curved bodies with highly cooled walls. Typical results with Lees' method are displayed in figures 9(a) and 9(b). In figure 9(a) are shown data and theories for a hemisphere at a Mach number of 12 plotted as the ratio q_w/q_w ,s against x/R. The predicted real-gas effect is small, as expected, because the pressure distributions are so little different. The data, obtained from X-17 flight tests, scatter about both theories.

In figure 9(b) is plotted a similar figure for the G. E. Mark II nose cone. The perfect-air and real-air theoretical curves, plotted as $q_{\rm w}/q_{\rm w,s}$ against ${\rm x/R_b}$, were computed by using Lees' method and theoretical pressure distributions shown in figure 2. Again, a small real-gas effect may be noted. The experimental data were obtained from Atlas firings and tend to scatter about the theories.

Thus, the laminar stagnation and flat-plate heat-transfer parameters, and the laminar heat-transfer distribution (ratio), are essentially unaffected by real-air properties. The heat-transfer rates themselves show a real-gas effect primarily through their dependence upon the local inviscid flow and transport properties, but are generally predictable within the scatter of experimental data.

NONEQUILIBRIUM EFFECTS

The theory of finite-rate processes is in its infancy at the present time and various estimates of the reaction-rate parameters differ by orders of magnitude. Some estimates of characteristic relaxation lengths have been made; for example, the dissociation and vibration relaxation lengths are sufficiently short for chemical equilibrium to be assumed for flow behind normal shocks with $\rm M_{\infty}>15$ below 250,000 feet of altitude if the characteristic flow length is 1 foot (ref. 28). On





the other hand, for an oblique shock with a flow deflection angle of 25° at $M_{\infty}=22$, nonequilibrium effects may enter above about 150,000 feet of altitude (ref. 28). In any event, finite-rate pressures immediately behind all portions of the primary shock wave should be roughly between the extremes predicted by perfect (frozen) and equilibrium real-air computations (seen previously to be at most of the order of 20 percent). Surface pressures close to the stagnation point will also be within the perfect and equilibrium real-air pressures, that is, within relatively narrow limits (around 5 percent).

Less can be said regarding downstream effects of finite relaxation rates. It is clear that in regions of rapid expansion, such as near the vertex of a Prandtl-Meyer expansion fan, nonequilibrium rates may cause relatively large local pressure disturbances, but the effects upon body forces and moments cannot be estimated. Separation and reattachment might be strongly affected by finite rates, as illustrated qualitatively in figure 10. Shown is the corner region of a typical ballistic capsule. Separation was assumed to occur at the rearward corner, and the flow was then assumed to expand to a given pressure (corresponding to flight measurements) for perfect air, and for frozen and equilibrium real air. The initial slope of the separation streamline shown in the figure, and hence flow reattachment on the afterbody, is seen to depend strongly upon the assumed reaction rates. Corners and afterbodies of this type occur on the G. E. Mark II and Mercury capsules. It is interesting that no reattachment was observed during Mark II flights, although an equilibrium expansion around the corners to the measured afterbody pressure indicated the likelihood of flow reattachment.

Nonequilibrium effects upon heat-transfer dimensionless parameters have been shown by Fay and Riddell (ref. 20) and by Chung and Anderson (ref. 29), to be negligible for stagnation and flat-plate flows, respectively, provided the wall is cold and catalytic. If the wall were non-catalytic, on the other hand, significant reductions in heat transfer could be obtained with cold walls, because some of the energy of dissociation would be retained by those atoms not recombining at the surface.

CONCLUSIONS

It has been shown that equilibrium real-gas behavior does not, in general, drastically affect inviscid flow forces and moments and aero-dynamic heat-transfer rates for most of the simple shapes considered. In fact, the scatter in the real-air experimental pressure and heat-transfer data on these shapes was shown to be larger than the predicted real-gas effect. Significant real-gas effects in inviscid flow were predicted only for some unswept two-dimensional shapes having discontinuities in surface slope at small angles of attack, and for swept flat plates near the shock detachment angle.



On the basis of the results obtained on most of the simple shapes considered here, real-gas effects are expected to be small on the more complicated configurations presently being investigated for use as reentry vehicles, because these shapes are characterized by highly swept surfaces and are designed, for the most part, for flight at relatively high angles of attack. It therefore appears that for such configurations where performance cannot be computed accurately for either real or perfect air, perfect-gas tests, used in conjunction with those analytic studies which are possible, will provide useful design data for flight conditions where equilibrium real-gas behavior is expected.

Lastly, nonequilibrium effects on inviscid flow appear important mainly in regions immediately downstream of rapid expansions. With cold, catalytic walls, the heat-transfer parameters are essentially independent of finite rate processes.



REFERENCES

- 1. Gilmore, F. R.: Equilibrium Composition and Thermodynamic Properties of Air to 24,000° K. U.S. Air Force Project RAND Res. Memo. RM-1543, The RAND Corp., Aug. 24, 1955. (Also Available From ASTIA as AD-84052.)
- 2. Hilsenrath, Joseph, and Beckett, Charles W.: Tables of Thermodynamic Properties of Argon-Free Air to 15,000° K. AEDC-TN-56-12, Arnold Eng. Dev. Center, Sept. 1956. (Also Available From ASTIA as Doc. No. AD-98974.)
- 3. Treanor, C. E., and Logan, J. G., Jr.: Tables of Thermodynamic Properties of Air From 3,000° K to 10,000° K. Rep. No. AD-1052-A-2 (Contract No. AF 40(600)-6, AF 18(603)-10), Cornell Aero. Lab., Inc., June 1956.
- 4. Feldman, Saul: Hypersonic Gas Dynamic Charts for Equilibrium Air. AVCO Res. Lab., Jan. 1957.
- 5. Moeckel, W. E., and Weston, Kenneth C.: Composition and Thermodynamic Properties of Air in Chemical Equilibrium. NACA TN 4265, 1958.
- 6. Gravalos, F. G., Edelfelt, I. H., and Emmons, H. W.: The Supersonic Flow About a Blunt Body of Revolution for Gases at Chemical Equilibrium. Doc. No. R58SD245, Missile and Ord. Syst. Dept., Gen. Elec. Co., June 16, 1958.
- 7. Holt, Maurice: Calculation of Pressure Distribution on Hypersonic Bodies of Revolution by Belotserkovskii's Method. RAD-2-TM-58-45, AVCO Res. and Advanced Dev. Div., Mar. 31, 1958 (Reissued Sept. 30, 1959).
- 8. Van Dyke, Milton D.: The Supersonic Blunt-Body Problem Review and Extension. Jour. Aero/Space Sci., vol. 25, no. 8, Aug. 1958, pp. 485-496.
- 9. Vaglio-Laurin, Roberto, and Ferri, Antonio: Theoretical Investigation of the Flow Field About Blunt-Nosed Bodies in Supersonic Flight.

 Jour. Aero/Space Sci., vol. 25, no. 12, Dec. 1958, pp. 761-770.
- 10. Beckwith, Ivan E., and Gallagher, James J.: Heat Transfer and Recovery Temperatures on a Sphere With Laminar, Transitional, and Turbulent Boundary Layers at Mach Numbers of 2.00 and 4.15. NACA TN 4125, 1957.



L1050

.



- 11. Lehnert, R., and Schermerhorn, V. L.: Wake Investigation on Sharp and Blunt Nose Cones at Supersonic Speeds. NAVORD Rep. 5668, U.S. Naval Ord. Lab. (White Oak, 'Md.), Jan. 28, 1958.
- 12. Cooper, Morton, and Mayo, Edward E.: Measurements of Local Heat Transfer and Pressure on Six 2-Inch-Diameter Blunt Bodies at a Mach Number of 4.95 and at Reynolds Numbers Per Foot up to 81 × 10⁶. NASA MEMO 1-3-59L, 1959.
- 13. Oliver, Robert E.: An Experimental Investigation of Flow Over Simple Blunt Bodies at a Nominal Mach Number of 5.8. GALCIT Memo. No. 26 (Contract No. DA-04-495-Ord-19), June 1, 1955.

L

0 5

0

- 14. Crawford, Davis H., and McCauley, William D.: Investigation of the Laminar Aerodynamic Heat-Transfer Characteristics of a Hemisphere-Cylinder in the Langley 11-Inch Hypersonic Tunnel at a Mach Number of 6.8. NACA Rep. 1323, 1957. (Supersedes NACA TN 3706.)
- 15. X-17 Re-Entry Test Vehicle R-22 Final Flight Report. Rep. IMSD-3042, Lockheed Aircraft Corp., May 14, 1957.
- 16. X-17 Re-Entry Test Vehicle R-26 Final Flight Report. Rep. IMSD-2600, Lockheed Aircraft Corp., Nov. 22, 1957.
- 17. Hansen, C. Frederick: Approximations for the Thermodynamic and Transport Properties of High-Temperature Air. NACA TN 4150, 1958.
- 18. Bauer, Ernest, and Zlotnick, Martin: Transport Coefficients of Air to 8,000° K. RAD-TR-58-12, AVCO Res. and Advanced Dev. Div., Sept. 29, 1958.
- 19. Green, Melville S.: The Transport Properties of Air at Elevated Temperatures. Viscosity, Thermal Conductivity, and Prandtl Number of Air From 1,000° K to 10,000° K at Normal Densities of 1, .1, and .01. Unpublished Report, Nat. Bur. Standards, 1957.
- 20. Fay, J. A., and Riddell, F. R.: Theory of Stagnation Point Heat Transfer in Dissociated Air. Jour. Aero. Sci., vol. 25, no. 2, Feb. 1958, pp. 73-85, 121.
- 21. X-17 Re-Entry Test Vehicle R-2 Final Flight Report. Rep. MSD-3003, Lockheed Aircraft Corp., Oct. 17, 1956.
- 22. X-17 Re-Entry Test Vehicle R-8 Final Flight Report. Rep. MSD-3028, Lockheed Aircraft Corp., Jan. 1, 1957.
- 23. X-17 Re-Entry Test Vehicle R-9 Final Flight Report. Rep. MSD-3029, Lockheed Aircraft Corp., Jan. 5, 1957.



0

8

- 24. X-17 Re-Entry Test Vehicle R-11 Final Flight Report. Rep. MSD-3031, Lockheed Aircraft Corp., Jan. 18, 1957.
- 25. Van Driest, E. R.: Investigation of Laminar Boundary Layer in Compressible Fluids Using the Crocco Method. NACA TN 2597, 1952.
- 26. Jones, Jim J.: Resumé of Experiments Conducted in the High-Pressure Shock Tube of the Gas Dynamics Laboratory at NASA. Proc. Third Shock Tube Symposium. SWR-TM-59-2, Air Force Special Weapons Center, Mar. 10-12, 1959.
- 27. Lees, Lester: Laminar Heat Transfer Over Blunt-Nosed Bodies at Hypersonic Flight Speeds. Jet Propulsion, vol. 26, no. 4, Apr. 1956, pp. 259-269.
- 28. Anon.: Aerodynamics Report. Vol. II. ER 10372 (Contract No. AF 33(600)-37705), Martin Space Flight, Mar. 1959.
- 29. Chung, Paul M., and Anderson, Aemer D.: Dissociative Relaxation of Oxygen Over an Adiabatic Flat Plate at Hypersonic Mach Numbers. NASA TN D-140, 1960.
- 30. Sibulkin, M.: Heat Transfer Near the Forward Stagnation Point of a Body of Revolution. Jour. Aero. Sci. (Readers' Forum), vol. 19, no. 8, Aug. 1952, pp. 570-571.
- 31. Beckwith, Ivan E.: Similar Solutions for the Compressible Boundary Layer on a Yawed Cylinder With Transpiration Cooling. NASA TR R-42, 1959. (Supersedes NACA TN 4345.)
- 32. Kemp, Nelson H., Rose, Peter H., and Detra, Ralph W.: Laminar Heat Transfer Around Blunt Bodies in Dissociated Air. Jour. Aero/Space Sci., vol. 26, no. 7, July 1959, pp. 421-430.
- 33. Fluid Motion Panel of the Aeronautical Research Committee and Others:
 Modern Developments in Fluid Dynamics. Vol. II, ch. XIV, sec. 270,
 S. Goldstein, ed., The Clarendon Press (Oxford), 1938, p. 631.





HEMISPHERE PRESSURE-COEFFICIENT DISTRIBUTIONS LOW MACH NUMBER

O EXPERIMENT (4.15 \leq M_O \leq 6.8)

10

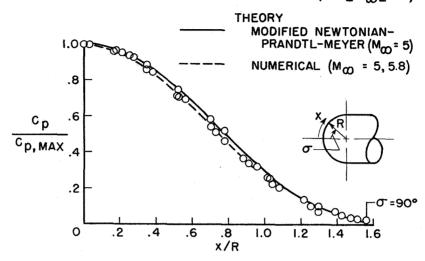


Figure 1(a)

HEMISPHERE PRESSURE-COEFFICIENT DISTRIBUTIONS HIGH MACH NUMBER

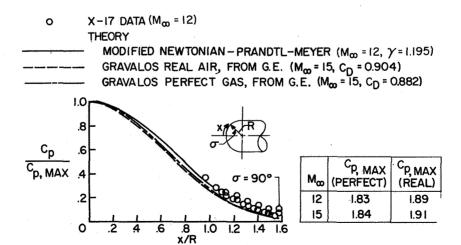


Figure 1(b)





PRESSURE-COEFFICIENT DISTRIBUTIONS ON ATLAS MARK II

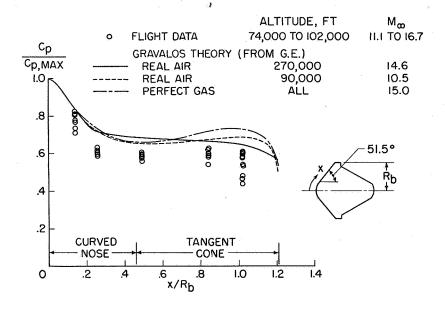


Figure 2

PRESSURE - COEFFICIENT DISTRIBUTION ON ATLAS MARK III. $M_{\infty} = 20$

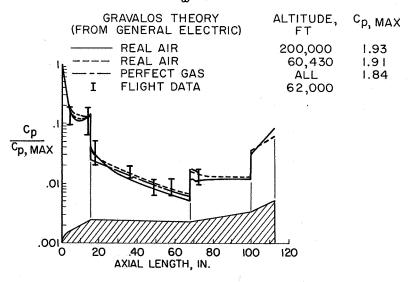


Figure 3



RATIO OF PERFECT TO REAL, AIR SURFACE PRESSURE SWEPT FLAT PLATES AT ANGLE OF ATTACK; Mo=20; ALTITUDE, 200,000 FT

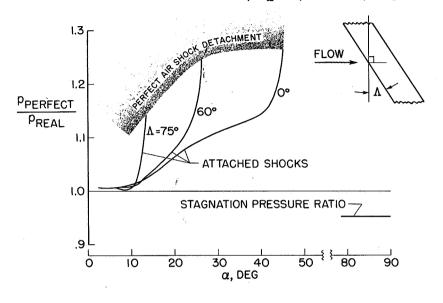


Figure 4

AERODYNAMIC CHARACTERISTICS OF A BLUNTED HALF-CONE

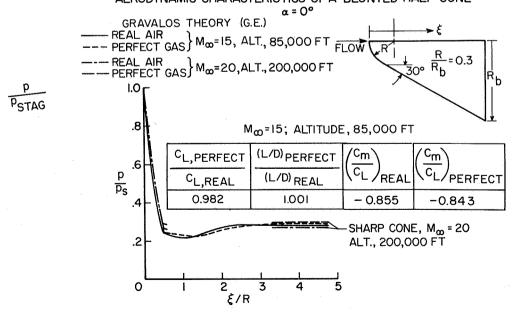
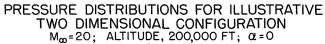


Figure 5



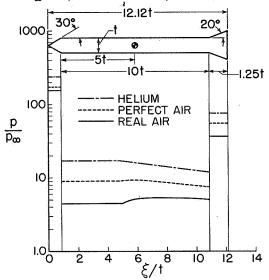


Figure 6(a)

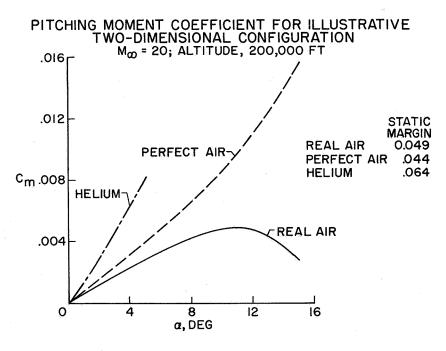


Figure 6(b)



STAGNATION-POINT HEAT-TRANSFER RATES FOR A BODY OF REVOLUTION

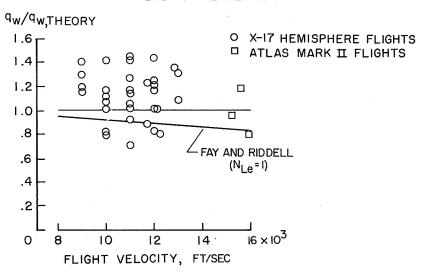


Figure 7

REAL-AIR LAMINAR-HEAT-TRANSFER PARAMETER FOR A FLAT PLATE

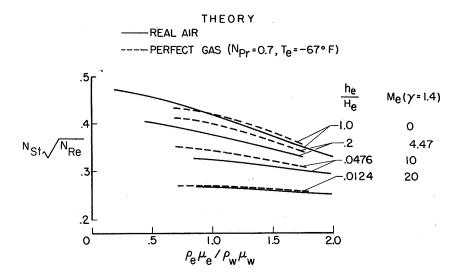


Figure 8(a)

HEAT TRANSFER FOR A 10° WEDGE IN SHOCK-TUBE FLOW

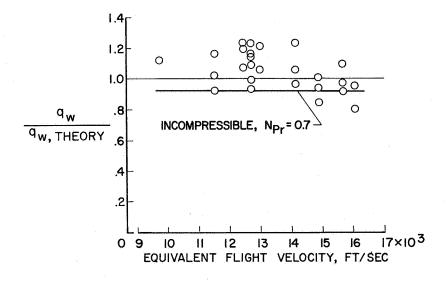


Figure 8(b)



HEAT-TRANSFER DISTRIBUTIONS ON A HEMISPHERE $M_{\infty} \approx 12$

18

1

狘.

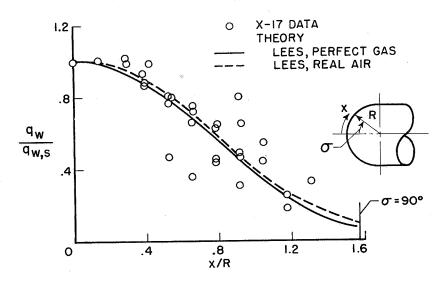


Figure 9(a)

HEAT-TRANSFER DISTRIBUTION ON ATLAS MARK II

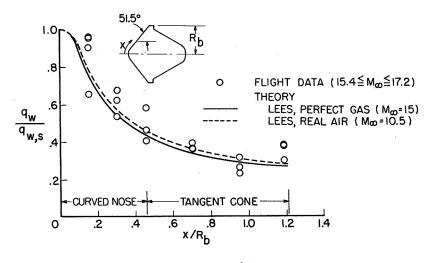


Figure 9(b)



NONEQUILIBRIUM EFFECT ON AFTERBODY FLOW M_{∞} = 20; ALTITUDE, 200,000 FT

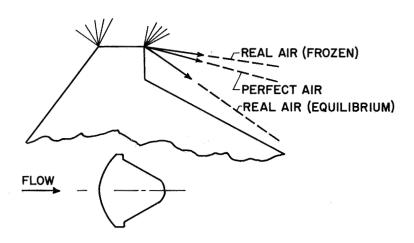


Figure 10

Page intentionally left blank



STUDIES OF STABILITY AND CONTROL OF

WINGED REENTRY CONFIGURATIONS

By Robert W. Rainey and William H. Close Langley Research Center

SUMMARY

LO

4

0

A study of the static stability and control problem areas of winged reentry vehicles capable of maximum lift-drag ratios of about 2 at hypersonic speeds has been made. Throughout the Mach number and angle-of-attack ranges of the tests, it appears that the center-of-gravity location will be a compromise between operation at maximum lift-drag ratio at subsonic speeds and at maximum lift at hypersonic speeds, where the aerodynamic center is significantly aft of its location at subsonic speeds. At maximum lift at hypersonic speeds, combinations of nose and flap deflections will trim the vehicle with reasonable longitudinal stability, and the static directional stability may be increased by use of wing-tip-fin roll-out. At hypersonic speeds, care must be exercised to tailor the forward portions of the vehicle in order to avoid longitudinal and directional instability in the low-angle-of-attack range; at low angles of attack the longitudinal control effectiveness is very low and auxiliary control devices may be required.

INTRODUCTION

A study has been made of several static longitudinal, directional, and lateral stability and control problems associated with winged reentry vehicles capable of maximum lift-drag ratios of about 2 at hypersonic speeds. This study was carried out at speeds from subsonic to a Mach number of 18 and in the angle-of-attack range from 0° to that for maximum lift (near 55°). Several problem areas are discussed herein along with possible solutions.





SYMBOLS

 iI

P.

69.

<\$.

$\mathbf{c}_{\mathbf{L}}$	lift coefficient, $\frac{\text{Lift}}{q_{\infty}S_{\text{WING}}}$
c_{i}	rolling-moment coefficient, $\frac{\text{Rolling moment}}{q_{\infty}S_{\text{WING}}^b}$
$C_{\mathbf{m}}$	pitching-moment coefficient, $\frac{\text{Pitching moment}}{q_{\infty}S_{\text{WING}}\bar{c}}$
$C_{\mathbf{N}}$	normal-force coefficient, $\frac{\text{Normal force}}{q_{\infty}S_{\text{WING}}}$
C_n	yawing-moment coefficient, $\frac{\text{Yawing moment}}{q_{\infty}S_{\text{WING}^b}}$
$c_{1_{\beta}}$	effective dihedral parameter, $\frac{\partial C_l}{\partial \beta}$, per deg
$c_{n_{\beta}}$	static directional stability parameter, $\frac{\partial C_n}{\partial \beta}$, per deg
$(\Delta^{c_{n_{\beta}}})_{fin}$	fin contribution to static directional stability parameter, per deg
$\frac{9C^{M}}{9C^{m}}$	static longitudinal stability parameter
ъ	wing span, in.
ē	mean aerodynamic chord, in.
L/D	lift-drag ratio
М	Mach number
$\frac{(p_{r}/p_{\infty}) - 1}{(p_{i}/p_{\infty}) - 1}$	real-gas pressure parameter, ratio of real-gas to ideal- gas pressure coefficients





p	static pressure
đ	dynamic pressure, lb/sq in.
S_{FLAP}	flap planform area, sq in.
$s_{ ext{FIN}}$	single fin area, sq in.
s _{NOSE}	nose planform area, sq in.
$s_{ t WING}$	total wing planform area, sq in.
α	angle of attack, deg
β	angle of sideslip, deg
$\delta_{\mathbf{n}}$	nose-panel-deflection angle, deg
$\delta_{ extsf{f}}$	flap-panel-deflection angle, deg
ø	fin roll-out angle referenced from the vertical plane
Subscripts:	
MAX	maximum
t t	trim
∞	free-stream conditions
r	real-gas conditions

L 1 0

0

i

DISCUSSION

ideal-gas conditions

Longitudinal Stability and Control

Angles of attack for maximum L/D or less.— The stability of several wings and winged vehicles is presented in figure 1 for an angle of attack of 10° which is approximately that for maximum L/D. The aerodynamic-center location relative to the mean aerodynamic chord is plotted against Mach number. These results are from references 1 to 5 and unpublished results from Boeing Airplane Co. In the lower portion



Á

Ĺ

1

4

0

3

of the figure are presented results from tests of simple, symmetrical delta wings: these results show that there is a large rearward shift in aerodynamic center in the transonic speed range. At Mach numbers above about 1, the aerodynamic center is located close to 50-percent mean aerodynamic chord which is the centroid of area. However, for the four reentry vehicles shown, which have bodies and fins in combination with wings of unsymmetrical airfoil section, large aerodynamic-center shifts are exhibited throughout the transonic and supersonic speed ranges. At hypersonic speeds the aerodynamic-center location is ahead of the 50percent mean aerodynamic chord and is invariant with Mach number. Additional tests have been made for two of the configurations reported in reference 1 in the air nozzle $(M_{\infty} = 9.6)$ and the helium nozzles $(M_{\infty} \approx 10$ and 18) of the Langley 11-inch hypersonic tunnel by Charles L. Ladson; whereas at a Mach number near 18, results are also available from AEDC Hotshot 1 using air (ref. 2). It can be seen that there is little effect of the variation in fluid properties upon the stability of the vehicles tested. Furthermore, for these vehicles, the results for M = 6.8 and 9.6 are representative of the results for higher Mach numbers. It is obvious that from a stability consideration for these vehicles, the results for the delta wings should not be depended upon. In general, the variation in the aerodynamic-center location with Mach number is similar for the four reentry vehicles. In addition, the trend in center-of-pressure location is quite similar to the aerodynamic-center shifts shown in this figure, and the problem of providing sufficient control to trim the vehicle even at low lift coefficients through the supersonic-speed range is evident. At angles of attack higher than that of 100 shown in figure 1 and at hypersonic speeds, the aerodynamic center and center of pressure move rearward, and, generally speaking, the centerof-gravity location would involve a compromise between the high-angleof-attack trim at hypersonic speeds and the low-angle-of-attack stability at subsonic speeds. From considerations for subsonic speeds, a centerof-gravity location at 42-percent mean aerodynamic chord appears reasonable and will be used for the remainder of this presentation.

At angles of attack lower than that of 10° shown in figure 1, the shape of the forward portions of the vehicle and the wing airfoil section have a marked influence on the stability. Examples of this are presented in figure 2, in which for a Mach number of 9.6, the pitching moment is plotted against normal force for two of the vehicles of figure 1 for flap deflections of 0° and -10° for the upper vehicle and for 0° for the lower. In the higher angle-of-attack range, the upper vehicle in stable and flap effectiveness is high. However, as the angle of attack is reduced below that for $(L/D)_{MAX}$ the large variations in the downloads on the fuselage nose and airfoil section with α resulted in marked instability. Furthermore, the flap effectiveness is very low. Modification of the fuselage nose from the triangular cross section of the upper vehicle to a higher fineness-ratio, "D" cross section of the

lower vehicle along with a reduction in the airfoil thickness was sufficient to alleviate the longitudinal instability; however, although the results are not presented herein, the problem of low flap effectiveness is still prevalent. Other results not reported herein show that for flap deflections up to -45°, the flap effectiveness is still quite low for flaps with an area approximately 10 percent of the wing area. Consequently, larger flaps or auxiliary devices or both appear to be in order. It should be noted for figure 2, as was pointed out for figure 1, that the body, and to some degree the fins, influence strongly the longitudinal characteristics in the low angle-of-attack range and wingalone data are not indicative of the complete-vehicle characteristics.

Angles of attack near maximum lift .- At the angles of attack greater than about 250, the effects of components on top of the wing are essentially nonexistent, and insofar as the vehicle characteristics are concerned, the complete vehicle may be simulated by a simple wing alone. In order to examine the high angle-of-attack trim problem at hypersonic speeds, an investigation was undertaken with a 70° swept, flat-plate delta wing at $M_m = 6.7$; the pitching-moment coefficients of this wing about the 42-percent mean aerodynamic chord are plotted in figure 3 against angle of attack for flap deflections of 0°, -10°, and -20°. test-point symbols denote the measured results, and the lines denote the results from computations which utilized the correlation of measured deltawing data at angles of attack in excess of leading-edge-shock detachment. (See ref. 6.) For the wing with the undeflected flap, the large negative pitching moments in the maximum-lift range which must be trimmed out are evident; consequently, a relatively large flap is in order. For the results presented herein the flap area was 19 percent of the wing area. The use of flap deflection at these angles of attack provides sizable increments in pitching moments, and as expected, the effects of flap deflection are destabilizing. The computations underestimate somewhat both the pitching-moment increments and the destabilizing effects of negative flap deflection in the range of $C_{L,MAX}$. Larger negative flap deflections will provide trim in the maximum-lift range but with a further decrease in the stability. The longitudinal stability may be increased somewhat by the use of nose deflection as shown in figure 4, in which the results show the increase in stability throughout the angleof-attack range along with the increments in pitching moment which are smaller at the higher angles of attack. The computations overestimated the moment increments and underestimated the stability increase near maximum lift.

From a stability and control standpoint, it appears feasible to consider the combined use of nose and flap deflection to provide trim with stability at angles of attack near maximum lift. In figure 5 are summarized some of the high-angle-of-attack trim characteristics of the 70° swept wing at $M_{\rm m}=6.7$. The computed results, shown as solid lines,



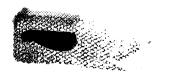
ζ4.

are presented as the trim stability parameter $(\partial C_m/\partial C_N)_+$ plotted against the trim angle of attack $\alpha_{t.}$ for nose deflections of 0° , 5° , and 10°. Along each line of constant nose deflection, the flap deflection angle varies from a small negative value to -400. The dashed lines are the computed contours of constant trim lift coefficient. For these trim conditions, an increase in nose deflection angle increased the vehicle stability as was noted previously for the untrimmed case (fig. 4). By use of combined nose and flap deflections, it is possible to provide trim with stability at maximum lift (fig. 5). The maximum value of trim $C_{T.}$ is 0.62 based on total planform area including flaps. If the center of gravity could be located more rearward, trim CL could obviously be increased. However, such a rearward shift in center of gravity would not necessarily reduce the overall stability inasmuch as less destabilizing negative flap deflections would be needed to trim. Experimental trim results, shown in figure 5 by the test-point symbols, have been obtained for several combinations of nose and flap deflections (ref. 6). Arrows from each test-point symbol connect the experimental point with its comparative computed point. In general, good agreement exists between the experimental and computed results except that the computations yield slightly higher stability. The highest measured trim lift coefficient obtained throughout this experimental investigation was 0.63 while the highest value of lift coefficient measured for the undeflected, untrimmed delta wing was 0.72. Of major interest also are the trim characteristics at higher Mach numbers, and in figure 6 are summarized the results of computations for a Mach number of 18 for the same 70° swept delta wing utilizing the computational method of reference 6 for ideal-gas conditions. These computed results are similar to those at $M_{\infty} = 6.7$ (fig. 5) except that the value of maximum trim lift is slightly lower. Included for comparison is the computed value of maximum trim lift for a vehicle with a wing loading of 25 lb/sq ft at an altitude of 242,000 feet where the real-gas effects have been approximated as follows:

The method of reference 6 for computing longitudinal stability for ideal-gas conditions was extended to the approximate real-gas conditions by the use of references 7 and 8. For the two-dimensional case of reference 7 up to shock detachment and for the normal-shock case of reference 8, a variation with flow deflection angle was obtained for the

parameter $\frac{(p_r/p_\infty)-1}{(p_i/p_\infty)-1}$ for the case of a Mach number of 18 and an alti-

tude of 242,000 feet (1956 ARDC model atmosphere). At the various panel flow-deflection angles, the individual ideal-gas panel pressure coefficients previously obtained were multiplied by this real-gas pressure parameter and the product is the approximate real-gas pressure coefficient.



1

ĵħ

Ž

1

()A

THE REAL PROPERTY.

These approximate real-gas effects did not alter the value of the maximum trim lift appreciably as compared with the ideal-gas value although the angle of attack at which it occurred was significantly higher and the control geometry required was slightly altered.

It should be emphasized that while effects of variation in nose deflection have been discussed herein, a reentry vehicle would utilize a fixed nose. Care must be exercised in the selection of such a nose with regard to exceeding the temperature limitation on this deflected area and with regard to the reduction in stability produced by the nose at angles of attack near $(L/D)_{MAX}$ or lower. Past experience (ref. 9) indicates that about $5^{\rm O}$ of nose deflection in combination with a small negative flap deflection will trim a similar vehicle at angles of attack in the range of $(L/D)_{MAX}$ with essentially no performance penalty and with reasonable longitudinal stability. The results presented herein (figs. 5 and 6) indicate that these angles of nose deflection may be used in combination with large negative flap deflections to provide trim with stability at maximum lift.

Directional and Lateral Stability

Basic stability derivatives .- With regard to directional and lateral stability, results from tests of two vehicles (from ref. 1 and unpublished results from Boeing Airplane Co.) are presented in figure 7 for an angle of attack approximately that for $(L/D)_{MAX}$. The static C_{n_R} (body axes) are presented as functions of Mach number. For both vehicles the decay in $C_{n_{\mathsf{R}}}$ with Mach number increase due to the reduction in tipfin effectiveness is evident. For this type of vehicle, the positive value of ClB can be removed by a small amount of dihedral of the lower wing surface. Angle of attack also has an appreciable influence on directional and lateral stability as seen in figure 8. At low angles of attack the static $C_{n_{\boldsymbol{\beta}}}$ increased with α as a result of the reduction in the destablizing influence of the fuselage nose. At higher angles of attack, the effectiveness of the tip fins falls off and static directional instability results. However, for these vehicles with highly swept wings, $C_{l_{\mathrm{R}}}$ becomes large negatively and may offset the directional instability for the dynamic case.

Method to improve static $C_{n_{\beta}}$. If it is desirable to have positive values of static $C_{n_{\beta}}$ at these high angles of attack, one method of improving static $C_{n_{\beta}}$ is the use of fin roll-out (fig. 9). The fin



roll-out angle \emptyset is that angle between the plane of the fin and the vertical. The use of roll-out causes the maximum deflection angle of the flow relative to the fin to occur at higher angles of attack; thus, the initiation of $\,C_{n_{\mathsf{R}}}\,\,$ decay is delayed to a higher angle of attack. It is seen that in this angle-of-attack range, fin roll-out may be used to nullify the familiar decay shown for $\emptyset = 0^{\circ}$ and to produce an invariant or an increasing $\,{\tt C}_{n_{\beta}}\,\,$ contribution of the fins with $\,\alpha$ increase. Of course, with fin roll-out there is an input to the pitching moment of the vehicle, and an increment in negative flap deflection $\Delta\delta_{\mathbf{r}}$ is necessary to overcome this pitching-moment input and to retrim the vehicle as shown by the dashed curves. In this regard the longitudinal trim limit at which the flaps become streamwise and lose their effectiveness is shown by the cross-hatched boundary in this figure. From consideration of cross-control effects due to rudder deflection, roll-out should be limited to small amounts, probably about 100 or 150. Also roll-out of this magnitude would require only about 20 additional negative flap deflection to retrim the vehicle at hypersonic speeds and would improve the longitudinal stability at subsonic speeds by about 2-percent mean aerodynamic chord.

L

1

0

0

CONCLUDING REMARKS

In conclusion, several aspects and problems of major importance to the stability and control of winged reentry vehicles have been discussed along with possible solutions for the problem areas. Although the magnitudes of the problems for specific vehicles would undoubtedly be altered from those contained within this generalized discussion, the principles behind which these solutions were reached should be applicable.





- 1. Ladson, Charles L., Johnston, Patrick J., and Trescott, Charles D., Jr.: Effects of Planform Geometry on the Aerodynamic Characteristics of a Hypersonic Glider at Mach Numbers Up to 9.6. NASA TM X-286.
- 2. Wallace, A. R., and Swain, W. N.: Force, Heat Transfer, and Pressure Distribution Tests of Martin-Bell Dyna-Soar Glider Models at Mach Numbers 15 21. AEDC TN 60-25 (Contract No. AF 40(600)-800), Arnold Eng. Dev. Center, Feb. 1960.
- 3. McDevitt, John B., and Rakich, John V.: The Aerodynamic Characteristics of Several Thick Delta Wings at Mach Numbers to 6 and Angles of Attack to 50°. NASA TM X-162, 1960.
- 4. Mueller, James N.: An Investigation of the Effect of Varying the Maximum-Thickness Position Upon the Aerodynamic Characteristics of a Series of 3 Percent-Thick Delta Wings. NACA RM L55D26, 1955.
- 5. Shanks, Robert E.: Effects of Wing Crank and Sweepback on the Low Subsonic Stability and Control Characteristics of a Model of a Hypersonic Boost-Glide Type Airplane. NASA TM X-181, 1960.
- 6. Close, William H.: Hypersonic Longitudinal Trim, Stability, and Control Characteristics of a Delta-Wing Configuration at High Angles of Attack. NASA TM X-240, 1960.
- 7. Trimpi, Robert L., and Jones, Robert A.: A Method of Solution With Tabulated Results for the Attached Oblique Shock-Wave System for Surfaces at Various Angles of Attack, Sweep, and Dihedral in an Equilibrium Real Gas Including the Atmosphere. NASA TR R-63, 1960.
- 8. Huber, Paul W.: Tables and Graphs of Normal-Shock Parameters at Hypersonic Mach Numbers and Selected Altitudes. NACA TN 4352, 1958.
- 9. Rainey, Robert W., Fetterman, David E., Jr., and Smith, Robert: Summary of Static Stability and Control Results of a Hypersonic Glider Investigation. NASA TM X-277, 1960.



TABLE I.- AXISYMMETRIC STAGNATION-POINT HEAT-TRANSFER PARAMETER

$$\mathbb{N}_{\text{Le}} = \mathbb{1}$$

Solution	Reference	Gas	Transport properties			
			μ	N _{Pr}	A	m
Sibulkin	30	Incompressible	Constant	Constant	0.763	0.5
Beckwith	31	Perfect compressible	Sutherland	Constant	.76	.4
Fay and Riddell	20	Equilibrium dissociated air	Sutherland	Constant	.76	.4
Kemp, Rose, and Detra	32	Equilibrium dissociated air	Sutherland	Constant	•793	.438
*Cohen and Beckwith		Equilibrium dissociated air	Hansen, ref. 18	Variable, Hansen, ref. 18	.767	.45

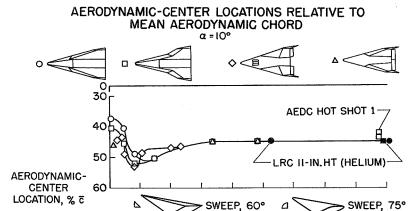
TABLE II.- YAWED-INFINITE-CYLINDER STAGNATION-LINE LAMINAR HEAT TRANSFER

$$[N_{Le} = 1]$$

Solution	Reference	Gas	Transport properties		A	-
			μ	$\mathtt{N}_\mathtt{Pr}$	A	m
Squire	33	Incompressible	Constant	Constant	0.570	0.5
Beckwith	31	Perfect compressible	Sutherland	Constant	.577	.44
Kemp, Rose, and Detraa	32	Equilibrium dissociated air	Sutherland	Constant	.576	.438
Cohen and Beckwith		Equilibrium dissociated air	Hansen, ref. 18	Variable, Hansen, ref. 18	-594	•5

^aSolutions for zero yaw only.

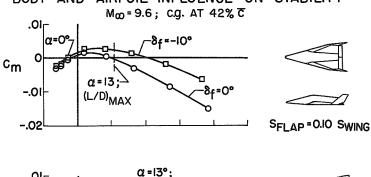




50 2 4 6 8 10 12 14 16 18 M_∞

Figure 1

BODY AND AIRFOIL INFLUENCE ON STABILITY



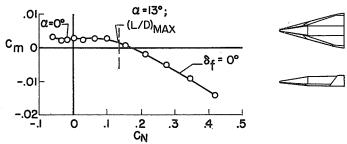


Figure 2



ী



EFFECT OF FLAP DEFLECTION ON DELTA-WING CHARACTERISTICS

 M_{∞} =6.7; c.g. AT 42% \overline{c} ; S_{FLAP} =0.19 S_{WING}

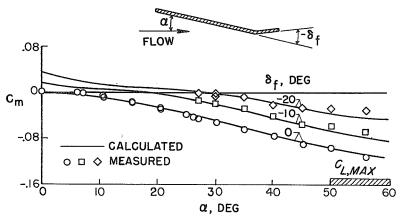


Figure 3

EFFECT OF NOSE DEFLECTION ON DELTA-WING CHARACTERISTICS

 M_{\odot} = 6.7; c.g. AT 42% \overline{c} ; S_{NOSE} = 0.16 S_{WING} ; S_{FLAP} = 0.19 S_{WING}

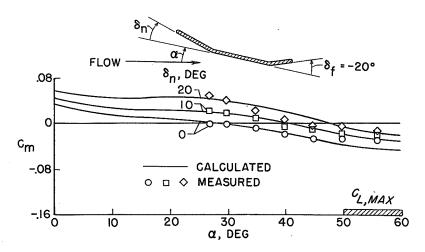


Figure 4



c E

3



(

 M_{∞} = 6.7; c.g. AT 42 % \overline{c} ; S_{NOSE} = 0.16 S_{WING} ; S_{FLAP} = 0.19 S_{WING}

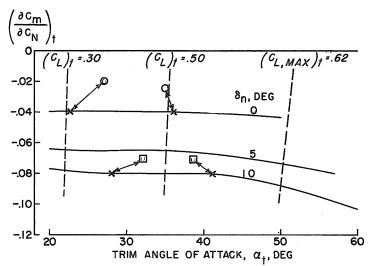


Figure 5

COMPUTED HIGH-ANGLE-OF-ATTACK LONGITUDINAL TRIM CHARACTERISTICS

 M_{\odot} = 18; c.g. AT 42% \bar{c} ; S_{NOSE} = 0.16 S_{WING} ; S_{FLAP} = 0.19 S_{WING}

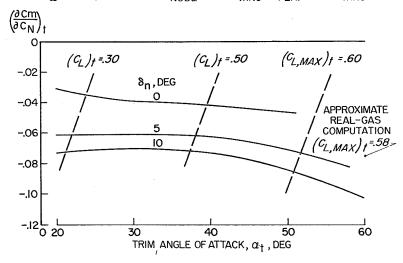


Figure 6





MACH NUMBER EFFECT ON DIRECTIONAL AND LATERAL STABILITY $$\alpha = 10^{\circ}$$

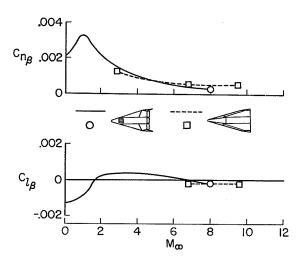


Figure 7

ANGLE-OF-ATTACK EFFECT ON DIRECTIONAL AND LATERAL STABILITY

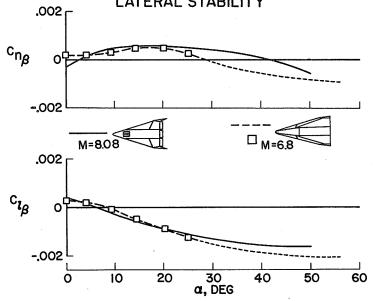


Figure 8

3

1

Å

EFFECTS OF FIN ROLLOUT ON DIRECTIONAL STABILITY SFIN = 0.08SWING; SFLAP = 0.19SWING

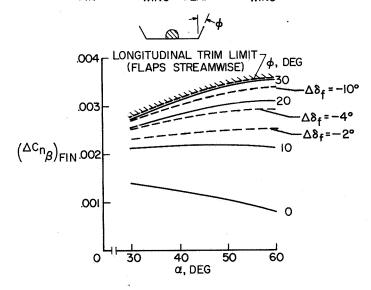


Figure 9

